

**Investigations into the Requirements for Homogeneous Platinum-  
and Iridium-Catalyzed Oxidative C-H Bond Functionalization**

**Thesis by**

**David R. Weinberg**

In Partial Fulfillment of the Requirements  
for the Degree of Doctor of Philosophy

California Institute of Technology

Pasadena, CA

2009

(Defended November 26, 2008)

© 2009

David R. Weinberg

All Rights Reserved

*For my family:*

*Interpretations of a person's behavior almost always begin with that person's family;  
therefore, they deserve the most credit for one's achievements.*

## Acknowledgements

It will be nearly impossible for me to thank everyone who has helped me to complete this thesis over the last seven plus years, and it would definitely be impossible for me to thank everyone who has influenced me or impacted my life, allowing me to reach this point. Nonetheless I will do my best to thank a small portion of the people who have helped me during my time at Caltech. If your name does not appear in the following pages, it does not mean that my appreciation for your impact on this thesis or on my life is lacking. Furthermore, I know that I cannot thank the people mentioned herein nearly enough. With that said...

First, I would like to thank my advisor, John Bercaw. Based on his reputation as a person and as a scientist, I knew that I wanted to work for John before I came to Caltech, and he did not disappoint me. John has been a great advisor. He has helped me to learn how to think about chemistry; but more importantly, he has taught me how to attack problems in general. He has also provided me with a kick in the ass when necessary. My favorite thing about John is that he treats everyone with respect, and he encourages everybody to ask questions. It is clear that John truly cares for his students, and he is more than willing to help them out when they are in trouble.

In addition to John, I was fortunate to have Jay Labinger as an advisor. Jay has been fantastic in that he is extremely insightful, and this allows him to see positive points of experiments that could otherwise be missed. He has often been crucial in helping me to communicate the reasons for performing reactions; and in general, he has had very

useful and unique suggestions for attacking problems. Thank you, Jay. I am glad that in the past two years I have been able to talk to Jay more about things outside of chemistry and to play tennis with him. The most memorable part, and possibly my favorite part, of my experiences playing tennis here has been trying to return Jay's serves; they destroyed me, but I was overjoyed by every small victory.

I have had a great advisory committee during my time at Caltech, including Harry Gray, Bob Grubbs, Nate Lewis, and David MacMillan. They have all provided valuable insight and direction, which has helped in the completion of this thesis and in my general understanding of how to attack problems in chemistry. Harry Gray has been an integral part of my time at Caltech. Harry has provided fantastic insight into chemistry; but probably more importantly, he has been a very good friend to me. Harry has lifted my spirits whenever I needed it, and he has always helped me to see things in a positive light. He is fun to be around, and one cannot help to feel intoxicated with Harry around, both literally and figuratively. Harry, I will never even nearly be able to thank you enough for all that you have done for me and how much you have inspired me and given me confidence. Thank you!!

Bob Grubbs has been my committee chair, and he has been exceedingly beneficial to me in providing me with direction. He has helped me in meetings with my committee, and he has given me valuable insight into chemistry. Thank you very much, Bob. I have enjoyed talking to Bob about rock climbing, canyoneering, and mountaineering. I was even fortunate to go with Bob on at least one rock-climbing trip.

Nate Lewis inspired me, like many others, to get involved with energy-related research and to try gaining a small understanding of energy-related politics. He made me think in greater depth about my research proposals, and he provided me with much-needed help in my search for a postdoctoral position. Thank you, Nate.

Next, I would like to thank the other people who directly contributed to this thesis. I greatly appreciate Larry Henling and Mike Day for their work on the crystallographic studies and their patience; Mona Shahgholi and Naseem Torian for help obtaining mass spectra; Angelo Di Bilio for help performing and analyzing the EPR experiments; David VanderVelde, Scott Ross, and Chris Daeffler for help with NMR experiments; Nilay Hazari for performing the DFT calculations and proofreading this manuscript; Aaron D. Wilson for help with the electrochemical studies; Victor Diakov for help with the GC-MS work in chapter 2; George Chen for help with the high-pressure NMR setup; Rick Gerhart for making custom glassware and reconstructing broken glassware; Theodor Agapie for help designing the custom glassware used in chapter 2; Greg Girolami for suggestions leading to the crystallization of anionic complexes; and, bp for funding and support.

An extremely large part of what I have learned during my time here has come from the people in the Bercaw group. They have provided me with insight, support, good times, and friendship. I believe that the composition of the group and group dynamics are a reflection on John, and I have always been impressed by the people surrounding me. The first two people that I would like to thank are Theodor Agapie and Nilay Hazari. My experience here would have been exceedingly different without these two fantastic

individuals. They have taught me an immense amount about chemistry and about life in general. I consider them both to be great role models, and I strive to be like them in many ways. The world would be very fortunate to have these two individuals mentoring people for the foreseeable future. They are great friends, and I have required their support on numerous occasions. They have each taken more time than they probably should have to help me out with chemistry and with outside issues. Somehow, they seem to have unending patience with me. I cannot say enough good things about these two people, and I cannot possibly thank them enough for all they have done for me. Thank you, both.

My training at Caltech really began with Theodor Agapie and Jonathon Owen. During my time here, Jonathon has been one of the biggest contributors to group dynamics and discussions about chemistry. He was always organizing social events, and I never saw anybody in the group talk so much to each group member about that person's chemistry. The group thoroughly misses not having him around; just ask George. Jonathon really helped me to gain intuition about platinum chemistry and to learn about working in the lab. The students at whatever institution Jonathon ends up at will be very lucky. He has remained a steadfast friend since leaving Caltech, and his friendship is truly appreciated.

Endy Min is one of the people that really convinced me to join the Bercaw group. She has become one of my best friends during her time here and since leaving the group. While our discussions have mostly been on topics not directly related to chemistry, they have been an integral part of my learning experience. She has supported me through

tough times, given me confidence, and stood by me when I did not take time for her. Thank you Endy for all that and for introducing me to Lindy Groove.

Steve Baldwin and Jeff Byers were both here for the majority of my time. They have been great friends, and they have also provided me with valuable insight into chemistry. I have thoroughly enjoyed spending a lot of time with Steve watching football and playing poker. He has cooked me fantastic meals, and he has allowed me to vent on many occasions. Thank you, Steve. I would like to thank Jeff for getting me back into reading classic literature by starting a book club. I thoroughly enjoyed the book club, and now I feel the need to read on a daily basis. This has provided me with valuable insight into the world in general, and it has helped to improve my writing. I have sincerely enjoyed Jeff's friendship, and I miss our day-to-day interactions on sports and literature.

Many thanks go to Alex Miller who has provided me with extremely valuable insight on chemistry, politics, and sports. Alex is a fantastic chemist and teacher. Another person who provided me with great ideas for chemistry is Bolin Lin. Bolin has come a long ways during my time here with his knowledge of chemistry and his grasp of the English language. Your ability to integrate new ideas will take you far. George "Shaq" Chen has also been very helpful and a good friend. George looks at things from very unique perspectives, and we can all benefit from this. Similarly, Ross Fu has provided me with very unique perspectives, especially with regard to chemistry and politics. I am very happy that he is picking up the iridium project.

I would like to thank Ted Weintrob because his patience with respect to the NMR facility has been fantastic, and I have always respected the job he has done. You will go far in chemistry due to your passion and your desire to do things rigorously.

Thanks go to Lily Ackerman. I have thoroughly enjoyed your friendship, and I am always impressed by your knowledge of chemistry and your approaches toward life.

I would also like to point out Susan Schofer who has been an invaluable friend to me; I greatly miss her. I would like to thank Sara Klamo who is one of the most hardcore people that I know and yet is an extremely fun person to be around. I have greatly appreciated overlapping with Paul Elowe during my time here. He is more like me than he realizes, and that is part of the reason that we get along so well at times and so much less well at other times. I have learned a lot from my discussions with Paul. Thanks also go to Heather Weincko. Heather is one of the nicest people that I know, and my only regret is that we did not spent more time together. I am also happy to have overlapped with Brian Zeglis and Antek Wong-Foy.

Many people in the current group have helped me to enjoy the last few years of my time here. I have really enjoyed talking to Paul O'blad, one of the most considerate people that I know. Archie (Ian Tonks) has been a great person to hang out with in lab and out, and I have thoroughly enjoyed our discussions on bonding. I have also really enjoyed hanging out with Suzanne Golisz and Shane Arney. Oh, and I do think that Suz is a safe chemist regardless of how I have tried to push her buttons in the past. Valerie Scott has been a welcome addition to the group. She is a very interesting person and quite the character. I look forward to hearing about her domination of gold chemistry. I

am happy that Miss Phoebe Lynne Davis (Rachel Klet) was kicked out of her old desk by George Chen because I really enjoy her friendship. She is a very hard worker, and my one wish for her is that she has more fun.

The postdocs during my time in the Bercaw group, including Christoph Balzarek, Tom Driver, Travis Williams, Aaron Wilson, Reto Dorta, Cliff Baar, Parisa Mehrkodavandi, Patrick Vagner, Xingwei Li, Alan Heyduk, and Ned West have provided me with exceedingly valuable knowledge, and I have really enjoyed the time spent with all of you.

There have been great undergrads in the lab as well, including Alexandra Velian, Daniel Tofan, Caroline Wei, Pasha Hunt, and Smaranda Marinescu. I expect great things from all of them, and I thoroughly enjoyed my time with each of them.

The staff at Caltech also has been fantastic. Pat Anderson has been exceedingly beneficial and patient. I would also like to thank Cora Carriedo, Joe Drew, and Tom Dunn. All these people have been very helpful, and I have enjoyed interacting with them all.

The number of people that I would like to thank from other groups at Caltech is really overwhelming, but I would like to point out a few that have really helped me out along the way. Brian Stoltz really taught me humility while getting me even more interested in chemistry through his synthesis class. Bruce MacKay and Cora Macbeth of the Peters group were very helpful for my initiation into electrochemistry. I would also like to thank John Carpenter and Jonathon Galownia of the Davis group for helpful advice on a variety of topics related to chemical engineering and heteropoly-acids.

I have had a number of friends in other groups at Caltech, and I would like to thank all of them. I will only point out a few though. Jason Jordan and Ramez Elgammel in particular have been great friends during my time here, and I look forward to seeing them on the east coast. I am grateful to many people from the Grubbs, Gray, Stoltz, and Barton groups, including Raissa Trend, Andrew Waltman, Jenn Stockdill, Jennifer Roizen, Andy Hejl, Pam Sontz, Eric Olmon, Josh Palmer, Jillian Dempsey, Crystal Shih, Melanie Yen, Tim Funk, Greg Drummond, Ted Corcovilos, and many more.

I would especially like to thank Yen Nguyen. I really enjoyed our time together, and she taught me a lot about food. She will forever influence what I consume. Furthermore, I constantly find her to be a source of inspiration. She seems to always follow her heart, and she does not flinch at even the most impressive challenges.

There are many non-Caltech people that I would like to thank as well. I would like to thank Jennifer Grady for her support and friendship. My learning experience at Caltech would not have been complete without her, and she is like a sister to me. I would like to thank Brad and Velika Patterson, as well as the rest of their family. They have provided me with great enjoyment, and they are good friends who have helped me through the worst of times. Thanks also go to my friends Tyler (T-Bone) Lamb and Jessica. I only wish that we could have spent more time together.

My deepest thanks go to Jeff Kistler. If it was not for you, I literally might not be here today. You have helped me through my absolute darkest moments. You have always brought me back to the light, and our conversations have always rejuvenated me. Thank you very much.

I want to thank Gretchen Keller for everything she has done for me the last couple years. I thoroughly enjoy our time together, and she has supported me through probably one of the most difficult years of both of our lives. I have a great deal of respect for her because of her strength and because of the way she treats those around her. She is both a great person and a great friend, and I love her dearly.

I am deeply indebted to my family. They have been fantastic, from my parents and brother to my cousins, aunts, uncles, and grandparents. I could not ask to be raised by a better group of people, and I love you all very much. As mentioned in the dedication, I believe the most important part of a person's development is their family, and you have been amazing. In particular, I would like to point out my Grandma and Grandpa Rich who really deserve a large portion of the credit for this strong family support group. I love my grandparents very much, and I cannot begin to enumerate all the things they have done for me and for the rest of the family. Next, I would like to thank my Aunt Linda and Uncle Paul. I was very luck to have them visiting southern California during some of my darkest moments, and they really helped me out.

Finally, I would like to thank my immediate family: Mom, Dad, and Jason. They have been great, and I love them all dearly. They have really defined who I am as a person, and they have helped me out through the entirety of my education, which I suppose goes back to when I was born. I really have a hard time picking out individual things for each one of them because they have all had such huge impacts on me throughout my life, and they have helped me so very much. I am really impressed by all

the things they have accomplished in their lives and by the way they have treated people through it all. Without them, I would not be me.

## Abstract

Investigations have been performed to determine the requirements for homogeneous platinum- and iridium-catalyzed oxidative alkane functionalization. Previous platinum-catalyzed systems have involved initial C-H bond activation to generate a platinum(II)-alkyl, followed by two-electron oxidation of this species to activate the alkyl towards nucleophilic displacement from the metal center. The factors affecting C-H bond activation by platinum(II) complexes and oxidation of alkylplatinum(II) complexes have been probed, while the possibility of using a diphenolate imidazolyl-carbene ligand to stabilize iridium complexes in a variety of oxidation states has been explored.

Relative oxidation and protonation rates for trichloro(methyl)platinum(II) dianion have been screened under a variety of conditions, using several different oxidants. Both one- and two-electron oxidants were shown to compete effectively with protonation of trichloro(methyl)platinum(II) dianion, including  $\text{CuCl}_2$ ,  $\text{CuBr}_2$ ,  $\text{FeCl}_3$ ,  $\text{Na}_3[\text{H}_3\text{PMo}_9\text{V}_3\text{O}_{40}]$ ,  $\text{Br}_2$ ,  $\text{Na}_2\text{Ir}^{\text{IV}}\text{Cl}_6$ , and  $(\text{NH}_4)_2\text{Ce}^{\text{IV}}(\text{NO}_3)_6$ . Oxidation by copper(II) proved to be highly dependent on the counteranion.

Disodium (2,2'-biindolyl)dimethylplatinum(II) has been synthesized for the purpose of probing the C-H bond activation chemistry of electron rich platinum(II) complexes. This complex decomposes rapidly in air, and deuterolysis of both platinum-methyls as well as the 2,2'-biindolyl ligand occurs when it is dissolved in methanol-d<sub>4</sub>. Methide abstraction from (2,2'-biindolyl)dimethylplatinum(II), either by protonolysis or

by reaction with  $B(C_6F_5)_3$ , generates monomethylplatinum(II) species capable of activating C-H and C-D bonds.

In the search for ligands capable of stabilizing iridium complexes in a variety of oxidation states, the first iridium complexes containing a diphenolate imidazolyl-carbene ligand have been synthesized.  $1,3\text{-Di}(2\text{-hydroxy-5-}tert\text{-butylphenyl})\text{imidazolium chloride}$  was synthesized and then reacted with chloro-1,5-cyclooctadiene iridium(I) dimer to generate potassium  $(1,5\text{-cyclooctadiene})\{1,3\text{-di}(2\text{-hydroxy-5-}tert\text{-butylphenyl})\text{imidazolyl}\}\text{iridium(I)}$ . Oxidation of this complex with two equivalents of ferrocenium(III) hexafluorophosphate generates  $(\text{acetonitrile})(1,5\text{-cyclooctadiene})\{1,3\text{-di}(2\text{-hydroxy-5-}tert\text{-butylphenyl})\text{imidazolyl}\}\text{iridium(III)}$  hexafluorophosphate. Reaction of this complex with dihydrogen generates a species capable of catalyzing olefin hydrogenations. Heating  $(\text{acetonitrile})(1,5\text{-cyclooctadiene})\{1,3\text{-di}(2\text{-hydroxy-5-}tert\text{-butylphenyl})\text{imidazolyl}\}\text{iridium(III)}$  hexafluorophosphate with greater than two equivalents of tricyclohexylphosphine in acetonitrile followed by treatment with tetramethylammonium chloride results in  $(\text{chloro})\text{bis}(\text{tricyclohexylphosphine})\{1,3\text{-di}(2\text{-hydroxy-5-}tert\text{-butylphenyl})\text{imidazolyl}\}\text{iridium(III)}$ . As indicated by cyclic voltammetry and bulk electrolysis, this complex undergoes two reversible one-electron oxidations in methylene chloride at -0.22 V and at 0.58 V.

**Table of Contents**

<b>Dedication</b> .....	iii
<b>Acknowledgements</b> .....	iv
<b>Abstract</b> .....	xiv
<b>Table of Contents</b> .....	xvi
<b>List of Figures</b> .....	xix
<b>List of Schemes</b> .....	xxii
<b>List of Tables</b> .....	xxv
<b>Chapter 1</b> .....	1
Introduction to Oxidative C-H Bond Functionalization with	
Homogeneous Organometallic Catalysts	
References and Notes.....	6
<b>Chapter 2</b> .....	7
Competitive Oxidation and Protonation of Aqueous	
Monomethylplatinum(II) Complexes: A Comparison of Oxidants	
Abstract.....	8
Introduction.....	9
Results and Discussion.....	12
Conclusions.....	22
Experimental Section.....	23
References and Notes.....	30

<b>Chapter 3.....</b>	<b>33</b>
The Synthesis, Protonolysis, and C-H Bond Activation Chemistry of	
Platinum(II) Complexes Containing the Dianionic 2,2'-Biindolyl Ligand	
Abstract.....	34
Introduction.....	35
Results and Discussion.....	39
Conclusions.....	48
Experimental Section.....	49
References and Notes.....	56
<b>Chapter 4.....</b>	<b>59</b>
The Synthesis and Characterization of Iridium Complexes	
Containing a Diphenolate Imidazolyl-Carbene Ligand	
Abstract.....	60
Introduction.....	62
Results and Discussion.....	66
Conclusions.....	101
Experimental Section.....	104
References and Notes.....	125

<b>Appendix 1.....</b>	<b>132</b>
Preliminary Studies on the Synthesis, Oxidation, and Protonation of	
Water-Soluble Methylplatinum(II) Complexes Containing Sulfonated,	
Bidentate Ligands	
Introduction.....	133
Results.....	133
Discussion and Conclusions.....	137
Experimental Section.....	139
References and Notes.....	143
<b>Appendix 2.....</b>	<b>145</b>
Tables for X-ray Crystal Structures	
Structure in Chapter 3.....	146
Structures in Chapter 4.....	153

## List of Figures

### Chapter 2

<b>Figure 2.1.</b> The dependence of $k_{MeH}/k_{MeCl}$ for <b>1</b> on $[H^+]$ ( $[Cu^{2+}] = 0.05\text{ M}$ , $[Cl^-] = 4\text{ M}$ ).....	15
---	----

<b>Figure 2.2.</b> The dependence of $k_{MeCl}/k_{MeH}$ for <b>1</b> on $[Cu^{2+}]$ and on $[Fe^{3+}]$ ( $[H^+] = 2\text{ M}$ , $[Cl^-] = 4\text{ M}$ ).....	15
---	----

### Chapter 3

<b>Figure 3.1.</b> Structural drawing of <b>2</b> with 15-crown-5 ether coordinating to the sodium counterions.....	41
--	----

### Chapter 4

<b>Figure 4.1.</b> Illustration (a) and structural drawings (b) of <b>5a</b> .....	68
--	----

<b>Figure 4.2.</b> The $^1H$ NMR spectrum of <b>6</b> in $THF-d_8$ .....	69
--	----

<b>Figure 4.3.</b> Structural drawing of <b>6</b> with 18-crown-6 ether coordinating to potassium.....	70
---	----

<b>Figure 4.4.</b> A dimer, synthesized and crystallized by Ross Fu, of (1,5-cyclooctadiene)iridium(I) centers each containing a diphenolate pyridine ligand with a sodium countercation.....	72
---	----

<b>Figure 4.5.</b> $^1H$ NMR spectrum of <b>6</b> in methanol- $d_4$ .....	73
--	----

<b>Figure 4.6.</b> Illustration (a) and structural drawings (b) of <b>7</b> .....	76
---	----

<b>Figure 4.7.</b> Illustration (a) and structural drawing (b) of <b>8</b> .....	77
--	----

<b>Figure 4.8.</b> Catalysis of cyclohexene hydrogenation using catalyst precursor <b>9</b> in THF-d <sub>8</sub> under 900 psi of dihydrogen.....	79
<b>Figure 4.9.</b> Structural drawings obtained from the crystals containing an approximately 4:1 mixture of <b>12</b> and <b>15</b> .....	85
<b>Figure 4.10.</b> Structural drawing of the two conformers in the unit cell of <b>16</b> .....	88
<b>Figure 4.11.</b> Cyclic voltammogram of a 3 mM CH <sub>2</sub> Cl <sub>2</sub> solution of <b>16</b> .....	89
<b>Figure 4.12.</b> Cyclic voltammogram of a 0.3 mM DMF solution of <b>2</b> .....	90
<b>Figure 4.13.</b> EPR spectrum at 7 K of the solution resulting from one coulometric oxidation (0.92 faradays per mole) of <b>16</b> .....	91
<b>Figure 4.14.</b> EPR spectrum at 18 K of the resulting solution from two coulometric oxidations (each approximately 1 faraday per mole) of <b>16</b> .....	92
<b>Figure 4.15.</b> Illustration (a) and fully optimized gas-phase structural drawings (b) of <b>17</b> .....	94
<b>Figure 4.16.</b> Illustration (a) and fully optimized gas-phase structural drawings (b) of <b>18</b> .....	95
<b>Figure 4.17.</b> The optimized gas-phase structure of <b>16</b> determined by QMMM calculations.....	97
<b>Figure 4.18.</b> Depiction of the HOMO for the fully optimized gas-phase structure of <b>17</b> .....	98
<b>Figure 4.19.</b> Depiction of the HOMO for the fully optimized gas-phase structure of <b>16</b> determined by QMMM calculations.....	98

<b>Figure 4.20.</b> The relative energies for optimized structures of <b>17</b> when the C <sub>ipso</sub> -O1-O2-C <sub>ipso</sub> torsion angle is set at various angles between 0° and 90°.....	99
<b>Figure 4.21.</b> Depiction of the HOMO for the fully optimized gas-phase structure of <b>18</b> .....	100
<b>Figure 4.22.</b> The relative energies for optimized structures of <b>18</b> when the C <sub>ipso</sub> -O1-O2-C <sub>ipso</sub> torsion angle is set at various angles between -25° and 35°.....	101
<b>Figure 4.23.</b> Coulometric oxidation of <b>16</b> at a potential positive of the first oxidation wave (0.25 V).....	121
<b>Figure 4.24.</b> Second coulometric oxidation of <b>16</b> at a potential positive of the second oxidation wave of <b>16</b> (0.96 V).....	121

**List of Schemes****Chapter 1**

<b>Scheme 1.1.</b> Two possible outer-sphere C-H bond functionalization pathways.....	4
--	---

<b>Scheme 1.2.</b> Inner-sphere C-H bond functionalization.....	5
---	---

**Chapter 2**

<b>Scheme 2.1.</b> The proposed mechanism for the functionalization of alkanes catalyzed by platinum(II/IV) salts.....	9
---	---

<b>Scheme 2.2.</b> The proposed mechanism for oxidation of monomethylplatinum(II) by hexachloroplatinate(IV).....	10
--	----

<b>Scheme 2.3.</b> The <i>in situ</i> generation of <b>1</b> in aqueous solutions with high chloride concentrations at 95 °C.....	13
--	----

<b>Scheme 2.4.</b> Possible pathways for the oxidation of <b>1</b> by CuCl <sub>2</sub> .....	16
---	----

<b>Scheme 2.5.</b> Dissolution of the <b>1</b> , <b>4</b> , and [Pt <sup>II</sup> Cl <sub>4</sub> ] <sup>2-</sup> mixture containing NaCl in a D <sub>2</sub> O solution of [Pt <sup>IV</sup> Cl <sub>6</sub> ] <sup>2-</sup> .....	19
--	----

**Chapter 3**

<b>Scheme 3.1.</b> The oxidation of methane to methyl bisulfate reported by Periana et al. and catalyzed by (bipyrimidine)dichloro- platinum(II) in fuming sulfuric acid.....	36
---	----

<b>Scheme 3.2.</b> The proposed mechanism for bipyrimidineplatinum(II)-catalyzed methane oxidation reported by Periana <i>et al</i> .....	36
<b>Scheme 3.3.</b> Possible platinum(II) C-H bond activation routes.....	38
<b>Scheme 3.4.</b> Deprotonation of 2,2'-biindolyl and generation of <b>2</b> .....	40
<b>Scheme 3.5.</b> Deuterolysis of <b>2</b> in CD <sub>3</sub> OD.....	43
<b>Scheme 3.6.</b> Protonation of <b>2</b> in THF-d <sub>8</sub> with TFE leading to C-D bond activation of THF-d <sub>8</sub> .....	44
<b>Scheme 3.7.</b> The reaction of <b>2</b> with 1 equivalent of TFE-d <sub>3</sub> in CD <sub>3</sub> CN to generate <b>3</b> .....	45
<b>Chapter 4</b>	
<b>Scheme 4.1.</b> A potential catalytic cycle for oxidative iridium-catalyzed C-H bond functionalization.....	63
<b>Scheme 4.2.</b> The oxidative functionalization of <b>1</b> as demonstrated by Periana <i>et al</i> .....	64
<b>Scheme 4.3.</b> Potential binding of <b>2</b> to iridium(III).....	64
<b>Scheme 4.4.</b> The synthesis of titanium and zirconium complexes with a diphenolate imidazolyl-carbene ligand as demonstrated by Kawaguchi <i>et al</i> .....	66
<b>Scheme 4.5.</b> The synthesis of potential ligand precursors, <b>2a</b> and <b>4a</b> .....	67
<b>Scheme 4.6.</b> Metallation of <b>2a</b> to generate <b>6</b> .....	68
<b>Scheme 4.7.</b> Reversible formation of <b>6'</b> in methanol-d <sub>4</sub> .....	74

<b>Scheme 4.8.</b> A possible isomerization of <b>6'</b> in methanol-d <sub>4</sub> that is not observed.....	75
<b>Scheme 4.9.</b> The synthesis of <b>9</b> and <b>10</b> from <b>6</b> .....	78
<b>Scheme 4.10.</b> Displacements of cyclooctadiene from <b>9</b> with trialkylphosphines.....	82
<b>Scheme 4.11.</b> The reaction of <b>12</b> with 1.5 equivalents of trimethylphosphine... <b>83</b>	
<b>Scheme 4.12.</b> Equilibrium between <b>12</b> and <b>15</b> which occurs in acetonitrile at 90 °C under an atmosphere of carbon monoxide.....	84
<b>Scheme 4.13.</b> Reaction of <b>12</b> with tetramethylammonium chloride to generate <b>16</b> .....	87
<b>Appendix 1</b>	
<b>Scheme A1.1.</b> The synthesis of <b>1</b> .....	134
<b>Scheme A1.2.</b> The synthesis of <b>2</b> .....	135
<b>Scheme A1.3.</b> Protonolysis of <b>2</b> to generate isomers <b>3a</b> and <b>3b</b> .....	135
<b>Scheme A1.4.</b> Oxidations of <b>1</b> and <b>2</b> with CuCl <sub>2</sub> .....	137
<b>Scheme A1.5.</b> Oxidation of <b>1</b> with Cu(ClO <sub>4</sub> ) <sub>2</sub> in the presence of triethylamine.....	137

## List of Tables

### Chapter 2

<b>Table 2.1.</b> The $k_{ox}/k_{H^+}$ for a variety of oxidants reacting with	
$[\text{Pt}^{\text{II}}(\text{CH}_3)\text{Cl}_3]^{2-}$ ( <b>1</b> ) at constant $[\text{H}^+]$ .....	14
<b>Table 2.2.</b> The ability of Cu(II) salts to oxidize $[\text{Pt}^{\text{II}}(\text{CH}_3)\text{Cl}_3]^{2-}$ ( <b>1</b> ) to	
$[\text{Pt}^{\text{IV}}(\text{CH}_3)\text{Cl}_5]^{2-}$ ( <b>3</b> ) under different conditions.....	21
<b>Table 2.3.</b> Dependence of $k_{ox}/k_{D^+}$ and $k_{ox}/k_{H^+}$ on $\text{Na}_2[\text{Pt}^{\text{IV}}\text{Cl}_6]$ for <b>1</b> and <b>4</b>	
$([\text{D}_2\text{SO}_4] = 0.35 \text{ M}, [\text{Cl}^-] = 3.0 \text{ M})$ .....	28
<b>Table 2.4.</b> Dependence of $k_{ox}/k_{D^+}$ and $k_{ox}/k_{H^+}$ on $[\text{Cl}^-]$ for <b>1</b> and <b>4</b>	
$(\text{Na}_2[\text{Pt}^{\text{IV}}\text{Cl}_6] = 0.12 \text{ M}, [\text{D}_2\text{SO}_4] = 0.35 \text{ M})$ .....	29
<b>Table 2.5.</b> Dependence of $k_{ox}/k_{D^+}$ and $k_{ox}/k_{H^+}$ on $[\text{Cl}^-]$ for <b>1</b> and <b>4</b>	
$([\text{Cu}^{\text{II}}\text{Cl}_2] = 0.25 \text{ M}, [\text{D}_2\text{SO}_4] = 0.35 \text{ M})$ .....	29

### Chapter 3

<b>Table 3.1.</b> Crystal and refinement data for the structure of <b>2</b> with	
15-crown-5 ether.....	55

### Chapter 4

<b>Table 4.1.</b> Selected bond lengths (Å) and angles (°)	
for <b>16'</b> , <b>16''</b> , <b>17</b> , and <b>18</b> .....	96
<b>Table 4.2.</b> Crystal and refinement data for the structures of <b>5a</b> , <b>6</b> , and <b>7</b> .....	122
<b>Table 4.3.</b> Crystal and refinement data for the structures	
of <b>12/15</b> , and <b>16</b> .....	123

## Appendix 2

<b>Table A2.1.</b> Atomic coordinates ( x 10 <sup>4</sup> ) and equivalent isotropic displacement parameters (Å <sup>2</sup> x 10 <sup>3</sup> ) for <b>2</b> (CCDC 706858).....	147
<b>Table A2.2.</b> Bond lengths [Å] and angles [°] for <b>2</b> (CCDC 706858).....	148
<b>Table A2.3.</b> Anisotropic displacement parameters (Å <sup>2</sup> x 10 <sup>4</sup> ) for <b>2</b> (CCDC 706858).....	151
<b>Table A2.4.</b> Atomic coordinates ( x 10 <sup>4</sup> ) and equivalent isotropic displacement parameters (Å <sup>2</sup> x 10 <sup>3</sup> ) for <b>5a</b> (CCDC 640093).....	153
<b>Table A2.5.</b> Bond lengths [Å] and angles [°] for <b>5a</b> (CCDC 640093).....	156
<b>Table A2.6.</b> Anisotropic displacement parameters (Å <sup>2</sup> x 10 <sup>4</sup> ) for <b>5a</b> (CCDC 640093).....	160
<b>Table A2.7.</b> Atomic coordinates ( x 10 <sup>4</sup> ) and equivalent isotropic displacement parameters (Å <sup>2</sup> x 10 <sup>3</sup> ) for <b>6</b> (CCDC 635046).....	163
<b>Table A2.8.</b> Bond lengths [Å] and angles [°] for <b>6</b> (CCDC 635046).....	165
<b>Table A2.9.</b> Anisotropic displacement parameters (Å <sup>2</sup> x 10 <sup>4</sup> ) for <b>6</b> (CCDC 635046).....	167
<b>Table A2.10.</b> Atomic coordinates ( x 10 <sup>4</sup> ) and equivalent isotropic displacement parameters (Å <sup>2</sup> x 10 <sup>3</sup> ) for <b>7</b> (CCDC 704157).....	170
<b>Table A2.11.</b> Bond lengths [Å] and angles [°] for <b>7</b> (CCDC 704157).....	171
<b>Table A2.12.</b> Anisotropic displacement parameters (Å <sup>2</sup> x 10 <sup>4</sup> ) for <b>7</b> (CCDC 704157).....	174

<b>Table A2.13.</b> Atomic coordinates ( x 10 <sup>4</sup> ) and equivalent isotropic displacement parameters (Å <sup>2</sup> x 10 <sup>3</sup> ) for <b>12/15</b> (CCDC 700172).....	176
<b>Table A2.14.</b> Bond lengths [Å] and angles [°] for <b>12/15</b> (CCDC 700172).....	179
<b>Table A2.15.</b> Anisotropic displacement parameters (Å <sup>2</sup> x 10 <sup>4</sup> ) for <b>12/15</b> (CCDC 700172).....	182
<b>Table A2.16.</b> Atomic coordinates ( x 10 <sup>4</sup> ) and equivalent isotropic displacement parameters (Å <sup>2</sup> x 10 <sup>3</sup> ) for <b>16</b> (CCDC 676694).....	186
<b>Table A2.17.</b> Bond lengths [Å] and angles [°] for <b>16</b> (CCDC 676694).....	190
<b>Table A2.18.</b> Anisotropic displacement parameters (Å <sup>2</sup> x 10 <sup>4</sup> ) for <b>16</b> (CCDC 676694).....	195

## **Chapter 1**

### **Introduction to Oxidative C-H Bond Functionalization with Homogeneous Organometallic Catalysts**

Although the abundance and low cost of alkanes make them valuable chemical feedstocks, they have not been utilized to their full potential due to difficulties associated with their selective functionalization.<sup>1-7</sup> The high homolytic and heterolytic bond strengths of the C-C and C-H bonds composing alkanes make it challenging to achieve efficient conversion of these molecules into more valuable products such as unsaturated hydrocarbons, alcohols, aldehydes, and carboxylic acids.<sup>2,5,7</sup> Currently, alkane conversion in the petrochemical industry is dominated by the use of heterogeneous catalysis;<sup>1</sup> and in general, heterogeneous alkane conversion requires temperatures in excess of 200 °C and is energy intensive.<sup>1,4,5</sup> While oxidative alkane conversion is thermodynamically favorable, heterogeneous catalysts for these processes still require high temperatures.<sup>1,5</sup> The selectivities of these processes are limited by the use of high temperatures and the involvement of an initial homolytic C-H bond cleavage.<sup>5</sup> Since the thermodynamic products of alkane oxidation are carbon dioxide and water, kinetic control of selectivity is required. Unfortunately, the rates of C-H bond homolysis tend to vary inversely with C-H bond strengths, and the products of C-H bond functionalization usually have one or more C-H bonds that are weaker than those in the starting alkane.<sup>5</sup> This puts severe limitations on the amounts of desirable, partially oxidized products that can be accumulated because the products should be more reactive than the starting alkanes.<sup>5</sup>

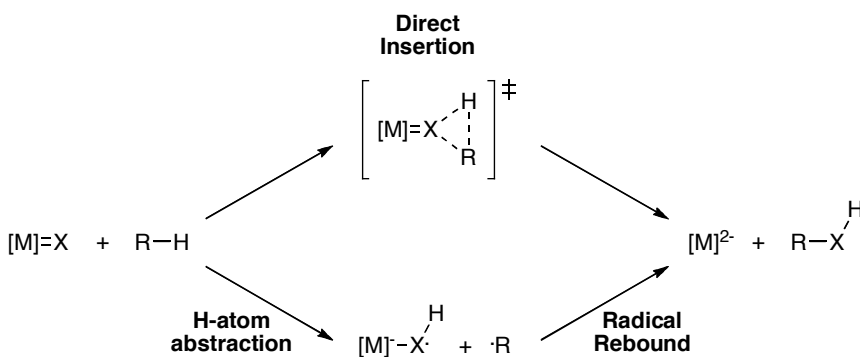
One alternative to heterogeneous alkane functionalization is enzymatic catalysis. A variety of enzymes have been shown to efficiently and selectively catalyze alkane oxidation, and these enzymes operate at physiological temperatures and pressures which are mild compared to the conditions required for heterogeneous alkane conversion.<sup>4,5,8,9</sup>

An additional benefit of enzyme-mediated alkane functionalization is that it involves the use of degradable catalysts and nontoxic cosubstrates.<sup>9</sup> Unfortunately, large-scale catalysis is currently impractical due to low enzymatic activity and stability as well as the demand for expensive electron donors in the form of cofactors.<sup>9</sup>

Homogeneous transition metal catalysis is the other major alternative to heterogeneous catalysis for alkane conversion.<sup>2-7</sup> Relatively low-temperature activation and functionalization of alkane C-H bonds has been demonstrated with homogeneous transition metal complexes, and these complexes offer the advantage over enzymatic systems that their reactivity can often be adjusted simply by ligand modification.<sup>2-7</sup> The selectivities of homogeneous transition metal systems are largely dictated by the pathway involved in the C-H bond breaking, or activation, step.<sup>3,10</sup> Based on how they activate C-H bonds, most transition metal catalysts for alkane functionalization can be divided into two general categories, complexes that react by an outer-sphere, or coordination chemistry, pathway and complexes that react via an inner-sphere, or organometallic pathway.<sup>3,10</sup>

The characteristic feature of outer-sphere C-H bond functionalization is that the metal center does not directly interact with the C-H bond during the activation step.<sup>3,10</sup> Instead, the metal center may catalyze decomposition of the primary oxidant to generate reactive oxidant-derived fragments, typically oxygen-centered radicals, that react with the C-H bond; alternatively, the C-H bond may be cleaved by a reactive ligand bound to the metal center.<sup>3,10</sup> In the latter case, the ligand may directly insert into the C-H bond, or it may simply abstract a hydride or hydrogen atom to generate a reactive alkyl fragment as depicted in scheme 1.1.<sup>3</sup> Outer-sphere C-H bond functionalization typically occurs for

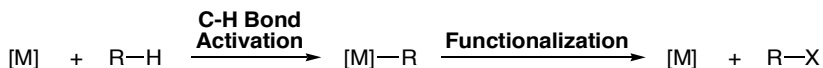
metals in high oxidation states, often with reactive oxo, imido, or carbene ligands.<sup>10</sup> As most of these reactions involve homolytic C-H bond cleavage, the selectivity is typically determined by C-H bond strength.<sup>3,10</sup> Selectivity thus favors the reaction of weaker C-H bonds such as those that are tertiary, benzylic, allylic, or alpha to heteroatoms; and as observed in heterogeneous alkane functionalization systems, overoxidation can be a problem.<sup>3,5,10</sup>



**Scheme 1.1.** Two possible outer-sphere C-H bond functionalization pathways.

Homogeneous inner-sphere C-H bond functionalization involves direct reaction of a C-H bond with the transition metal center to form a metal-alkyl as depicted in scheme 1.2.<sup>3,10</sup> Functionalization then proceeds by reaction of the coordinated alkyl either with a ligand bound to the metal center or with an external reagent.<sup>3,10</sup> In contrast to outer-sphere pathways, inner-sphere pathways are favored by diamagnetic complexes that perform two-electron chemistry, avoiding one-electron changes in oxidation state and radical pathways.<sup>3</sup> The selectivity is typically related to the propensity of the metal center to bind a particular C-H bond, and it is often significantly different from the selectivity observed for outer-sphere reactions.<sup>3,10</sup> Regioselective alkane functionalization via inner-sphere C-H bond activation often occurs at the stronger,

terminal C-H bonds due to steric factors, and favorable chemoselectivities have been observed for some of these systems; however, many factors can affect selectivity, including the ligand environment at the metal center and the specific mechanism of the C-H bond cleavage step.<sup>2-7,10</sup> Inner-sphere, homogeneous transition metal catalyzed C-H bond functionalization is thus promising due to the mild conditions under which it can be achieved and due to the potential for controlling regio- and chemo-selectivity via subtle system modifications. This thesis focuses on determining the requirements for selective, homogeneous, inner-sphere C-H bond functionalization using complexes of platinum and iridium.



**Scheme 1.2.** Inner-sphere C-H bond functionalization.

## References and Notes

---

<sup>1</sup> Olah, G. A.; Molnár, Á. *Hydrocarbon Chemistry*, 2<sup>nd</sup> ed.; Wiley & Sons: New Jersey, 2003.

<sup>2</sup> Shilov, A. E.; Shul'pin, G. B. *Activation and Catalytic Reactions of Saturated Hydrocarbons in the Presence of Metal Complexes*; Kluwer, Academic Publishers: Dordrecht, 2000.

<sup>3</sup> Crabtree, R. H. *J. Chem. Soc., Dalton Trans.* **2001**, 2437-2450.

<sup>4</sup> Labinger, J. A.; Bercaw, J. E. *Nature* **2002**, 417, 507-514.

<sup>5</sup> Labinger, J. A. *J. Mol. Catal. A: Chemical* **2004**, 220, 27-35.

<sup>6</sup> Periana, R. A.; Bhalla, G.; Tenn, W. J., III; Young, K. J. H.; Liu, X. Y.; Mironov, O.; Jones, C. J.; Ziatdinov, V. R. *J. Mol. Catal. A: Chemical* **2004**, 220, 7-25.

<sup>7</sup> Lersch, M.; Tilset, M. *Chem. Rev.* **2005**, 105, 2471-2526.

<sup>8</sup> van Beilen, J. B.; Funhoff, E. G. *Curr. Opin. Biotech.* **2005**, 16, 308-314.

<sup>9</sup> Ayala, M.; Torres, E. *Appl. Catal., A: General* **2004**, 28, 1-13.

<sup>10</sup> Dick, A. R.; Sanford, M. S. *Tetrahedron* **2006**, 62, 2439-2463.

## Chapter 2

### **Competitive Oxidation and Protonation of Aqueous Monomethylplatinum(II) Complexes: A Comparison of Oxidants**

*This chapter was reproduced in part with permission from Weinberg, D. R.; Labinger, J. A.; Bercaw, J. E. *Organometallics* 2007, 26, 167-172.*

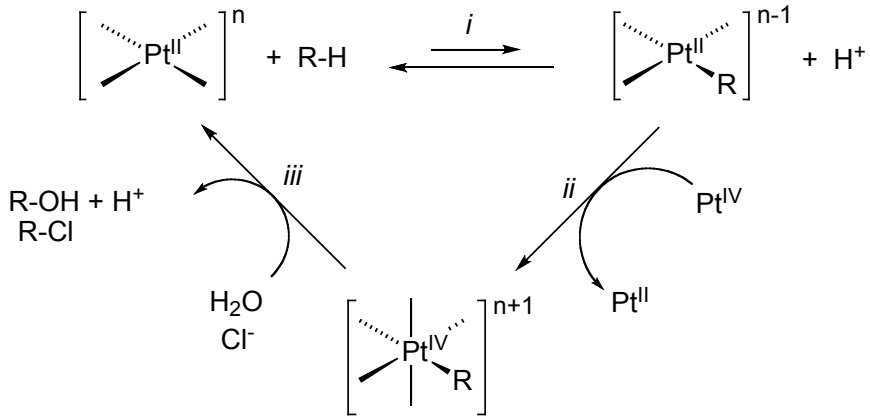
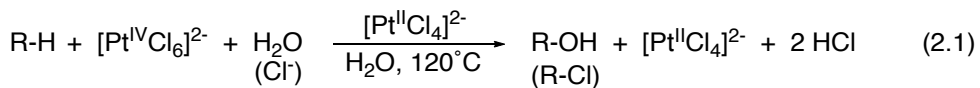
Copyright 2007 American Chemical Society.

## Abstract

$[\text{Pt}^{\text{II}}(\text{CH}_3)\text{Cl}_3]^{2-}$  (**1**), generated at 95 °C *in situ* from  $\text{Cs}_2[\text{Pt}^{\text{IV}}(\text{CH}_3)_2\text{Cl}_4]$  in an aqueous solution of high chloride concentration and  $[\text{H}^+] = 0.2\text{ M}$ , undergoes competitive oxidation vs. protonation ( $k_{\text{ox}}/k_{\text{H}^+}$ ) with several oxidants. A first-order dependence on oxidant concentration was determined for both  $\text{CuCl}_2$  and  $\text{FeCl}_3$  oxidations of **1**, and  $k_{\text{ox}}/k_{\text{H}^+}$  was determined to be  $191 \pm 24$  and  $14 \pm 3$ .  $\text{CuCl}_2$  was shown to catalyze the oxidation of **1** by dioxygen; however,  $[\text{Pt}^{\text{II}}\text{Cl}_4]^{2-}$  was also oxidized under these conditions. Anion **1**, generated in a mixture of platinum(II) salts,  $[\text{Cp}_2\text{Co}^{\text{III}}]_2\{[\text{Pt}^{\text{II}}\text{Cl}_4] + \mathbf{1} + [\text{Pt}^{\text{II}}(\text{CH}_3)_2\text{Cl}_2]\}$  (**4**) ·  $x\text{ NaCl}$  (**5**), also undergoes competitive oxidation and protonation at room temperature in  $\text{D}_2\text{O}$  when in the presence of oxidants. Increasing chloride decreases the ratio  $k_{\text{ox}}/k_{\text{H}^+}$  for **1** when  $\text{Na}_2[\text{Pt}^{\text{IV}}\text{Cl}_6]$  is used as the oxidant, but when  $\text{CuCl}_2$  is used as the oxidant, added chloride increases  $k_{\text{ox}}/k_{\text{H}^+}$ . The one-electron oxidants,  $\text{Na}_2[\text{Ir}^{\text{IV}}\text{Cl}_6]$  and  $(\text{NH}_4)_2[\text{Ce}^{\text{IV}}(\text{NO}_3)_6]$ , were also shown to oxidize **1**.

## Introduction

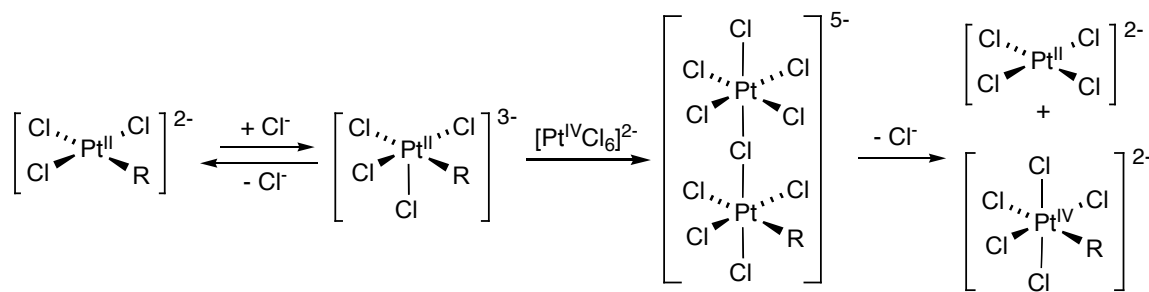
About 35 years ago Shilov et al. reported that the homogeneous oxidation of alkanes by an aqueous mixture of platinum(II) and platinum(IV) salts at 120 °C gives the corresponding alcohols or alkyl chlorides with moderate selectivity (eq 2.1).<sup>1</sup> Mechanistic studies indicate that the catalysis occurs by an inner-sphere pathway, and it involves three major steps as shown in scheme 2.1: (i) Pt(II) activates an alkane C-H bond to generate a Pt(II) alkyl; (ii) the Pt(II) alkyl is oxidized by hexachloroplatinate(IV) to a Pt(IV) alkyl; (iii) nucleophilic attack by water or chloride on the Pt(IV) alkyl affords the alcohol or alkyl chloride, respectively, and regenerates Pt(II).<sup>2</sup>



**Scheme 2.1.** The proposed mechanism for the functionalization of alkanes catalyzed by platinum(II/IV) salts.<sup>2</sup>

While the C-H activation step (i) is rate and selectivity limiting in the catalysis, the oxidation step (ii) provides the thermodynamic driving force for the reaction.

Furthermore, since step (i) is highly reversible, oxidation of  $[\text{Pt}^{\text{II}}\text{-R}]$  by  $[\text{Pt}^{\text{IV}}\text{Cl}_6]^{2-}$  must be remarkably fast in order to compete with protonolysis. Studies on model complexes indicate that the oxidation step proceeds via a chloride bridged intermediate, as shown in scheme 2.2,<sup>3</sup> a common mechanism for Pt(II)-Pt(IV) redox reactions.<sup>4</sup> Isotopic labeling experiments have placed an upper limit on the rate of the self-exchange reaction between tetrachloroplatinate(II) and hexachloroplatinate(IV)<sup>5</sup> that would be much too slow to compete with protonolysis. Nonetheless, two studies have demonstrated that the rate constant for oxidation of  $[\text{Pt}^{\text{II}}\text{-CH}_3]$  is comparable to (at room temperature)<sup>6</sup> or much faster than (at 95 °C)<sup>7</sup> the competing protonolysis. The reasons for this great enhancement of reactivity are not entirely clear; possible factors include the lower oxidation potential of methylated Pt(II) complexes and/or the lower energy required for formation of the five-coordinate species as a consequence of the greater *cis* and *trans* effects of a methyl ligand.<sup>8</sup>



**Scheme 2.2.** The proposed mechanism for oxidation of monomethylplatinum(II) by hexachloroplatinate(IV).<sup>3</sup>

A major practical limitation of the Shilov oxidation of alkanes is the use of  $[\text{Pt}^{\text{IV}}\text{Cl}_6]^{2-}$  as a stoichiometric oxidant. Labeling studies indicate that this step occurs by

electron transfer, not alkyl transfer, to Pt(IV); hence in principle it should be possible to substitute an inexpensive stoichiometric oxidant.<sup>2e</sup> There are strict constraints on suitable alternative oxidants, though: they must be fast enough to oxidize  $[\text{Pt}^{\text{II}}\text{-R}]$  competitively with protonolysis, but must not rapidly oxidize inorganic Pt(II), *i.e.*  $[\text{Pt}^{\text{II}}\text{Cl}_n(\text{H}_2\text{O})_{4-n}]^{2-n}$ , since that would deplete the species responsible for alkane activation. (Note that all inorganic ligands have been represented as chloride in schemes and structural formulae for simplicity; the species actually present will generally be a mixture of chloro/aquo complexes whose composition will vary with conditions.)

A variety of alternative oxidants, including chlorine,<sup>9</sup> hydrogen peroxide,<sup>10</sup> peroxydisulfate,<sup>11</sup> and the anode of an electrochemical cell,<sup>12</sup> have been used with limited success. The most interesting examples are Wacker-like systems that use catalytic amounts of an oxidant that can in turn be reoxidized by dioxygen, making the latter the stoichiometric oxidant; significant numbers of turnovers have been achieved with both  $\text{Cu}^{\text{II}}\text{Cl}_2$ <sup>13</sup> and a polyoxometalate.<sup>14</sup> All of the above still fall far short of what would be required for practical application, due in large part to catalyst inactivation, usually by deposition of metallic platinum. A bipyrimidine platinum(II) complex has been found to catalyze oxidation of methane to methyl bisulfate in high yield, using sulfuric acid as the oxidant and solvent;<sup>15</sup> while it does not suffer from catalyst inactivation by deposition of metallic platinum, it still falls short of a practical process.<sup>16</sup>

A systematic approach toward replacing Pt(IV) with a more practical oxidant would be facilitated if we better understood how various oxidants function in the actual oxidation step; such information is difficult to glean from overall performance of a complex catalytic system. While, as noted above, the presumed Pt(II) alkyl that

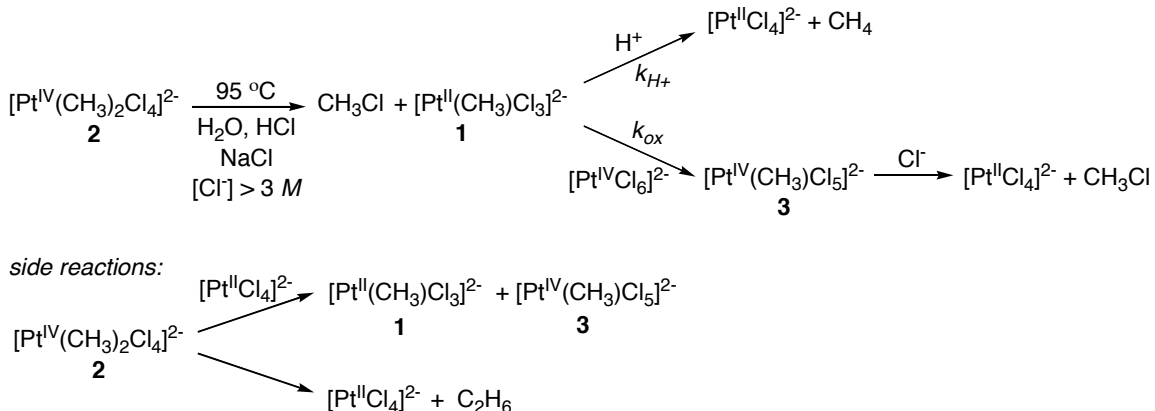
undergoes oxidation in the Shilov system is highly unstable to protonolysis, methods<sup>6,7</sup> that were developed for generating this species *in situ* and assessing its reactivity towards  $[\text{Pt}^{\text{IV}}\text{Cl}_6]^{2-}$  may be readily extended to other oxidants. We report here the results of these studies.

## Results and Discussion

### Competitive oxidation and protonation at elevated temperature:

**Cu-mediated oxidation by O<sub>2</sub>.** Zamashchikov and co-workers determined the relative rates of protonolysis and oxidation of  $[\text{Pt}^{\text{II}}(\text{CH}_3)\text{Cl}_3]^{2-}$  (**1**) by means of the system shown in scheme 2.3.<sup>7</sup> Here nucleophilic attack of chloride on the *dimethyl* complex  $[\text{Pt}^{\text{IV}}(\text{CH}_3)_2\text{Cl}_4]^{2-}$  (**2**) generates **1** (along with an equivalent of methyl chloride), which is competitively protonated to generate methane and  $[\text{Pt}^{\text{II}}\text{Cl}_4]^{2-}$ , and oxidized by  $[\text{Pt}^{\text{IV}}\text{Cl}_6]^{2-}$  to monomethyl  $[\text{Pt}^{\text{IV}}(\text{CH}_3)\text{Cl}_5]^{2-}$  (**3**). Complex **3** is unstable under the reaction conditions, undergoing nucleophilic attack by chloride (step (*iii*) of the overall Shilov mechanism) to generate an additional equivalent of  $\text{CH}_3\text{Cl}$  and  $[\text{Pt}^{\text{II}}\text{Cl}_4]^{2-}$ .

As shown in scheme 2.3, there are two side reactions. Nucleophilic attack by  $[\text{Pt}^{\text{II}}\text{Cl}_4]^{2-}$  on **2** generates **1** and **3**; however, this has no net effect on the final product distribution. Also, some ethane is reductively eliminated from **2**, but this is sufficiently slow relative to nucleophilic attack that only a very small amount of ethane (<5%) is generated. Hence the ratio of second-order rate constants for oxidation and protonation ( $k_{\text{ox}}/k_{\text{H}^+}$ ) could be determined from the relative yields of products along with the stoichiometry of reagents used, and was found to be  $18.4 \pm 0.5$ .



**Scheme 2.3.** The *in situ* generation of **1** in aqueous solutions with high chloride concentrations at 95 °C.<sup>7</sup>

In our hands, heating an aqueous solution of  $\text{Cs}_2[\text{Pt}^{\text{IV}}(\text{CH}_3)_2\text{Cl}_4]$  (0.002 M) containing greater than 3 M chloride concentration at 95 °C for nine days resulted in complete disappearance of  $[\text{Pt}^{\text{IV}}(\text{CH}_3)_2\text{Cl}_4]^{2-}$  and generation of one equivalent of methane, as determined by GC-MS. Under these reaction conditions  $\text{CH}_3\text{Cl}$  substantially decomposes (to  $\text{CH}_3\text{OH}$ ) and cannot be accurately quantified; nonetheless the extent of competing oxidation (when an oxidant is present) can be calculated from the reduction in methane yield. Assuming the reaction is first-order in both oxidant and **1**, as is the case for  $\text{Na}_2[\text{Pt}^{\text{IV}}\text{Cl}_6]$ , the ratios of the “observed” rate constants for formation of  $\text{CH}_3\text{Cl}$  vs. methane ( $k_{\text{MeCl}}/k_{\text{MeH}}$ ) and the second-order rate constants for oxidation vs. protonation ( $k_{\text{ox}}/k_{\text{H}^+}$ ) are found using equations (2) and (3), respectively, where  $n$  is the number of moles of the corresponding species.<sup>7</sup>

$$\frac{k_{\text{MeCl}}}{k_{\text{MeH}}} = \frac{2n_{\text{Cs}_2\text{Pt}^{\text{IV}}(\text{CH}_3)_2\text{Cl}_4} - n_{\text{EtH}} - n_{\text{MeH}}}{n_{\text{MeH}}} \quad (2)$$

$$\frac{k_{Ox.}}{k_{H^+}} = \frac{1}{2} \left( \frac{k_{MeCl}}{k_{MeH}} - 1 \right) \frac{[H^+]}{[Ox.]} \quad (3)$$

The results for several different oxidants are shown in table 2.1; that for  $\text{Na}_2[\text{Pt}^{\text{IV}}\text{Cl}_6]$ ,  $20 \pm 4$ , is within experimental error of the previously reported value. As noted above, the calculation assumes first-order dependence on reagent concentration. Protonolysis was shown to be first-order in  $[\text{H}^+]$  (for  $\text{CuCl}_2$  as oxidant), as shown in figure 2.1, while oxidation was shown to be first-order in oxidant for both  $\text{CuCl}_2$  and  $\text{FeCl}_3$ , as shown in figure 2.2.

**Table 2.1.** The  $k_{ox.}/k_{H^+}$  for a variety of oxidants reacting with  $[\text{Pt}^{\text{II}}(\text{CH}_3)\text{Cl}_3]^{2-}$  (**1**) at constant  $[\text{H}^+]$ . Except as noted,  $[\text{Cs}_2\text{Pt}^{\text{IV}}(\text{CH}_3)_2\text{Cl}_4] = 0.002 \text{ M}$ ;  $[\text{H}^+] = 0.2 \text{ M}$ ; [oxidant] =  $0.02 \text{ M}$ ;  $[\text{Cl}^-] = 4 \text{ M}$ . <sup>a</sup> $[\text{Cu}^{\text{II}}\text{Cl}_2] = 0.001 \text{ M}$ , under excess  $\text{O}_2$  (1 atm). <sup>b</sup> $[\text{Cl}^-] = 3 \text{ M}$ .

entry	Oxidant	$k_{Ox.}/k_{H^+}$
1	$\text{Na}_2\text{Pt}^{\text{IV}}\text{Cl}_6$	$20 \pm 4$
2	$\text{Cu}^{\text{II}}\text{Cl}_2$	$191 \pm 24$
3	$\text{O}_2/\text{Cu}^{\text{II}}\text{Cl}_2$ <sup>a</sup>	$173 \pm 35$
4	$\text{Fe}^{\text{III}}\text{Cl}_3$	$14 \pm 3$
5	$\text{Na}_3[\text{H}_3\text{PMo}_9\text{V}_3\text{O}_{40}]$ <sup>b</sup>	$15 \pm 3$
6	$\text{Br}_2$ <sup>b</sup>	$210 \pm 40$

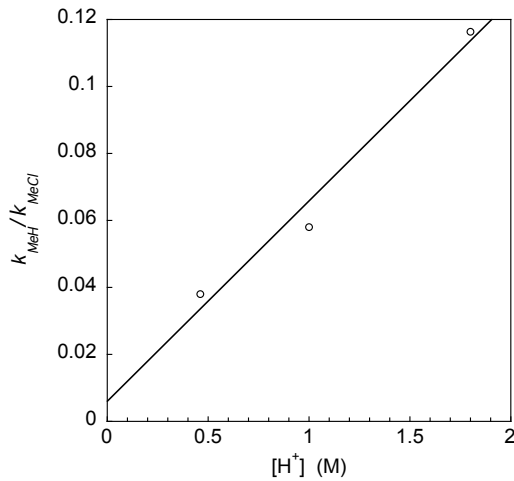


**Figure 2.1.** The dependence of  $k_{MeH}/k_{MeCl}$  for **1** on  $[H^+]$  ( $[Cu^{2+}] = 0.05\text{ M}$ ,  $[Cl^-] = 4\text{ M}$ ).

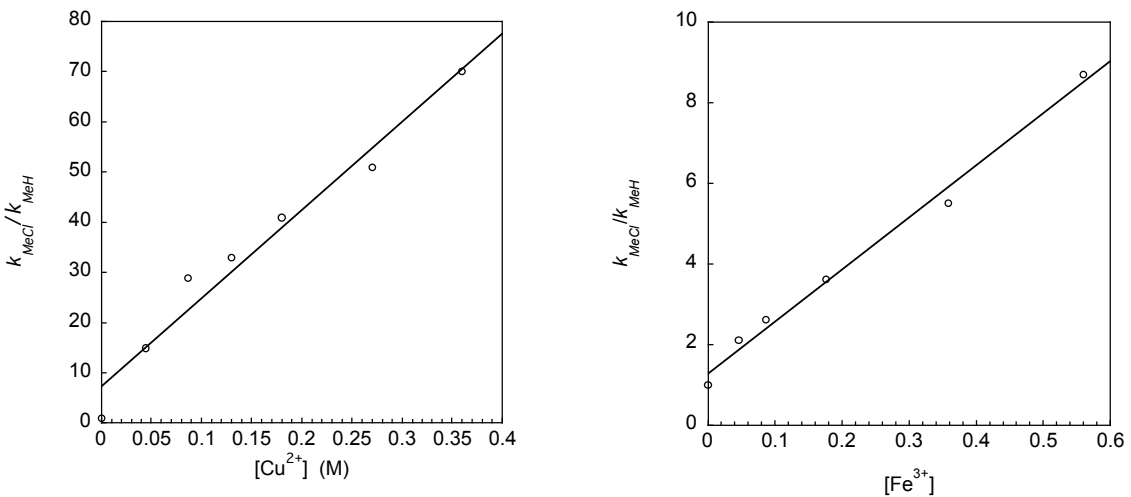
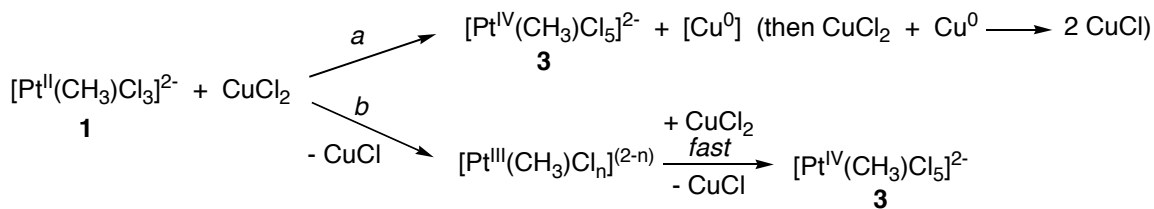


**Figure 2.2.** The dependence of  $k_{MeCl}/k_{MeH}$  for **1** on  $[Cu^{2+}]$  (left) and  $[Fe^{3+}]$  (right) ( $[H^+] = 2\text{ M}$ ,  $[Cl^-] = 4\text{ M}$ ).

The rapid oxidation by  $CuCl_2$  is particularly striking. Oxidation of platinum(II) complexes by copper(II) halides could in principle proceed via either one- or two-electron mechanisms, as shown in scheme 2.4. In (a) an initial two-electron

oxidation is followed by comproportionation of copper(0) and copper(II), while in (b) initial (rate-determining) one-electron oxidation generates  $[\text{Pt}^{\text{III}}(\text{CH}_3)]$ , which undergoes fast one-electron oxidation by a second Cu(II). The first-order dependence on  $[\text{Cu}(\text{II})]$  could be consistent with either of these possibilities. For the all-inorganic analog, for which the thermodynamics lie in the opposite direction ( $[\text{PtCl}_6]^{2-}$  oxidizes Cu(I)), a one-electron route was proposed based on kinetics;<sup>17</sup> but in fact, the kinetics could be consistent with the two-electron path as well. In a later study on oxidation of (N,C)-ligated Pt(II) complexes by  $\text{CuX}_2$  the authors also preferred alternative (b), though not decisively so.<sup>18</sup>



**Scheme 2.4.** Possible pathways for the oxidation of **1** by  $\text{CuCl}_2$ .

The three oxidants  $\text{Cu}^{\text{II}}$ ,  $\text{Fe}^{\text{III}}$ , and  $\text{Na}_3[\text{H}_3\text{PMo}_9\text{V}_3\text{O}_{40}]$  are all capable of reoxidation by  $\text{O}_2$  under certain conditions. (Bromine, the most reactive oxidant, would not be useful in a catalytic system because it is known to oxidize  $[\text{Pt}^{\text{II}}\text{Cl}_4]^{2-}$ .<sup>19</sup>) As noted above, efficient catalytic oxidation of substrates such as ethanesulfonic acid has been achieved with a Pt/Cu/ $\text{O}_2$  system; in that case catalyst deactivation apparently does *not* involve Pt metal deposition.<sup>13</sup> That finding implies that (as in the Wacker process) reoxidation of  $\text{Cu}^{\text{I}}$  by  $\text{O}_2$  is fast relative to other steps. Indeed, when **1** is generated from

$[\text{Pt}^{\text{IV}}(\text{CH}_3)_2\text{Cl}_4]^{2-}$  (**2**) under an atmosphere of dioxygen in the presence of only half an equivalent of  $\text{CuCl}_2$ , the same rate constant ratio is observed (within experimental error) as with excess  $\text{CuCl}_2$  (entry 3, table 2.1). A similar result could not be obtained with  $\text{FeCl}_3$ , as  $k_{\text{ox}}/k_{\text{H}^+}$  varied from run to run when only half an equivalent of  $\text{FeCl}_3$  was used under an atmosphere of dioxygen.

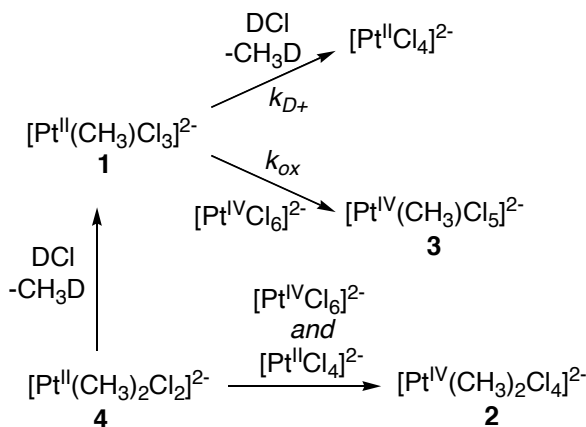
As for the polyoxometalate ( $\text{Na}_3[\text{H}_3\text{PMo}_9\text{V}_3\text{O}_{40}]$ ), it is known to be reoxidizable by dioxygen; however, it is also difficult to obtain as a pure trivanadium species;<sup>20</sup> furthermore, it proved to be partially insoluble under our reaction conditions, so it was not tested in the presence of dioxygen. It is encouraging though that stoichiometric oxidation of **1** could be observed, at a rate close to that of  $[\text{Pt}^{\text{IV}}\text{Cl}_6]^{2-}$  (table 2.1).

One likely mode of catalyst inactivation with the  $\text{CuCl}_2/\text{O}_2$  system is suggested by the observation that  $\text{Cs}_2[\text{Pt}^{\text{IV}}\text{Cl}_6]$  crystallizes out of solution during the course of this reaction, indicating oxidation of  $[\text{Pt}^{\text{II}}\text{Cl}_4]^{2-}$ . That would not be effected by either  $\text{CuCl}_2$  (the reverse reaction takes place: see above) or  $\text{O}_2$  alone. Presumably, peroxidic species (possibly free peroxide or some sort of copper-peroxide complex) formed during the reoxidation of copper(I) with dioxygen<sup>21</sup> are responsible. Because in the accepted mechanism  $[\text{Pt}^{\text{II}}\text{Cl}_4]^{2-}$  is required for C-H activation, such a process would gradually remove a crucial component of the system and shut down the catalytic reaction.

**Competitive oxidation and protonation at room temperature: chloride effects.** The above probe generates the key intermediate  $[\text{Pt}^{\text{II}}(\text{CH}_3)\text{Cl}_3]^{2-}$  (**1**) by reaction of  $[\text{Pt}^{\text{IV}}(\text{CH}_3)_2\text{Cl}_4]^{2-}$  (**2**) with chloride, and hence requires high  $[\text{Cl}^-]$ . This may be problematic in several regards. First, since excess chloride inhibits the C-H activation

step in the Shilov system,<sup>1</sup> the chloride level for this experiment differs significantly from that of the “real” reaction, potentially affecting the platinum speciation in solution. Second, the rate at which **1** is oxidized is likely to be  $[Cl^-]$ -dependent in the mechanism of scheme 2.2. Finally, the chloride concentration affects the oxidation potential of a variety of oxidants,<sup>22</sup> including some of those examined here.

We have previously reported an alternate route to transient **1** that does not require excess  $Cl^-$ . Reduction of  $Na_2[Pt^{IV}(CH_3)Cl_5]$  with cobaltocene in tetrahydrofuran (THF) precipitates a mixture of cobaltocenium salts of  $[Pt^{II}(CH_3)Cl_3]^{2-}$  (**1**),  $[Pt^{II}(CH_3)_2Cl_2]^{2-}$  (**4**), and  $[Pt^{II}Cl_4]^{2-}$  (along with some  $NaCl$ ), which upon addition to a solution of  $Na_2[Pt^{IV}Cl_6]$  in  $D_2O$  exhibits competitive protonolysis and oxidation of **1**; the relative rates can be determined from the yield of  $[Pt^{IV}(CH_3)Cl_5]^{2-}$  (**3**) (scheme 2.5). In that earlier study, carried out under a limited range of acid and oxidant concentrations, it appeared that **4** was completely oxidized to  $[Pt^{IV}(CH_3)_2Cl_4]^{2-}$  (**2**) (which is stable under the reaction conditions), even at low levels of  $[Pt^{IV}Cl_6]^{2-}$ , indicating that  $[Pt^{II}Cl_4]^{2-}$  is also capable of effecting oxidation of **4**, presumably with formation of  $Pt^0$ . The rate constant ratio for oxidation vs. deuterolysis ( $k_{ox}/k_{D+}$ ) at 22 °C was estimated at approximately 2.55; using an independent determination of the isotope effect ( $k_{H+}/k_{D+} \approx 9$ )<sup>23</sup> gave  $k_{ox}/k_{H+} \approx 0.3$ , around two orders of magnitude lower than at 95 °C.<sup>6</sup>



**Scheme 2.5.** Dissolution of the **1**, **4**, and  $[\text{Pt}^{\text{II}}\text{Cl}_4]^{2-}$  mixture containing  $\text{NaCl}$  in a  $\text{D}_2\text{O}$  solution of  $[\text{Pt}^{\text{IV}}\text{Cl}_6]^{2-}$ .

On repeating those experiments, we find the results are not quite so straightforward as previously reported. In the first place, deuterolysis is competitive with oxidation for *both* **1** and **4** as shown in scheme 2.5: increasing the amount of acid (by adding  $\text{D}_2\text{SO}_4$ ) results in a reduction of the yields of both **2** and **3**. Since **2** was used as an internal standard for NMR quantitation, the assumption that its yield was invariant introduced some error. Secondly, the yields are not as reproducible as suggested by the earlier limited study. This is not too surprising because of the way the experiment is (necessarily) performed: the solid mixture of Pt(II) salts is dissolved directly in the solution with which it reacts, probably causing the local concentrations of reagents to change drastically and irreproducibly as the solid dissolves. From an extensive series of experiments measuring the amounts of **2** and **3** generated, rate constant ratios for oxidation vs. deuterolysis ( $k_{\text{ox}}/k_{\text{D}+}$ ) at  $22\text{ }^{\circ}\text{C}$  were determined to be  $7.7 \pm 0.9$  for **1** and  $14 \pm 2$  for **4**. This translates into a  $k_{\text{ox}}/k_{\text{H}+}$  of about 0.9 for **1**. (Tabular results for the specific experiments are provided in the Experimental Section.)

The difference between the two findings suggest that the  $k_{ox}/k_{H+}$  value determined by this method is only accurate to within a factor of three or so, but it is clearly significantly lower than that obtained at 95 °C with high chloride concentrations. Previously, this was attributed to the large temperature difference between the two studies; however, the large difference in chloride concentration between the two studies could also affect  $k_{ox}/k_{H+}$ , if the kinetic order in chloride for oxidation and protonation differ. Under the same conditions but with 3.0 M added chloride,  $k_{ox}/k_{D+}$  was determined to be  $3.5 \pm 0.4$  for **1** and  $5.0 \pm 0.9$  for **4**. Thus there is a chloride dependence on the ratio, with  $k_{ox}/k_{H+}$  for **1** about 0.4 under high chloride (vis-à-vis 0.9 at low chloride concentration) at 22 °C.

An analogous determination of  $k_{ox}/k_{H+}$  and its dependence on chloride concentration for CuCl<sub>2</sub> is complicated by the effect of paramagnetic copper(II), which makes it difficult to integrate <sup>1</sup>H NMR peaks in the spectrum; hence only qualitative results can be obtained (table 2.2). It is clear that some additional halide (there is always a small amount of chloride present in these experiments, as the precipitated mixed cobaltocenium/Pt(II) salts contain some NaCl) is needed for the oxidation even in the absence of added acid, and quite high [Cl<sup>-</sup>] is needed to compete at low pH. This requirement for relatively high chloride concentration could be due to the role of bridging halide, if an inner-sphere oxidation mechanism (schemes 2.2 and 2.4a) is followed. It is also well known that Cu(II) is a stronger oxidant at higher halide concentrations, and further that one-electron oxidations are favored in the presence of chloride or bromide.<sup>24</sup> Substantial oxidation of [Pt<sup>II</sup>(CH<sub>3</sub>)<sub>2</sub>Cl<sub>2</sub>]<sup>2-</sup> (**4**) to [Pt<sup>IV</sup>(CH<sub>3</sub>)<sub>2</sub>Cl<sub>4</sub>]<sup>2-</sup> (**2**) was observed in all

these experiments, confirming that it is more facile than that of  $[\text{Pt}^{\text{II}}(\text{CH}_3)\text{Cl}_3]^{2-}$  (**1**) to  $[\text{Pt}^{\text{IV}}(\text{CH}_3)\text{Cl}_5]^{2-}$  (**3**).

**Table 2.2.** The ability of Cu(II) salts to oxidize  $[\text{Pt}^{\text{II}}(\text{CH}_3)\text{Cl}_3]^{2-}$  (**1**) to  $[\text{Pt}^{\text{IV}}(\text{CH}_3)\text{Cl}_5]^{2-}$  (**3**) under different conditions.  $[\text{Cs}_2\text{Pt}^{\text{IV}}(\text{CH}_3)_2\text{Cl}_4] = 0.002 \text{ M}$ ;  $[\text{Cu}^{\text{II}}] = 0.24 \text{ M}$ . <sup>a</sup>X = perchlorate, triflate, acetate, sulfate.

entry	oxidant	added $\text{Cl}^-$	added $\text{H}^+$	<b>3</b> formed (>35%)
1	$\text{Cu}^{\text{II}}\text{Cl}_2$	—	—	Yes
2	$\text{Cu}^{\text{II}}\text{Cl}_2$	—	$0.35 \text{ N D}_2\text{SO}_4$	No
3	$\text{Cu}^{\text{II}}\text{Cl}_2$	$3 \text{ M}$	$0.35 \text{ N D}_2\text{SO}_4$	Yes
4	$\text{Cu}^{\text{II}}\text{Br}_2$	—	—	Yes
5	$\text{Cu}^{\text{II}}\text{X}_2$ <sup>a</sup>	—	—	No

To test the possibility of a one-electron pathway (such as that depicted in scheme 2.4b) for oxidation of  $[\text{Pt}^{\text{II}}(\text{CH}_3)\text{Cl}_3]^{2-}$  (**1**),  $\text{Na}_2[\text{Ir}^{\text{IV}}\text{Cl}_6]$  and  $(\text{NH}_4)_2[\text{Ce}^{\text{IV}}(\text{NO}_3)_6]$  were examined. These are known one-electron oxidants, which could not be tested by the high temperature route ( $\text{Na}_2[\text{IrCl}_6]$  because it directly oxidizes methane;<sup>25</sup> Ce(IV) because at high chloride concentrations it oxidizes chloride<sup>22</sup>). Indeed, addition of the mixed Pt(II) salts to a  $\text{D}_2\text{O}$  solution containing an excess of either  $\text{Na}_2[\text{IrCl}_6]$  or  $(\text{NH}_4)_2[\text{Ce}(\text{NO}_3)_6]$

resulted in significant oxidation of both **1** and  $[\text{Pt}^{\text{II}}(\text{CH}_3)_2\text{Cl}_2]^{2-}$  (**4**), indicating that a one-electron oxidation pathway can be rapid for these oxidants—and, by extension, may be plausible for Cu(II) and Fe(III) as well. Finally,  $\text{Na}_3[\text{H}_3\text{PMo}_9\text{V}_3\text{O}_{40}]$ , bromine and hydrogen peroxide also were shown to oxidize **1** (and **4**) in  $\text{D}_2\text{O}$  at room temperature in the absence of added chloride.

## Conclusions

The competitive oxidation and protonation of the monomethylplatinum(II) salt (**1**) involved in the Shilov system was studied in order to gain insight into the possibility of using an inexpensive stoichiometric oxidant for the replacement of  $\text{Na}_2[\text{Pt}^{\text{IV}}\text{Cl}_6]$ . When  $\text{Na}_2[\text{Pt}^{\text{IV}}\text{Cl}_6]$  is used as the oxidant, chloride has been shown to decrease the ratio of oxidation to protonation of **1**, while high temperatures have been shown to increase the ratio of oxidation to protonation. This implies that oxidation has a considerably higher activation energy than does protonolysis. The chloride dependence of  $k_{\text{ox}}/k_{\text{H}^+}$  is modest, and may represent either inhibition of oxidation or acceleration of protonolysis (or both) by chloride. From the mechanism of scheme 2.2, oxidation is expected to be accelerated by chloride, but this could be balanced by a similar effect on protonolysis.<sup>26</sup> Shifting the speciation equilibrium could then favor more highly chlorinated species that are harder to oxidize. In any case, the conditions of the “real” Shilov system (low chloride concentrations, temperatures of about 120 °C) highly favor oxidation by Pt(IV) over protonation, and any alternative oxidant must also compete quite efficiently with protonation.

Ideally, the Shilov oxidation of alkanes would be performed under an atmosphere of oxygen with an oxidant that could oxidize **1**, generating a reduced form that could be reoxidized by dioxygen. To this end, a variety of oxidants were shown to oxidize **1**, including  $\text{CuCl}_2$ ,  $\text{FeCl}_3$ , and  $\text{Na}_3[\text{H}_3\text{PMo}_9\text{V}_3\text{O}_{40}]$ , all of which could potentially be reoxidized by dioxygen.  $\text{CuCl}_2$  was actually shown to oxidize **1** catalytically in the presence of excess dioxygen; however under these conditions, the catalyst in the Shilov system,  $[\text{Pt}^{\text{II}}\text{Cl}_4]^{2-}$ , is also oxidized. This could prove problematic for the use of  $\text{CuCl}_2$  as a catalytic co-oxidant for the Shilov system.

Both  $\text{CuCl}_2$  and  $\text{FeCl}_3$  oxidize **1** with first-order dependence on oxidant. The oxidation of **1** by copper(II) was shown to be highly dependent on the counteranion—only chloride and bromide proved competent—and oxidations by  $\text{CuCl}_2$  are highly dependent on chloride concentration. In contrast to the case of  $\text{Na}_2\text{Pt}^{\text{IV}}\text{Cl}_6$ , decreasing the chloride concentration decreases the rate at which  $\text{CuCl}_2$  oxidizes **1**.

At this time we cannot determine whether oxidation by Cu(II) goes via a one- or a two-electron pathway. The fact that one-electron oxidants such as  $\text{Na}_2\text{Ir}^{\text{IV}}\text{Cl}_6$  and  $(\text{NH}_4)_2\text{Ce}^{\text{IV}}(\text{NO}_3)_6$  rapidly oxidize **1** imply the former is quite reasonable, but the kinetics could be consistent with either, and the  $[\text{Cl}^-]$  dependence might reflect the effect of chloride concentration on the one-electron oxidation potential of copper(II) or the chloride requirement of a bridged intermediate in a two-electron pathway.

## Experimental Section

**General considerations.** Platinum salts were obtained from Strem. Anhydrous lithium chloride was purchased from Aldrich. 6.25 M hydrochloric acid (aq.) was

purchased from VWR. All deuterated solvents were purchased from Cambridge Isotope Laboratories, Inc.  $\text{Na}_3[\text{H}_3\text{PMo}_9\text{V}_3\text{O}_{40}]^{27}$  was prepared according to literature procedures. NMR spectra were acquired on a Varian Mercury 300 ( $^1\text{H}$ , 299.8 MHz) spectrometer at 23 °C. NMR shifts were referenced relative to internal solvent: 4.80 (s) (deuterium oxide) and 2.50 (m) (dimethyl sulfoxide- $d_6$ ). GC-MS data were collected using a Hewlett-Packard 5890 gas chromatograph with a HP-PLOT Q column and a Hewlett-Packard 5973 mass spectrometer.

**Synthesis of cesium dimethyltetrachloroplatinate(IV).** The procedure described below was generated from the procedure outlined by Zamashchikov et al.<sup>7</sup> as well as information provided to J. A. Labinger in a personal communication from S. L. Litvinenko.<sup>28</sup>

Potassium tetrachloroplatinate(II) (8.3 g, 0.020 mol) was dissolved in 50 mL of water. 19 mL (0.21 mol) of anhydrous dimethylsulfate was added, and the solution was stirred for 24 hours. Then, 1.07 g (0.011 mol) of hydrazine dihydrochloride was added. After 5 minutes, 38 mL (0.41 mol) of dimethylsulfate was added. After 5 minutes, 100 mL of methanol was added; and after another 5 minutes, 50 mL of water was added. This generated a yellow solution. After 5 minutes, 102.5 g of sodium carbonate were added very slowly. The solution slowly turned brown with a small amounts of black precipitate. Stirring of the solution continued with 50 mL of water being added after 1, 2, and 3 hours. After 6 hours, the solution was filtered through celite, and the filtrate was acidified with 6 M hydrochloric acid to a pH of about 1. The solvent was removed under reduced pressure. The residue was then dissolved in 50 mL of water, and this solution

was neutralized with sodium carbonate. An extraction was performed with about 500 mL of acetone. The organic phase was filtered through celite, and then acidification of the filtrate was repeated. The solvent and volatiles were removed under reduced pressure. The resulting residue was dissolved in 40 mL of water, and this solution was filtered through celite. Solvent was removed from the filtrate under reduced pressure. The residue was dissolved in a minimal amount of water, and then the solution was filtered. An aqueous saturated cesium chloride solution at 0 °C was added to the filtrate until precipitation occurred. The solid was isolated by filtration and washed 3 times with 5 mL of water at 0 °C. It was then washed 3 times with 5 mL of methanol at 0 °C. Next, the solid was dissolved in about 2.5 mL of water, and chlorine gas was bubbled through the solution for about 5 minutes. During this time, a yellow solid formed which was subsequently removed by filtration. Solvent and volatiles were removed from the filtrate under reduced pressure in order to isolate a yellow solid (550 mg, 0.82 mmol, 4%).

**Oxidation vs. protonolysis of monomethylplatinum(II) complex (1) at elevated temperature.** To determine the baseline methane yield, a solution of 1.94 g anhydrous lithium chloride in about 8 mL deionized water was cooled to room temperature, and 34.8 mg of  $\text{Cs}_2[\text{Pt}^{\text{IV}}(\text{CH}_3)_2\text{Cl}_4]$  added. This solution was then injected into the reaction vessel using a plastic syringe with a Teflon needle, and washed in with additional deionized water to give a total of 17 mL of solution in the reaction vessel. The reaction vessel consisted of a round-bottom flask with a small stir bar sealed inside. The only opening to the flask was a stopcock with a short (1.5 cm) hose adaptor on the other side. The total internal volume of the flask was about 31 mL. The solution was then

degassed and filled with helium. With the stopcock open and connected via a rubber hose to a helium source and a mercury bubbler, the flask was heated to 368 K. Then, 7.0 mL of 6.25 M hydrochloric acid (aq) was injected into the flask through the hose connected to the stopcock, using a plastic syringe with a Teflon needle. The stopcock was sealed, and the rubber hose was removed. The hose adapter on the stopcock was then capped with a rubber septum held down by copper wire. Using a syringe, the capped hose adapter was then filled with silicon oil in order to minimize exchange of gases between the air and the headspace of the reaction vessel during sampling. The air in the capped hose adapter was drained with a needle as it was being filled with silicon oil. 200  $\mu$ L of argon at 1 atm, for use as an internal standard, was added to the head space inside the vessel via syringe. The reaction was stirred at 368 K for 9 days, at which point consumption of **2** was complete as determined by  $^1\text{H}$  NMR spectroscopy. A 50  $\mu$ L sample of the headspace gas was injected into the GC-MS for analysis of argon, methane, ethane, carbon dioxide, and methyl chloride. (In a separate experiment, methyl chloride was found to decompose under the reaction conditions in the absence of  $\text{Cs}_2[\text{Pt}(\text{CH}_3)_2\text{Cl}_4]$ , while methane, ethane, and carbon dioxide were stable.) The final volume of solution in the vessel was measured at 368 K using a graduated cylinder in order to determine the exact concentrations of reagents.

For determination of relative rates, the desired amount of appropriate oxidant was added to the solution before heating, and the reaction carried out as above. Some reactions were carried out under an atmosphere of dioxygen instead of helium. The crystals that deposited at the end of the reaction using  $\text{CuCl}_2$  and dioxygen were

identified as  $\text{Cs}_2[\text{Pt}^{\text{IV}}\text{Cl}_6]$  by matching the X-ray crystallographic unit cell parameters to published values.

**Oxidation vs. protonolysis of monomethylplatinum(II) complex (1) at room temperature.** The solid mixture of cobaltocenium salts containing **1** was prepared as previously described.<sup>6</sup> A solution containing the desired amounts of oxidant, lithium chloride, and (in some cases)  $\text{D}_2\text{SO}_4$  in 1.0 mL  $\text{D}_2\text{O}$  was added to 20 mg of the solid mixture with vigorous stirring. The reaction was stirred for 20 minutes before being centrifuged. The supernatant was then transferred to an NMR tube for analysis by  $^1\text{H}$  NMR spectroscopy. Quantification was achieved using the signals of either added sodium *p*-toluenesulfonate or THF (present in the solid mixture) as internal standard; separate experiments showed that the amount of THF relative to sodium *p*-toluenesulfonate remained the same under all reaction conditions tested.  $k_{\text{Ox.}}/k_{\text{D}^+}$  was determined for **4** and for **1** using eq. (2.4) and eq. (2.5), respectively.  $[\mathbf{1}]_0$  and  $[\mathbf{4}]_0$  represent the initial concentrations of the respective platinum(II) species in solution. This was determined from the reaction in which **5** was dissolved in  $\text{D}_2\text{O}$  with a 0.12 *M*  $[\text{Na}_2\text{Pt}^{\text{IV}}\text{Cl}_6]$  because in this reaction both **1** and **4** were completely oxidized. The concentrations of the methylplatinum(IV) species were determined by  $^1\text{H}$  NMR spectroscopy at the end of the reaction. The  $k_{\text{Ox.}}/k_{\text{D}^+}$  and  $k_{\text{Ox.}}/k_{\text{H}^+}$  for **1** and **4** under various conditions are presented in tables 2.3, 2.4, and 2.5.

$$\mathbf{4}: \frac{k_{\text{Ox.}}}{k_{\text{D}^+}} = \frac{[\mathbf{2}]}{[\mathbf{4}]_0 - [\mathbf{2}]} \frac{[\text{D}^+]}{[\text{Ox.}]} \quad (2.4)$$

$$\mathbf{1}: \frac{k_{Ox.}}{k_{D^+}} = \frac{[3]}{([1]_0 + [4]_0) - [3] - [2]} \frac{[D^+]}{[Ox.]} \quad (2.5)$$

**Table 2.3.** Dependence of  $k_{Ox.}/k_{D^+}$  and  $k_{Ox.}/k_{H^+}$  on  $\text{Na}_2[\text{Pt}^{\text{IV}}\text{Cl}_6]$  for **1** and **4** ( $[\text{D}_2\text{SO}_4] = 0.35 \text{ M}$ ,  $[\text{Cl}^-] = 3.0 \text{ M}$ ). \*These numbers differ from those reported in the text: the latter are based only on the data for  $[\text{Na}_2\text{Pt}^{\text{IV}}\text{Cl}_6] = 0.12 \text{ M}$ , for the purpose of using the same conditions to compare low and high  $[\text{Cl}^-]$ .

$\text{Na}_2[\text{Pt}^{\text{IV}}\text{Cl}_6]$	<b>1</b>		<b>4</b>	
(M)	$k_{Ox.}/k_{D^+}$	$k_{Ox.}/k_{H^+}$	$k_{Ox.}/k_{D^+}$	$k_{Ox.}/k_{H^+}$
0.12	3.2	0.35	4.1	0.45
0.12	3.4	0.37	4.5	0.50
0.12	4.1	0.46	5.8	0.64
0.12	3.3	0.36	5.8	0.64
0.25	3.6	0.40	4.0	0.44
0.37	3.2	0.36	3.2	0.35
0.37	2.5	0.27	3.3	0.37
0.50	2.6	0.29	2.8	0.31
0.50	4.1	0.46	3.5	0.39
average*	3.3	0.37	4.1	0.46
standard deviation*	0.6	0.06	1.1	0.12

**Table 2.4.** Dependence of  $k_{Ox}/k_{D+}$  and  $k_{Ox}/k_{H+}$  on  $[Cl^-]$  for **1** and **4** ( $Na_2[Pt^{IV}Cl_6] = 0.12 M$ ,  $[D_2SO_4] = 0.35 M$ ).

[Cl <sup>-</sup> ] (M)	<b>1</b>		<b>4</b>	
	$k_{ox}/k_{D+}$	$k_{ox}/k_{H+}$	$k_{ox}/k_{D+}$	$k_{ox}/k_{H+}$
0.72	8.099	0.900	8.55	0.95
0.72	10.877	1.209	9.21	1.02
0.72	6.871	0.763	12.54	1.394
0.72	7.723	0.858	16.44	1.827
0.72	8.625	0.958	14.23	1.582
1.5	5.677	0.631	6.70	0.74
2.2	4.521	0.502	6.06	0.67
3.0	3.165	0.352	4.09	0.45
3.0	3.352	0.372	4.49	0.499
3.0	4.125	0.458	5.78	0.642
3.0	3.282	0.365	5.77	0.641

**Table 2.5.** Dependence of  $k_{Ox}/k_{D+}$  and  $k_{Ox}/k_{H+}$  on  $[Cl^-]$  for **1** and **4** ( $[Cu^{II}Cl_2] = 0.25 M$ ,  $[D_2SO_4] = 0.35 M$ ).

[Cl <sup>-</sup> ] (M)	<b>1</b>		<b>4</b>	
	$k_{ox}/k_{D+}$	$k_{ox}/k_{H+}$	$k_{ox}/k_{D+}$	$k_{ox}/k_{H+}$
0.496	0.00	0.00	44.25	4.92
3.0	0.776	0.086	48.41	5.38

## References and Notes

---

<sup>1</sup> Goldshlegger, N. F.; Tyabin, M. B.; Shilov, A. E.; Shteinman, A. A. *Zh. Fiz. Khim.* **1969**, *43*, 2174-2175.; Goldshlegger, N. F.; Eskova, V. V.; Shilov, A. E.; Shteinman, A. A. *Zh. Fiz. Khim.* **1972**, *46*, 1353-1354. See also Shilov, A. E.; Shul'pin, G. B. *Activation and Catalytic Reactions of Saturated Hydrocarbons in the Presence of Metal Complexes*; Kluwer Academic Publishers: Dordrecht, 2000, pp. 259-317.

<sup>2</sup> (a) Kushch, L. A.; Lavrushko, V. V.; Misharin, Y. S.; Moravskii, A. P.; Shilov, A. E. *Nouv. J. Chim.* **1983**, *7*, 729-733. (b) Luinstra, G. A.; Labinger, J. A.; Bercaw, J. E. *J. Am. Chem. Soc.* **1993**, *115*, 3004-3005. (c) Labinger, J. A.; Herring, A. M.; Lyon, D. K.; Luinstra, G. A.; Bercaw, J. E.; Horvath, I. T.; Eller, K. *Organometallics* **1993**, *12*, 895-905. (d) Luinstra, G. A.; Wang, L.; Stahl, S. S.; Labinger, J. A.; Bercaw, J. E. *Organometallics* **1994**, *13*, 755-756. (e) Luinstra, G. A.; Wang, L.; Stahl, S. S.; Labinger, J. A.; Bercaw, J. E. *J. Organomet. Chem.* **1995**, *504*, 75-91. (f) Hutson, A. C.; Lin, M.; Basickes, N.; Sen, A. *J. Organomet. Chem.* **1995**, *504*, 69-74.

<sup>3</sup> Scollard, J. D.; Day, M.; Labinger, J. A.; Bercaw, J. E. *Helv. Chim. Acta* **2001**, *84*, 3247-3268.

<sup>4</sup> One-electron pathways are also known for some redox systems involving Pt(II) and/or Pt(IV). See Basolo, F.; Pearson, R. G. *Mechanisms of Inorganic Reactions*; 2<sup>nd</sup> ed.; John Wiley & Sons: New York, 1967, pp. 494-497.

<sup>5</sup> Rich, R. L.; Taube, H. *J. Am. Chem. Soc.* **1954**, *76*, 2608-2611.

<sup>6</sup> Wang, L.; Stahl, S. S.; Labinger, J. A.; Bercaw, J. E. *J. Mol. Cat. A* **1997**, *116*, 269-275.

<sup>7</sup> Zamashchikov, V. V.; Popov, V. G.; Litvinenko, S. L. *Russian Chemical Bulletin* **1993**, *42*, 352-358.

---

<sup>8</sup> Basolo, F.; Pearson, R. G. *Mechanisms of Inorganic Reactions*; 2nd ed.; John Wiley & Sons: New York, 1967, pp. 375-382.

<sup>9</sup> Horvath, I. T.; Cook, R. A.; Millar, J. M.; Kiss, G. *Organometallics* **1993**, *12*, 8-10.

<sup>10</sup> Devries, N.; Roe, D. C.; Thorn, D. L. *J. Mol. Cat. A* **2002**, *189*, 17-22.

<sup>11</sup> Basickes, N.; Hogan, T. E.; Sen, A. *J. Am. Chem. Soc.* **1996**, *118*, 13111-13112.

<sup>12</sup> Freund, M. S.; Labinger, J. A.; Lewis, N. S.; Bercaw, J. E. *J. Mol. Cat.* **1994**, *87*, L11-L16.

<sup>13</sup> Lin, M.; Shen, C.; Garcia-Zayas, E. A.; Sen, A. *J. Am. Chem. Soc.* **2001**, *123*, 1000-1001.

<sup>14</sup> Bar-Nahum, I.; Khenkin, A. M.; Neumann, R. *J. Am. Chem. Soc.* **2004**, *126*, 10236-10237.

<sup>15</sup> Periana, R. A.; Taube, D. J.; Gamble, S.; Taube, H.; Satoh, T.; Fujii, H. *Science* **1998**, *280*, 560-564.

<sup>16</sup> Labinger, J. A.; Bercaw, J. E. *Nature* **2002**, *417*, 507-514.

<sup>17</sup> Moodley, K. G.; Nicol, M. J. *J. Chem. Soc. Dalton Trans.* **1977**, 239-243.

<sup>18</sup> van Beek, J. A. M.; van Koten, G.; Wehman-Ooyevaar, I. C. M.; Smeets, W. J. J.; van der Sluis, P.; Spek, A. L. *J. Chem. Soc. Dalton Trans.* **1991**, 883-893.

<sup>19</sup> Preetz, W.; Rimkus, G. *Z. Naturforsch, B: Chem. Sci* **1983**, *38B*, 442-445.

<sup>20</sup> Kozhevnikov, I. V. *Chem. Rev.* **1998**, *98*, 171-198.

<sup>21</sup> (a) Henry, P. M. *Inorg. Chem.* **1966**, *5*, 668-669. (b) Jhaveri, A. S.; Sharma, M. M. *Chem. Eng. Sci.* **1967**, *22*, 1-6. (c) Gray, R. D. *J. Am. Chem. Soc.* **1969**, *91*, 56-62. (d)

---

Stevanato, R.; Argese, E.; Viglino, P. *Inorg. Chim. Acta*. **1984**, *92*, 177-180. (e)

Goldstein, S.; Czapski, G. *Inorg. Chem.* **1985**, *24*, 1087-1092.

<sup>22</sup> Latimer, W. M. *The Oxidation States of the Elements and Their Potentials in Aqueous Solutions*; 2nd ed.; Prentice Hall: New York, 1952; Cotton, F. A.; Wilkinson, G.; Murillo, C. A.; Bochmann, M. *Advanced Inorganic Chemistry*; 6th ed.; Wiley & Sons: New York, 1999.

<sup>23</sup> Stahl, S. S.; Labinger, J. A.; Bercaw, J. E. *J. Am. Chem. Soc.* **1996**, *118*, 5961-5976.

<sup>24</sup> Malyszko, J.; Kaczor, M. *J. Chem. Educ.* **2003**, *80*, 1048-1050.

<sup>25</sup> Control experiments revealed that under these conditions,  $\text{Na}_2[\text{Ir}^{\text{IV}}\text{Cl}_6]$  oxidizes methane in the absence of platinum. There is precedent for iridium(IV) oxidation of alkanes. See: Shilov, A. E. *Activation of Saturated Hydrocarbons with Transition Metal Complexes*; D. Reidel: Dordrecht, The Netherlands, 1984, pp. 66-67.

<sup>26</sup> For a previous indication of the possible involvement of chloride in the protonolysis of platinum(II) methyl species, see Hill, G. S.; Rendina, L. M.; Puddephatt, R. J. *Organometallics*, **1995**, *14*, 4966-4968.

<sup>27</sup> Grate, J. H.; Hamm, D. R.; Saxton, R. J. International Patent Application Publication Number WO 91/13681, 1991.

<sup>28</sup> Litvinenko, S. L. Personal communication to J. A. Labinger, 2003.

## **Chapter 3**

### **The Synthesis, Protonolysis, and C-H Bond Activation Chemistry of Platinum(II) Complexes Containing the Dianionic 2,2'-Biindolyl Ligand**

## Abstract

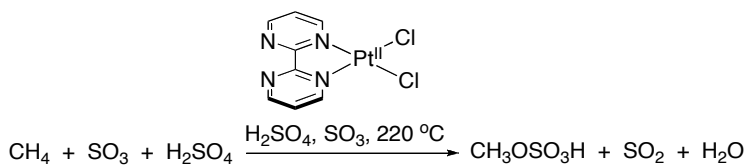
Electron rich platinum(II) complexes containing the 2,2'-biindolyl ligand were synthesized and probed for C-H bond activation chemistry. 2,2'-biindolyl was deprotonated with greater than two equivalents of sodium hydride, and it was subsequently reacted with dimethyl(1,5-cyclooctadiene)platinum(II) to generate disodium (2,2'-biindolyl)dimethylplatinum(II) (**2**). Crystals of **2** with 15-crown-5 ether were grown from diethyl ether. **2** decomposes rapidly in air, and deuterolysis of both platinum-methyls as well as the 2,2'-biindolyl ligand occurs when **2** is dissolved in methanol-d<sub>4</sub>. Protonolysis of a single platinum(II)-methyl bond occurs when **2** is reacted with one equivalent of 2,2,2-trifluoroethanol-d<sub>3</sub> in either tetrahydrofuran-d<sub>8</sub> (THF-d<sub>8</sub>) or acetonitrile-d<sub>3</sub> (CD<sub>3</sub>CN). This protonolysis occurs much more rapidly in CD<sub>3</sub>CN than in THF-d<sub>8</sub>. In THF-d<sub>8</sub>, C-D bond activation of THF-d<sub>8</sub> follows protonolysis, and C-D bond activation occurs faster than the protonolysis as no intermediate is observed. The reaction of **2** with B(C<sub>6</sub>F<sub>5</sub>)<sub>3</sub> in C<sub>6</sub>D<sub>6</sub> also led to a species capable of activating C-D bonds as indicated by the generation of CH<sub>4</sub>, CH<sub>3</sub>D, CH<sub>2</sub>D<sub>2</sub>, and possibly CHD<sub>3</sub>.

## Introduction

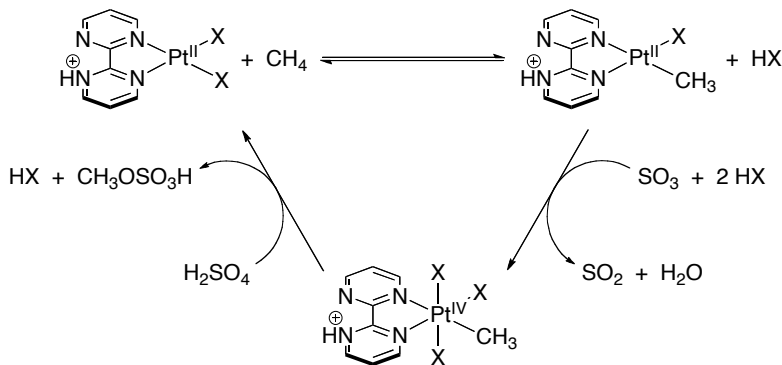
In the development of homogeneous catalysts for the conversion of alkanes into more valuable products, selective alkane functionalization has been achieved using a mixture of platinum(II) and platinum(IV) salts as discovered by Shilov et al. and described in chapter 2.<sup>1-3</sup> In order to make this system practical,  $[\text{Pt}^{\text{IV}}\text{Cl}_6]^{2-}$  needs to be replaced by an inexpensive stoichiometric oxidant, but improvements in catalytic rates and in catalyst stability are also necessary.<sup>4,5</sup> Unfortunately further studies on this system are hindered by the number of species present in solution, the limited number of methods available to characterize these species, and the instability of these species.

The use of chelating ligands can limit the number of species in solution, can aid in characterization, and can be used to modify the chemistry of metal complexes.<sup>4,6</sup> With regards to alkane functionalization using platinum complexes containing chelating ligands, the benchmark system was developed by Periana et al. at Catalytica Advanced Technology Inc.<sup>7</sup> This system, depicted in scheme 3.1, involves the oxidation of methane to methyl bisulfate catalyzed by (bipyrimidine)dichloroplatinum(II) in fuming sulfuric acid. The proposed mechanism for this reaction is closely related to the one proposed for the catalysis described by Shilov et al., and it is depicted in scheme 3.2.  $\text{SO}_3$  or  $\text{H}_2\text{SO}_4$  functions as the stoichiometric oxidant in this system; however, the  $\text{SO}_2$  generated following oxidation of platinum could in principle be reoxidized to  $\text{SO}_3$  or  $\text{H}_2\text{SO}_4$  by dioxygen, meaning that dioxygen would function as the stoichiometric oxidant.<sup>7</sup> Furthermore, the combination of the chelating ligand and the use of hot, fuming sulfuric acid prevents metal precipitation, and turnover numbers greater than 300 can be

achieved.<sup>5</sup> The generation of methylbisulfate as the product allows yields to be achieved in excess of 70% based on methane.<sup>5</sup>



**Scheme 3.1.** The oxidation of methane to methyl bisulfate reported by Periana et al. and catalyzed by (bipyrimidine)dichloroplatinum(II) in fuming sulfuric acid.<sup>7</sup>



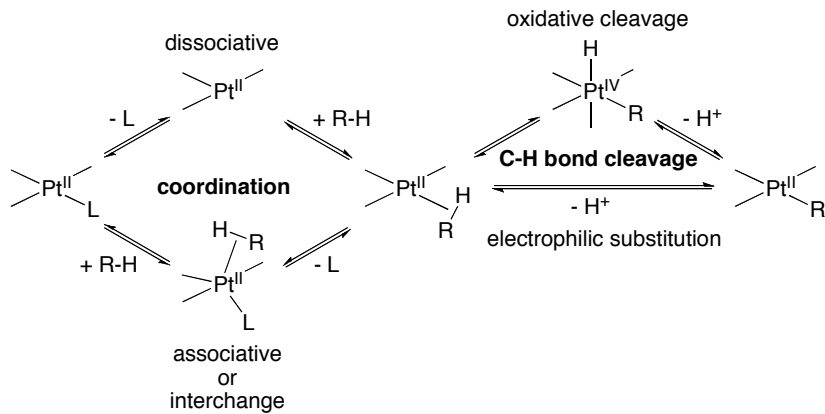
**Scheme 3.2.** The proposed mechanism for bipyrimidineplatinum(II)-catalyzed methane oxidation reported by Periana et al. (X =  $\text{HSO}_4^-$  or  $\text{Cl}^-$ ).<sup>4-7</sup>

This system does, however, suffer from at least two major drawbacks. First, methyl bisulfate is of little direct use.<sup>4</sup> While methyl bisulfate can be converted by hydrolysis to methanol, a more useful product, this process is not yet economically practical for industrial use.<sup>4,7</sup> Second, the catalyst is severely inhibited by both water and methanol.<sup>5</sup> This is problematic because water is generated during the catalysis by oxidation of platinum with either  $\text{SO}_3$  or  $\text{H}_2\text{SO}_4$ .<sup>7</sup> While water could potentially be used

to hydrolyze methyl bisulfate, the resulting methanol also inhibits catalysis. In the absence of water and methanol, methane C-H bond activation is proposed to occur by initial displacement of bisulfate from platinum(II) with methane.<sup>5</sup> Under the reaction conditions, water and methanol form stronger bonds with platinum(II) than bisulfate; thus, there is a larger barrier to displacement of water and methanol from platinum(II) by methane, and the overall barrier to methane C-H bond activation is increased.<sup>5</sup> This has also been proposed to account for slow rates of catalysis in the alkane functionalization system developed by Shilov et al., as C-H bond activation in that system is also rate limiting.<sup>5</sup>

In order to increase rates of platinum-catalyzed alkane functionalization, conditions need to be found which decrease the barriers to C-H bond activation. C-H bond activation at platinum(II) can generally be divided into two steps as shown in scheme 3.3.<sup>6</sup> The first step involves coordination of the C-H  $\sigma$ -bond to the metal center, and this is followed by C-H bond cleavage to generate a metal-carbon  $\sigma$ -bond. Previous studies indicate that each step can occur by one of two different pathways (scheme 3.3), and the spectator ligands bound to platinum have a strong influence over which pathway is taken.<sup>6</sup> C-H bond coordination can occur either by a dissociative exchange pathway or by an associative exchange pathway, while C-H bond cleavage can occur either by oxidative addition, to generate an (alkyl)hydridoplatinum(IV) species, followed by deprotonation or by electrophilic substitution.<sup>6</sup> Ligands which make the platinum(II) metal center more electron deficient favor the generation of an alkylplatinum(II) species via associative C-H bond coordination followed by electrophilic substitution. In contrast,

dissociative exchange and oxidative cleavage are favored by electron rich and strongly  $\sigma$ -donating ligands.



**Scheme 3.3.** Possible platinum(II) C-H bond activation routes.

C-H bonds are poor nucleophiles; therefore in order for C-H bond coordination to be kinetically and thermodynamically accessible, it is necessary to design systems in which the ligand being displaced is relatively weakly bound to the platinum(II) metal center.<sup>5,6</sup> In the case of electron deficient metal centers, this means that poorly coordinating solvents and counterions are necessary; however, product inhibition can still occur, as in the alkane functionalization system developed by Periana et al.<sup>5,6</sup> Electron rich metal centers with electron donating ligands could be envisioned to destabilize complexes in which relatively strong nucleophiles are bound, thereby facilitating C-H bond coordination via a dissociative exchange pathway.<sup>5,6</sup> The use of electron donating ligands should also make the resulting alkylplatinum(II) complex more prone to oxidation. This is important as oxidation follows C-H bond activation in both of the platinum-catalyzed, alkane functionalization systems described above.<sup>3,5,7</sup>

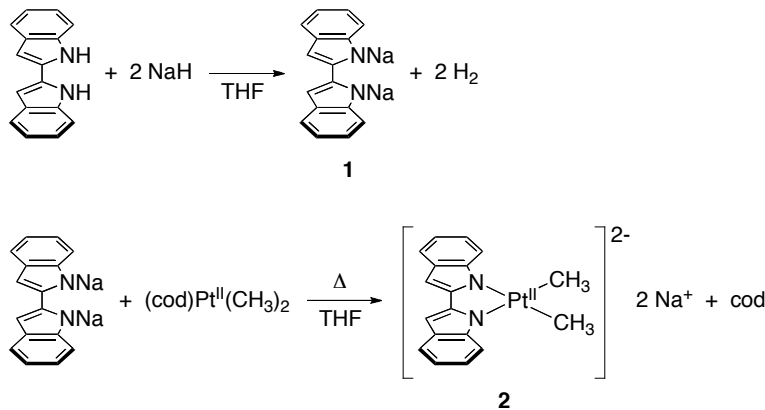
Unfortunately, few ligands have been shown to induce dissociative exchange at platinum(II).<sup>6,8</sup> Dissociative exchange has been demonstrated for platinum(II) complexes containing *cis*-coordinating, anionic carbon spectator ligands.<sup>8,9</sup> Dissociative exchange in some of these complexes has even led to C-H bond activation via cyclometallation, but one of the original anionic carbon ligands is reductively eliminated with the proton of the C-H bond being cyclometallated.<sup>8,10,11</sup> As this indicates, one of the problems with using anionic carbon donors as spectator ligands for C-H bond functionalization at platinum(II) is that C-H bond activation generates an anionic carbon donor for functionalization.<sup>3,4,5</sup> Development of a platinum-catalyzed C-H bond functionalization system involving anionic carbon spectator ligands is thus likely to be difficult. It would therefore be useful to probe other anionic donors, while incorporation of these donors into chelating ligands could aid in stabilization.

While C-H bond activation studies are lacking for platinum(II) complexes supported by chelating ligands containing two anionic nitrogen donors, bidentate ligands containing one anionic nitrogen donor have been used to support platinum(II) complexes capable of catalyzing C-H bond functionalization.<sup>12,13</sup> These complexes seem to activate C-H bonds by an associative exchange mechanism, and catalysis is relatively slow;<sup>12,13</sup> therefore, the use of a dianionic biindolyl ligand will be probed to determine whether it can increase rates of C-H bond activation and potentially functionalization.

## Results and Discussion

The disodium salt of 2,2'-biindolyl (**1**) was generated by deprotonation of 2,2'-biindolyl with excess sodium hydride in tetrahydrofuran (THF) as illustrated in

scheme 3.4. Excess sodium hydride was removed by filtration through celite, and **1** was recrystallized from a 1:1 mixture of THF and diethyl ether. Heating a THF solution of **1** and dimethyl(1,5-cyclooctadiene)platinum(II) in a Schlenk bomb at 100 °C generated 1,5-cyclooctadiene and disodium (2,2'-biindolyl)dimethylplatinum(II) (**2**, scheme 3.4) over the course of 8 days, and **2** could be isolated in 57% yield. **2** was isolated with two equivalents of THF per equivalent of **2**, probably because THF was coordinated to the sodium counterions. The amount of THF isolated with **2** was quantified by <sup>1</sup>H NMR spectroscopy following dissolution of **2** in CD<sub>3</sub>CN. In order to facilitate crystallization of **2**, an excess of 15-crown-5 ether was added to a solution of **2** in diethyl ether. Crystals of **2** with two equivalents of 15-crown-5 ether were grown at -35 °C, and the structure is depicted in figure 3.1.



**Scheme 3.4.** Deprotonation of 2,2'-biindolyl and generation of **2** (cod = 1,5-cyclooctadiene).

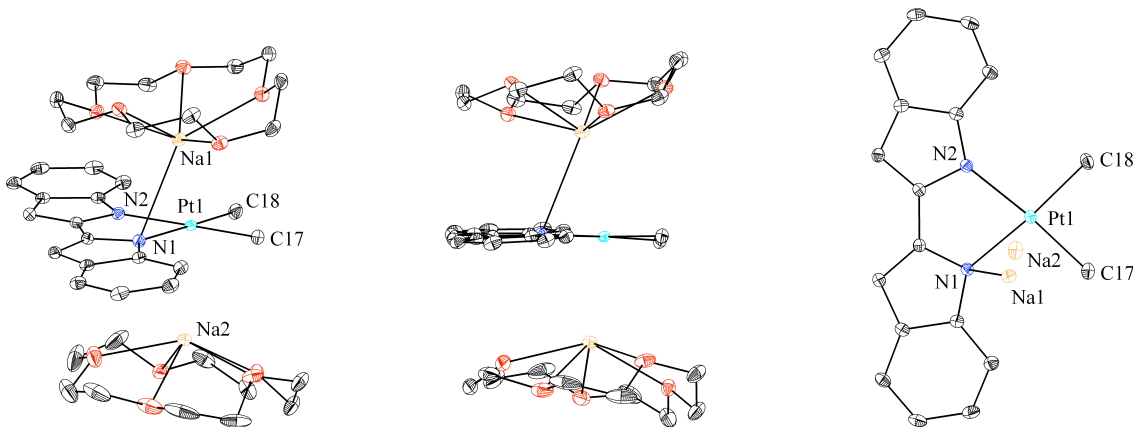


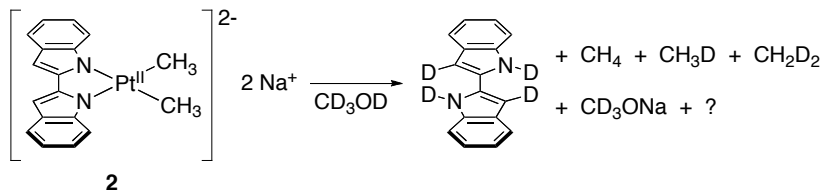
**Figure 3.1.** Structural drawing of **2** with 15-crown-5 ether coordinating to the sodium countercations. Three perspectives are shown; the 15-crown-5 ethers have been removed from the view on the right. One molecule of diethyl ether is present in the unit cell, but it is not shown here. Displacement ellipsoids are drawn at the 50% probability level. Selected bond lengths (Å) and angles (°): Pt1-C18 2.0469(16); Pt1-C17 2.0536(16); Pt1-N2 2.1210(12); Pt1-N1 2.1265(13); Pt1-Na2 2.9821(6); Pt1-Na1 3.0565(6); Na1-N1 2.8602(14); Na2-N1 3.071(1); Na1-N2 3.898(1); Na2-N2 3.916(1); C18-Pt1-C17 87.71(7); C18-Pt1-N2 96.97(6); C17-Pt1-N2 175.22(6); C18-Pt1-N1 175.28(6); C17-Pt1-N1 96.82(6); N2-Pt1-N1 78.52(5); Na2-Pt1-Na1 129.051(19).

Only two other transition metal complexes with the 2,2'-biindolyl functionality have been synthesized and published; in these complexes, 2,2'-biindolyl was incorporated into a tetradentate ligand framework for nickel(II).<sup>14</sup> The crystal structure of **2** with 15-crown-5 ether, shown in figure 3.1, is the first crystal structure of a transition metal complex with the 2,2'-biindolyl functionality bound directly to the metal center. In the crystal structure, the distances between the sodium ions and platinum as well as between the sodium ions and one nitrogen atom (N1) are within the sum of the

van der Waals radii for these atoms; however, the distances are still relatively long, indicating only weak interactions.<sup>15</sup>

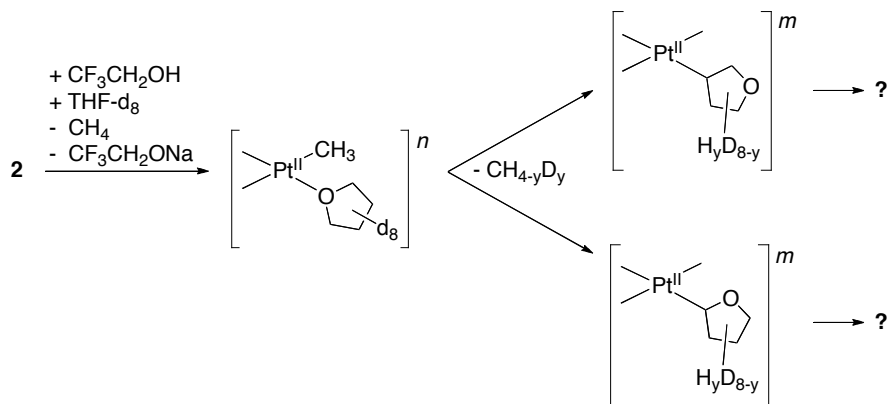
**2** decomposes rapidly when exposed to air, either in the solid state or in solution. While **2** reacts rapidly with oxidants such as N-bromosuccinimide and copper(II) chloride, a clean oxidation of **2** has not yet been achieved. The reaction of **2** with proton sources was also investigated. Protonolysis of a platinum(II)-methyl bond is the microscopic reverse of methane C-H bond activation at platinum(II); and therefore, it may provide insight into potential C-H bond activations. Furthermore, it has been demonstrated previously that dimethylplatinum(II) complexes containing a chelating ligand can be induced to activate C-H and C-D bonds following removal of a methide either by protonolysis or by abstraction with a Lewis acid.<sup>6,16</sup>

When **2** is dissolved in anhydrous methanol-d<sub>4</sub> (CD<sub>3</sub>OD) under anaerobic conditions, both platinum-methyls are rapidly protonolyzed as well as the 2,2'-biindolyl ligand (scheme 3.5). A <sup>1</sup>H NMR of the reaction was taken within 35 minutes, and peaks corresponding to **2** can no longer be observed. Instead, peaks can be observed which correspond to CH<sub>4</sub>, CH<sub>3</sub>D, and CH<sub>2</sub>D<sub>2</sub>. H/D isotopic scrambling prior to displacement of methane from platinum is well precedented, and it could account for the generation of CH<sub>2</sub>D<sub>2</sub> and CH<sub>4</sub>.<sup>6,17,18</sup> Deuterolysis of 2,2'-biindolyl was indicated by peaks matching those of the 4, 4', 5, 5', 6, 6', 7, and 7' protons in non-ligated 2,2'-biindolyl. The absence of peaks corresponding to the 3 and 3' protons of 2,2'-biindolyl is likely due to deuteration in these positions; deuteration in the 3 position of indole has been demonstrated previously in acidic solutions.<sup>19</sup>



**Scheme 3.5.** Deuterolysis of **2** in CD<sub>3</sub>OD.

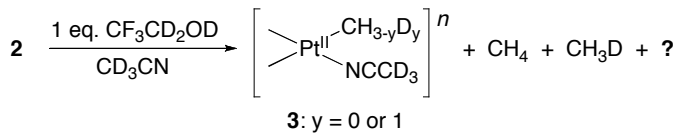
In order to better control and observe the protonation of **2**, **2** was reacted with only one equivalent of trifluoroethanol (TFE) both in THF-d<sub>8</sub> and in acetonitrile-d<sub>3</sub> (CD<sub>3</sub>CN). When the reaction of **2** with one equivalent of either TFE or TFE-d<sub>3</sub> was performed in THF-d<sub>8</sub> and monitored by <sup>1</sup>H NMR spectroscopy, the peaks corresponding to **2** disappeared slowly over the course of approximately 4 days, while new peaks appeared, including peaks corresponding to CH<sub>4</sub>, CH<sub>3</sub>D, and CH<sub>2</sub>D<sub>2</sub>. The reaction occurred at approximately the same rate whether TFE or TFE-d<sub>3</sub> was used; although, further experiments need to be performed in order to obtain a more accurate measurement of the isotopic effect on the rate of protonolysis. The observance of CH<sub>3</sub>D and CH<sub>2</sub>D<sub>2</sub> even when the protonolysis is performed with protio-TFE indicates C-D bond activation of THF-d<sub>8</sub> by a methylplatinum(II) species as illustrated in scheme 3.6. The natural abundance of deuterium, 0.0156%, is too low for any other source to account for the amounts of CH<sub>3</sub>D and CH<sub>2</sub>D<sub>2</sub> generated.<sup>20</sup> A new platinum-methyl species is never observed, and it is unclear at this time what happens to the 2,2'-biindolyl ligand because multiple overlapping peaks are observed between 6.2 and 7.8 ppm.



**Scheme 3.6.** Protonation of **2** in THF-d<sub>8</sub> with TFE leading to C-D bond activation of THF-d<sub>8</sub>. Outside of the ligands specified, it is unclear what is bound to platinum.

This reaction likely proceeds by protonolysis of a platinum(II)-methyl bond in **2** to generate a monomethylplatinum(II) complex with THF-d<sub>8</sub> coordinated, as depicted in scheme 3.6. Intramolecular C-D bond activation could then occur from the methyl(THF-d<sub>8</sub>)platinum(II) complex (scheme 3.6) since oxygen-bound THF adducts of other monomethylplatinum(II) complexes have been shown to undergo intramolecular C-H bond activation and subsequent reductive elimination of methane.<sup>21,22</sup> It should be noted that protonolysis of a bond between platinum(II) and 2,2'-biindolyl could also allow coordination of THF-d<sub>8</sub>, leading to C-D bond activation, and this pathway cannot be ruled out at this time. A methylplatinum(II) species other than **2** is never observed during the course of the reaction; so, C-D bond activation of THF-d<sub>8</sub> seems to be fast relative to protonolysis. Further experiments need to be performed in order to determine which C-D bonds of THF-d<sub>8</sub> are activated and to determine the specific platinum species involved in the reaction.

When **2** was reacted with one equivalent of either TFE or TFE-d<sub>3</sub> in CD<sub>3</sub>CN and the reaction was monitored by <sup>1</sup>H NMR spectroscopy, the peaks corresponding to **2** disappeared over the course of about 4 hours, while CH<sub>4</sub> and CH<sub>3</sub>D were generated along with a new methylplatinum(II) species (**3**, scheme 3.7). Only trace amounts of CH<sub>3</sub>D are generated when protio-TFE is used. In the <sup>1</sup>H NMR spectrum, **3** exhibits a Pt-CH<sub>3</sub> peak that is shifted downfield from the corresponding peak for **2**, and the Pt-CH<sub>3</sub> peak of **3** has <sup>195</sup>Pt satellites with a coupling constant of 78 Hz. This is a significant decrease in <sup>195</sup>Pt-CH<sub>3</sub> coupling constant relative to **2** (<sup>2</sup>J<sub>PtH</sub> = 84 Hz). Previous protonolyses of dimethylplatinum(II) species to generate monomethylplatinum(II) species have also been accompanied by a decrease in <sup>195</sup>Pt-CH<sub>3</sub> coupling constants.<sup>23,24</sup> Based on this evidence, along with the generation of methane isotopologues and the results for the protonolysis of **2** in THF-d<sub>8</sub>, **3** is tentatively assigned as an (acetonitrile)(monomethyl)platinum(II) complex (scheme 3.7).



**Scheme 3.7.** The reaction of **2** with 1 equivalent of TFE-d<sub>3</sub> in CD<sub>3</sub>CN to generate **3**.

At the same rate as the Pt-CH<sub>3</sub> peak of **3** appears in the <sup>1</sup>H NMR spectrum, new peaks are observed in the aryl region for at least one species, possibly **3**, containing 2,2'-biindolyl. Unfortunately, the nature of this species is unclear due to the presence of overlapping multiplets in the aryl region. Binding of 2,2'-biindolyl in **3** is supported by the presence of a peak corresponding to the mass of (acetonitrile)(2,2'-

biindolyl)methylplatinum(II) in the MALDI mass spectrum. While it seems likely that 2,2'-biindolyl is bound to platinum in **3**, its binding mode is unclear, and further characterization of this species is necessary.

Deuterium incorporation into the platinum(II)-methyl of **3** is indicated by a triplet at 1.13 ppm for Pt-CH<sub>2</sub>D in the <sup>1</sup>H NMR spectrum. This peak is significantly smaller when protio-TFE is used, and it exhibits a coupling constant of 1.5 Hz, indicative of two-bond coupling to deuterium.<sup>25</sup> The Pt-CH<sub>2</sub>D peak occurs only slightly upfield of the singlet with <sup>195</sup>Pt satellites for Pt-CH<sub>3</sub> at 1.15 ppm. There appear to be <sup>195</sup>Pt satellites for the triplet as well, but they are hard to resolve due to overlap with the <sup>195</sup>Pt satellites of the Pt-CH<sub>3</sub> peak. Incorporation of deuterium into the platinum(II)-methyl of **3** indicates reversible H/D isotopic exchange following protonation of **2** and prior to loss of methane as formulated for the deuterolysis of **2** in CD<sub>3</sub>OD and similar to protonolyses of dimethylplatinum(II) complexes described previously.<sup>6,17,18</sup>

Preliminary investigations were made into the activation of benzene-d<sub>6</sub> (C<sub>6</sub>D<sub>6</sub>) C-D bonds by platinum species containing the 2,2'-biindolyl ligand. It was envisioned that methide abstraction by B(C<sub>6</sub>F<sub>5</sub>)<sub>3</sub> would lead to a monomethylplatinum(II) complex capable of activating C-H or C-D bonds similarly to the species involved in the activation of THF-d<sub>8</sub> described above. Previously, other methylplatinum(II) complexes have been shown to undergo methide abstraction by B(C<sub>6</sub>F<sub>5</sub>)<sub>3</sub> in benzene, leading to the activation of benzene C-H bonds at platinum(II).<sup>16</sup> **2** was therefore dissolved in C<sub>6</sub>D<sub>6</sub> containing B(C<sub>6</sub>F<sub>5</sub>)<sub>3</sub>. While **2** is only sparingly soluble in C<sub>6</sub>D<sub>6</sub>, partial dissolution of **2** was observed in the presence of one equivalent of B(C<sub>6</sub>F<sub>5</sub>)<sub>3</sub>, and complete dissolution of **2** occurred when greater than two equivalents were used. Regardless of whether one or two

equivalents of  $\text{B}(\text{C}_6\text{F}_5)_3$  were dissolved in  $\text{C}_6\text{D}_6$ , reaction of this solution with **2** immediately resulted in a mixture of  $\text{CH}_4$ ,  $\text{CH}_3\text{D}$ ,  $\text{CH}_2\text{D}_2$ , and  $\text{CHD}_3$ , as observed by  $^1\text{H}$  NMR spectroscopy. Thus, a monomethylplatinum(II) complex, similar to the one involved in  $\text{THF-d}_8$  activation (scheme 3.6), was likely generated by methide abstraction or labilization with  $\text{B}(\text{C}_6\text{F}_5)_3$ . Similar to systems characterized previously, reversible activation of the C-D bonds in  $\text{C}_6\text{D}_6$  by the monomethylplatinum(II) complex, followed by irreversible loss of methane, would account for generation of the deuterated methane isotopologues observed in the reaction.<sup>24</sup>

As evidence for this pathway, no methane was generated when the reaction was attempted in a 2.5:1 volume:volume mixture of  $\text{CD}_3\text{CN}$  and  $\text{C}_6\text{D}_6$ ; and based on  $^1\text{H}$  NMR spectroscopy, generation of what seems to be a new monomethylplatinum(II) complex (**4**) containing 2,2'-biindolyl occurred. **4** has a  $\text{Pt-CH}_3$  peak at 1.29 ppm, and the  $^{195}\text{Pt}$  satellites for this peak have a coupling constant of 80 Hz, intermediate between the coupling constants observed for **2** (84 Hz) and **3** (78 Hz). Coordination of  $\text{CD}_3\text{CN}$  in **4** may block C-D bond activation of  $\text{C}_6\text{D}_6$ . This reaction was not clean, but **4** can be generated cleanly by the reaction of  $\text{B}(\text{C}_6\text{F}_5)_3$  with **2** in  $\text{CD}_3\text{CN}$ . The peaks for **4** are significantly different from those of **3**, and this could be due to an interaction of  $[\text{BCH}_3(\text{C}_6\text{F}_5)_3]^-$  with **4**, due to coordination of trifluoroethoxide in **3**, or due to different coordination modes of 2,2'-biindolyl in the two complexes. When **4** was generated *in situ*, a peak could not be observed in the  $^1\text{H}$  NMR spectrum for  $[\text{BCH}_3(\text{C}_6\text{F}_5)_3]^-$ ; however, it may precipitate out of solution, or it may be broadened out due to an as yet unidentified process. Further studies need to be performed in order to fully characterize **4** and to gain

more insight into activation of the C-D bonds in C<sub>6</sub>D<sub>6</sub> using (2,2'-biindolyl)platinum(II) complexes.

## Conclusions

In an attempt to find a ligand capable of facilitating C-H bond activation and stable to subsequent reductive elimination, the chelating, dianionic bisnitrogen donor ligand, 2,2'-biindolyl, was used to synthesize sodium (2,2'-biindolyl)dimethylplatinum(II) (**2**). This is one of the first examples of a 2,2'-biindolyl functionality bound directly to a transition metal center.<sup>14</sup> **2** is relatively electron rich as evidenced by its reactivity with mild oxidants and proton sources.

Methide abstraction from **2**, either by protonolysis or by reaction with B(C<sub>6</sub>F<sub>5</sub>)<sub>3</sub>, generates monomethylplatinum(II) species capable of activating C-H and C-D bonds. Protonolysis of a platinum(II)-methyl bond is observed when **2** is reacted with one equivalent of trifluoroethanol-d<sub>3</sub> in either THF-d<sub>8</sub> or CD<sub>3</sub>CN. The protonolysis occurs significantly faster in CD<sub>3</sub>CN than in THF-d<sub>8</sub>, and a species is observed which has tentatively been identified as an (acetonitrile)monomethylplatinum(II) complex. In THF-d<sub>8</sub>, C-D bond activation of THF-d<sub>8</sub> follows protonolysis, likely via a similar (solvento)monomethylplatinum(II) species. In addition, activation of the C-D bonds in C<sub>6</sub>D<sub>6</sub> was indicated by the generation of deuterated methane isotopologues following methide abstraction from **2** using B(C<sub>6</sub>F<sub>5</sub>)<sub>3</sub>. While these results are promising for the development of a C-H bond functionalization system involving 2,2'-biindolyl-ligated platinum(II) complexes, further studies need to be performed in order to determine the platinum species involved in and resulting from these C-D bond activation reactions.

## Experimental Section

**General considerations.** All air- and/or moisture-sensitive compounds were manipulated using standard Schlenk techniques or in a glovebox under a nitrogen atmosphere as described previously.<sup>26</sup> Under standard glovebox conditions purging was not performed between uses of petroleum ether, diethyl ether, benzene, toluene and tetrahydrofuran; thus when any of these solvents were used, traces of all these solvents were in the atmosphere and could be found intermixed in the solvent bottles. All NMR solvents were purchased from Cambridge Isotopes Laboratories, Inc. The solvents for air- and moisture-sensitive reactions were dried by passage through a column of activated alumina followed by storage under dinitrogen. 2, 2, 2-trifluoroethanol-d<sub>3</sub> (TFE-d<sub>3</sub>) was purchased from Cambridge Isotopes Laboratories, Inc and then dried over 3 Å molecular sieves. Next, it was vacuum distilled onto tris(pentafluorophenyl)borane (B(C<sub>6</sub>F<sub>5</sub>)<sub>3</sub>) before being distilled into a Strauss flask and stored under dinitrogen. 2, 2, 2-trifluoroethanol (TFE) was purchased from Aldrich. It was dried over 3 Å molecular sieves, degassed by the freeze-pump-thaw method, and then stored in a Schlenk bomb under dinitrogen. All other materials were used as received. Sodium hydride, B(C<sub>6</sub>F<sub>5</sub>)<sub>3</sub>, and chlorotrimethylsilane were purchased from Aldrich. 2, 2'-biindolyl was synthesized according to a previously reported procedure<sup>27</sup> or purchased from Syntastic. Dimethyl(1, 5-cyclooctadiene)platinum (II) was purchased from Strem Chemicals, Inc. <sup>1</sup>H, <sup>13</sup>C and <sup>19</sup>F NMR spectra were recorded on Varian Mercury 300 spectrometers at room temperature, unless indicated otherwise. Chemical shifts are reported with respect to

residual internal protio solvent for  $^1\text{H}$  and  $^{13}\text{C}\{^1\text{H}\}$  NMR spectra.  $\text{CFCl}_3$  was used as an external standard to reference  $^{19}\text{F}$  NMR spectra at 0 ppm.

The single crystal X-ray diffraction sample was prepared by coating the crystal with Paratone N oil under nitrogen and then transferring the crystals to a microscope slide under argon. The sample was selected and mounted on a glass fiber with Paratone N oil. Data collection was carried out on a Bruker Smart 1000 CCD diffractometer. The structure was solved by direct methods. All non-hydrogen atoms were refined anisotropically.

**Generation of the disodium salt of 2,2'-biindolyl (1).** In a glovebox, 2, 2'-biindolyl (500 mg, 2.2 mmol) was dissolved in about 40 mL of THF, and sodium hydride was suspended in about 20 mL of THF. The sodium hydride suspension was slowly added to the solution of 2,2'-biindolyl, and bubbling occurred. This solution was stirred for 6 hours, and then it was filtered through Celite to remove unreacted sodium hydride. The solvent was evaporated under vacuum, and the solid was then precipitated overnight from a 1:1 mixture of diethyl ether and THF by cooling it to 0° C. This solid was washed with diethyl ether and dried *in vacuo*. A white solid (97%, 875 mg, 2.1 mmol) was isolated, and it contains about two equivalents of THF per molecule of **1** based on  $^1\text{H}$  NMR spectroscopy. The THF likely coordinates to sodium, making it difficult to remove.  $^1\text{H}$  NMR (300 MHz, THF- $d_8$ ):  $\delta$  1.78 (m, 8H, 2 eq. THF), 3.61 (m, 8H, 2 eq. THF), 6.52 (td,  $^3J_{\text{HH}} = 6.8$  Hz,  $^4J_{\text{HH}} = 1.5$  Hz, 2H), 6.57 (td,  $^3J_{\text{HH}} = 7.1$  Hz,  $^4J_{\text{HH}} = 1.7$  Hz, 2H), 6.65 (s, 2H), 7.18 (br d,  $^3J_{\text{HH}} = 7.3$  Hz, 2H), 7.28 (m, 2H).  $^{13}\text{C}\{^1\text{H}\}$  NMR (75 MHz,

THF-d<sub>8</sub>):  $\delta$  26.4 (THF), 68.3 (THF), 95.6, 115.1, 115.8, 116.2, 118.2, 135.1, 149.9, 150.3.

**Synthesis of disodium dimethyl(2,2'-biindolyl)platinum (II) (2).** In a glovebox, **1** (120 mg, 0.285 mmol), containing 2 equivalents of THF, and dimethyl(1, 5-cyclooctadiene)platinum (II) (165 mg, 0.495 mmol) were dissolved in 30 mL THF in a Schlenk tube. The tube was sealed and heated for 8 days at 100 °C. The tube was then cooled to 23 °C. The solvent and volatiles were removed under reduced pressure. The resulting solid was washed with toluene. It was then extracted with THF, and the THF solution was filtered through celite. Removal of solvent from the filtrate under reduced pressure yielded a light yellow powder (57%, 105 mg, 0.163 mmol) that decomposes rapidly when exposed to air. Based on <sup>1</sup>H NMR in CD<sub>3</sub>CN, two equivalents of THF-d<sub>8</sub> remained coordinated to sodium in the product. <sup>1</sup>H NMR (300 MHz, CD<sub>3</sub>CN):  $\delta$  0.94 (s, <sup>2</sup>*J*<sub>PtH</sub> = 84 Hz, 6H), 1.80 (m, 8H, 2 eq. THF), 3.64 (m, 8H, 2 eq. THF), 6.43 (d, <sup>4</sup>*J*<sub>HH</sub> = 0.86 Hz, 2H), 6.60 (m, 4H), 7.28 (m, 2H), 7.71 (m, 2H); <sup>1</sup>H NMR (300 MHz, THF-d<sub>8</sub>):  $\delta$  1.08 (s, <sup>2</sup>*J*<sub>PtH</sub> = 83 Hz, 6H), 6.54 (s, 2H), 6.60 (td, <sup>3</sup>*J*<sub>HH</sub> = 6.8 Hz, <sup>4</sup>*J*<sub>HH</sub> = 1.7 Hz, 2H), 6.64 (td, <sup>3</sup>*J*<sub>HH</sub> = 6.8 Hz, <sup>4</sup>*J*<sub>HH</sub> = 1.7 Hz, 2H), 7.26-7.33 (m, 2H), 7.72-7.82 (m, 2H). <sup>13</sup>C {<sup>1</sup>H} NMR (75 MHz, THF-d<sub>8</sub>):  $\delta$  -21.4, 94.1, 115.0, 115.7, 117.3, 118.7, 134.6, 148.5, 150.52.

**Crystallization of 2 with 15-crown-5 ether.** In a glovebox, approximately 10 mg (0.02 mmol) of **2** were dissolved in a minimal amount of diethyl ether. Approximately 0.3 mL (1.5 mmol) of 15-crown-5 ether were added, and some precipitate

formed. The solution was filtered, and the filtrate was stored at -35 °C. Yellow crystals formed over the course of approximately two weeks.

**Deuterolysis of **2** in **CD<sub>3</sub>OD**.** In a glovebox, **2** (6 mg, 0.009 mmol) was dissolved in about 0.6 mL of **CD<sub>3</sub>OD**. The solution was initially bright red; but within 30 minutes, it turned brownish red. A <sup>1</sup>H NMR spectrum was taken within 35 minutes, and no peaks corresponding to **2** could be observed. New peaks corresponding to CH<sub>4</sub>, CH<sub>3</sub>D, and CH<sub>2</sub>D<sub>2</sub> were apparent along with new peaks in the aryl region. The peaks in the aryl region match those of the 4, 4', 5, 5', 6, 6', 7, and 7' protons in free 2,2'-biindolyl: <sup>1</sup>H NMR (300 MHz, **CD<sub>3</sub>OD**) δ 7.00 (m, 2H), 7.10 (m, 2H), 7.38 (d of m, <sup>3</sup>J = 8.10 Hz, 2H), 7.53 (d of m, <sup>3</sup>J = 7.93 Hz). The absence of peaks corresponding to the 3 and 3' protons of 2,2'-biindolyl is likely due to deuteration in these positions; deuteration in the 3 position of indole has been demonstrated in acidic solutions. Based on the <sup>1</sup>H NMR spectrum, the reaction was fairly clean, but it should be noted that broad peaks were present at 6.77 ppm and at -0.17 ppm.

**Protonation of **2** with TFE-d<sub>3</sub> in THF-d<sub>8</sub>.** Initial silylation of a J-Young NMR tube was performed by washing it with a 20% solution of chlorotrimethylsilane in methylene chloride. It was then heated for about 6 hours at 98 °C. In a glovebox, 5.0 mg (0.010 mmol) of **2** was dissolved in approximately 200 μL of THF-d<sub>8</sub> and transferred to the J-Young NMR tube with another 200 μL of THF-d<sub>8</sub>. 3.6 μL (0.051 mmol) of TFE-d<sub>3</sub> was then used to make a 1.0 mL THF-d<sub>8</sub> solution in a volumetric flask. 150 μL of this solution (0.0076 mmol of TFE-d<sub>3</sub>) was added to the J-Young tube. The tube was quickly

sealed, and the solution was mixed, thoroughly. The reaction was then monitored by  $^1\text{H}$  NMR spectroscopy. Over the course of about 4 days, the peaks in the  $^1\text{H}$  NMR corresponding to **2** slowly disappeared, while new biindolyl peaks grew in along with  $\text{CH}_4$ ,  $\text{CH}_3\text{D}$ , and  $\text{CH}_2\text{D}_2$ . A new peak in the  $^1\text{H}$  NMR corresponding to  $\text{Pt-CH}_3$  was never observed. Since less than one equivalent of TFE was used relative to **2**, some **2** remained unreacted.

**Protonation of 2 with TFE in  $\text{THF-d}_8$ .** The procedure used for the protonation of **2** with TFE- $\text{d}_3$  was repeated, but the J-Young NMR tube was not silylated prior to the reaction. Also, 3.6  $\mu\text{L}$  (0.049 mmol) of TFE was instead used to make the 1.0 mL  $\text{THF-d}_8$  solution in a volumetric flask. 150  $\mu\text{L}$  of this solution (0.0074 mmol of TFE) was added to the J-Young tube. This reaction also took about 4 days, and similar results were obtained as with TFE- $\text{d}_3$ .

**Protonation of 2 with TFE- $\text{d}_3$  and TFE in  $\text{CD}_3\text{CN}$ .** In a glovebox, 10.7 mg (0.0213 mmol) of **2** was dissolved in approximately 200  $\mu\text{L}$  of  $\text{THF-d}_8$  and transferred to a J-Young NMR tube with another 200  $\mu\text{L}$  of  $\text{THF-d}_8$ . 7.5  $\mu\text{L}$  (0.11 mmol) of TFE- $\text{d}_3$  was then used to make a 1.0 mL  $\text{THF-d}_8$  solution in a volumetric flask. 200  $\mu\text{L}$  of this solution (0.021 mmol of TFE- $\text{d}_3$ ) was added to the J-Young tube. The tube was quickly sealed, and the solution was mixed, thoroughly. The reaction was then monitored by  $^1\text{H}$  NMR spectroscopy. Over the course of about 4 hours, the peaks in the  $^1\text{H}$  NMR corresponding to **2** slowly disappeared, while peaks corresponding to  $\text{CH}_4$  and  $\text{CH}_3\text{D}$  grew in along with a new set of peaks likely corresponding to an

(acetonitrile)methylplatinum(II) complex (**3**) containing 2,2'-biindolyl. It is not clear at this time how 2,2'-biindolyl binds to platinum(II) in **3**, and more than one species may be present. Deuterium incorporation into the platinum-methyl was evidenced by Pt-CH<sub>3</sub> and Pt-CH<sub>2</sub>D peaks. Similar results were obtained when the reaction was performed with protio-TFE, but the peaks for CH<sub>3</sub>D and Pt-CH<sub>2</sub>D decreased in intensity. <sup>1</sup>H NMR of **3** (300 MHz, CD<sub>3</sub>CN):  $\delta$  1.13 (t, <sup>2</sup>J<sub>DH</sub> = 1.5 Hz, coupling to <sup>195</sup>Pt was hard to resolve, 2H, Pt-CH<sub>2</sub>D), 1.15 (s, <sup>2</sup>J<sub>PtH</sub> = 78 Hz, 2H, Pt-CH<sub>3</sub>), 6.46 (m, 1H), 6.74 (m, 5H), 7.36 (m, 3H); 7.64 (br d, 1H). MALDI-TOF MS m/z calcd. for (acetonitrile-d<sub>3</sub>)(2,2'-biindolyl)methylplatinum(II) (C<sub>19</sub>H<sub>13</sub>D<sub>3</sub>N<sub>3</sub>Pt): 484.12. Found: 484.2.

**C-D bond activation of C<sub>6</sub>D<sub>6</sub> with 2.** **2** (6 mg, 0.012 mmol) and B(C<sub>6</sub>F<sub>5</sub>)<sub>3</sub> (15 mg, 0.029 mmol) were dissolved in 0.4 mL C<sub>6</sub>D<sub>6</sub>. The solution bubbled rapidly, and a yellow solution with red oil at the bottom was formed. <sup>1</sup>H NMR spectroscopy revealed multiple products, including CH<sub>4</sub>, CH<sub>3</sub>D, CH<sub>2</sub>D<sub>2</sub>, and possibly CHD<sub>3</sub>. When this reaction was attempted with less than 2 equivalents of B(C<sub>6</sub>F<sub>5</sub>)<sub>3</sub>, not all of **2** reacted, and some solid remained. This reaction was also attempted by first dissolving **2** (11 mg, 0.025 mmol) in 0.25 mL CD<sub>3</sub>CN. Separately, B(C<sub>6</sub>F<sub>5</sub>)<sub>3</sub> (14 mg, 0.027 mmol) was dissolved in 0.25 mL CD<sub>3</sub>CN. 0.1 mL C<sub>6</sub>D<sub>6</sub> was added to each solution, and then the solution with B(C<sub>6</sub>F<sub>5</sub>)<sub>3</sub> was slowly added to the solution of **2**. An orange solution was formed, and multiple products were observed by <sup>1</sup>H NMR spectroscopy, including **4** (<sup>1</sup>H NMR described below); however, there were no peaks corresponding to methane or its isotopologues.

**In situ generation of 4 by the reaction of 2 with B(C<sub>6</sub>F<sub>5</sub>)<sub>3</sub> in CD<sub>3</sub>CN** (6.0 mg, 0.014 mmol) and B(C<sub>6</sub>F<sub>5</sub>)<sub>3</sub> (14.1 mg, 0.028 mmol) were dissolved separately, each in 0.2 mL CD<sub>3</sub>CN. The B(C<sub>6</sub>F<sub>5</sub>)<sub>3</sub> solution was then added to the solution of **2**. A yellow solution was formed in which **3** could be identified by <sup>1</sup>H NMR spectroscopy. <sup>1</sup>H NMR (300 MHz, CD<sub>3</sub>CN):  $\delta$  1.29 (s, <sup>2</sup>*J*<sub>PtH</sub> = 80 Hz, 3H), 6.76 (t, <sup>3</sup>*J*<sub>HH</sub> = 14 Hz, 1H), 6.88-7.00 (m, 3H), 7.01-7.17 (m, 3H), 7.61-7.69 (m, 2H), 7.72 (d, <sup>3</sup>*J*<sub>HH</sub> = 8 Hz, 1H).

**Table of Crystal Data and Structure Refinement.**

**Table 3.1.** Crystal and refinement data for the structure of **2** with 15-crown-5 ether.

Empirical formula	[C <sub>18</sub> H <sub>16</sub> N <sub>2</sub> Pt] <sup>2-</sup> 2 [C <sub>10</sub> H <sub>20</sub> NaO <sub>5</sub> ] <sup>+</sup> • 0.5 C <sub>4</sub> H <sub>10</sub> O	Crystal system	Orthorhombic
Formula weight	987.98	Space group	Pbca
T (K)	100(2)	<i>d</i> <sub>calc</sub> , g/cm <sup>3</sup>	1.566
<i>a</i> , Å	14.2417(7)	θ range, deg	1.88 to 37.82
<i>b</i> , Å	17.5788(9)	<i>μ</i> , mm <sup>-1</sup>	3.459
<i>c</i> , Å	33.1713(16)	Abs. correction	Semiempirical from equivalents
Z	6	GOF	2.356
Volume, Å <sup>3</sup>	4499.5(7)	<i>R</i> <sub>1</sub> , <sup>a</sup> <i>wR</i> <sub>2</sub> , <sup>b</sup> [I > 2σ(I)]	0.0303, 0.0484

<sup>a</sup> *R*<sub>1</sub> =  $\sum ||F_o| - |F_c|| / \sum |F_o|$ . <sup>b</sup> *wR*<sub>2</sub> =  $[\sum [w(F_o^2 - F_c^2)^2] / \sum [w(F_o^2)^2]]^{1/2}$ .

## References and Notes

---

<sup>1</sup> Goldshlegger, N. F.; Tyabin, M. B.; Shilov, A. E.; Shteinman, A. A. *Zh. Fiz. Khim.* **1969**, *43*, 2174-2175.

<sup>2</sup> Goldshlegger, N. F.; Eskova, V. V.; Shilov, A. E.; Shteinman, A. A. *Zh. Fiz. Khim.* **1972**, *46*, 1353-1354.

<sup>3</sup> Shilov, A. E.; Shul'pin, G. B. *Activation and Catalytic Reactions of Saturated Hydrocarbons in the Presence of Metal Complexes*; Kluwer, Academic Publishers: Dordrecht, 2000; pp 259-317.

<sup>4</sup> Labinger, J. A.; Bercaw, J. E. *Nature* **2002**, *417*, 507-514.

<sup>5</sup> Periana, R. A.; Bhalla, G.; Tenn, W. J.; Young, K. J. H.; Liu, X. Y.; Mironov, O.; Jones, C.; Ziatdinov, V. R. *J. Mol. Catal. A* **2004**, *220*, 7-25.

<sup>6</sup> Lersch, M.; Tilset, M. *Chem. Rev.* **2005**, *105*, 2471-2526.

<sup>7</sup> Periana, R. A.; Taube, D. J.; Gamble, S.; Taube, H.; Satoh, T.; Fujii, H. *Science* **1998**, *280*, 560-564.

<sup>8</sup> Plutino, M. R.; Scolaro, L. M.; Albinati, A.; Romeo, R. *J. Am. Chem. Soc.* **2004**, *126*, 6470-6484.

<sup>9</sup> Plutino, M. R.; Scolaro, L. M.; Romeo, R.; Grassi, A. *Inorg. Chem.* **2000**, *39*, 2712-2720.

<sup>10</sup> Romeo, R.; Plutino, M. R.; Romeo, A. *Helv. Chim. Acta* **2005**, *88*, 507-522.

<sup>11</sup> Simhai, N.; Iverson, C. N.; Edelbach, B. L.; Jones, W. D. *Organometallics* **2001**, *20*, 2759-2766.

<sup>12</sup> West, N. M.; White, P. S.; Templeton, J. L. *J. Am. Chem. Soc.* **2007**, *129*, 12372-12373.

---

<sup>13</sup> Karshtedt, D.; McBee, J. L.; Bell, A. T.; Tilley, T. D. *Organometallics* **2006**, *25*, 1801-1811.

<sup>14</sup> Black, D. S. C.; Kumar, N.; Wang, L. C. H. *J. Chem. Soc., Chem. Commun.* **1985**, 1174-1175.

<sup>15</sup> Bondi, A. *J. Phys. Chem.* **1964**, *68*, 441-451.

<sup>16</sup> Liang, L.-C.; Lin, J.-M.; Lee, W.-Y. *Chem. Commun.* **2005**, 2462-2464.

<sup>17</sup> Stahl, S. S.; Labinger, J. A.; Bercaw, J. E. *J. Am. Chem. Soc.* **1996**, *118*, 5691-5976.

<sup>18</sup> Holtcamp, M. W.; Labinger, J. A.; Bercaw, J. E. *Inorg. Chim. Acta* **1997**, *265*, 117-125.

<sup>19</sup> Williams, T. J.; Labinger, J. A.; Bercaw, J. E. *Organometallics* **2007**, *26*, 281-287.

<sup>20</sup> Drago, R. S. *Physical Methods in Chemistry*; W. B. Saunders: Philadelphia, PA, 1977; inside cover.

<sup>21</sup> Holtcamp, M. W.; Labinger, J. A.; Bercaw, J. E. *J. Am. Chem. Soc.* **1997**, *119*, 848-849.

<sup>22</sup> Holtcamp, M. W.; Henling, L. M.; Day, M. W.; Labinger, J. A.; Bercaw, J. E. *Inorg. Chim. Acta* **1998**, 467-478.

<sup>23</sup> Johansson, L.; Ryan, O. B.; Tilset, M. *J. Am. Chem. Soc.* **1999**, *121*, 1974-1975.

<sup>24</sup> Zhong, H. A.; Labinger, J. A.; Bercaw, J. E. *J. Am. Chem. Soc.* **2002**, *124*, 1378-1399.

<sup>25</sup> Heyduk, A. F.; Driver, T. G.; Labinger, J. A.; Bercaw, J. E. *J. Am. Chem. Soc.* **2004**, *126*, 15034-15035.

---

<sup>26</sup> Burger, B. J.; Bercaw, J. E. *New Developments in the Synthesis, Manipulation, and Characterization of Organometallic Compounds*; Wayda, A.; Dahrensbourg, M. Y., Eds.; American Chemical Society: Washington, DC, **1987**; Vol. 357.

<sup>27</sup> Bergman, J.; Koch, E.; Pelzman, B. *Tetrahedron* **1995**, *51*, 5631-5642.

## **Chapter 4**

### **The Synthesis and Characterization of Iridium Complexes Containing a Diphenolate Imidazolyl-Carbene Ligand**

## Abstract

1,3-di(2-hydroxy-5-*tert*-butylphenyl)imidazolium chloride (**2a**) was synthesized in 42% yield, and then it was reacted with chloro-1,5-cyclooctadiene iridium(I) dimer to generate potassium (1,5-cyclooctadiene){1,3-di(2-hydroxy-5-*tert*-butylphenyl)imidazolyl} iridium(I) (**6**). **6** is the first iridium complex stabilized by a diphenolate imidazolyl-carbene ligand. In the solid-state structure of **6** with 18-crown-6 ether, only one phenoxide is actually bound to the metal center, while the other phenoxide is coordinated to the potassium counterocation along with 18-crown-6 ether. The solution-phase structure of this complex is fluxional and highly solvent dependent.

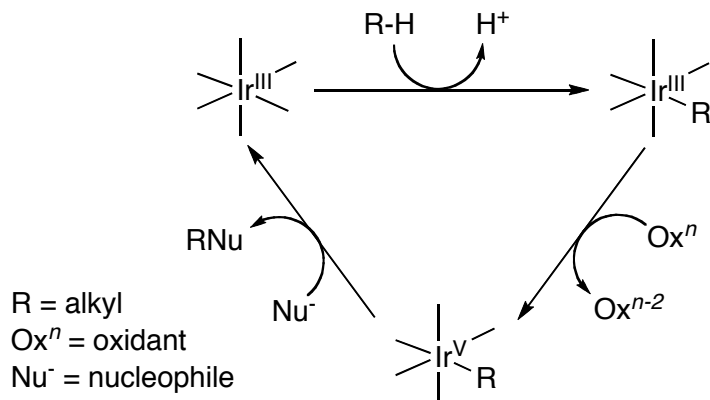
(Acetonitrile)(1,5-cyclooctadiene){1,3-di(2-hydroxy-5-*tert*-butylphenyl)imidazolyl}-iridium(III) hexafluorophosphate (**9**) is generated by the oxidation of **6** with two equivalents of ferrocenium(III) hexafluorophosphate in acetonitrile. Reaction of this complex with dihydrogen results in the generation of cyclooctane and a species capable of catalyzing the hydrogenation of cyclohexene to cyclohexane. Displacement of cyclooctadiene from **9** is achieved by heating **9** in acetonitrile to generate tris(acetonitrile){1,3-di(2-hydroxy-5-*tert*-butylphenyl)imidazolyl} iridium(III) hexafluorophosphate (**10**). Heating **9** in acetonitrile containing greater than three equivalents of trimethylphosphine results in the generation of tris(trimethylphosphine){1,3-di(2-hydroxy-5-*tert*-butylphenyl)imidazolyl} iridium(III) hexafluorophosphate (**11**), while a similar reaction with three equivalents of tricyclohexylphosphine yields (acetonitrile)bis(tricyclohexylphosphine){1,3-di(2-hydroxy-5-*tert*-butylphenyl)imidazolyl} iridium(III) hexafluorophosphate (**12**).

The reaction of **12** with carbon monoxide in acetonitrile at 90 °C generates an equilibrium mixture of **12** and (carbon monoxide)bis(tricyclohexylphosphine){1,3-di(2-hydroxy-5-*tert*-butylphenyl)imidazolyl}iridium(III) hexafluorophosphate (**15**). **15** has a CO-stretching frequency of 2064 cm<sup>-1</sup>. Acetonitrile can also be displaced from **12** by reaction with chloride to generate (chloro)bis(tricyclohexylphosphine){1,3-di(2-hydroxy-5-*tert*-butylphenyl)imidazolyl}iridium(III) (**16**). In the solid-state structure of **16**, the diphenolate imidazolyl-carbene ligand is distorted from C<sub>2v</sub>-symmetry toward C<sub>2</sub>-symmetry. Based on DFT calculations, this may be due to an antibonding interaction between the phenolates and the metal center in the highest occupied molecular orbital (HOMO) of the complex. As indicated by cyclic voltammetry and bulk electrolysis, **16** undergoes two reversible one-electron oxidations in methylene chloride at -0.22 V and at 0.58 V. Based on EPR spectra, mass spectra, and DFT calculations, the first oxidation seems to generate [(chloro)bis(tricyclohexylphosphine){1,3-di(2-hydroxy-5-*tert*-butylphenyl)imidazolyl}iridium]<sup>+</sup> (**16**<sup>+</sup>) with the unpaired electron occupying a molecular orbital that is delocalized over both the metal center and the diphenolate imidazolyl-carbene ligand.

## Introduction

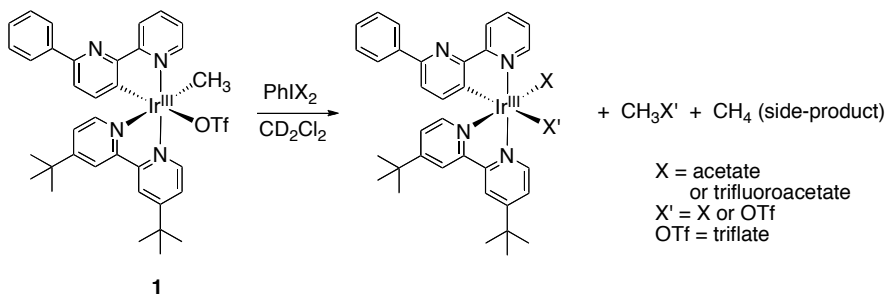
In the search for new homogeneous organometallic alkane functionalization catalysts, iridium has shown a significant amount of potential. Iridium has previously been shown to catalyze alkane dehydrogenation, and iridium(III) complexes have been shown to perform some of the lowest temperature electrophilic alkane C-H bond activations yet reported.<sup>1-3</sup> Rapid C-H bond activation is important because it is often the rate-limiting step in organometallic alkane functionalization systems.<sup>4</sup> Similar to the methylplatinum(II) complexes involved in platinum-catalyzed methane functionalization, methyliridium(III) complexes have been shown to react with strong oxidants to release methyl-containing organic products.<sup>4,5</sup> This is promising for the development of an iridium-catalyzed alkane functionalization system akin to the ones demonstrated with platinum(II).<sup>4</sup>

A potential catalytic cycle for oxidative iridium-catalyzed C-H bond functionalization is illustrated in scheme 4.1. Similar to platinum-catalyzed C-H bond functionalization, an initial electrophilic C-H bond activation could generate an alkyliridium(III) complex. A two-electron oxidation could then be used to activate this complex toward either nucleophilic attack or reductive elimination, both of which would result in release of a functionalized alkyl and regeneration of the initial iridium(III) catalyst. Alternatively, reductive elimination could occur from the alkyliridium(III) to generate a functionalized alkyl and an iridium(I) complex, which could be reoxidized; however, functionalization of an iridium(III) alkyl by reductive elimination or nucleophilic attack is difficult.<sup>5</sup>



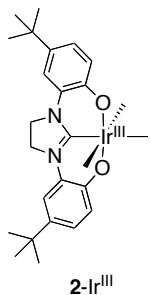
**Scheme 4.1.** A potential catalytic cycle for oxidative iridium-catalyzed C-H bond functionalization.

While there is a significant amount of precedent for the electrophilic activation of alkane C-H bonds with iridium(III) complexes,<sup>3,6</sup> there is less precedence for the oxidation and functionalization steps.<sup>5</sup> Periana et al. demonstrated that reaction of a methyliridium(III) complex (**1**) with strong oxidants such as iodobenzene diacetate resulted in the release of functionalized methyl-containing organic products such as methyl acetate (scheme 4.2).<sup>5</sup> While methane was produced as a side-product in reactions of **1** with  $\text{PhIX}_2$  (X = acetate or trifluoroacetate), the use of either bromine or iodine as the oxidant resulted in quantitative formation of the corresponding methyl halide.<sup>5</sup> The mechanisms of these reactions are not clear; however, it is plausible that two-electron oxidation of **1** activates it toward reductive elimination or nucleophilic attack. Unfortunately, a complex similar to **1** has not yet been generated via alkane C-H bond activation.<sup>5</sup> Ideally, a ligand system could be found for iridium(III) which would facilitate both alkane C-H bond activation and oxidative functionalization of the resulting alkyliridium(III) complex.



**Scheme 4.2.** The oxidative functionalization of **1** as demonstrated by Periana et al.<sup>5</sup>

To this end, iridium(III) complexes containing a diphenolate imidazolyl-carbene ligand (**2**, scheme 4.3) were targeted. The relatively *trans*-effecting imidazolyl-carbene functionality should facilitate ligand substitution.<sup>7</sup> Iridium(III) complexes often suffer from exceedingly slow rates of ligand substitution, and this could hinder C-H bond activation, which is likely to require initial coordination of the C-H bond to the metal center.<sup>8-11</sup>

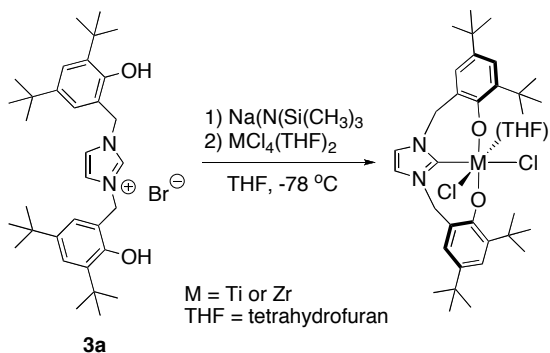


**Scheme 4.3.** Potential binding of **2** to iridium(III).

In order to facilitate two-electron oxidation of potential alkyliridium(III) complexes, **2** incorporates two phenolate functionalities. Although several iridium(V) complexes have been isolated and characterized previously, the generation of iridium(V) species often requires strongly donating ligands and/or harsh oxidants.<sup>8,12-21</sup> Phenolates

have previously been demonstrated to stabilize relatively high oxidation state complexes of other transition metals.<sup>22,23</sup> Furthermore, phenolate ligands can be oxidized to generate stable ligand-centered radicals.<sup>23,24</sup> Phenolate oxidation may occur at a lower potential than that required for generation of iridium(V), and similar ligand-centered oxidations have previously been used to facilitate reductive elimination from otherwise stable zirconium(IV) complexes.<sup>25</sup> Thus, phenolate ligands could possibly reduce the potentials required for two-electron oxidation of iridium(III) complexes while still promoting reductive elimination following oxidation.<sup>26,27</sup>

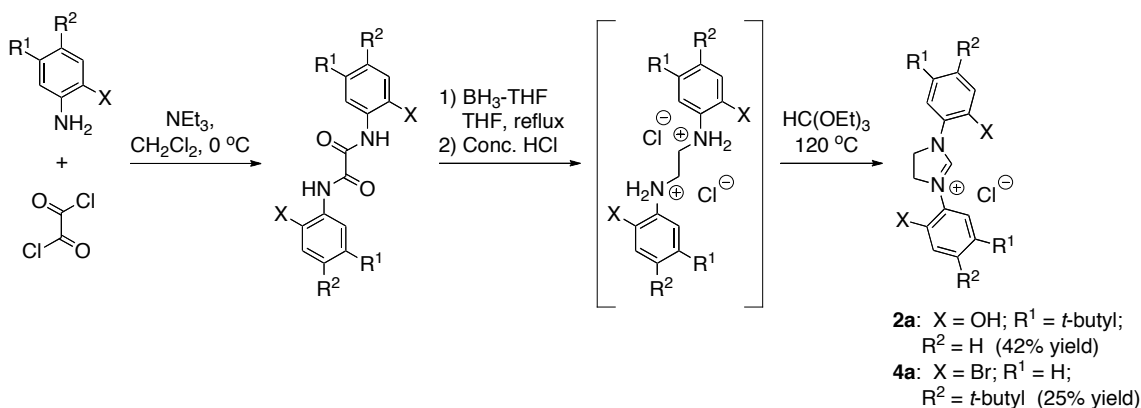
Currently, there are very few examples of diphenolate imidazolyl-carbene ligands.<sup>28,29,30</sup> A diphenolate imidazolyl-carbene ligand precursor (**3a**) has been synthesized previously in which a methylene unit bridges each phenolate to the imidazolyl ring as shown in scheme 4.4.<sup>30</sup> The deprotonated ligand is unstable to a 1,2 benzyl migration reaction at room temperature; so, metallations must be performed at low temperature. Upon ligation, this tridentate ligand forms seven-membered metallacycles, and it has been used to support titanium and zirconium complexes. Published reports are lacking on the synthesis and metallation of a diphenolate imidazolyl-carbene ligand such as **2** (scheme 4.3), in which methylenes do not bridge the phenolates to the imidazolyl ring; although, the synthesis of a similar ligand for ruthenium has been reported concurrently to the work described below.<sup>31</sup> It is envisioned that this type of ligand will be more thermally robust and will form more stable six-membered metallacycles.



**Scheme 4.4.** The synthesis of titanium and zirconium complexes with a diphenolate imidazolyl-carbene ligand as demonstrated by Kawaguchi et al.<sup>30</sup>

## Results and Discussion

**Synthesis of potential ligands and an iridium(I) complex.** The precursor to the diphenolate imidazolyl-carbene ligand, 1,3-di(2-hydroxy-5-*tert*-butylphenyl)imidazolium chloride (**2a**), was synthesized in 42% overall yield using the procedure illustrated in scheme 4.5. This procedure was adapted from the synthesis of monophenolate imidazolium salts by Waltman et al.<sup>32</sup> Another potential precursor to an imidazolyl-carbene ligand, 1,3-di(2-bromo-4-*tert*-butylphenyl)imidazolium chloride (**4a**) was synthesized in a similar manner (scheme 4.5). It was envisioned that activation of the bromo-phenyl bonds of **4a** by iridium could generate an iridium complex with a tridentate diphenyl imidazolyl-carbene ligand. Attempts at metallating **3a** involved initial deprotonation or reaction with silver(I) cations, followed by reaction with chloro-1,5-cyclooctadiene iridium(I) dimer. Unfortunately, a clean iridium species was never isolated from reactions involving **4a**.



**Scheme 4.5.** The synthesis of potential ligand precursors, **2a** and **4a**. Overall yields are shown.

Attempts were made to metallate **2a** and another potential ligand precursor, 2,6-di(2-hydroxy-3,5-*tert*-butylphenyl)pyridine (**5a**, figure 4.1), with a variety of iridium(I), iridium(III), and iridium(IV) starting materials. A clean iridium complex was never obtained in reactions involving **5a**; however, crystals of **5a** were obtained when it was heated with dihydrogen hexachloroiridate (IV) hydrate in ethanol-d<sub>6</sub>. The structure of **5a** is shown in figure 4.1.

A clean iridium complex was obtained when **2a** was deprotonated with potassium hexamethyldisilazide (KHMDS) and then reacted with chloro-1,5-cyclooctadiene iridium(I) dimer at room temperature as shown in scheme 4.6. Based on <sup>1</sup>H NMR spectroscopy, clean deprotonation of **2a** occurred at room temperature when it was reacted with greater than 3 equivalents of potassium hexamethyldisilazide in THF-d<sub>8</sub>. 1,5-cyclooctadiene iridium(I) dimer was then added to the resulting solution, and potassium (1,5-cyclooctadiene){1,3-di(2-hydroxy-5-*tert*-butylphenyl)imidazolyl}iridium(I) (**6**) was generated quantitatively as observed by <sup>1</sup>H

NMR spectroscopy (fig. 4.2). The 18-crown-6 etherate of **6** was crystallized from benzene, and the structure is depicted in figure 4.3.

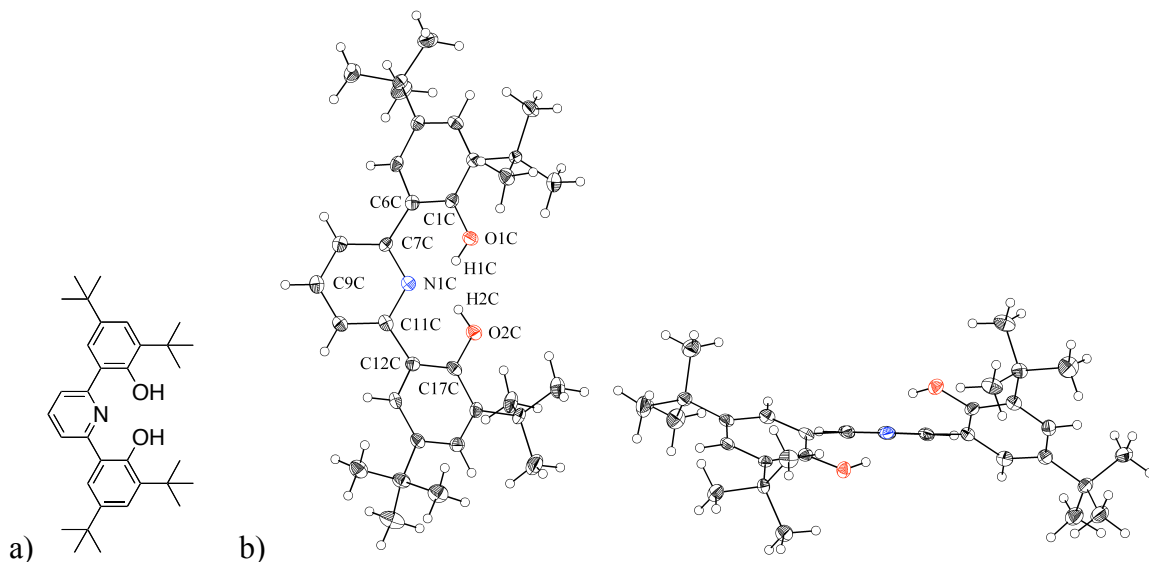
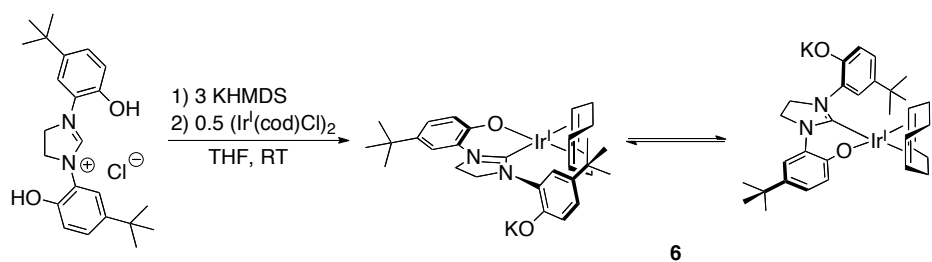


**Figure 4.1.** Illustration (a) and structural drawings (b) of **5a**. Displacement ellipsoids are drawn at the 50% probability level. The positions of the hydrogen atoms were calculated from geometrical considerations. The unit cell contains two more molecules of **5a**. Selected bond lengths (Å) and angles (°): C1C-O1C 1.366(3); C17C-O2C 1.378(3); O1C-N1C 2.629(3); O2C-N1C 2.704(3); N1C-C7C-C6C-C1C -27.61(36); N1C-C11C-C12C-C17C -38.28(36); C1C-O1C-O2C-C17C -127.61(20).



**Scheme 4.6.** Metallation of **2a** to generate **6**.

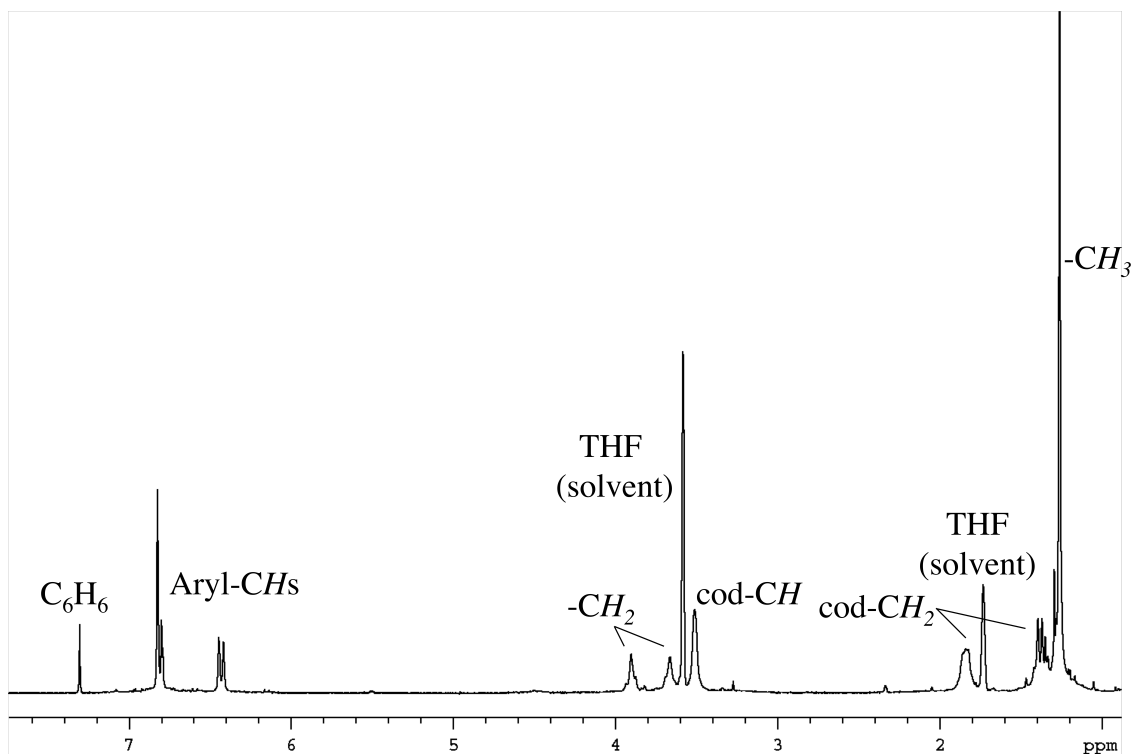


**Figure 4.2.**  $^1\text{H}$  NMR spectrum of **6** in  $\text{THF-d}_8$ . Note some benzene was isolated with **6**, and it is present in solution. Also, the “- $\text{CH}_3$ ” peak is truncated as it has a much greater intensity than the other peaks.

**2** is one of only a few diphenolate imidazolyl-carbenes that have been synthesized.<sup>28-31</sup> It has improved thermal stability over previously synthesized diphenolate imidazolyl-carbenes that have a methylene group bridging each phenolate to the imidazolyl ring (scheme 4.4).<sup>30</sup> Imidazolium salts such as **3a** require deprotonation and metallation at  $-78\text{ }^\circ\text{C}$ , while **2a** can be deprotonated and metallated at room temperature.<sup>30</sup> **6** is the first iridium complex with a diphenolate imidazolyl-carbene ligand to be isolated, and the crystal structure of **6** with 18-crown-6 ether is the first example of an iridium(I) complex with a pendant, non-binding phenolate or alkoxide.

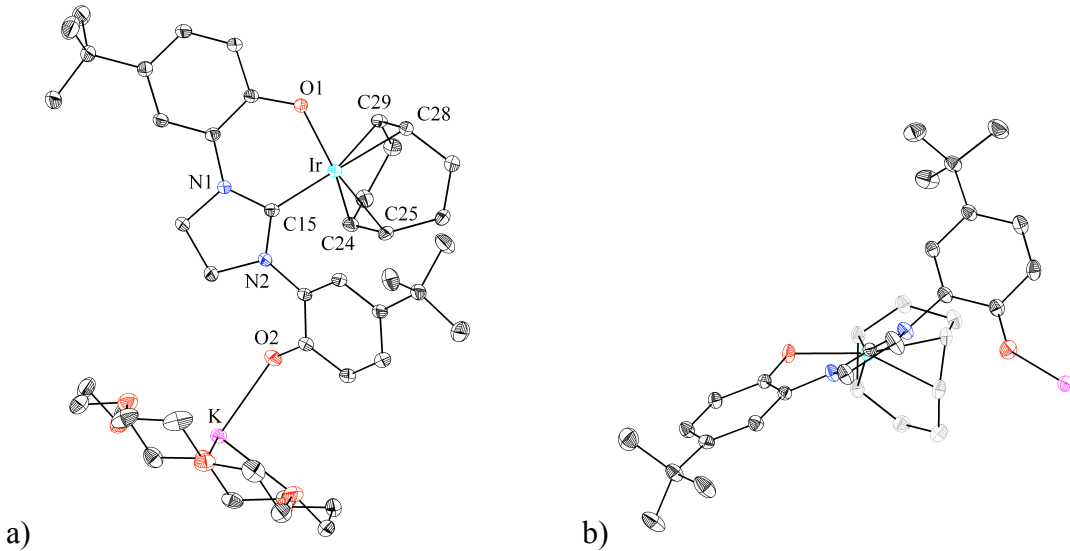


**Figure 4.3.** Structural drawing of **6** with 18-crown-6 ether coordinating to potassium. Displacement ellipsoids are drawn at the 50% probability level. A molecule of benzene is in the unit cell, but it is not shown here. (a) Perspective taken perpendicular to the square plane of the complex. (b) Perspective taken facing down the C15–Ir bond, and the 18-crown-6 ether was removed for clarity. Selected bond lengths (Å) and angles (°): Ir–C15 2.041(3); Ir–O1 2.0423(19); Ir–C(24) 2.093(3); Ir–C25 2.145(3); Ir–C28 2.159(3); Ir–C29 2.174(3); N1–C15 1.369(4); N2–C15 1.348(4); O2–K 2.576(2); C15–Ir–O1 87.56(10); C15–Ir–C24 93.31(12); O1–Ir–C24 153.01(11); C15–Ir–C25 100.71(10); C15–Ir–C25 39.06(12); C15–Ir–O1 87.56(10); C15–Ir–C24 93.31(12); O1–Ir–C24 153.01(11); C15–Ir–C25 100.71(12); O1–Ir–C25 165.77(10); C24–Ir–C25 39.06(12); C15–Ir–C28 164.27(12); O1–Ir–C28 88.10(10); C24–Ir–C28 97.40(12); C25–Ir–C28 80.84(11); C15–Ir–C29 156.85(12); O1–Ir–C29 86.99(10); C24–Ir–C29 81.68(12); C25–Ir–C29 89.62(12); C28–Ir–C29 37.61(12).

Similar NMR spectra were obtained for **6** with 18-crown-6 ether in THF-d<sub>8</sub> and in C<sub>6</sub>D<sub>6</sub>, as well as for **6** in the absence of 18-crown-6 ether in THF-d<sub>8</sub>, in CD<sub>3</sub>CN, and in DMSO-d<sub>6</sub>. One set of peaks is observed in the <sup>1</sup>H NMR (fig. 4.2) for both phenolates, and only three peaks are observed for the cyclooctadiene. Two peaks are observed for the two -CH<sub>2</sub> groups in the imidazolyl ring. These were assigned after a 2D-COSY <sup>1</sup>H NMR spectrum was used to identify the three cyclooctadiene peaks. The one-dimensional <sup>1</sup>H NMR experiment was repeated at various temperatures between -70 and 60 °C. All the peaks broaden significantly below -40 °C. Between -40 and -70 °C, the two imidazolyl -CH<sub>2</sub> peaks coalesce, and the cyclooctadiene -CH peak splits. In the <sup>13</sup>C NMR spectrum at ambient temperature, only one peak appears for the -CH<sub>2</sub> groups, and one set of peaks appears for both phenolates and for cyclooctadiene. It should be noted that the -CH peak of cyclooctadiene is not observed in the <sup>13</sup>C NMR spectrum because it overlaps with the THF solvent peak at 67.45 ppm (referenced to the other THF peak at 25.37 ppm), and this was confirmed by <sup>1</sup>H-<sup>13</sup>C HMQC.<sup>33,34</sup>

Determination of the solution-phase structure of **6** has proven difficult. The solid-state structure of **6** with 18-crown-6 ether is not static in solution as two sets of peaks would be expected for the phenolates, and six peaks would be expected for the cyclooctadiene. Two isomers of **6** could be in equilibrium as depicted in scheme 4.6. Unfortunately, it is still not clear why two peaks are observed in the <sup>1</sup>H NMR spectra for the imidazolyl -CH<sub>2</sub> groups. This would seem to indicate that rotation about the nitrogen-phenolate bonds is slower than conversion between the two isomers shown in scheme 4.6;<sup>35</sup> however, it is not apparent why the two imidazolyl -CH<sub>2</sub> peaks converge around -70 °C. Slow rotation about the nitrogen-phenolate bonds at room temperature

should also cause the three cyclooctadiene  $^1\text{H}$  NMR peaks to split into six peaks. While only three peaks are observed for cyclooctadiene, this explanation may still be valid because these peaks are relatively broad.

Understanding the solution-phase chemistry of **6** is complicated by the fact that its  $^1\text{H}$  NMR spectrum is significantly different at high concentrations, in  $\text{C}_6\text{D}_6$ , and in methanol- $\text{d}_4$ . Both in  $\text{C}_6\text{D}_6$  and at high concentrations in  $\text{THF-d}_8$  the  $^1\text{H}$  NMR peaks for **6** in the absence of 18-crown-6 ether broaden significantly. This is possibly indicative of the equilibrium, shown in scheme 4.6, being slowed down by intermolecular interactions between iridium complexes. Dimers of a similar (1,5-cyclooctadiene)iridium(I) complex, containing a diphenolate pyridine ligand with a sodium counterocation and depicted in figure 4.4 have been synthesized and crystallized by Ross Fu from non-polar solvents.<sup>36</sup> In these dimers, a pendant phenoxide from each iridium center bridges the two sodium counterocations. In  $\text{C}_6\text{D}_6$ , this interaction could be disrupted in the presence of 18-crown-6 ether as indicated by sharpening of the  $^1\text{H}$  NMR peaks for **6**.

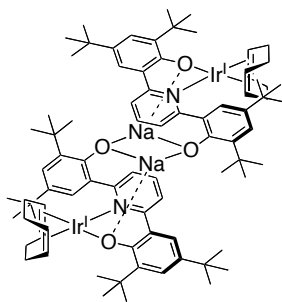


**Figure 4.4.** A dimer, synthesized and crystallized by Ross Fu, of (1,5-cyclooctadiene)iridium(I) centers each containing a diphenolate pyridine ligand with a sodium countercation.<sup>36</sup>

The  $^1\text{H}$  NMR spectrum of **6** in methanol-d<sub>4</sub>, shown in fig. 5, is similar to the spectrum of **6** in THF-d<sub>8</sub>; however, there are two -CH peaks and four -CH<sub>2</sub> peaks for cyclooctadiene bound to iridium(I). The rest of the peaks are fairly sharp with one set of peaks for the phenolates and two imidazolyl -CH<sub>2</sub> peaks. Removal of methanol and dissolution in THF-d<sub>8</sub> simply leads back to a spectrum resembling the one shown in figure 4.2.

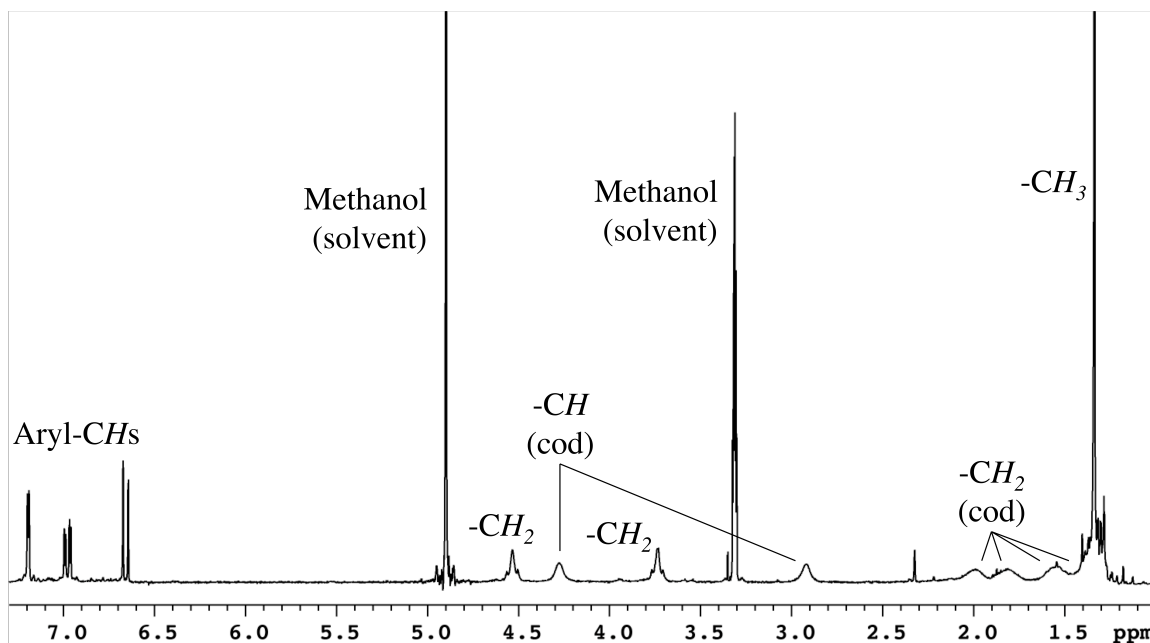
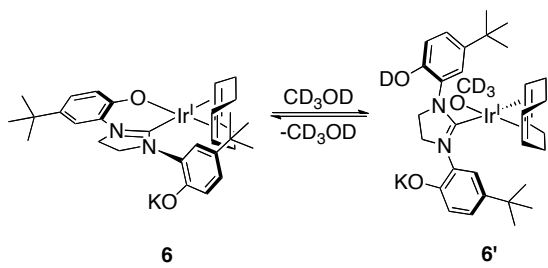


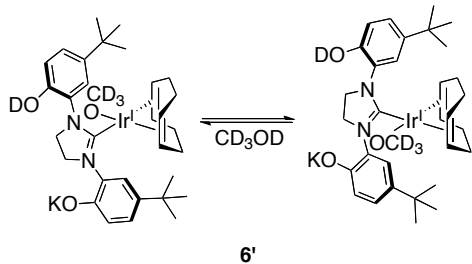
**Figure 4.5.**  $^1\text{H}$  NMR spectrum of **6** in methanol-d<sub>4</sub>. The methanol peak at 4.90 ppm and the “-CH<sub>3</sub>” peak are truncated.

It is unclear why in methanol-d<sub>4</sub> the  $^1\text{H}$  NMR peaks for coordinated cyclooctadiene split into two sets. Simple phenoxide stabilization by the protic solvent, decreasing the rate of isomerization is unlikely since two sets of peaks for the phenolates would also be expected. It is possible that reversible protonation of a phenolate leads to a

methoxoiridium(I) complex (**6'**) as illustrated in scheme 4.7. While the  $pK_a$  of methanol should be much higher than that of the phenol, this should be compensated for by the formation of a bond between iridium and methoxide and by the high concentration of methanol; thus, it is possible that **6'** is the major species in solution, and it gives rise to the  $^1H$  NMR spectrum shown in figure 4.5. This structure would explain why only a protic solvent gives rise to six peaks for iridium-coordinated cyclooctadiene. An isomerization similar to the one depicted in scheme 4.8 might be expected in which the bound methoxide is protonated and displaced by a molecule of methanol in solution. This type of isomerization could equivalence the two sets of cyclooctadiene peaks in a similar manner to the isomerization proposed for **6** in THF and shown in scheme 4.6; however, this isomerization must be relatively slow on the NMR time scale as it would lead to only three peaks for iridium-coordinated cyclooctadiene. The carbene may only shift to a position *trans* to the other olefin of cyclooctadiene in the phenolate isomerization (scheme 4.6) because the non-ligating phenolate is positioned to effect this isomerization by being on the other side of the carbene. Further studies need to be performed in order to confirm these hypotheses on the solution-phase structure of **6** and on its solvent dependence.



**Scheme 4.7.** Reversible formation of **6'** in methanol-d<sub>4</sub>.



**Scheme 4.8.** A possible isomerization of **6'** in methanol-d<sub>4</sub> that is not observed.

An interesting result was obtained when attempts were made to grow crystals of **6** following salt metathesis with bis(triphenyl-phosphoranylidene)ammonium ( $[\text{PPN}]^+$ ) chloride. **6** reacted slowly with PPN to generate crystals of  $\mu$ -(amidotriphenylphosphorus)- $\mu$ -hydroxobis((1,5-cyclooctadiene)iridium(I)) (**7**) and bis(triphenylphosphoranylidene)ammonium bis{1,3-di(2-hydroxy-5-*tert*-butylphenyl)imidazolyl} iridium(III) (**8**), the structures of which are shown in figures 4.6 and 4.7, respectively. Although the crystal structure of **8** is of poor quality, it is of interest because it shows that **2** can bind facially; there are relatively few examples of facial coordination for similar diphenolate pincer ligands.<sup>37-39</sup> The crystal structure of **7** is the first of an iridium-ligated phosphoraniminate, and **7** is the first example of a phosphoraniminate ligand bridging two iridium centers. The phosphorus-nitrogen bond length for **7** (1.551(11) Å) is characteristic of a phosphorus-nitrogen double bond.<sup>40</sup>

$[\text{PPN}]^+$  has been shown previously to react with alkoxides and hydroxides to generate  $\text{Ph}_2\text{P}(\text{O})\text{NPPPh}_3$ , a small amount of triphenylphosphine oxide, and some other unidentified products.<sup>41</sup> The presence of triphenylphosphine oxide indicates cleavage of the phosphorus-nitrogen bond although the nitrogen-containing product was not identified. A similar reaction with the non-ligating phenoxide of **6** could explain the

generation of the bridging triphenylphosphoraniminate ligand in **7**. Contamination of the sample with water or dioxygen could account for the bridging hydroxide. The generation of **8** requires an oxidant; so, this could also be accounted for by contamination with dioxygen.

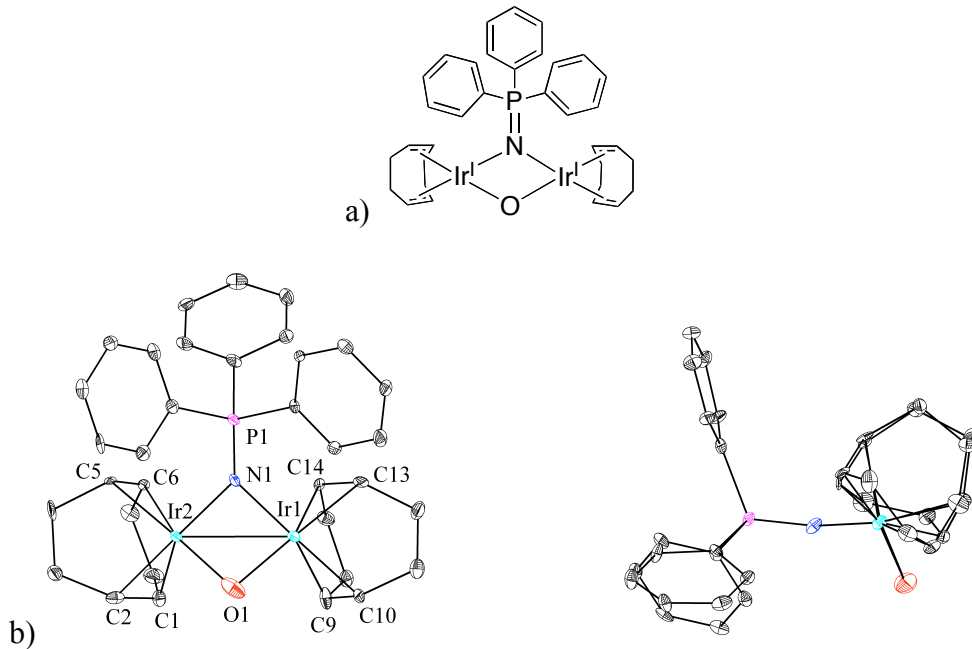


**Figure 4.6.** Illustration (a) and structural drawings (b) of **7** with displacement ellipsoids drawn at the 50% probability level. Selected bond lengths ( $\text{\AA}$ ) and angles ( $^\circ$ ): Ir1-N1 2.069(10); Ir1-C9 2.071(14); Ir1-C10 2.088(12); Ir1-O1 2.093(9); Ir1-C14 2.112(12); Ir1-C13 2.127(12); Ir1-Ir2 2.7709(9); Ir2-C1 2.067(13); Ir2-O1 2.076(11); Ir2-C5 2.089(11); Ir2-C6 2.093(11); Ir2-C2 2.096(11); Ir2-N1 2.098(10); P1-N1 1.551(11); P1-C23 1.807(15); P1-C29 1.823(12); P1-C17 1.842(14); P1-N1-Ir1 137.9(6); P1-N1-Ir2 137.1(6); Ir1-N1-Ir2 83.4(4); Ir2-O1-Ir1 83.3(4).

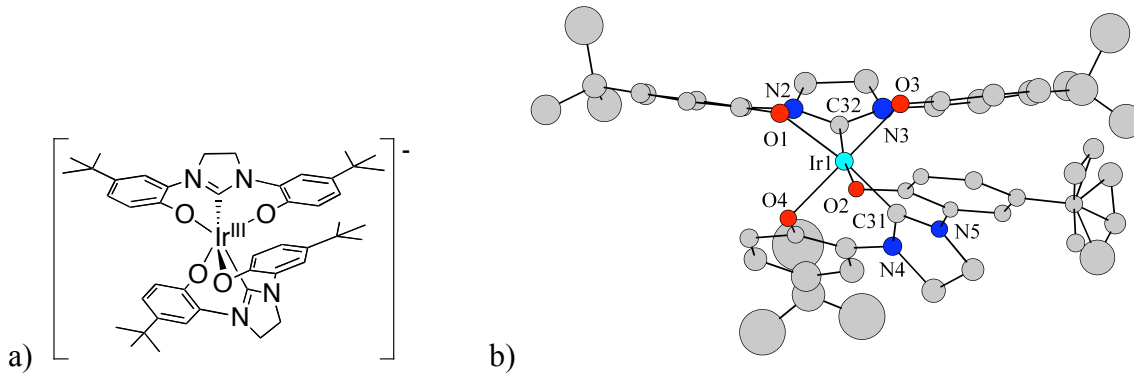
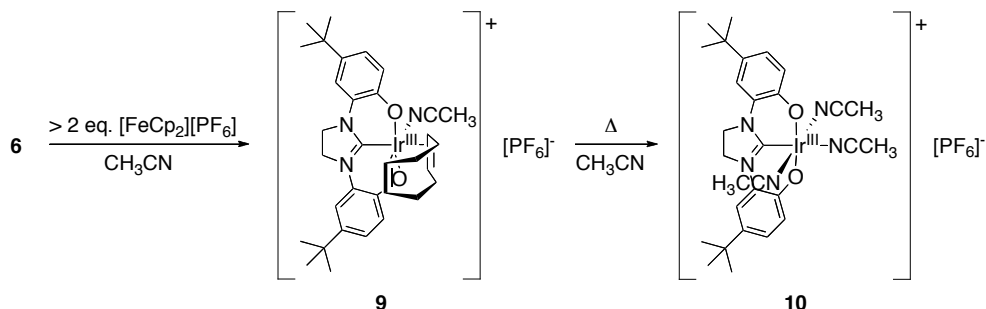


**Figure 4.7.** Illustration (a) and structural drawing (b) of **8**.  $[\text{PPN}]^+$  and solvent fragments have been removed for clarity. Disorder in the *tert*-butyl groups should be noted.

**Synthesis and chemistry of iridium(III) complexes.** In acetonitrile, **6** was fairly cleanly oxidized to (acetonitrile)(1,5-cyclooctadiene){1,3-di(2-hydroxy-5-*tert*-butylphenyl)imidazolyl}iridium(III) hexafluorophosphate (**9**) using ferrocenium(III) hexafluorophosphate as illustrated in scheme 4.9. This complex was characterized by  $^1\text{H}$ ,  $^{13}\text{C}$ ,  $^{31}\text{P}$ , and  $^{19}\text{F}$  NMR spectroscopy as well as fast atom bombardment (FAB+) high resolution mass spectrometry (HRMS). In the  $^1\text{H}$  NMR spectrum, there is one set of peaks for the two phenolates; there are two peaks for the  $-\text{CH}_2$  groups of the imidazolyl ring; and, there are six peaks for iridium-coordinated cyclooctadiene. The peaks for coordinated cyclooctadiene are shifted significantly downfield from their positions in **6**. Based on the NMR data and the observance of the molecular ion in the mass spectrum, **9** was identified as an octahedral iridium (III) complex with the diphenolate carbene ligand bound meridionally.

Simply heating **9** at 90 °C in acetonitrile results in the displacement of cyclooctadiene by acetonitrile to generate tris(acetonitrile){1,3-di(2-hydroxy-5-*tert*-butylphenyl)imidazolyl}iridium(III) hexafluorophosphate (**10**) as shown in scheme 4.9.

Free cyclooctadiene is observed when the reaction is performed in  $\text{CD}_3\text{CN}$ . When **10** is generated in  $\text{CH}_3\text{CN}$ , isolated, and then redissolved in  $\text{CD}_3\text{CN}$ , the two peaks for iridium-coordinated  $\text{CH}_3\text{CN}$  appear in the  $^1\text{H}$  NMR spectrum at 2.53 and 2.68 ppm with an approximate ratio of 2:1. These peaks are not present when **10** is generated in  $\text{CD}_3\text{CN}$ . Furthermore, these peaks disappear over time in  $\text{CD}_3\text{CN}$ , while the peak for uncoordinated  $\text{CH}_3\text{CN}$  at 1.97 increases by approximately the same amount. Mass spectrometry confirmed the assignment of **10** as tris(acetonitrile){1,3-di(2-hydroxy-5-*tert*-butylphenyl)imidazolyl}iridium(III) hexafluorophosphate (scheme 4.9). The fact that cyclooctadiene can simply be displaced from **9** by acetonitrile indicates weak binding to iridium(III) by cyclooctadiene.



**Scheme 4.9.** The synthesis of **9** and **10** from **6**.

**9** reacts with dihydrogen to generate cyclooctane at room temperature in THF under 1 atm of dihydrogen. This leads to a species that catalyzes the hydrogenation of cyclohexene to cyclohexane. In order to monitor the reaction, catalytic hydrogenation of cyclohexene was performed under 900 psi of dihydrogen in a high pressure sapphire NMR tube. The concentrations of cyclohexene, cyclohexane, and dihydrogen in solution were monitored by  $^1\text{H}$  NMR spectroscopy, and the results are plotted in figure 4.8. As

shown by the graph in figure 4.8a, diffusion of dihydrogen from the gas phase into solution was slow, and the concentration of dihydrogen in solution was lower than the concentration of olefin. Surprisingly, the disappearance of cyclohexene and the generation of cyclohexane still followed a first-order dependence on cyclohexene concentration (figure 4.8b). This seems to indicate a zero-order dependence on dihydrogen concentration, meaning that reaction of the catalyst with dihydrogen is much faster than reaction of the catalyst with cyclohexene; however, further studies need to be performed in order to confirm this preliminary result.

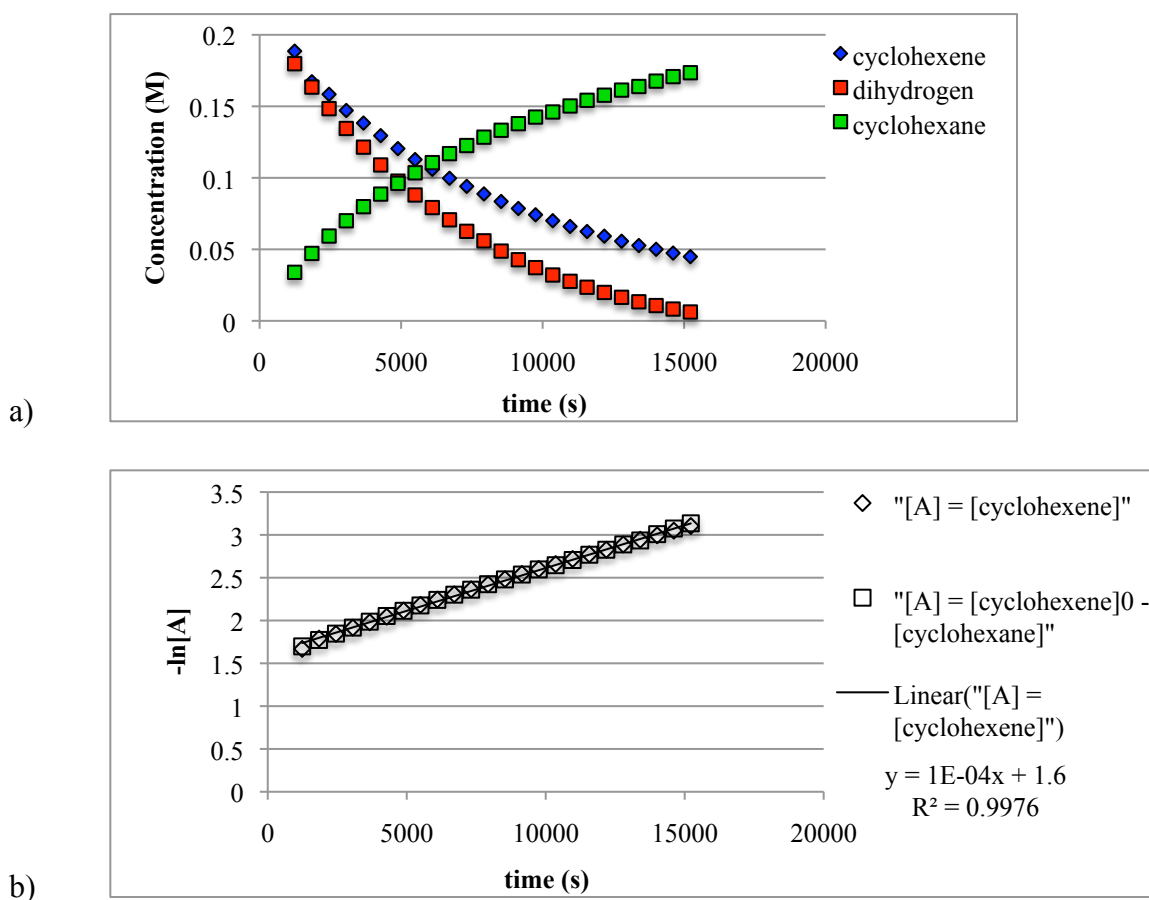


**Figure 4.8.** Catalysis of cyclohexene hydrogenation using catalyst precursor **9** in THF-d<sub>8</sub> under 900 psi of dihydrogen. a) Plot of cyclohexene, cyclohexane, and dihydrogen concentrations vs. time. b) The first-order dependence of the reaction on cyclohexene

concentration as determined both from cyclohexene disappearance ( $[A] = [\text{cyclohexene}]$ ) and from cyclohexane appearance ( $[A] = [\text{cyclohexene}]_0 - [\text{cyclohexane}]$ ). It should be noted that  $[\text{cyclohexene}]_0$  represents the initial concentration of cyclohexene.

While further studies need to be performed in order to determine the exact rate of catalysis, a minimum first-order rate constant for hydrogenation of cyclohexene can be approximated at  $1 \times 10^{-4} \text{ s}^{-1}$  (figure 4.8b). This rate is fairly low in comparison to many other iridium-catalyzed olefin hydrogenations, but most other iridium-catalyzed hydrogenations involve either an iridium(I) catalyst precursor or a dihydridoiridium(III) catalyst precursor.<sup>42-45</sup> While generation of an iridium(I) complex or a dihydridoiridium(III) complex from **9** is unlikely to occur at least initially, **9** may be converted to a monohydrido iridium(III) complex by displacement of acetonitrile with dihydrogen, followed by deprotonation with a coordinated phenoxide. Similar monohydrido iridium(III) complexes have been generated by coordination of dihydrogen and subsequent deprotonation; furthermore, some of these monohydrido iridium(III) complexes have proved to be competent precursors to hydrogenation catalysts.<sup>45-49</sup>

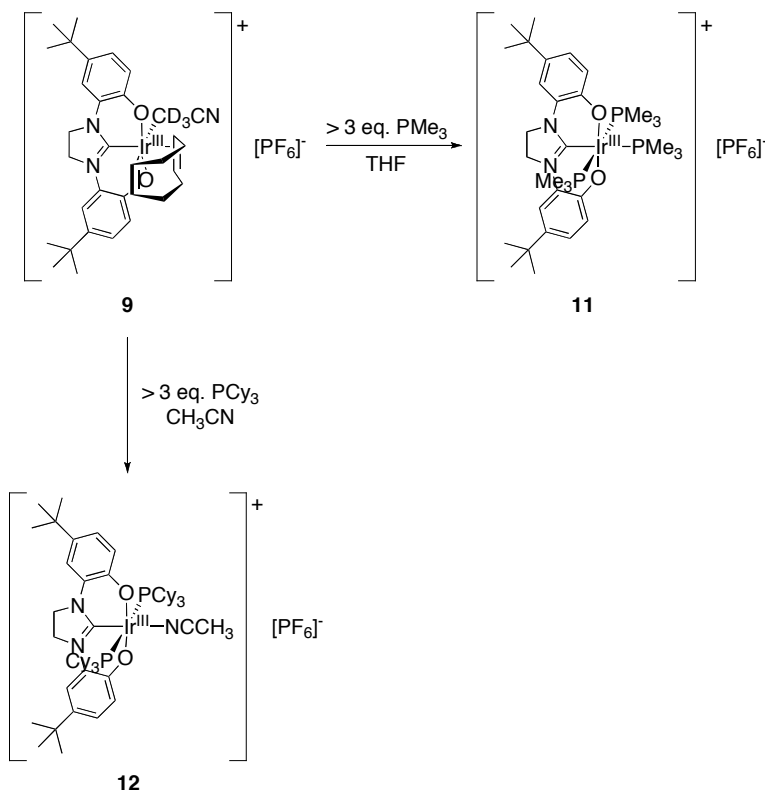
In an attempt to determine the fate of iridium in hydrogenations with **9**, **9** was dissolved in THF-d<sub>8</sub> and sealed in a J-Young NMR tube at room temperature under 1 atm of dihydrogen (the ratio of H<sub>2</sub> to **9** in the tube was approximately 10:1). By <sup>1</sup>H NMR spectroscopy, only trace amounts of cyclooctene were ever observed; no iridium-hydride signals were observed; and, only broad peaks were observed for the diphenolate carbene ligand. When the solvent and other volatiles were then removed under reduced pressure and the resulting solid was heated in CD<sub>3</sub>CN at 90 °C, **10** was generated. The generation

of **10** seems to indicate that the diphenolate imidazolyl-carbene ligand remains bound to iridium throughout the catalysis; however, it is still unclear what other ligands are bound to iridium during the catalysis. While iridium hydrides were not observed during hydrogenation, it is still possible that they are generated in small amounts or that they react rapidly. Furthermore, it would be difficult to observe an iridium hydride due the broadening which occurs for the peaks of the other ligands bound to iridium.

In order to further probe the coordination environment of the diphenolate carbene iridium(III) complexes, **9** was reacted, in separate experiments, with trimethylphosphine and tricyclohexylphosphine as shown in scheme 4.10. In each case, greater than three equivalents of phosphine were used. Based on  $^1\text{H}$  NMR spectroscopy, the reactions occurred slowly at room temperature, but they went to completion when heated for greater than 12 hours at 90 °C. During this time, cyclooctadiene was cleanly displaced from the metal center. In the reaction with trimethylphosphine, three equivalents of phosphine reacted to generate tris(trimethylphosphine){1,3-di(2-hydroxy-5-*tert*-butylphenyl)imidazolyl}iridium(III) hexafluorophosphate (**11**) as shown in scheme 4.10; however when greater than three equivalents of tricyclohexylphosphine were reacted with **9**, only two equivalents of phosphine bound to the metal center, resulting in the formation of (acetonitrile)bis(tricyclohexylphosphine){1,3-di(2-hydroxy-5-*tert*-butylphenyl)imidazolyl}iridium(III) hexafluorophosphate (**12**) (scheme 4.10).

With respect to **12**, only one singlet is observed for the coordinated tricyclohexylphosphines in the  $^{31}\text{P}$  NMR spectrum, and only one set of peaks is observed in the  $^1\text{H}$  NMR spectrum for both phenolates. Taken together, this data indicates that the tricyclohexylphosphine ligands bind *trans* to each other, while the diphenolate carbene is

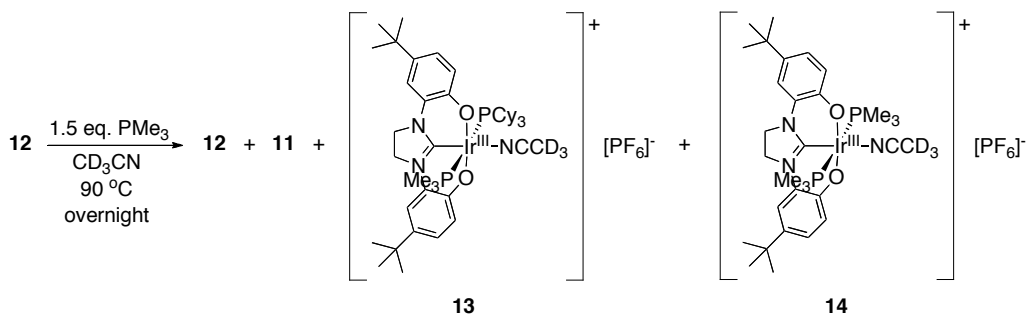
bound meridionally as shown in scheme 4.10. The  $^1\text{H}$  NMR spectrum of **11** also contains only one set of peaks for both phenolates, but the  $^{31}\text{P}$  NMR spectrum of **11** contains a doublet and a triplet with a 2:1 ratio of intensities. The identity of each complex was confirmed by high resolution mass spectrometry (FAB $^+$ ), and an elemental analysis was obtained for **12**.



**Scheme 4.10.** Displacements of cyclooctadiene from **9** with trialkylphosphines.

**12** was reacted with 1.5 equivalents of trimethylphosphine in order to probe the steric requirements for coordination *trans* to the carbene. After heating the reaction for approximately 12 hours at 90 °C, a mixture of iridium(III) phosphine complexes was generated as indicated by  $^{31}\text{P}$  NMR spectroscopy (scheme 4.11). **11** and unreacted **12**

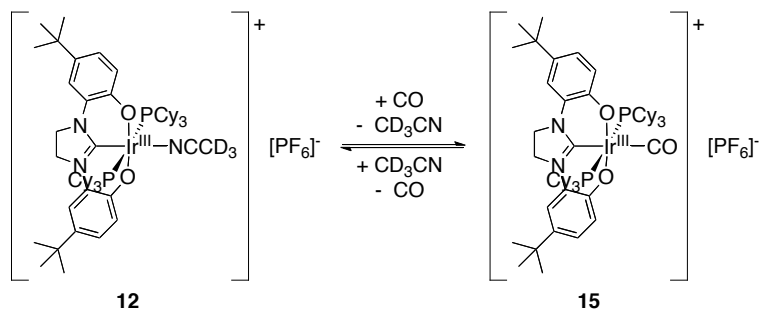
were present in this mixture as well as (acetonitrile)(tricyclohexylphosphine)-(trimethylphosphine){1,3-di(2-hydroxy-5-*tert*-butylphenyl)imidazolyl}iridium(III) hexafluorophosphate (**13**) and (acetonitrile)bis(trimethylphosphine){1,3-di(2-hydroxy-5-*tert*-butylphenyl)imidazolyl}iridium(III) hexafluorophosphate (**14**) which were tentatively identified based on the  $^{31}\text{P}$  NMR spectrum. The only triplet in the  $^{31}\text{P}$  NMR spectrum belonged to **11**. This indicates that significant amounts of bis(tricyclohexylphosphine)(trimethylphosphine){1,3-di(2-hydroxy-5-*tert*-butylphenyl)imidazolyl}iridium(III) hexafluorophosphate were not generated, likely due to the imposition of substantial steric constraints by the tricyclohexylphosphine ligands.



**Scheme 4.11.** The reaction of **12** with 1.5 equivalents of trimethylphosphine.

**12** was reacted with carbon monoxide in order to probe electronic effects on ligands binding *trans* to the carbene. In acetonitrile, an equilibrium mixture of **12** and (carbon monoxide)bis(tricyclohexylphosphine){1,3-di(2-hydroxy-5-*tert*-butylphenyl)imidazolyl}iridium(III) hexafluorophosphate (**15**) (scheme 4.12) forms over the course of about 3 days when the reaction is performed at  $90^\circ\text{C}$  under approximately 2.8 mL of carbon monoxide at 1.3 atm. The maximum ratio of **12** to **15** in solution is approximately 2:1. **15** is converted back to **12** when the solution is degassed and

reheated to 90 °C. This indicates that generation of **15** from **12** is reversible at 90 °C. Determination of an equilibrium constant is complicated by the formation of yellow crystals above the surface of the solution during the reaction. Single crystal X-ray diffraction indicated that these crystals contain a 4:1 mixture of **12** and **15** (figure 4.9). Both complexes have the diphenolate carbene ligand coordinated meridionally with the tricyclohexylphosphine ligands *trans* to each other as depicted in figure 4.9. It should be noted that the diphenolate carbene ligand is relatively planar in this structure with a C<sub>ipso</sub>-O1-O2-C<sub>ipso</sub> torsion angle of only 2.9°. **9** was also reacted with carbon-<sup>13</sup>C monoxide to confirm the solution-phase geometry of **15** and to check for an isotope shift in the infrared spectrum. The resulting iridium(III)complex containing carbon-<sup>13</sup>C monoxide (**15'**) displays a triplet in the <sup>13</sup>C NMR spectrum and a doublet in the <sup>31</sup>P NMR spectrum as expected. The infrared CO-stretching frequency of **15** is 2064 cm<sup>-1</sup>; and as expected, an isotopic shift is observed for **15'**, which has a <sup>13</sup>CO-stretching frequency of 2016 cm<sup>-1</sup> (2018 cm<sup>-1</sup> calculated).



**Scheme 4.12.** Equilibrium between **12** and **15** which occurs in acetonitrile at 90 °C under an atmosphere of carbon monoxide.

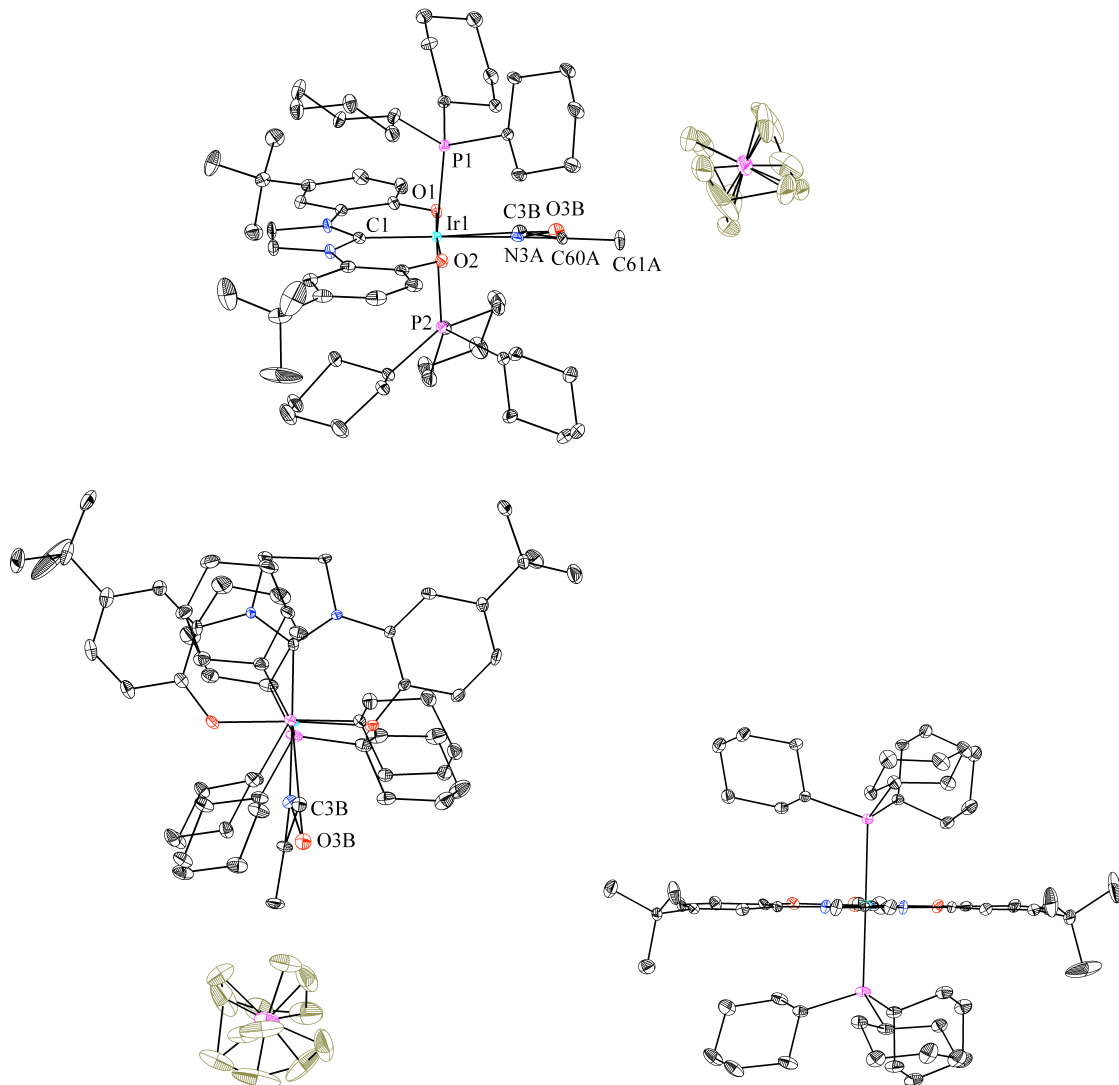


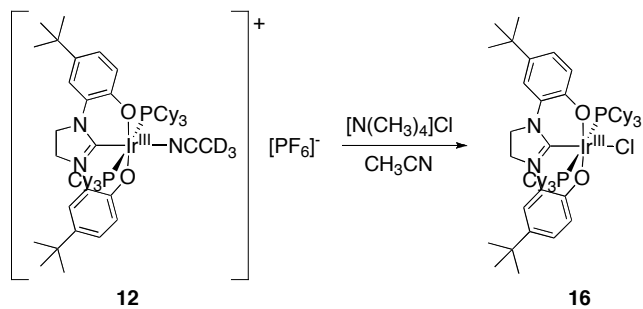
**Figure 4.9.** Structural drawings obtained from the crystals containing an approximately 4:1 mixture of **12** and **15**. Displacement ellipsoids are drawn at the 50% probability level.  $[\text{PF}_6]^-$  has been removed from the bottom-right structure. In the unit cell, there is a 78% occupancy of positions N3A, C60A, and C61A of **12** and a 22% occupancy of positions C3B and O3B of **15**. The  $\text{C}_{\text{ipso}}\text{-O1-O2-C}_{\text{ipso}}$  torsion angle is  $2.9^\circ$ . Selected bond lengths ( $\text{\AA}$ ) and angles ( $^\circ$ ): Ir1-C1 1.9694(19); Ir1-O2 2.0331(14); Ir1-O1 2.0390(13); Ir1-N3A 2.055(8); Ir1-C3B 2.14(4); Ir1-P2 2.4348(5); Ir1-P1 2.4437(5); C1-Ir1-O2 91.57(8); C1-Ir1-O1 92.21(7); O2-Ir1-O1 176.10(5); C1-Ir1-N3A 178.8(2); O2-Ir1-N3A 87.8(2);

O1-Ir1-N3A 88.5(2); C1-Ir1-C3B 174.1(10); O2-Ir1-C3B 94.4(10); O1-Ir1-C3B 81.9(10); N3A-Ir1-C3B 6.7(12); C1-Ir1-P2 92.79(6); O2-Ir1-P2 91.00(5); O1-Ir1-P2 89.77(4); N3A-Ir1-P2 86.2(2); C3B-Ir1-P2 87.5(11); C1-Ir1-P1 94.97(6); O2-Ir1-P1 89.17(5); O1-Ir1-P1 89.56(4); N3A-Ir1-P1 86.0(2); C3B-Ir1-P1 84.8(11); P2-Ir1-P1 172.229(16); Ir1-C3B-O3B 178(4); Ir1-N3A-C60A 175.1(7); N3A-C60A-C61A 177.1(7); C<sub>ipso</sub>-O1-O2-C<sub>ipso</sub> -2.71(22).

While the infrared CO-stretching frequency is within the range of other cationic diphosphine iridium(III) carbonyl complexes,<sup>50-52</sup> it is toward the upper end of the normal range for transition metal carbonyl complexes (1820-2150 cm<sup>-1</sup>).<sup>45</sup> This is indicative of relatively weak  $\pi$ -donation from iridium to the carbonyl  $\pi^*$ -orbital, and this is consistent with the fact that the carbonyl- (**15**) and acetonitrile- (**12**) iridium(III) complexes are in equilibrium at elevated temperatures. While the crystal structure shown in figure 4.9 of **15** and **12** could provide additional insight into bonding between the iridium and the carbonyl, this analysis is precluded by inaccuracy in the bond lengths possibly due to only 22% occupancy of **15** in the unit cell.

Acetonitrile can also be displaced from **12** by chloride to generate the air-stable complex, (chloro)bis(tricyclohexylphosphine){1,3-di(2-hydroxy-5-*tert*-butylphenyl)imidazolyl}iridium(III) (**16**), as shown in scheme 4.13. Crystals of **16** were obtained from methylene chloride (CH<sub>2</sub>Cl<sub>2</sub>), and the structure, as determined by single crystal X-ray diffraction, is illustrated in figure 4.10. Two isomers of **16** (**16'** and **16''**) occupy the unit cell along with two molecules of methylene chloride. The metal center, the chloride, the two oxygens, and the carbene carbon lie approximately in one plane for

both isomers; however, the rings of the diphenolate imidazolyl ligand do not lie in this plane for either isomer. Instead, the diphenolate imidazolyl ligand is approximately C<sub>2</sub>-symmetric. In order to compare the degree to which the diphenolate imidazolyl ligand of each isomer is distorted from C<sub>2v</sub>-symmetry towards C<sub>2</sub>-symmetry, the C<sub>ipso</sub>-O1-O2-C<sub>ipso</sub> torsion angle can be compared. For **16'**, this angle is -15.72(26) $^{\circ}$ ; whereas for **16''**, this angle is 35.19(26) $^{\circ}$ . The diphenolate imidazolyl ligand of **16''** is thus significantly more distorted from C<sub>2v</sub>-symmetry than the corresponding ligand on **16'**. It should be noted though that there is some disorder in the crystal structure, and this could affect the observed angles; furthermore, differences between the two isomers may be caused to some extent by the packing of the molecules in the crystal. Still, each isomer is significantly distorted from C<sub>2v</sub> symmetry.



**Scheme 4.13.** Reaction of **12** with tetramethylammonium chloride to generate **16**.

Cyclic voltammograms of **16** have been obtained with 0.3 M tetrabutylammonium tetrafluoroborate ( $[\text{NBu}_4][\text{BF}_4]$ ) as the supporting electrolyte in  $\text{CH}_2\text{Cl}_2$ , THF, and dimethylformamide (DMF). In methylene chloride, two reversible oxidations are observed, as shown in figure 4.11. One occurs at -0.22 V ( $\Delta E_p = 98$  mV at a scan rate of 0.100 V/s), and the other occurs at 0.58 V ( $(\Delta E_p = 98$  mV at a scan rate of 0.100 V/s)). In

THF, oxidation waves are centered at approximately the same positions, but  $\Delta E_p$  increases to about 200 mV for each oxidation at a scan rate of 0.100 V/s; however,  $\Delta E_p$  for the ferrocene(II)/ferrocenium(III) couple is also about 200 mV. **16** was only sparingly soluble in DMF, and the wave for the second oxidation became only quasi-reversible. This was indicated by significantly less current being passed for the reduction peak relative to the oxidation peak. Furthermore, overlap of the first oxidation wave with the ferrocene(II)/ferrocenium(III) wave hampered an accurate measurement of its potential.

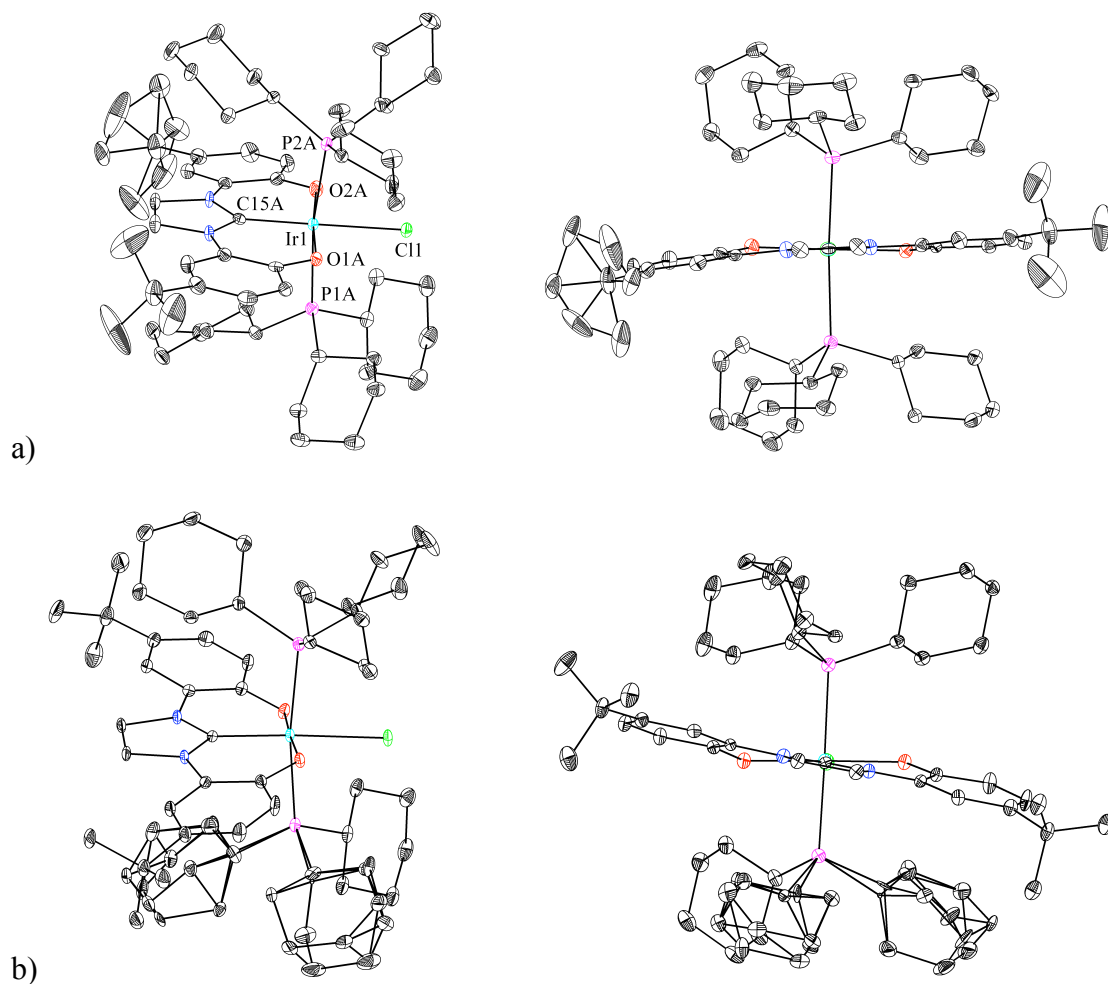


**Figure 4.10.** Structural drawing of the two conformers in the unit cell of **16** with displacement ellipsoids drawn at the 50% probability level. Two molecules of methylene

chloride are also in the unit cell. a) Isomer **16'** is shown. The perspective in the first view is directed approximately bisecting the P1A-Ir1-O1A angle; the perspective in the second view is directed down the C15A-Ir1 bond. The C<sub>ipso</sub>-O1-O2-C<sub>ipso</sub> torsion angle is -15.72(26)°. b) Isomer **16''** shown with approximately the same perspectives. The C<sub>ipso</sub>-O1-O2-C<sub>ipso</sub> torsion angle is 35.19(26)°.

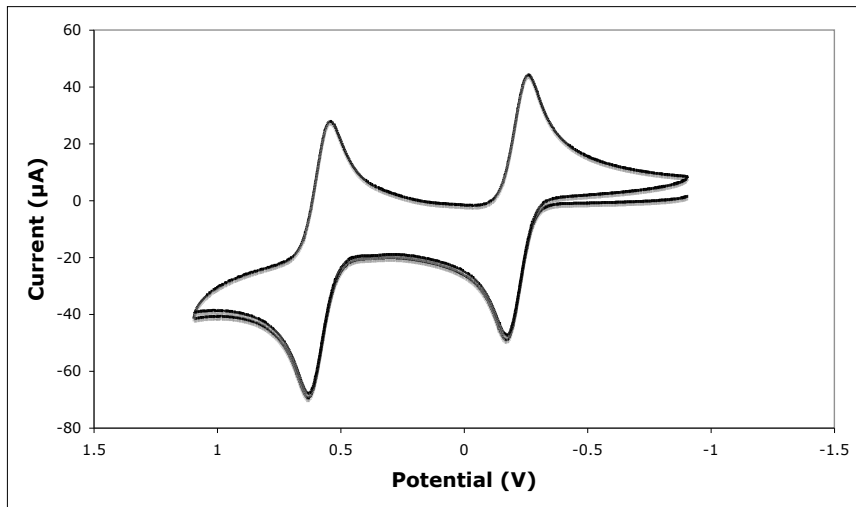


**Figure 4.11.** Cyclic voltammogram of a 3 mM CH<sub>2</sub>Cl<sub>2</sub> solution of **16** at a scan rate of 100 mV/s with 0.3 M [NBu<sub>4</sub>][BF<sub>4</sub>] as the supporting electrolyte.

Controlled potential electrolysis of **16** in CD<sub>2</sub>Cl<sub>2</sub> was used to determine how many electrons are involved per molecule of **16** in each oxidation. Coulometric oxidation of **16** at a potential positive of the first oxidation wave (0.25 V) resulted in the passage of 0.92 faradays per mole, indicating that the wave at -0.22 V corresponds to a one-electron oxidation of **16**. The controlled potential electrolysis was continued at a potential positive of the second wave (0.96 V), and this resulted in the passage of 0.99 faradays per mole, indicating that the wave at 0.58 V also corresponds to a one-electron oxidation.

In order to probe whether the diphenolate imidazolyl ligand of **16** is being oxidized, a cyclic voltammogram of **2** was obtained in DMF, and it is shown in figure 4.12. Two irreversible oxidations occur at 0.73 and 0.94 V. Even though the oxidations of **2** occur at significantly higher potentials than even the highest potential at which **16** is oxidized, oxidation of the diphenolate imidazolyl-carbene ligand cannot be ruled out in the oxidation of **16** because the metallated ligand is likely to have significantly different oxidation potentials from the triply protonated, non-ligated diphenol imidazolium chloride (**2**).<sup>53,54</sup>

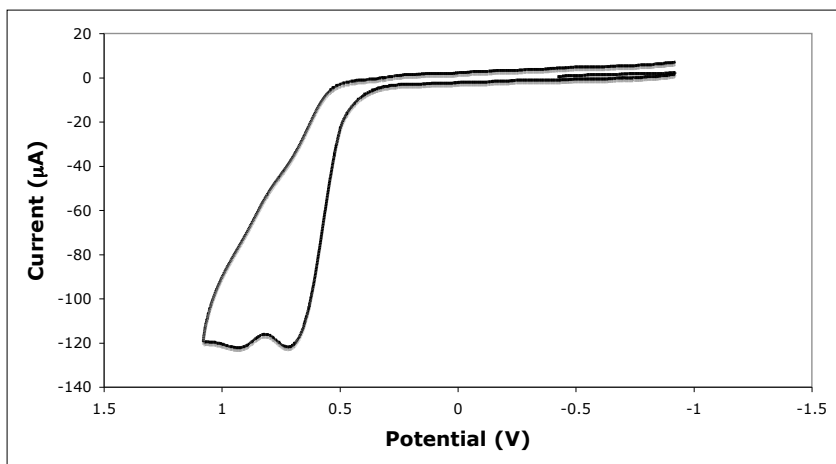


**Figure 4.12.** Cyclic voltammogram of a 0.3 mM DMF solution of **2** at a scan rate of 100 mV/s with 0.3 M  $[\text{NBu}_4][\text{BF}_4]$  as the supporting electrolyte.

EPR samples were obtained from the controlled potential electrolysis of **16**, both before and after the second oxidation. The sample obtained after the first oxidation of **16** had the EPR spectrum shown in figure 4.13. The EPR spectrum is indicative of an  $S = 1/2$  species with  $g_{\parallel} = 2.19$  and  $g_{\perp} \approx 1.94$ . It should be noted that at temperatures as low as 7 K, hyperfine splitting cannot be resolved. The same spectrum is obtained when

**16** is oxidized with less than one equivalent of ferrocenium(III) hexafluorophosphate. Mass spectroscopy of the EPR sample from the controlled potential electrolysis indicated a molecular ion with the mass of **16**.

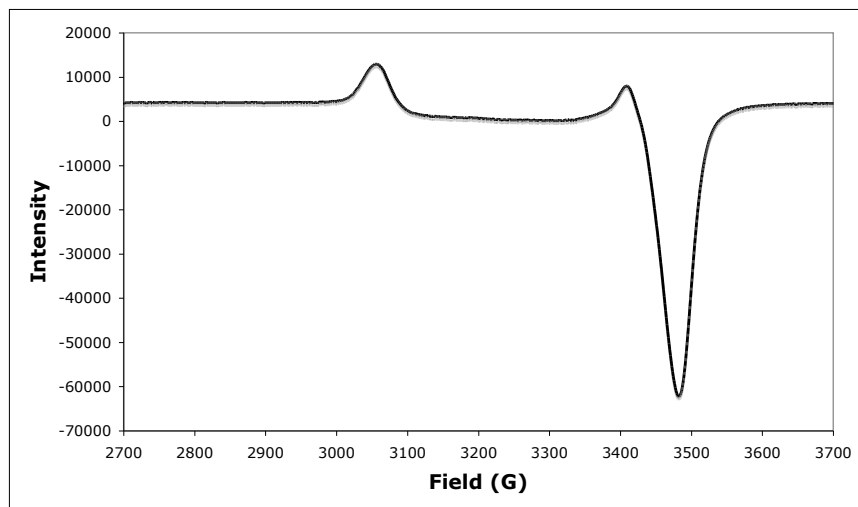


**Figure 4.13.** EPR spectrum at 7 K of the solution resulting from one coulometric oxidation (0.92 faradays per mole) of **16**.

After the second one-electron coulometric oxidation of **16** was completed, the resulting solution was analyzed by both EPR spectroscopy and  $^{31}\text{P}$  NMR spectroscopy. The EPR spectrum is shown in figure 4.14. It should be noted that it is unclear whether ferrocenium(III) hexafluorophosphate contributes to this spectrum; it is present in trace amounts because it was used as the sacrificial oxidant. Ferrocenium(III) hexafluorophosphate also has a peak in its EPR spectrum at approximately 1500 G; however, the rest of its spectrum at 18 K does not match the one shown in figure 4.14. Mass spectrometry of the EPR sample obtained from the second coulometric oxidation of **16** indicated a molecular ion with the mass of **16**. The dominant peak in the  $^{31}\text{P}$  NMR

spectrum was for hexafluorophosphate from the ferrocenium(III); however, three other peaks were present, and they appeared at 138.86, 130.71, and 31.08 ppm.

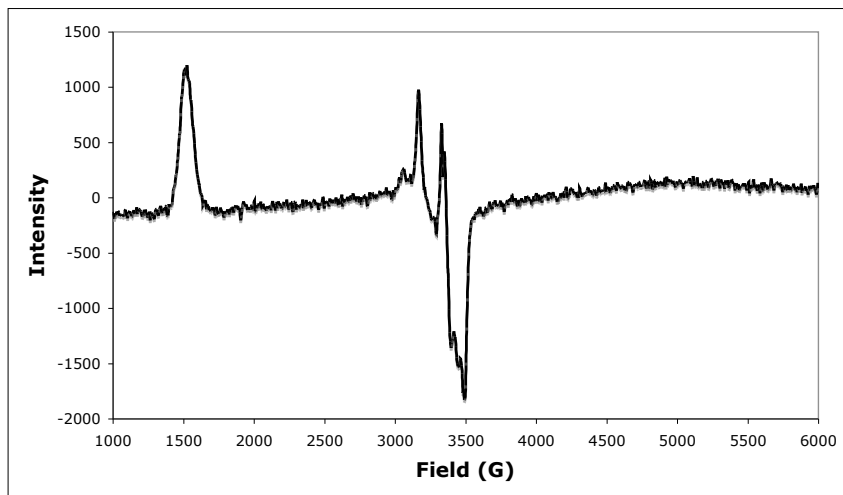


**Figure 4.14.** EPR spectrum at 18 K of the solution resulting from two coulometric oxidations (each approximately 1 faraday per mole) of **16**.

The one-electron oxidation product of **16** is likely  $[(\text{chloro})\text{bis}(\text{tricyclohexylphosphine})\{1,3\text{-di}(2\text{-hydroxy-5-}tert\text{-butylphenyl})\text{imidazolyl}\}\text{iridium}]^+$  (**16** $^+$ ) as evidenced by the reversible one-electron oxidation of **16** under electrochemical conditions, the generation of the same species by chemical oxidation with one equivalent of ferrocenium, and the observance of a mass corresponding to **16** $^+$  for this species. More than one possibility exists for the type of orbital in **16** from which the electron is removed to generate the relatively stable radical-cation, **16** $^+$ . The oxidation of iridium(III) complexes to generate iridium(IV) complexes and the oxidation of phenolates to generate phenoxyl radicals are both well precedented. While oxidations of iridium(III) to iridium(IV) and oxidations of phenolate ligands to

generate phenoxy radicals typically occur at potentials greater than the oxidation of **16** at -0.22 V, the oxidation of **16** falls within the range observed for both types of oxidation.<sup>53-64</sup> In the EPR spectrum, hyperfine coupling might be expected in either case because of spin coupling to the iridium nucleus (<sup>191</sup>Ir, 37%; <sup>193</sup>Ir, 63%; both  $I = 3/2$ ) and to the phosphorus nuclei (<sup>31</sup>P;  $I = 1/2$ ) or because of spin coupling to hydrogen (<sup>1</sup>H;  $I = 1/2$ ) and to nitrogen (<sup>14</sup>N, 99.635%;  $I = 1$ ; <sup>15</sup>N, 0.365%;  $I = 1/2$ ).<sup>55,65</sup> There is precedent, though, for iridium(IV) complexes in which the hyperfine splitting cannot be resolved at fairly low temperatures, and it is also possible that hyperfine coupling is not resolved due to a high degree of delocalization in the singly occupied orbital.<sup>63</sup> The  $g$ -values for the EPR spectrum are characteristic of a metal-centered radical as they differ significantly from the free electron value of 2.0023 and from values for previously characterized phenoxy radicals; however, this  $g$ -value could simply indicate some metal character in a singly occupied orbital that is delocalized over both the metal center and the ligands.<sup>53,60,65-67</sup>

With regards to the second one-electron oxidation of **16**, the reversibility of the second oxidation of **16** in the cyclic voltammogram and the appearance of the molecular ion in the mass spectrum for **16** following two-electron coulometric oxidation seem to indicate that  $[(\text{chloro})\text{bis}(\text{tricyclohexylphosphine})\{1,3\text{-di}(2\text{-hydroxy-5-}tert\text{-butylphenyl})\text{imidazolyl}\}\text{iridium}]^{2+}$  (**16**<sup>2+</sup>) is the initial product. Based on one-electron oxidation potentials obtained previously for iridium(IV) complexes and for phenolates, it is possible that **16**<sup>2+</sup> could be either an iridium(V) species or an iridium(IV) species with a ligand-centered radical.<sup>20,53,54,60,61,63,64</sup> Unfortunately, the appearance of peaks in both the EPR and NMR spectra of the two-electron oxidation product seems to indicate that

**16<sup>2+</sup>** is converted to other products over time, and this precludes a detailed electronic description of **16<sup>2+</sup>**.

In an attempt gain further insight into the one-electron oxidation of **16**, Dr. Nilay Hazari performed full geometry optimizations and calculations of the gas-phase SCF energies on the model complexes, [(chloro)bis(phosphine){1,3-di(2-hydroxyphenyl)imidazolyl}iridium(III)] (17) and [(chloro)bis(phosphine){1,3-di(2-hydroxyphenyl)imidazolyl}iridium]<sup>+</sup> (18), containing less steric bulk than the respective complexes **16** and **16<sup>+</sup>**.<sup>68</sup> The geometrical coordinates determined from the crystal structure of **16'** were used as a starting point for geometry optimization of **17**, and the optimized structure of **17** was used as a starting point for geometry optimization of **18**. The optimized structures of **17** and **18** are shown in figures 4.15 and 4.16, respectively, while a side-by-side comparison of the bond lengths and angles in **16'**, **16''**, **17**, and **18** is provided in table 4.1.

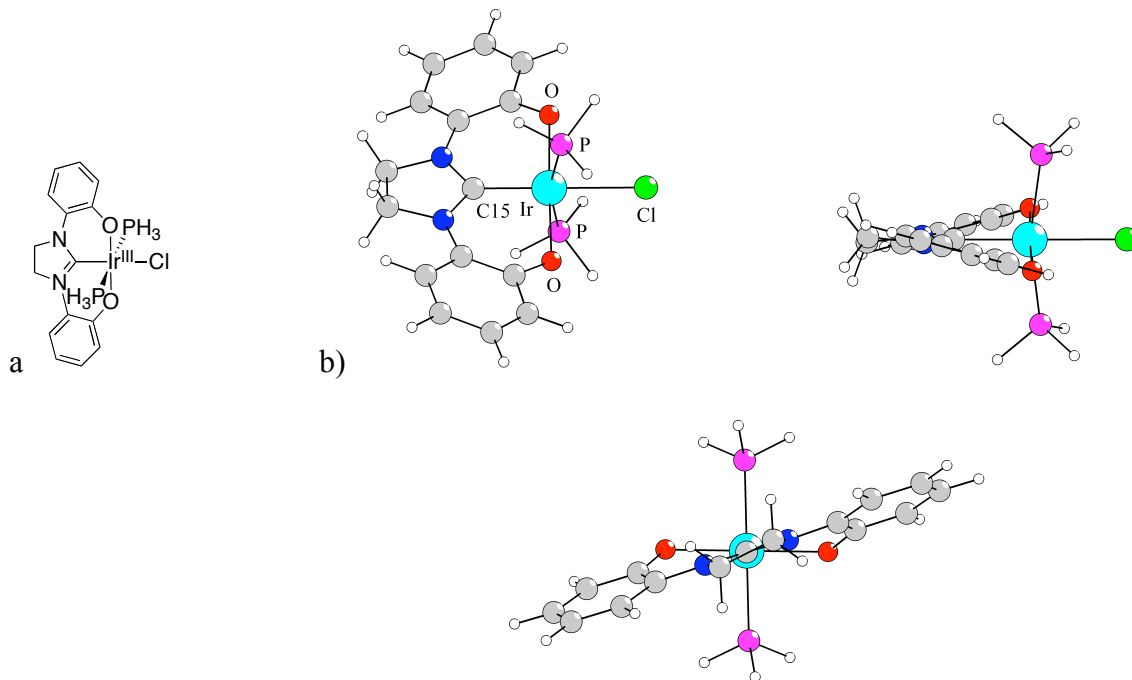


**Figure 4.15.** Illustration (a) and fully optimized gas-phase structural drawings (b) of **17**.

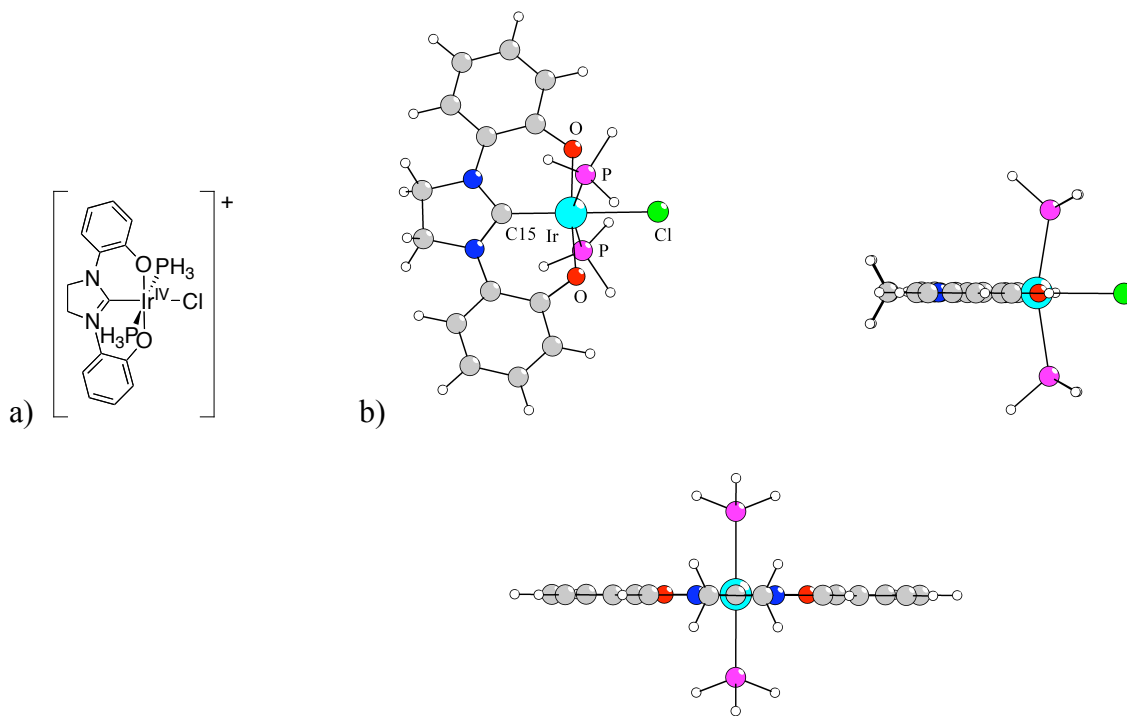


**Figure 4.16.** Illustration (a) and fully optimized gas-phase structural drawings (b) of **18**.

With the exception of the  $C_{ipso}$ -O1-O2- $C_{ipso}$  torsion angle, there is good agreement between the bond distances and angles of **16'**, **16''**, and **17**. Although this angle is much greater in **17** ( $-62.62^\circ$ ) than in either **16'** ( $-15.72(26)^\circ$ ) or **16''** ( $35.19(26)^\circ$ ), it is even significantly different between the two solid-state isomers of **16** (**16'** and **16''**). To probe whether the increased torsion angle of **17** is caused by a lack of steric bulk, QMMM calculations, in which all the steric bulk is included, were performed to determine the optimized gas-phase structure of **16**.<sup>68</sup> The resulting structure is shown in figure 4.17, and it has a  $C_{ipso}$ -O1-O2- $C_{ipso}$  torsion angle of  $-9.55^\circ$ . The steric bulk of **16** therefore seems to have a dramatic impact on the torsion angle, probably because the tricyclohexylphosphine ligands prevent a large distortion of the diphenolate imidazolyl-carbene ligand away from  $C_{2v}$ -symmetry to  $C_2$ -symmetry.

**Table 4.1.** Selected bond lengths (Å) and angles (°) for **16'**, **16''**, **17**, and **18**.

	Structure			
	<b>16'</b>	<b>16''</b>	<b>17</b>	<b>18</b>
<b>Bond Lengths</b>				
Ir-C15	1.944(2)	1.944(2)	1.95	1.96
Ir-O1	2.0343(16)	2.0307(17)	2.09	2.03
Ir-O2	2.0257(17)	2.0380(18)	2.09	2.03
Ir-P1	2.4365(7)	2.4102(8)	2.34	2.38
Ir-P2	2.4194(7)	2.4260(8)	2.34	2.38
Ir-Cl	2.4584(5)	2.4529(5)	2.49	2.46
<b>Angles</b>				
C15-Ir-O1	93.06(8)	92.75(9)	90.9	92.7
C15-Ir-O2	91.66(8)	90.14(9)	90.9	92.7
C15-Ir-P1	93.67(7)	93.81(8)	97.0	98.8
C15-Ir-P2	94.16(7)	94.60(8)	97.0	98.8
C15-Ir-Cl	179.44(8)	177.33(8)	180.0	180.0
O1-Ir-O2	175.24(6)	177.00(6)	178.3	174.5
O1-Ir-P1	87.51(5)	92.32(5)	87.7	89.6
O1-Ir-P2	88.45(5)	88.27(5)	92.1	89.6
O1-Ir-Cl	87.29(4)	85.42(4)	89.1	87.2
O2-Ir-P1	92.81(5)	86.70(5)	87.7	89.6
O2-Ir-P2	90.58(5)	92.29(6)	92.1	89.6
O2-Ir-Cl	87.99(4)	91.66(4)	89.1	87.2
P1-Ir-P2	171.367(19)	171.53(2)	166.0	162.4
P1-Ir-Cl	86.79(2)	84.32(2)	83.0	81.2
P2-Ir-Cl	85.40(2)	87.30(2)	83.0	81.2
<b>Dihedral Angle</b>				
C <sub>ipso</sub> -O1-O2-C <sub>ipso</sub>	-15.72(26)	35.19(26)	-62.6	0.3

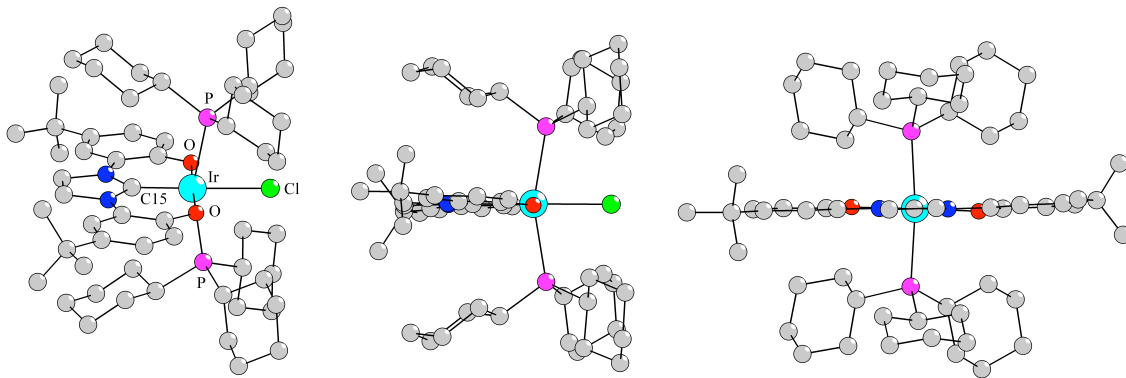


**Figure 4.17.** The optimized gas-phase structure of **16** determined by QMMM calculations. The  $C_{ipso}$ -O1-O2- $C_{ipso}$  torsion angle is  $-9.55^\circ$ . Hydrogen atoms have been removed for clarity.

One explanation for the increased torsion angle of **17** may be that it is favored by electronic effects. This conclusion is supported by the calculated HOMO of **17**, depicted in figure 4.18; a similar orbital was calculated for the optimized gas-phase structure of **16**, and it is shown in figure 4.19.<sup>68</sup> This orbital has a  $\pi$ -antibonding interaction between the phenolate ligands and the metal center. The increased  $C_{ipso}$ -O1-O2- $C_{ipso}$  torsion angle of **17** probably decreases overlap between the  $\pi$ -orbitals of the phenolates and the metal center, thus diminishing the antibonding interaction and lowering the energy of the HOMO. In order to probe the degree to which changes in this torsion angle affect the overall energy of the molecule, multiple geometry optimizations and calculations of the gas-phase SCF energies for **17** were performed with the  $C_{ipso}$ -O1-O2- $C_{ipso}$  torsion angle held constant at various angles between  $0^\circ$  and  $90^\circ$ .<sup>68</sup> The relative energies of the resulting structures are plotted against their respective  $C_{ipso}$ -O1-O2- $C_{ipso}$  torsion angles in figure 4.20. These results indicate that the energy of **17** changes relatively little (less than 4 kJ/mol) for torsion angles between  $0^\circ$  and  $90^\circ$ . Furthermore, increasing the torsion

angle from the optimized angle of  $-62.62^\circ$  causes a greater increase in energy than decreasing the torsion angle. This explains why factors such as steric bulk and crystal packing can cause such dramatic decreases in the  $C_{ipso}$ -O1-O2- $C_{ipso}$  torsion angle of **16**.

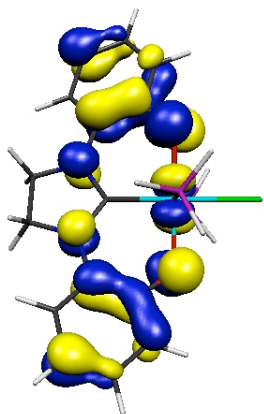


**Figure 4.18.** Depiction of the HOMO for the fully optimized gas-phase structure of **17**.

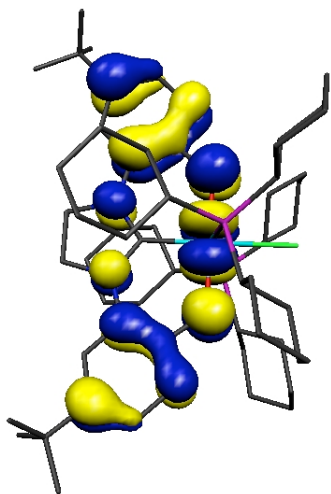


**Figure 4.19.** Depiction of the HOMO for the fully optimized gas-phase structure of **16** determined by QM/MM calculations. Hydrogen atoms have been removed for clarity.

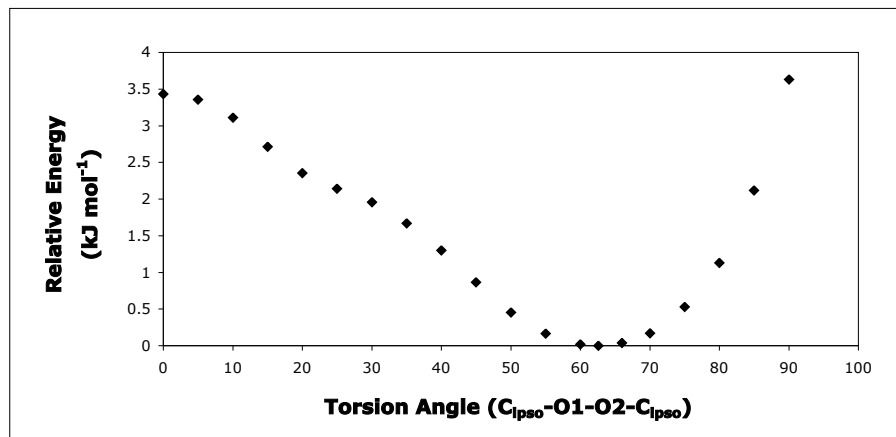


**Figure 4.20.** The relative energies for optimized structures of **17** when the C<sub>ipso</sub>-O1-O2-C<sub>ipso</sub> torsion angle is set at various angles between 0° and 90°.

In contrast to **17**, **18** is approximately C<sub>2v</sub>-symmetric, with a C<sub>ipso</sub>-O1-O2-C<sub>ipso</sub> torsion angle of only 0.3°. The singly occupied molecular orbital (SOMO) of **18**, depicted in figure 4.21, is similar to the HOMOs of **16** and **17**, and this may account for the small C<sub>ipso</sub>-O1-O2-C<sub>ipso</sub> torsion angle of **18**. As this orbital is only partially occupied, the energetic cost of the antibonding interaction between the phenolate ligands and the metal center should be significantly attenuated, and this cost may be outweighed by the corresponding bonding interactions in lower energy orbitals. Maximization of  $\pi$ -orbital overlap between the phenolates and the metal center should therefore be favorable; and based on the orbital symmetry, this should be accomplished by the diphenolate imidazolyl-carbene ligand adopting an approximately C<sub>2v</sub>-symmetric geometry, as observed for **18**.

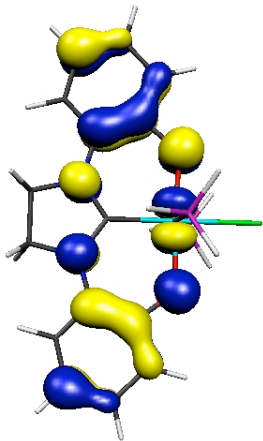


**Figure 4.21.** Depiction of the HOMO for the fully optimized gas-phase structure of **18**.

In order to determine the degree to which this geometry is favored, multiple geometry optimizations and calculations of the gas-phase SCF energies for **18** were performed with the C<sub>ipso</sub>-O1-O2-C<sub>ipso</sub> torsion angle held constant at various angles between -20° and 35°.<sup>68</sup> The relative energies of the resulting structures are plotted against their respective C<sub>ipso</sub>-O1-O2-C<sub>ipso</sub> torsion angles in figure 4.22. As for **17**, there is relatively little change in energy over a fairly wide range of torsion angles; therefore, sterics could play a significant role in dictating the geometry of **16<sup>+</sup>**. However, the use of sterically bulky tricyclohexyl phosphine axial ligands should also favor C<sub>2v</sub>-symmetric binding of the diphenolate imidazolyl-carbene ligand; so, **16<sup>+</sup>** is likely to adopt a similar geometry to **18**.

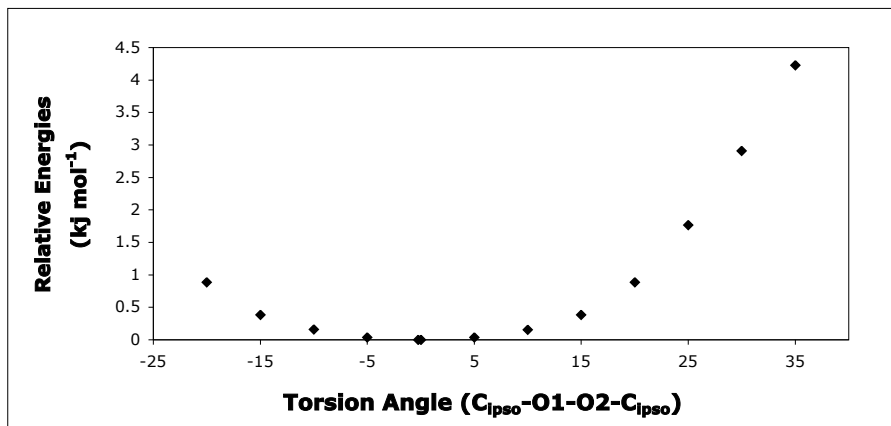


**Figure 4.22.** The relative energies for optimized structures of **18** when the C<sub>ipso</sub>-O1-O2-C<sub>ipso</sub> torsion angle is set at various angles between -25° and 35°.

Based on the SOMO of **18** as well as the HOMOs of **16** and **17**, it seems likely that one-electron oxidation of **16** to generate **16<sup>+</sup>** involves the removal of an electron from a highly delocalized molecular orbital containing orbital density on both the diphenolate imidazolyl-carbene ligand and the metal center. Stabilization of the unpaired electron in such a highly delocalized orbital may help to explain the lack of hyperfine splitting in the low temperature EPR spectrum of **16<sup>+</sup>**.

## Conclusions

For the first time, iridium complexes have been synthesized with a diphenolate imidazolyl-carbene ligand (**2**). Only a few diphenolate imidazolyl-carbene ligands have been synthesized previously. The precursor to **2**, 1,3-di(2-hydroxy-5-*tert*-butylphenyl)imidazolium chloride (**2a**) shows increased thermal stability over most similar ligand precursors due to the lack of a methylene group bridging each phenolate to the imidazolyl ring.<sup>28-31</sup> Deprotonation of **2a**, followed by reaction with chloro-1,5-

cyclooctadiene iridium(I) dimer generated a unique complex, potassium (1,5-cyclooctadiene){1,3-di(2-hydroxy-5-*tert*-butylphenyl)imidazolyl}iridium(I) (**6**). Only one of the phenoxides is bound to iridium in the solid-state structure of this complex, containing one equivalent of 18-crown-6 ether; the other phenoxide is coordinated to the potassium counterocation along with 18-crown-6-ether. The solution-phase structure of this complex seems to be fluxional, and it is highly solvent dependent.

Oxidation of **6** with two equivalents of ferrocenium(III) hexafluorophosphate in acetonitrile leads to the generation of (acetonitrile)(1,5-cyclooctadiene){1,3-di(2-hydroxy-5-*tert*-butylphenyl)imidazolyl}iridium(III) hexafluorophosphate (**9**). Reaction of this complex with dihydrogen results in the generation of cyclooctane and a species capable of catalyzing the hydrogenation of cyclohexene to cyclohexane. Heating **9** in acetonitrile results in the displacement of cyclooctadiene by acetonitrile to generate tris(acetonitrile){1,3-di(2-hydroxy-5-*tert*-butylphenyl)imidazolyl}iridium(III) hexafluorophosphate (**10**). This indicates relatively weak binding of cyclooctadiene to iridium in **9**. Cyclooctadiene can also be displaced from **9** at elevated temperatures with trialkylphosphines. The reaction of trimethylphosphine with **9** results in the generation of tris(trimethylphosphine){1,3-di(2-hydroxy-5-*tert*-butylphenyl)imidazolyl}iridium(III) hexafluorophosphate (**11**), while the reaction of **9** with tricyclohexylphosphine leads to the formation of (acetonitrile)bis(tricyclohexylphosphine){1,3-di(2-hydroxy-5-*tert*-butylphenyl)imidazolyl}iridium(III) hexafluorophosphate (**12**).

In order to probe electronic effects on ligands binding *trans* to the carbene, **12** was reacted with carbon monoxide. At 90 °C in acetonitrile, an equilibrium mixture of **12** and (carbon monoxide)bis(tricyclohexylphosphine){1,3-di(2-hydroxy-5-*tert*-butylphenyl)imidazolyl}iridium(III) hexafluorophosphate (**13**) was observed.

butylphenyl)imidazolyl} iridium(III) hexafluorophosphate (**15**) is generated. Consistent with the observed equilibrium mixture of **12** and **15**, the CO-stretching frequency of **15** ( $2064\text{ cm}^{-1}$ ) is indicative of relatively weak  $\pi$ -donation from iridium into the carbonyl  $\pi^*$ -orbital.

Acetonitrile can also be displaced from **12** by chloride, resulting in the formation of (chloro)bis(tricyclohexylphosphine){1,3-di(2-hydroxy-5-*tert*-butylphenyl)imidazolyl}-iridium(III) (**16**). Based on DFT calculations, the HOMO of this complex is a highly delocalized molecular orbital, containing an antibonding interaction between the phenolates and the metal center. This interaction seems to cause a distortion of the diphenolate imidazolyl-carbene ligand from  $C_{2v}$ -symmetry toward  $C_2$ -symmetry as observed in the solid-state structure of **16**. In methylene chloride, two reversible one-electron oxidations of **16** are observed at -0.22 and 0.58 V by cyclic voltammetry and bulk electrolysis. Based on EPR spectra and on DFT calculations, the SOMO of the complex resulting from the first oxidation is similar to the HOMO calculated for **16**, and it seems to have orbital density both on the metal center and on the diphenolate imidazolyl-carbene ligand. It is likely that the second oxidation occurs from a similar orbital, but further studies are required to characterize the two-electron oxidation product of **16**.

Overall, this diphenolate imidazolyl-carbene ligand (**2**) has proven capable of stabilizing both iridium(I) and iridium(III) complexes, including complexes with interesting structural and electronic properties and a complex capable of catalyzing olefin hydrogenations. The fact that **2** can support iridium(I) complexes, as well as iridium(III)

complexes capable of undergoing two reversible one-electron oxidations, is promising for the incorporation of this ligand into redox-active catalysts.

## Experimental Section

**General considerations.** All air- and/or moisture-sensitive compounds were manipulated using standard Schlenk techniques or in a glovebox under a nitrogen atmosphere as described previously.<sup>69</sup> Under standard glovebox conditions purging was not performed between uses of petroleum ether, diethyl ether, benzene, toluene and tetrahydrofuran; thus when any of these solvents were used, traces of all these solvents were in the atmosphere and could be found intermixed in the solvent bottles. All NMR solvents were purchased from Cambridge Isotopes Laboratories, Inc. The solvents for air- and moisture-sensitive reactions were dried by passage through a column of activated alumina followed by storage under dinitrogen. All other materials were used as received. 2-amino-4-*tert*-butylphenol, oxalyl chloride, triethylamine, BH<sub>3</sub>-THF (1M in THF), triethyl orthoformate, potassium hexamethyldisilazide (potassium bis(trimethylsilyl)amide), bis(triphenyl-phosphoranylidene)ammonium chloride, ferrocenium hexafluorophosphate<sup>70</sup> were purchased from Aldrich. 2-bromo-4-*tert*-butylaniline was purchased from Oakwood Products, Inc. Chloro-1,5-cyclooctadiene iridium(I) dimer was purchased from Strem Chemicals, Inc. 2,6-di(2-hydroxy-3,5-*tert*-butylphenyl)pyridine (**5a**) was obtained from Theodor Agapie.<sup>37</sup> <sup>1</sup>H, <sup>13</sup>C, <sup>31</sup>P, and <sup>19</sup>F NMR spectra were recorded on Varian Mercury 300 spectrometers at room temperature, unless indicated otherwise. Chemical shifts are reported with respect to residual internal protio solvent for <sup>1</sup>H and <sup>13</sup>C{<sup>1</sup>H} NMR spectra. H<sub>3</sub>PO<sub>4</sub> and CFCl<sub>3</sub> were used as external

standards to reference  $^{31}\text{P}$  and  $^{19}\text{F}$  NMR spectra, respectively, at 0 ppm. High resolution mass spectra (HRMS) were obtained at the California Institute of Technology Mass Spectral Facility. Elemental analyses were obtained by Midwest Microlab, LLC located in Indianapolis, IN and Columbia Analytical Services (formerly Desert Analytics) located in Tucson, AZ.

All electrochemical measurements were carried out on a Bioanalytcs BAS100B/W. These measurements were performed under a nitrogen or argon atmosphere in 0.3 M tetrabutylammonium tetrafluoroborate solutions. Ferrocene was used as an internal standard, and all potentials are referenced to the ferrocene/ferrocenium couple. For cyclic voltammetry experiments, the working electrode was a glassy carbon disk (2 mm diameter); the counter electrode was a coiled platinum wire; and, a silver wire was used as a pseudoreference electrode. In the bulk electrolysis experiments, the glassy carbon disk was replaced with a platinum wire basket for the working electrode.

The spectrometer used for all EPR experiments was an X-band Bruker EMX with a standard TE<sub>102</sub> cavity. Approximately 250  $\mu\text{L}$  samples were transferred to an EPR tube, frozen with liquid nitrogen, and then placed in a modified TE<sub>102</sub> cavity fit with a liquid helium-powered cryostat. This allowed EPR spectra to be obtained at temperatures between 7 and 77 K.

Single-crystal X-ray diffraction samples were prepared by decanting or pipetting off any solvent and then coating the crystals with Paratone N oil. The crystals were then transferred to a microscope slide. Samples were selected and mounted on a glass fiber with Paratone N oil. Data collection was carried out on a Bruker Smart 1000 CCD

diffractometer. The structures were solved by direct methods. With the exception of **8**, all non-hydrogen atoms were refined anisotropically.

Density functional calculations were carried out using Gaussian 03 Revision D.01.<sup>71</sup> Calculations on the model systems (with minimal steric bulk) were performed using the nonlocal exchange correction by Becke<sup>72,73</sup> and nonlocal correlation corrections by Perdew,<sup>74</sup> as implemented using the bvp86 keyword in Gaussian. The following basis sets were used: LANL2DZ<sup>75-77</sup> for iridium atoms, Stuttgart-Dresden<sup>78,79</sup> for phosphorus atoms and 6-31G\*\* basis set for all other atoms. Pseudopotentials were utilized for iridium and phosphorus atoms, using the LANL2DZ ECP for iridium and the Stuttgart-Dresden potential for phosphorus. For calculations on full experimental systems, QMMM calculations were performed using ONIOM(bvp86:UFF).<sup>80</sup> In these calculations the *tertiary*-butyl groups on the tridentate diphenolate imidazolyl-carbene ligands and the cyclohexyl groups on the phosphine ligands were calculated at the UFF level and the rest of the molecule was calculated using DFT. All optimized structures were verified using frequency calculations and did not contain any imaginary frequencies. Isosurface plots were made using the Molekel program.<sup>81</sup>

**Synthesis of N, N'-Di(2-hydroxy-5-*tert*-butylphenyl)oxalamide.** 4.0 mL (5.9 g, 0.046 mol) oxalyl chloride was combined with 35 mL CH<sub>2</sub>Cl<sub>2</sub> under argon in a Schlenk flask. 100 mL of CH<sub>2</sub>Cl<sub>2</sub> were then used to dissolve 15.0 g (0.091 mol) 2-amino-4-*tert*-butylphenol in a second Schlenk flask, and 12.6 mL (9.1 g, 0.090 mol) of triethylamine was added. Both solutions were then cooled to 273 K. The solution of 2-amino-4-*tert*-butylphenol and triethylamine was slowly cannula transferred into the solution of oxalyl

chloride, producing a white gas. Additional  $\text{CH}_2\text{Cl}_2$  was used to wash in any remaining 2-amino-4-*tert*-butylphenol and triethylamine. The resulting solution was stirred for 2 hours, and then 150 mL  $\text{H}_2\text{O}$  was added.  $\text{CH}_2\text{Cl}_2$  was used to extract the organic products. The solvent was removed under vacuum. The resulting solid was washed with both ethyl acetate and petroleum ether. Volatiles were removed under vacuum, and a white solid was isolated (9.77g, 0.0255 mol, 56.2% yield).  $^1\text{H}$  NMR (300 MHz, N,N-dimethylformamide (DMF)-d<sub>7</sub>)  $\delta$  = 10.61 (s, 2 H), 10.04 (s, 2H), 8.45 (d,  $^4J$  = 2.34 Hz, 2H), 7.11 (dd,  $^3J$  = 8.55 Hz,  $^4J$  = 2.33 Hz, 2H), 6.99 (d,  $^3J$  = 8.55 Hz, 2H), 1.31 (s, 18H);  $^{13}\text{C}$  { $^1\text{H}$ } NMR (75 MHz, DMF-d<sub>7</sub>):  $\delta$  157.7, 145.4, 142.5, 125.1, 122.4, 117.0, 114.8, 31.4. HRMS (FAB+) m/z calculated for  $\text{C}_{22}\text{H}_{28}\text{O}_4\text{N}_2$  + H: 385.2127. Found: 385.2108 (M + H). Analysis calculated for  $\text{C}_{22}\text{H}_{28}\text{O}_4\text{N}_2$ : C, 68.73; H, 7.34; N, 7.29. Found: C, 68.53; H, 7.25; N, 7.33.

#### **Synthesis of 1,3-di(2-hydroxy-5-*tert*-butylphenyl)imidazolium chloride (2a).**

1.00 g (2.60 mmol) N, N'-Di(2-hydroxy-5-*tert*-butylphenyl)oxalamide was weighed into an oven-dried Schlenk flask. N, N'-Di(2-hydroxy-5-*tert*-butylphenyl)oxalamide was dissolved in 26.5 mL  $\text{BH}_3$ -THF (1M in THF, 26.5 mmol). A large amount of bubbling occurred, and the solution turned bright orange. The reaction was heated and stirred for 19 hours at 70 °C. The reaction was then cooled to room temperature, yielding a transparent brown solution. While stirring, methanol was added until all bubbling ceased. 5.1 mL of 12 M HCl was then added, and the solvent was removed under reduced pressure. The resulting solid was redissolved in methanol, and then the solvent was again removed under reduced pressure. Methanol was added then removed two

more times. This resulted in a white solid, the dihydrochloride salt of the diimine, which was not characterized. In a Schlenk flask under argon, the solid was suspended in 10.5 mL triethylorthoformate and heated to 100 °C with vigorous stirring. The solid still did not dissolve, even when another 10 mL triethylorthoformate was added. The suspension was then heated for two hours at 120 °C, and the suspension started to become tan in color. The suspension was then filtered while still warm, and the resulting solid was washed with diethyl ether. A white solid was isolated. The filtrate was filtered again. The resulting solids were combined, and volatiles were removed under reduced pressure. A white solid was thus obtained (777 mg, 1.93 mmol, 74.2%). <sup>1</sup>H NMR (300 MHz, dimethylsulfoxide (DMSO)-d<sub>6</sub>) δ = 10.74 (br s, 2H), 9.49 (s, 1H), 7.38 (d, <sup>4</sup>J = 2.09 Hz, 2H), 7.27 (dd, <sup>3</sup>J = 8.69 Hz, <sup>4</sup>J = 2.09 Hz, 2H), 7.05 (d, <sup>3</sup>J = 8.69 Hz), 4.57 (s, 4H), 1.27 (s, 18H); <sup>13</sup>C {<sup>1</sup>H} NMR (75 MHz, DMSO-d<sub>6</sub>): δ 156.7, 148.0, 142.3, 125.7, 123.0, 120.3, 116.5, 49.8, 34.0, 31.2. HRMS (FAB+) m/z calculated for C<sub>23</sub>H<sub>31</sub>O<sub>2</sub>N<sub>2</sub>: 367.2386. Found: 367.2390 (M<sup>+</sup>). Analysis calculated for C<sub>23</sub>H<sub>31</sub>O<sub>2</sub>N<sub>2</sub>Cl: C, 68.55; H, 7.75; N, 6.95. Found: C, 68.30; H, 7.78; N, 6.85. CV in DMF: E<sub>p</sub>, V vs. ferrocene at 0.100 V/s: 0.73 V (irr.), 0.94 V (irr.).

**Synthesis of N, N'-di(2-bromo-4-*tert*-butylphenyl)oxalamide.** 0.60 mL (0.87 g, 0.0069 mol) oxalyl chloride was combined with 6 mL CH<sub>2</sub>Cl<sub>2</sub> under argon in a Schlenk flask. 10 mL of CH<sub>2</sub>Cl<sub>2</sub> were then used to dissolve 2.5 g (0.011 mol) 2-bromo-4-*tert*-butylaniline in a second Schlenk flask, and 1.93 mL (1.4 g, 0.014 mol) of triethylamine was added. Both solutions were then cooled to 273 K. The solution of 2-amino-4-*tert*-butylphenol and triethylamine was slowly cannula transferred into the solution of oxalyl

chloride, producing a white gas. 10 mL additional  $\text{CH}_2\text{Cl}_2$  was used to wash in any remaining 2-bromo-4-*tert*-butylaniline and triethylamine. The resulting solution was stirred for 2 hours, and then 20 mL  $\text{H}_2\text{O}$  was added.  $\text{CH}_2\text{Cl}_2$  was used to extract the organic products. The solvent was removed under vacuum. The resulting solid was redissolved in a minimal amount of methylene chloride. Impurities were precipitated out with petroleum ether and removed by filtration. Solvent was once again removed under vacuum yielding a solid (1.95 g, 0.00382 mol, 69.7% yield).  $^1\text{H}$  NMR (300 MHz,  $\text{CDCl}_3$ )  $\delta$  = 9.87 (s, 2H), 8.34 (d,  $^3J$  = 8.68 Hz, 2H), 7.60 (d,  $^4J$  = 2.10 Hz, 2H), 7.39 (dd,  $^3J$  = 8.68 Hz,  $^4J$  = 2.10 Hz, 2H), 1.32 (s, 18H).

#### **Synthesis of 1,3-di(2-bromo-4-*tert*-butylphenyl)imidazolium chloride (4a).**

4.00 g (7.84 mmol) N, N'-Di(2-bromo-4-*tert*-butylphenyl)oxalamide was weighed into an oven-dried Schlenk flask. N, N'-Di(2-bromo-4-*tert*-butylphenyl)-oxalamide was dissolved in 63 mL  $\text{BH}_3$ -THF (1M in THF, 63 mmol). Bubbling occurred. The reaction was heated and stirred for 19 hours at 70 °C. The reaction was then cooled to room temperature. While stirring, methanol was added until all bubbling ceased. 20 mL of 12 M HCl was then added, and the solvent was removed under reduced pressure. The resulting solid was redissolved in methanol, and then the solvent was again removed under reduced pressure. Methanol was added then removed two more times. This resulted in a white solid, the dihydrochloride salt of the diimine, which was not characterized. In a Schlenk flask under argon, the solid was suspended in 75 mL triethylorthoformate and heated to 100 °C while stirring. The vessel was heated for 25 minutes at 120 °C, and then the suspension started to darken in color. The suspension

was filtered while still warm, and the solid was washed with diethyl ether three times. The product was thus obtained as a white solid (1.5 mg, 2.8 mmol, 36%). <sup>1</sup>H NMR (300 MHz, dimethylsulfoxide (DMSO)-d<sub>6</sub>) δ 9.46 (s, 1H), 7.84 (d, <sup>4</sup>J = 1.95 Hz, 2H), 7.76 (d, <sup>3</sup>J = 8.46 Hz, 2H), 7.65 (dd, <sup>3</sup>J = 8.46 Hz, <sup>4</sup>J = 1.95 Hz, 2H), 4.57 (s, 4H), 1.31 (s, 18H); <sup>13</sup>C {<sup>1</sup>H} NMR (75 MHz, DMSO-d<sub>6</sub>): δ 159.9, 155.1, 132.2, 130.6, 128.0, 126.4, 119.3, 52.3, 34.9, 30.7. HRMS (FAB+) m/z calculated for C<sub>23</sub>H<sub>29</sub>Br<sub>2</sub>N<sub>2</sub>: 491.0698. Found: 491.0701 (M<sup>+</sup>). Analysis calculated for C<sub>23</sub>H<sub>29</sub>Br<sub>2</sub>Cl<sub>2</sub>N<sub>2</sub>: C, 52.25; H, 5.53; N, 5.30. Found: C, 52.07; H, 5.50; N, 5.30.

**Crystallization of 2,6-di(2-hydroxy-3,5-*tert*-butylphenyl)pyridine (5a).** 10 mg (0.021 mmol) of 2,6-di(2-hydroxy-3,5-*tert*-butylphenyl)pyridine and 11 mg of dihydrogen hexachloroiridate (IV) hydrate were dissolved in 0.7 mL ethanol-d<sub>6</sub> and transferred to a J-Young NMR tube. The tube was then sealed and heated to 90 °C. Crystals were observed after 3 days.

**Synthesis of potassium (1,5-cyclooctadiene){1,3-di(2-hydroxy-5-*tert*-butylphenyl)imidazolyl}iridium(I) (6).** In a glovebox, THF was used to dissolve 1.5 g (4.0 mmol) of **2a** and 2.4 g (12 mmol) potassium hexamethyldisilazide in an Erlenmeyer flask, and the solution was stirred for 30 minutes. In a separate flask, chloro-1,5-cyclooctadiene iridium(I) dimer (1.33 g, 1.98 mmol) was then dissolved in THF and slowly added to the solution of **2a** and potassium hexamethyldisilazide. The resulting bright orange solution was stirred for 30 minutes, and then the solvent was removed under reduced pressure. An orange solid was obtained which was then stirred in

methanol for 12 hours under argon. Solvent was again removed under reduced pressure. The resulting solid was dissolved in THF and stirred for 15 minutes. Then, the solvent was removed under reduced pressure. This solid was dissolved in benzene and filtered. Finally, volatiles were removed from the filtrate by lyophilization, yielding a bright orange powder (2.2 g, 3.1 mmol, 79%).  $^1\text{H}$  NMR (300 MHz, THF-d<sub>8</sub>)  $\delta$  6.81 (m, 4H), 6.43 (d,  $^3J = 8.62$  Hz, 2H), 3.90 (app. t,  $^3J = 8.81$  Hz, 2H), 3.66 (app. t,  $^3J = 8.81$  Hz, 2H), 3.51 (br s, 4H), 1.84 (br s, 4H), 1.38 (m, 4H), 1.26 (s, 18H);  $^1\text{H}$  NMR (300 MHz, CD<sub>3</sub>OD)  $\delta$  7.19 (d,  $^4J = 2.58$  Hz, 2H), 6.98 (dd,  $^3J = 8.37$  Hz,  $^4J = 2.58$  Hz, 2H), 6.66 (d,  $^3J = 8.37$  Hz, 2H), 4.53 (br s, 2H), 4.27 (br s, 2H), 2.40 (br s, 2H), 3.74 (br s, 2H), 2.92 (br s, 2H), 1.92 (br s, 2H), 1.55 (br s, 2H), 1.33 (br m, 20H);  $^{13}\text{C}$  { $^1\text{H}$ } NMR (75 MHz, THF-d<sub>8</sub>):  $\delta$  196.8, 161.1, 134.3, 132.6, 123.9, 119.6, 51.6, 34.3, 32.4, 32.2. HRMS (FAB+) m/z calculated for C<sub>31</sub>H<sub>40</sub>N<sub>2</sub>O<sub>2</sub>Ir: 665.2719. Found: 665.2745 (M<sup>+</sup>), 557.1913 (M<sup>+</sup> - cod).

**Crystallization of 6 with 18-crown-6 ether.** In a glovebox, saturated solutions of **6** (40 mg, 0.099 mmol) and 18-crown-6 ether (26.3 mg, 0.0995 mmol) in benzene were prepared. Another 0.5 mL of benzene were added to each solution, and the solution of 18-crown-6 ether was slowly added to the solution of **6** in a 20 mL vial. The vial was sealed, and orange crystals formed over the course of approximately one month.

**Crystallization of  $\mu$ -(amidotriphenylphosphorus)bis((1,5-cyclooctadiene)-iridium(I)) (**7**).** In a glovebox, a minimal amount of THF was used to dissolve 50 mg (0.071 mmol) of **6** in a vial. In a separate vial, 37 mg (0.064 mmol) of

bis(triphenylphosphoranylidene)ammonium chloride was also dissolved in a minimal amount of THF, and this solution was slowly added to the solution of **6**. The resulting solution was stored at room temperature in a capped vial for about two months. Orange crystals were then observed along with an oily orange solid.

**Crystallization of bis(triphenylphosphoranylidene)ammonium bis{1,3-di(2-hydroxy-5-*tert*-butylphenyl)imidazolyl}iridium(III) (8).** In a glovebox, a minimal amount of benzene was used to dissolve 50 mg (0.071 mmol) of **6** in a vial. In a separate vial, 37 mg (0.064 mmol) of bis(triphenylphosphoranylidene)ammonium chloride was also dissolved in a minimal amount of benzene, and this solution was slowly added to the solution of **6**. The resulting was sealed in a vial; and over the course of three months, yellow crystals formed which were characterized by single crystal X-ray diffraction.

**Synthesis of (acetonitrile)(1,5-cyclooctadiene){1,3-di(2-hydroxy-5-*tert*-butylphenyl)imidazolyl}iridium(III) hexafluorophosphate (9).** In a glovebox, acetonitrile was used to dissolve 1.00 g (1.42 mmol) of **6** in an Erlenmeyer flask. In a separate flask, 1.18 g (3.55 mmol) ferrocenium(III) hexafluorophosphate was dissolved in acetonitrile. The ferrocenium(III) solution was slowly added to the solution of **6**. The resulting solution was stirred for 30 minutes and filtered. The solvent was removed from the filtrate under reduced pressure, and the resulting solid was washed with petroleum ether and diethyl ether. Volatiles were then removed from the solid under reduced pressure; 550 mg (0.65 mmol, 46% yield) of yellow solid was isolated.  $^1\text{H}$  NMR (300 MHz,  $\text{CD}_3\text{CN}$ )  $\delta$  7.02 (dd,  $^3J = 8.41$  Hz,  $^4J = 2.29$  Hz, 2H), 6.95 (d,  $^3J = 2.29$  Hz, 2H),

6.87 (d,  $^3J = 8.41$  Hz, 2H), 6.35 (m, 2H), 5.12 (m, 2H), 4.51 (m, 2H), 4.29 (m, 2H), 2.59 (br m, 2H), 2.46 (br m, 2H), 2.35 (br m, 2H), 2.17 (br m, 2H), 1.30 (s, 18H);  $^{13}\text{C}\{^1\text{H}\}$  NMR (75 MHz, THF-d<sub>8</sub>):  $\delta$  152.3, 141.4, 128.3, 127.4, 123.8, 120.3, 115.4, 94.0, 49.3, 35.1, 34.9, 31.8, 26.9;  $^{31}\text{P}\{^1\text{H}\}$  NMR (CD<sub>3</sub>CN, 121 MHz):  $\delta$  -141 (septet,  $^1J = 700$  Hz);  $^{19}\text{F}\{^1\text{H}\}$  NMR (CD<sub>3</sub>CN, 282 MHz):  $\delta$  -72.2 (d), -151.2 (s, [BF<sub>4</sub>]<sup>-</sup>). <sup>70</sup> HRMS (FAB+) m/z calculated for C<sub>33</sub>H<sub>43</sub>N<sub>3</sub>O<sub>2</sub>Ir: 706.2984. Found: 706.2987 (M<sup>+</sup>), 665.2721 (M<sup>+</sup> - CH<sub>3</sub>CN), 557.1781 (M<sup>+</sup> - (CH<sub>3</sub>CN + cyclooctadiene)).

**In situ generation of tris(acetonitrile){1,3-di(2-hydroxy-5-*tert*-butylphenyl)imidazolyl}iridium(III) hexafluorophosphate (10).** In a glovebox, 100 mg (0.118 mmol) of **9** were dissolved in about 25 mL of acetonitrile and transferred into a 50 mL Schlenk bomb. The bomb was sealed and heated at 90 °C for about 12 hours. It was then cooled to room temperature, and the solvent was removed under reduced pressure. This solid was extracted with diethyl ether, and again the solvent was removed under reduced pressure. 45 mg (0.054 mmol, 46%) of brown solid was isolated. The peaks in the  $^1\text{H}$  NMR at 2.53 and 2.68 ppm disappear over time in CD<sub>3</sub>CN, while the CH<sub>3</sub>CN peak at 1.97 peak increases by approximately the same amount.  $^1\text{H}$  (300 MHz, CD<sub>3</sub>CN)  $\delta$  6.94 (m, 4H), 6.67 (d,  $^3J = 8.37$  Hz, 2H), 4.50 (s, 4H), 2.68 (s, < 3H), 2.53 (s, < 6H), 1.97 (s, CH<sub>3</sub>CN), 1.29 (s, 18H);  $^{13}\text{C}\{^1\text{H}\}$  NMR (75 MHz, CD<sub>3</sub>CN, taken after peak at 2.68 ppm in  $^1\text{H}$  NMR disappeared):  $\delta$  153.8, 139.4, 128.3, 122.9, 119.9, 115.4, 48.8, 34.5, 31.8, 4.1, 1.8 (CH<sub>3</sub>CN);  $^{31}\text{P}\{^1\text{H}\}$  NMR (CD<sub>3</sub>CN, 121 MHz):  $\delta$  -144 (septet,  $^1J = 700$  Hz);  $^{19}\text{F}\{^1\text{H}\}$  NMR (CD<sub>3</sub>CN, 282 MHz):  $\delta$  -72.1 (d,  $^1J = 704$  Hz), -150.7

(s,  $[\text{BF}_4]^-$ ), -150.8 (s,  $[\text{BF}_4]^-$ ).<sup>70</sup> HRMS (FAB+, performed on the tris(acetonitrile-d<sub>3</sub>) complex) m/z calculated for  $\text{C}_{29}\text{H}_{28}\text{IrO}_2\text{N}_5\text{D}_9$ : 689.341. Found: 689.3156 ( $\text{M}^+$ ).

**Hydrogenation of **9**.** In a glovebox, 10 mg (0.012 mmol) of **9** was dissolved in about 0.6 mL THF-d<sub>8</sub> and sealed inside a 3.3 mL J-Young NMR tube. The solution was degassed by three freeze-pump-thaw cycles. The tube was then filled with 1 atm dihydrogen. The solution turned from yellow to orange over the course of about 15 minutes, and cyclooctane began to appear at 1.54 ppm in the <sup>1</sup>H NMR spectrum. Very small amounts of cyclooctene were observed after 1.5 hours by <sup>1</sup>H NMR, while the cyclooctane peak continued to grow. Another <sup>1</sup>H NMR spectrum was taken after 18 hours; the spectrum indicated that the coordinated 1,5-cyclooctadiene of **9** was completely hydrogenated to cyclooctane. No signals were observed in the <sup>1</sup>H NMR at less than 0 ppm, even after the sample was heated at 90 °C for 12 hours. After this period of heating, the solvent was removed under reduced pressure, and the sample was redissolved in CD<sub>3</sub>CN. Heating the sample for at least 12 hours generated **10** as the major product.

**Hydrogenation of cyclohexene catalyzed by **9**.** In a glovebox, a 1.0 mL THF-d<sub>8</sub> solution containing 10 mg (0.012 mmol) of **9** and 22.0  $\mu\text{L}$  (17.8 mg, 0.217 mmol) cyclohexene was prepared in a 1.0 mL volumetric flask. 500  $\mu\text{L}$  of this solution was syringed into a 1.5 mL high pressure, sapphire NMR tube. The tube was sealed and then was filled to a pressure of 900 psi with dihydrogen. The NMR tube was inverted several

times to ensure mixing between the headspace and the solution.  $^1\text{H}$  NMR spectra were taken every 608 seconds starting about 630 seconds after mixing commenced.

**In situ generation of tris(trimethylphosphine){1,3-di(2-hydroxy-5-*tert*-butylphenyl)imidazolyl}iridium(III) hexafluorophosphate (11).** In a glovebox, 10 mg (0.012 mmol) of **9** was dissolved in approximately 0.6 mL THF-d<sub>8</sub> and transferred to a J-Young NMR tube. 5.0  $\mu\text{L}$  (0.048 mmol) of trimethylphosphine was added to the solution. The NMR tube was then sealed, and the solution was mixed. The NMR tube was then heated at 90 °C in an oil bath for greater than 12 hours. Solvent and other volatiles were removed under reduced pressure, leaving a yellow solid.  $^1\text{H}$  (300 MHz, THF-d<sub>8</sub>)  $\delta$  6.97 (d,  $^4J = 2.34$  Hz, 2H), 6.85 (dd,  $^3J = 8.59$  Hz,  $^4J = 2.34$  Hz, 2H), 6.52 (d,  $^3J = 8.59$  Hz, 2H), 4.48 (s, 4H), 1.66 (d,  $^2J = 9.18$  Hz, 9H), 1.36 (app. t,  $J = 3.75$  Hz, 18H), 1.28 (s, 18H);  $^{31}\text{P}\{^1\text{H}\}$  NMR (THF-d<sub>8</sub>, 121 MHz):  $\delta$  -32.8 (d,  $^2J = 28.1$  Hz, 2P), -44.1 (t,  $^2J = 28.1$  Hz, 1P), -144 (septet,  $^1J = 700$  Hz, 1P). HRMS (FAB+) m/z calculated for C<sub>32</sub>H<sub>55</sub>IrN<sub>2</sub>O<sub>2</sub>P<sub>3</sub>: 785.3105. Found: 785.3097 (M $^+$ ).

**Synthesis of (acetonitrile)bis(tricyclohexylphosphine){1,3-di(2-hydroxy-5-*tert*-butylphenyl)imidazolyl}iridium(III) hexafluorophosphate (12).** In a glovebox, 810 mg (0.952 mmol) of **9** and 587 mg (2.09 mmol) of tricyclohexylphosphine were combined in a 500 mL Schlenk bomb with a Teflon stir bar. CH<sub>3</sub>CN was added until both solids went into solution. The bomb was then sealed and heated at 90 °C for 16 hours while stirring. The solvent and volatiles were removed under reduced pressure. The solid was washed consecutively with petroleum ether, benzene, and diethyl ether.

Finally, the solid was washed with a minimal amount of acetonitrile. Volatiles were again removed under reduced pressure. The solid was redissolved in acetonitrile and filtered. The solvent was removed from the filtrate under reduced pressure, and this yielded a bright yellow solid (750 mg, 0.57 mmol, 60%).  $^1\text{H}$  (300 MHz,  $\text{CD}_3\text{CN}$ )  $\delta$  6.89 (dd,  $^3J = 8.44$  Hz,  $^4J = 2.31$  Hz, 2H), 6.84 (d,  $^4J = 2.31$  Hz, 2H), 6.39 (d,  $^3J = 8.44$  Hz, 2H), 4.27 (s, 4H), 2.14 (m, 6H), 1.90 (br, 12H, overlaps with solvent peak), 1.67 (br m, 24H), 1.26 (s, 18H, overlaps with peak at 1.23 ppm), 1.23 (br m, 24H, overlaps with peak at 1.26 ppm);  $^{13}\text{C}\{^1\text{H}\}$  NMR (75 MHz,  $\text{CD}_3\text{CN}$ ):  $\delta$  150.8, 137.6, 127.3, 121.4, 119.3, 113.4, 46.5, 33.0 (apparent t,  $J = 11$  Hz), 30.5, 28.0, 27.2 (apparent t,  $J = 3.8$  Hz), 25.8;  $^{31}\text{P}\{^1\text{H}\}$  NMR ( $\text{CD}_3\text{CN}$ , 121 MHz):  $\delta$  -7.3, -143 (septet,  $^1J = 700$  Hz);  $^{19}\text{F}\{^1\text{H}\}$  NMR ( $\text{CD}_3\text{CN}$ , 282 MHz): -71.0 (d,  $^1J = 705$  Hz), -151.1. HRMS (FAB+, performed on the acetonitrile-d<sub>3</sub> complex) m/z calculated for  $\text{C}_{61}\text{H}_{94}\text{IrN}_2\text{O}_2\text{P}_2\text{D}_3 - \text{CD}_3\text{CN}$ : 1117.642. Found: 1117.6417 ( $\text{M}^+ - \text{CD}_3\text{CN}$ ), 837.4271 ( $\text{M}^+ - (\text{CD}_3\text{CN} + \text{PC}_{18}\text{H}_{33})$ ). Analysis calculated for  $\text{C}_{61}\text{H}_{97}\text{F}_6\text{IrN}_3\text{O}_2\text{P}_3$ : C, 56.20; H, 7.50; N, 3.22; F, 8.74; Ir, 14.75. Found: C, 56.19; H, 7.33; N, 3.12; F, 8.5; Ir, 15.0.

**The reaction of 12 with 1.5 equivalents of trimethylphosphine.** In a glovebox, 10 mg (0.0077 mmol) of **12** was dissolved in approximately 0.6 mL  $\text{CD}_3\text{CN}$  and transferred into a J-Young NMR tube. 1.2  $\mu\text{L}$  (0.012 mmol) of trimethylphosphine were added. The tube was sealed; and then, the solution was mixed thoroughly. The J-Young tube was heated for greater than 12 hours at 90 °C, and then the products were analyzed by  $^1\text{H}$  and  $^{31}\text{P}$  NMR spectroscopy. Based on the  $^{31}\text{P}$  NMR spectrum, **11** and **12** were present as well as two species, which were tentatively identified as

(acetonitrile)(tricyclohexylphosphine)(trimethylphosphine){1,3-di(2-hydroxy-5-*tert*-butylphenyl)imidazolyl}iridium(III) hexafluorophosphate **(13)** and (acetonitrile)bis(trimethylphosphine){1,3-di(2-hydroxy-5-*tert*-butylphenyl)imidazolyl}-iridium(III) hexafluorophosphate **(14)**.  $^{31}\text{P}\{\text{H}\}$  NMR (CD<sub>3</sub>CN, 121 MHz):  $\delta$  11.31 (br s, free  $PCy_3$ ), -2.99 (d,  $^2J = 390$  Hz,  $PCy_3$  of **13**), -7.33 (s,  $PCy_3$  of **12**), -20.21 (d,  $^2J = 390$  Hz,  $P(\text{CH}_3)_3$  of **13**), -23.88 (s,  $P(\text{CH}_3)_3$  of **14**), -32.66 (d,  $^2J = 27.8$  Hz,  $P(\text{CH}_3)_3$  of **11**), -43.53 (t,  $^2J = 27.8$  Hz,  $P(\text{CH}_3)_3$  of **11**, -143 (septet,  $^1J = 700$  Hz,  $PF_6$ ).

**In situ generation of (carbon monoxide)bis(tricyclohexylphosphine){1,3-di(2-hydroxy-5-*tert*-butylphenyl)imidazolyl}iridium(III) hexafluorophosphate (15).** In a glovebox, 10 mg (0.0077 mmol) of **12** was dissolved in 0.6 mL CD<sub>3</sub>CN and sealed in a 3.3 mL J-Young NMR tube. The solution was degassed by the freeze-pump-thaw method, then the tube was filled with one atmosphere of carbon monoxide at room temperature. The tube was heated at 90 °C, and the reaction was monitored by  $^1\text{H}$  NMR spectroscopy. Over the course of about 3 days, **15** appeared in the  $^1\text{H}$  NMR spectrum, and the peak did not grow in further with continued heating. Yellow crystals appeared in the J-Young tube slightly above the solvent level. These were identified as an approximately 4:1 ratio of **12** to **15** by single crystal X-ray diffraction. The  $^1\text{H}$  NMR spectrum of the solution phase indicated a ratio of **12** to **15** that was approximately 2:1. When the solution was degassed and heated for another 2 days, **15** was converted back to **12**, and the ratio of **12**:**15** increased to greater than 8:1 based on the  $^1\text{H}$  NMR spectrum. The following data are for **15**, only.  $^1\text{H}$  (300 MHz, CD<sub>3</sub>CN)  $\delta$  6.95 (dd overlapping with d at 6.95,  $^3J = 9.22$  Hz,  $^4J = 2.23$  Hz, 2H), 6.95 (d overlapping with dd at 6.95,  $^4J = 2.23$

Hz, 2H), 6.48 (d,  $^3J = 9.22$  Hz, 2H), 4.46 (s, 4H), 1.1-2.2 (br multiplets for PCy<sub>3</sub> overlapping with a water peak, which came from the carbon monoxide; the solvent peak; the *t*-butyl peak of **15**, and multiple peaks for **12**, 66 H), 1.28 (s overlapping with br multiplets for PCy<sub>3</sub> of **12** and **15**); <sup>31</sup>P{<sup>1</sup>H} NMR (CD<sub>3</sub>CN, 121 MHz):  $\delta$  1.43, -143 (septet,  $^1J = 700$  Hz). IR (CD<sub>3</sub>CN):  $\nu_{CO}$ , 2064 cm<sup>-1</sup>.

***In situ* generation of (carbon-<sup>13</sup>C monoxide)bis(tricyclohexylphosphine){1,3-di(2-hydroxy-5-*tert*-butylphenyl)imidazolyl}iridium(III) hexafluorophosphate (15').**

This complex was generated in a similar manner to **15**, but <sup>13</sup>C-enriched carbon monoxide was used. <sup>1</sup>H (300 MHz, CD<sub>3</sub>CN):  $\delta$  6.95 (dd overlapping with d at 6.95,  $^3J = 9.22$  Hz,  $^4J = 2.23$  Hz, 2H), 6.95 (d overlapping with dd at 6.95,  $^4J = 2.23$  Hz, 2H), 6.48 (d,  $^3J = 9.22$  Hz, 2H), 4.46 (s, 4H), 1.1-2.2 (br multiplets for PCy<sub>3</sub> overlapping with a water peak, which came from the carbon monoxide; the solvent peak; the *t*-butyl peak of **15'**, and multiple peaks for **12**, 66 H), 1.28 (s overlapping with br multiplets for PCy<sub>3</sub> of **12** and **15'**); <sup>13</sup>C {<sup>1</sup>H} NMR (75 MHz, CD<sub>3</sub>CN):  $\delta$  184.7 (free <sup>13</sup>CO), 174.8 (t,  $^2J = 9.7$  Hz); <sup>31</sup>P{<sup>1</sup>H} NMR (CD<sub>3</sub>CN, 121 MHz):  $\delta$  1.44 (d,  $^2J = 9.7$  Hz), -143 (septet,  $^1J = 700$  Hz). IR (CD<sub>3</sub>CN):  $\nu_{13CO}$ , 2015.5 cm<sup>-1</sup>.

**Synthesis of (chloro)bis(tricyclohexylphosphine){1,3-di(2-hydroxy-5-*tert*-butylphenyl)imidazolyl}iridium(III) (16).** In a glovebox, approximately 10 mL of CH<sub>3</sub>CN was used to dissolve 166 mg (0.127 mmol) of **12** in a 20 mL vial. 14 mg (0.13 mmol) of tetramethylammonium chloride was dissolved in about 2 mL of CH<sub>3</sub>CN and added to the solution of **12**. The resulting solution was transferred to a 100 mL Schlenk

bomb with a Teflon stir bar. The Schlenk bomb was then sealed, and the solution was allowed to stir for 3 days. During this time, a yellow precipitate formed. The precipitate was isolated by filtration and washed with acetonitrile. The yellow solid was then dissolved in benzene, which was then removed under reduced pressure. The resulting solid was redissolved in methylene chloride and filtered. Removal of solvent and other volatiles under reduced pressure resulted in the isolation of a yellow solid (95 mg, 0.082 mmol, 63%). Crystals were grown by cooling a concentrated methylene chloride solution of **16** to -20 °C.  $^1\text{H}$  (300 MHz,  $\text{CD}_2\text{Cl}_2$ )  $\delta$  6.81 (dd,  $^3J = 8.56$  Hz,  $^4J = 2.41$  Hz, 2H), 6.65 (d,  $^4J = 2.41$  Hz, 2H), 6.36 (d,  $^3J = 8.56$  Hz, 2H), 4.09 (s, 4H), 2.39 (br m, 6H), 2.08 (br m, 12H), 1.61 (br, 24H), 1.26 (s overlapping with the br multiplet at 1.12, 18H), 1.12 (br multiplet overlapping with s at 1.26, 24H);  $^{13}\text{C}$  { $^1\text{H}$ } NMR (75 MHz,  $\text{CD}_2\text{Cl}_2$ ):  $\delta$  153.0, 136.5, 128.6, 121.6, 121.0, 113.0, 47.2, 34.1, 33.4 (apparent t,  $J = 10.7$  Hz), 32.0, 30.3, 29.0, 28.5 (apparent t,  $J = 4.8$  Hz), 27.3;  $^{31}\text{P}$  { $^1\text{H}$ } NMR ( $\text{CD}_2\text{Cl}_2$ , 121 MHz):  $\delta$  -12.7. HRMS (FAB+) m/z calcd. for  $\text{C}_{59}\text{H}_{94}\text{ClIrN}_2\text{O}_2\text{P}_2$ : 1152.611. Found: 1152.6105 ( $\text{M}^+$ ); 1117.6425 ( $\text{M}^+ - \text{Cl}$ ). Analysis calculated for  $\text{C}_{59}\text{H}_{94}\text{IrN}_2\text{O}_2\text{P}_2$ : C, 61.46; H, 8.22; N, 2.43. Found: C, 61.7; H, 7.9; N, 2.3. CV in  $\text{CH}_2\text{Cl}_2$ :  $E_{1/2}$ , V vs. ferrocene at 0.100 V/s ( $\Delta E_p$ ): -0.22 V (98 mV), 0.58 V (98 mV); in THF at 0.050 V/s: -0.20 V (226 mV), 0.58 V (202 mV); in DMF at 0.100 V/s: -0.13 V (53 mV), 0.59 V (65 mV).

**Bulk electrolysis of **16** with EPR and mass spectra of the oxidation products.**

In a glovebox, 33 mg (0.029 mmol) of **16** and 1.01 g (3.07 mmol) of tetrabutylammonium tetrafluoroborate ( $[\text{NBu}_4][\text{BF}_4]$ ) were used to make a 10 mL  $\text{CD}_2\text{Cl}_2$  solution, which was transferred into the working electrode side of the bulk electrolysis

cell. 78 mg (0.24 mmol) of ferrocenium hexafluorophosphate(III) and 1.01 g (3.07 mmol) of  $[\text{NBu}_4][\text{BF}_4]$  were used to make a 10 mL  $\text{CD}_2\text{Cl}_2$  solution. About 6 mL of this solution was transferred into the auxiliary side of the bulk electrolysis cell. Coulometric oxidation of **16** was performed at a potential positive of the first oxidation wave (0.25 V), and the results are shown in figure 4.23. 0.92 Faradays per mole of **16** were passed. 250  $\mu\text{L}$  of solution was removed from the working electrode side of the bulk electrolysis cell and sealed in J-Young EPR tube. The solution in this tube was then frozen at 77 K. The EPR spectrum is shown in figure 4.13. After the EPR spectrum was obtained, the EPR sample was analyzed for **16** or its cation by mass spectroscopy. HRMS (FAB+) m/z calcd. for  $\text{C}_{59}\text{H}_{94}\text{ClIrN}_2\text{O}_2\text{P}_2$ : 1152.61. Found: 1152.66 ( $\text{M}^+$ ).

Coulometric oxidation of **16** was continued at a potential positive of the second oxidation wave (0.96 V), and the results are shown in figure 4.24. 0.99 Faradays per mole of **16** were passed. Another 250  $\mu\text{L}$  of solution was removed from the working electrode side of the bulk electrolysis cell and sealed in a J-Young EPR tube. The solution in the tube was then frozen at 77 K, and the EPR spectrum is shown in figure 4.14. After the EPR spectrum was obtained, the EPR sample was analyzed for **16** or its cation by mass spectroscopy. HRMS (FAB+) m/z calcd. for  $\text{C}_{59}\text{H}_{94}\text{ClIrN}_2\text{O}_2\text{P}_2$ : 1152.61. Found: 1152.67 ( $\text{M}^+$ ).

The remaining solution from the working electrode side of the bulk electrolysis cell was stored at about -20 °C for greater than two weeks. The solvent was then removed under reduced pressure, until about 4 mL remained. 0.6 mL were transferred to a J-Young NMR tube, and a  $^{31}\text{P}$  NMR spectrum was obtained.  $^{31}\text{P}\{\text{H}\}$  NMR ( $\text{CD}_2\text{Cl}_2$ , 121 MHz):  $\delta$  138.86, 130.71, 31.08, -143.52 (septet,  $^1J = 700$  Hz).

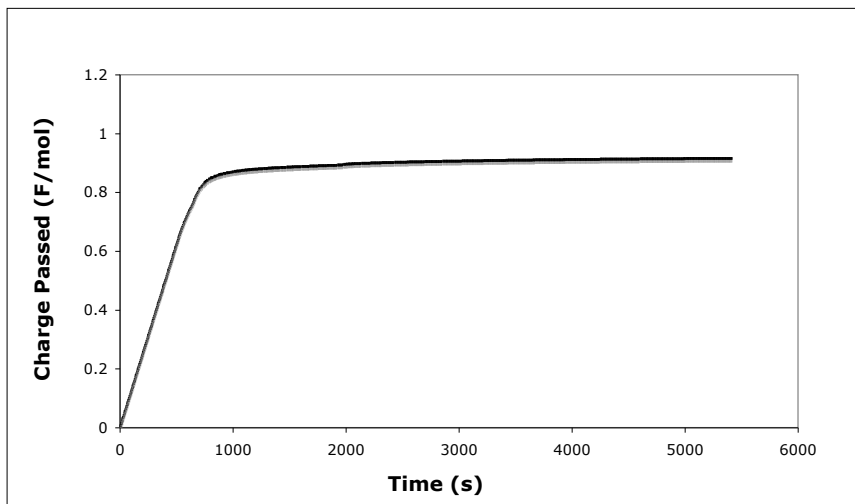


**Figure 4.23.** Coulometric oxidation of **16** at a potential positive of the first oxidation wave (0.25 V).

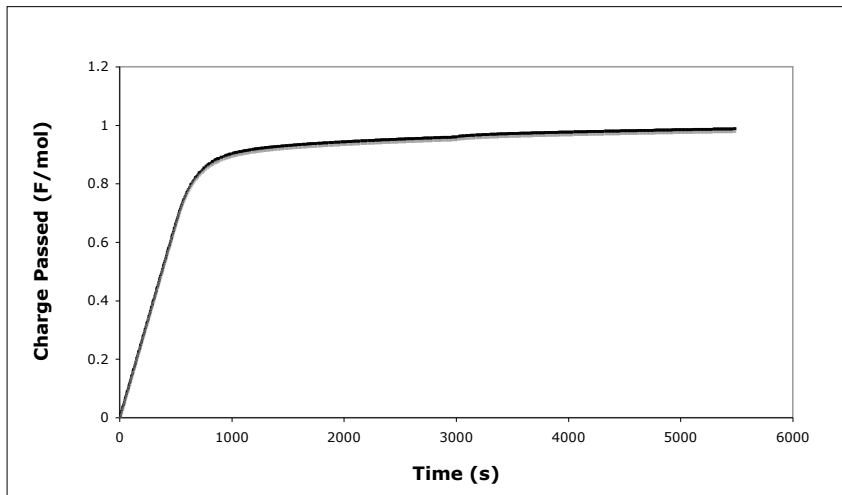


**Figure 4.24.** Second coulometric oxidation of **16** at a potential positive of the second oxidation wave of **16** (0.96 V).

**Oxidation of 16 with ferrocenium(III) hexafluorophosphate.** In a glovebox, 10 mg (8.7 mmol) of **16** was dissolved with 7 mL of  $\text{CH}_2\text{Cl}_2$  in a vial. In a separate vial,

2 mg (6 mmol) ferrocenium(III) hexafluorophosphate was dissolved in 1.7 mL CH<sub>2</sub>Cl<sub>2</sub>. The ferrocenium(III) solution was added to the solution of **16**, while stirring. 200  $\mu$ L of this solution was transferred to a J-Young EPR tube. The same EPR spectrum was obtained as for the one-electron oxidation product in the coulometric oxidation of **16**.

### Tables of Crystal Data and Structure Refinement.

**Table 4.2.** Crystal and refinement data for the structures of **5a**, **6**, and **7**.

	<b>5a</b>	<b>6</b>	<b>7</b>
Empirical formula	C <sub>33</sub> H <sub>45</sub> NO <sub>2</sub>	[C <sub>43</sub> H <sub>48</sub> N <sub>2</sub> O <sub>2</sub> Ir] <sup>-</sup> [C <sub>8</sub> H <sub>16</sub> O <sub>6</sub> K] <sup>+</sup> • $\frac{1}{2}$ (C <sub>6</sub> H <sub>6</sub> )	C <sub>34</sub> H <sub>40</sub> NOPIr
Formula weight	487.70	1007.32	894.04
T (K)	100(2)	100(2)	100(2)
<i>a</i> , Å	11.2818(11)	13.9766(6)	11.408(4)
<i>b</i> , Å	15.6956(15)	14.0671(7)	12.890(4)
<i>c</i> , Å	26.299(3)	14.2902(7)	20.209(7)
$\alpha$ , deg	92.992(2)	69.3360(10)	
$\beta$ , deg	94.515(2)	68.6020(10)	
$\gamma$ , deg	103.637(2)	64.4860(10)	
Volume, Å <sup>3</sup>	4499.5(7)	2295.88(19)	2971.8(17)
Z	6	2	4
Crystal system	Triclinic	Triclinic	Orthorhombic
Space group	P-1	P-1	P2 <sub>1</sub> 2 <sub>1</sub> 2 <sub>1</sub>

$d_{\text{calc}}$ , g/cm <sup>3</sup>	1.080	1.457	1.998
$\theta$ range, deg	1.87 to 25.06	1.88 to 42.81	1.87 to 28.32
$\mu$ , mm <sup>-1</sup>	0.066	3.051	9.028
Abs. correction	None	SADABS	Semiempirical from equivalents
GOF	1.162	1.328	1.253
$R_1$ , <sup>a</sup> $wR_2$ <sup>b</sup> [I>2σ(I)]	0.0612, 0.1087	0.0501, 0.0904	0.0505, 0.0833

<sup>a</sup>  $R_1 = \sum ||F_O| - |F_C|| / \sum |F_O|$ . <sup>b</sup>  $wR_2 = [\sum [w(F_O^2 - F_C^2)^2] / \sum [w(F_O^2)^2]]^{1/2}$ .

**Table 4.3.** Crystal and refinement data for the structures of **12/15**, and **16**.

	<b>12/15</b>	<b>16</b>
Empirical formula	$[\text{C}_{59}\text{H}_{94}\text{N}_2\text{O}_2\text{P}_2(\text{NC}_2\text{H}_3)_{0.78}(\text{CO})_{0.22}\text{Ir}]^+ [\text{PF}_6]^-$	$\text{C}_{59}\text{H}_{94}\text{N}_2\text{O}_2\text{P}_2\text{ClIr} \bullet \text{CH}_2\text{Cl}_2$
Formula weight	1300.60	1237.88
T (K)	100(2)	100(2)
$a$ , Å	15.8837(6)	13.5361(7)
$b$ , Å	17.9448(6)	38.3615(18)
$c$ , Å	21.1330(8)	22.7930(12)
$\beta$ , deg		96.738(3)
Volume, Å <sup>3</sup>	6023.5(4)	1173.9(10)
Z	4	8
Crystal system	Orthorhombic	Monoclinic

Space group	P2 <sub>1</sub> 2 <sub>1</sub> 2 <sub>1</sub>	P2 <sub>1</sub> /n
<i>d</i> <sub>calc</sub> , g/cm <sup>3</sup>	1.434	1.399
θ range, deg	1.60 to 33.58	1.39 to 31.90
<i>μ</i> , mm <sup>-1</sup>	2.359	2.505
Abs. correction	Semiempirical from equivalents	None
GOF	2.300	1.075
<i>R</i> <sub>1</sub> , <sup>a</sup> <i>wR</i> <sub>2</sub> <sup>b</sup> [ <i>I</i> >2σ( <i>I</i> )]	0.0277, 0.0481	0.0369, 0.0541

<sup>a</sup>  $R_1 = \sum ||F_o| - |F_c|| / \sum |F_o|$ . <sup>b</sup>  $wR_2 = [\sum [w(F_o^2 - F_c^2)^2] / \sum [w(F_o^2)^2]]^{1/2}$ .

## References and Notes

<sup>1</sup> Dick, A. R.; Sanford, M. S. *Tetrahedron* **2006**, *62*, 2439-2463.

<sup>2</sup> Jensen, C. M. *Chem. Commun.* **1999**, 2443-2449.

<sup>3</sup> Golden, J. T.; Anderson, R. A.; Bergman, R. G. *J. Am. Chem. Soc.* **2001**, *123*, 5837-5838.

<sup>4</sup> Shilov, A. E.; Shul'pin, G. B. *Activation and Catalytic Reactions of Saturated Hydrocarbons in the Presence of Metal Complexes*; James, B. R., Ed.; Catalysis by Metal Complexes 21; Kluwer Academic Publishers: Dordrecht, The Netherlands, 2000.

<sup>5</sup> Young, K. J. H.; Mironov, O. A.; Periana, R. A. *Organometallics* **2007**, *26*, 2137.

<sup>6</sup> Bhalla, G.; Periana, R. A. *Angew. Chem. Int. Ed.* **2005**, *44*, 1540-1543.

<sup>7</sup> Lee, M.-T.; Hu, C.-H. *Organometallics* **2004**, *23*, 976-983.

<sup>8</sup> Cotton, F. A.; Wilkinson, G.; Murillo, C. A.; Bochmann, M. *Advanced Inorganic Chemistry*, 6<sup>th</sup> ed.; Wiley & Sons: New York, 1999; pp 1039-1063.

<sup>9</sup> Crabtree, R. H. *J. Chem. Soc., Dalton Trans.* **2001**, 2437-2450.

<sup>10</sup> Strout, D. L.; Zaric, S.; Niu, S.; Hall, M. B. *J. Am. Chem. Soc.* **1996**, *118*, 6068-6069.

<sup>11</sup> Hinderling, C.; Plattner, D. A.; Chen, P. *Angew. Chem., Int. Ed. Engl.* **1997**, *36*, 243-244.

<sup>12</sup> Esteruelas, M. A.; Fernández-Alvarez, López, A. M.; Oñate, A. M.; Ruiz-Sánchez, P. *Organometallics* **2006**, *25*, 5131-5138.

<sup>13</sup> Panda, M.; Das, C.; Lee, G.-H.; Peng, S.-M.; Goswani, S. *Dalton Trans.* **2004**, 2655-2661.

<sup>14</sup> Webster, C. E.; Hall, M. B. *Coord. Chem. Rev.* **2003**, *238-239*, 315-331.

<sup>15</sup> Klei, S. R.; Tilley, T. D.; Bergman, R. G. *Organometallics* **2002**, *21*, 3376-3387.

---

<sup>16</sup> Jacobi, B. G.; Laitar, D. S.; Pu, L.; Wargocki, M. F.; DiPasquale, A. G.; Fortner, K. C.; Schuck, S. M.; Brown, S. N. *Inorg. Chem.* **2002**, *41*, 4815-4823.

<sup>17</sup> Alaimo, P. J.; Bergman, R. G. *Organometallics* **1999**, *18*, 2707-2717.

<sup>18</sup> Gutiérrez-Puebla, E.; Monge, A.; Paneque, M.; Poveda, M. L.; Taboada, S.; Trujillo, M.; Carmona, E. *J. Am. Chem. Soc.* **1999**, *121*, 346-354.

<sup>19</sup> Loza, M.; Faller, J. W.; Crabtree, R. H. *Inorg. Chem.* **1995**, *34*, 2937-2941.

<sup>20</sup> Castillo-Blum, S. E.; Richens, D. T.; Sykes, A. G. *Inorg. Chem.* **1989**, *28*, 954-960.

<sup>21</sup> Isobe, K.; Bailey, P. M.; Maitlis, P. M. *J. Chem. Soc., Chem. Commun.* **1981**, 808-809.

<sup>22</sup> Lomoth, R.; Huang, P.; Zheng, J.; Sun, L.; Hammarström, L.; Akermark, B.; Styring, S. *Eur. J. Inorg. Chem.* **2002**, 2965-974.

<sup>23</sup> Kurahashi, T.; Kikuchi, A.; Tosha, T.; Shiro, Y.; Kitagawa, T.; Fujii, H. *Inorg. Chem.* **2008**, *47*, 1674-1686.

<sup>24</sup> Mukherjee, A.; Lloret, F.; Mukherjee, R. *Inorg. Chem.* **2008**, *47*, 4471-4480.

<sup>25</sup> Haneline, M. R.; Heyduk, A. G. *J. Am. Chem. Soc.* **2006**, *128*, 8410-8411.

<sup>26</sup> Palmer, J. H.; Day, M. W.; Wilson, A. D.; Henling, L. M.; Gross, Z.; Gray, H. B. *J. Am. Chem. Soc.* **2008**, *130*, 7786-7787.

<sup>27</sup> Ringenberg, M. R.; Kokatam, S. L.; Heiden, Z. M.; Rauchfuss, T. B. *J. Am. Chem. Soc.* **2008**, *130*, 788-789.

<sup>28</sup> Liddle, S. T.; Edworthy, I. S.; Arnold, P. L. *Chem. Soc. Rev.* **2007**, *36*, 1732-1744.

<sup>29</sup> Aihara, H.; Matsuo, T.; Kawaguchi, H. *Chem. Commun.* **2003**, 2204-2205.

<sup>30</sup> Zhang, D.; Aihara, H.; Watanabe, T.; Matsuo, T.; Kawaguchi, H. *J. Organomet. Chem.* **2007**, *692*, 234-242.

---

<sup>31</sup> Macnaughtan, M. L.; Johnson, M. J. A. Needed: Modified Catalysts for Olefin Metathesis with Vinyl Halides. In *Program and Abstract Guide*, Proceedings of the International Symposium on Olefin Metathesis, Pasadena, CA, July 29 – August 3, 2007; p 39.

<sup>32</sup> Waltman, A. W.; Grubbs, R. H. *Organometallics* **2004**, *23*, 3105-3107.

<sup>33</sup> The <sup>13</sup>C NMR assignments of the imidazolyl –CH<sub>2</sub> peak and the cyclooctadiene –CH peak were made based on <sup>13</sup>C NMR spectra of **2** and **3** along with previously reported imidazolyl and cyclooctadiene complexes in references 28 and 30.

<sup>34</sup> Rodman, G. S.; Mann, K. R. *Inorg. Chem.* **1988**, *27*, 3338-3346.

<sup>35</sup> Karabiyik, H.; Kilinçarslan, R.; Aygün, M.; Çetinkaya, B.; Büyükgüngör, O. Z. *Naturforsch., B: Chem. Sci.* **2005**, *60*, 837-842.

<sup>36</sup> Fu, R. California Institute of Technology, Pasadena, CA. Unpublished work, 2008.

<sup>37</sup> Agapie, T. Ph.D. Thesis, California Institute of Technology, Pasadena, CA 2007.

<sup>38</sup> Tonks, Ian A. California Institute of Technology, Pasadena, CA. Unpublished work, 2008.

<sup>39</sup> Golisz, S. R. California Institute of Technology, Pasadena, CA. Unpublished work, 2008.

<sup>40</sup> Imrie, C.; Modro, T. A.; Rooyen, P. H. V.; Wagener, C. C. P.; Wallace, K.; Hudson, H. R.; McPartlin, M.; Nasirun, J. B.; Powroznyk, L. *J. Phys. Org. Chem.* **1995**, *8*, 41-46.

<sup>41</sup> Daresbourg, D. J.; Pala, M.; Rheingold, A. L. *Inorg. Chem.* **1986**, *25*, 125-127.

<sup>42</sup> Vazquez-Serrano, L. D.; Owens, B. T.; Buriak, J. M. *Inorg. Chim. Acta* **2006**, *359*, 2786-2797.

---

<sup>43</sup> Nagaraja, C. M.; Nethaji, M.; Jagirdar, B. R. *Organometallics* **2007**, *26*, 6307-6311.

<sup>44</sup> Roseblade, S. J.; Pfaltz, A. *Acc. Chem. Res.* **2007**, *40*, 1402-1411.

<sup>45</sup> Crabtree, R. H. *The Organometallic Chemistry of the Transition Metals*, 3<sup>rd</sup> ed.; Wiley & Sons: New York, 2001; pp 80-114, 222-258.

<sup>46</sup> Lee, D.-H.; Patel, B. P.; Clot, E.; Eisenstein, O.; Crabtree, R. H. *Chem. Commun.* **1999**, 297-298.

<sup>47</sup> Ogo, S.; Kabe, R.; Hayashi, H.; Harada, R.; Fukuzumi, S. *Dalton Trans.*, **2006**, 4657-4663.

<sup>48</sup> Sablong, R.; Osborn, J. A. *Tetrahedron: Asymmetry* **1996**, *7*, 3059-3062.

<sup>49</sup> Chan, Y. N. C.; Meyer, D.; Osborn, J. A. *J. Chem. Soc., Chem. Commun.* **1990**, 869-871.

<sup>50</sup> O'Connor, J. M.; Pu, L.; Rheingold, A. L. *J. Am. Chem. Soc.* **1990**, *112*, 6232-6247.

<sup>51</sup> Clark, H. C.; Reimer, K. J. *Inorg. Chem.* **1975**, *14*, 2133-2140.

<sup>52</sup> Thorn, D. L.; Fultz, W. C. *J. Phys. Chem.* **1989**, *93*, 1234-1243.

<sup>53</sup> Benisvy, L.; Bill, E.; Blake, A. J.; Collison, D.; Davies, E. S.; Garner, C. D.; McArdle, G.; McInnes, E. J. L.; McMaster, J.; Ross, S. H. K.; Wilson, C. *Dalton Trans.* **2006**, 258-267.

<sup>54</sup> Sokolowski, A.; Müller, J.; Weihermüller, T.; Schnepf, R.; Hildebrandt, P.; Hildenbrand, K.; Bothe, E.; Wieghardt, K. *J. Am. Chem. Soc.* **1997**, *119*, 8889-8900.

<sup>55</sup> Diversi, P.; de Biani, F. F.; Igrosso, G.; Laschi, F.; Lucherini, A.; Pinzino, C.; Zanello, P. *J. Organomet. Chem.* **1999**, *584*, 73-86.

---

<sup>56</sup> Panda, M.; Das, C.; Lee, G.-H.; Peng, S.-M.; Goswami, S. *Dalton Trans.* **2004**, 2655-2661.

<sup>57</sup> Acharyya, R.; Basuli, F.; Peng, S.-M.; Lee, G.-H.; Wang, R.-Z.; Mak, T. C. W.; Bhattacharya, S. *J. Organomet. Chem.* **2005**, 690, 3908-3917.

<sup>58</sup> Li, X.; Chen, Z.; Zhao, Q.; Shen, L.; Li, F.; Yi, T.; Cao, Y.; Huang, C. *Inorg. Chem.* **2007**, 46, 5518-5527.

<sup>59</sup> Wu, F.-I.; Su, H.-J.; Shu, C.-F.; Luo, L.; Diau, W.-G.; Cheng, C.-H.; Duan, J.-P.; Lee, G.-H. *J. Mater. Chem.* **2005**, 15, 1035-1042.

<sup>60</sup> Hoganson, C. W.; Babcock, G. T. *Biochemistry* **1992**, 31, 11874-11880.

<sup>61</sup> Halfen, J. A.; Jazdzewski, B. A.; Mahapatra, S.; Berreau, L. M.; Wilkinson, E. C.; Que, L., Jr.; Tolman, W. B. *J. Am. Chem. Soc.* **1997**, 119, 8217-8227.

<sup>62</sup> Chaudhuri, P.; Hess, M.; Müller, J.; Hildenbrand, K.; Bill, E.; Weyhermüller, T.; Wieghardt, K. *J. Am. Chem. Soc.* **1999**, 121, 9599-9610.

<sup>63</sup> Hay-Motherwell, R. S.; Wilkinson, G.; Hussain-Bates, B.; Hursthouse, M. B. *J. Chem. Soc., Dalton Trans.* **1992**, 3477-3482.

<sup>64</sup> Larsen, S. K.; Pierpont, C. G. *J. Am. Chem. Soc.* **1988**, 110, 1827-1832.

<sup>65</sup> Drago, R. S. *Physical Methods in Chemistry*; W. B. Saunders: Philadelphia, PA, 1977; pp 467-509.

<sup>66</sup> Hulsebosch, R. J.; van den Brink, J. S.; Nieuwenhuis, S. A. M.; Gast, P.; Raap, J.; Lugtenburg, J.; Hoff, A. J. *J. Am. Chem. Soc.* **1997**, 119, 8685-8694.

<sup>67</sup> Kim, S. H.; Aznar, C.; Brynda, M.; Silks, L. A. "P."; Michalczyk, R.; Unkefer, C. J.; Woodruff, W. H.; Britt, R. D. *J. Am. Chem. Soc.* **126**, 2328-2338.

---

<sup>68</sup> All density functional calculations were performed by Nilay Hazari.

<sup>69</sup> Burger, B. J.; Bercaw, J. E. *New Developments in the Synthesis, Manipulation, and Characterization of Organometallic Compounds*; Wayda, A.; Daresbourg, M. Y., Eds.; American Chemical Society: Washington, DC, **1987**; Vol. 357.

<sup>70</sup> Ferrocenium(III) hexafluorophosphate was obtained from the supplier with a small amount of the  $[\text{BF}_4]^-$ ; hence, all  $[\text{PF}_6]^-$  salts synthesized are contaminated with a small amount of the  $[\text{BF}_4]^-$  salt.

<sup>71</sup> Frisch, M. J.; Trucks, G. W.; Schlegel, H. B.; Scuseria, G. E.; Robb, M. A.; Cheeseman, J. R.; Montgomery, Jr., J. A.; Vreven, T.; Kudin, K. N.; Burant, J. C.; Millam, J. M.; Iyengar, S. S.; Tomasi, J.; Barone, V.; Mennucci, B.; Cossi, M.; Scalmani, G.; Rega, N.; Petersson, G. A.; Nakatsuji, H.; Hada, M.; Ehara, M.; Toyota, K.; Fukuda, R.; Hasegawa, J.; Ishida, M.; Nakajima, T.; Honda, Y.; Kitao, O.; Nakai, H.; Klene, M.; Li, X.; Knox, J. E.; Hratchian, H. P.; Cross, J. B.; Bakken, V.; Adamo, C.; Jaramillo, J.; Gomperts, R.; Stratmann, R. E.; Yazyev, O.; Austin, A. J.; Cammi, R.; Pomelli, C.; Ochterski, J. W.; Ayala, P. Y.; Morokuma, K.; Voth, G. A.; Salvador, P.; Dannenberg, J. J.; Zakrzewski, V. G.; Dapprich, S.; Daniels, A. D.; Strain, M. C.; Farkas, O.; Malick, D. K.; Rabuck, A. D.; Raghavachari, K.; Foresman, J. B.; Ortiz, J. V.; Cui, Q.; Baboul, A. G.; Clifford, S.; Cioslowski, J.; Stefanov, B. B.; Liu, G.; Liashenko, A.; Piskorz, P.; Komaromi, I.; Martin, R. L.; Fox, D. J.; Keith, T.; Al-Laham, M. A.; Peng, C. Y.; Nanayakkara, A.; Challacombe, M.; Gill, P. M. W.; Johnson, B.; Chen, W.; Wong, M. W.; Gonzalez, C.; Pople, J. A.; *Gaussian 03*, revision C.02, Gaussian, Inc., Wallingford CT, 2004.

---

<sup>72</sup> Becke, A. D. *Phys. Rev. A: At., Mol., Opt. Phys.* **1988**, *38*, 3098-3100.

<sup>73</sup> Becke, A. D. *J. Chem. Phys.* **1988**, *88*, 1053-1062.

<sup>74</sup> Perdew, J. P. *Phys. Rev. B* **1986**, *33*, 8800-8802.

<sup>75</sup> Hay, P. J.; Wadt, W. R. *J. Chem. Phys.* **1985**, *82*, 270-283.

<sup>76</sup> Wadt, W. R.; Hay, P. J. *J. Chem. Phys.* **1985**, *82*, 284-298.

<sup>77</sup> Hay, P. J.; Wadt, W. R. *J. Chem. Phys.* **1985**, *82*, 299-310.

<sup>78</sup> Andrae, D.; Häussermann, U.; Dolg, M.; Stoll, H.; Preuss, H. *Theor. Chim. Acta* **1990**, *77*, 123-141.

<sup>79</sup> Bergner, A.; Dolg, M.; Küchle, W.; Stoll, H.; Preuss, H. *Mol. Phys.* **1993**, *80*, 1431-1441.

<sup>80</sup> Svensson, M.; Humber, S.; Froese, R. D. J.; Matsubara, T.; Sieber, S.; Morokuma, K. J. *J. Phys. Chem.* **1996**, *100*, 19357-19363.

<sup>81</sup> Flukiger, P.; Portmann, H. P. L.; Weber, J. *MOLEKEL*; Swiss Centre for Scientific Computing: Manno, Switzerland, 2000; Vol. 1.

## **Appendix 1**

### **Preliminary Studies on the Synthesis, Oxidation, and Protonation of Water-Soluble Methylplatinum(II) Complexes Containing Sulfonated, Bidentate Ligands**

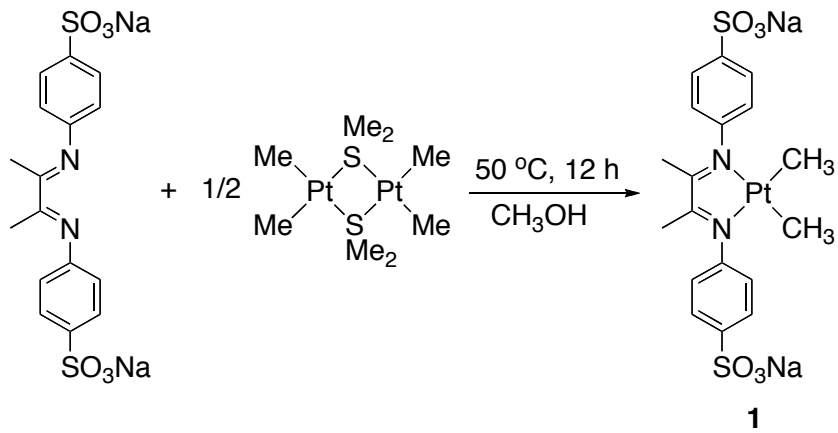
## Introduction

As stated in chapter 3, the platinum(II)-catalyzed alkane functionalization discovered by Shilov et al. requires improved catalyst stability in order to be practical.<sup>1-4</sup> The use of chelating ligands has the potential to improve catalyst stability and to aid in characterization, in part by limiting the number of species in solution.<sup>4,5</sup> Since the platinum(II) system used by Shilov et al. is performed in aqueous solutions, sulfonated, chelating ligands will be used to generate water-soluble methylplatinum(II) complexes relevant to this catalysis. In particular, oxidation of these complexes will be used to gain more information about possible factors affecting oxidation of the methylplatinum(II) species in the Shilov system.<sup>3</sup>

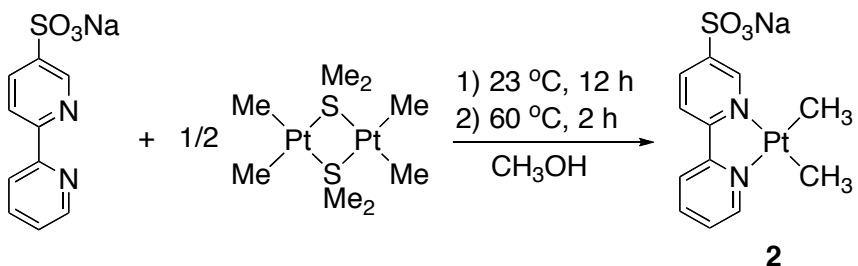
## Results

The sodium salt of 1,4-bis(4-phenylsulfonate)-2,3-dimethyl-1,4-diaza-1,3-butadiene was heated in methanol at 50 °C with bis(dimethyl(μ-dimethylsulfide))platinum(II) to generate (4-bis(4-phenylsulfonate)-2,3-dimethyl-1,4-diaza-1,3-butadiene)dimethylplatinum(II) (**1**) as depicted in scheme A1.1. Likely due to the thermal instability of the bis(dimethyl(μ-dimethylsulfide))platinum(II), some colloidal platinum(0) always formed, and it proved difficult to remove. Thus, in all reactions performed with this complex, there was a small amount of colloidal platinum(0). **1** is a dark red solid that is soluble in water, and it is sparingly soluble in methanol. When it is dissolved in water, it forms a yellow solution; however, the complex decomposes slowly in water, and a significant amount of decomposition can be observed by <sup>1</sup>H NMR spectroscopy after 1 day.

In order to circumvent problems associated with colloidal platinum removal and decomposition in aqueous solution, (2,2'-bipyridine-5-sulfonate)dimethylplatinum(II) (**2**) was synthesized. 2,2'-Bipyridine-5-sulfonic acid was synthesized by published procedures, and then it was deprotonated with an aqueous sodium hydroxide solution to form the sodium salt of 2,2'-bipyridine-5-sulfonate.<sup>6</sup> This was then reacted with bis(dimethyl( $\mu$ -dimethylsulfide))platinum(II) to generate (2,2'-bipyridine-5-sulfonate)dimethylplatinum(II) (**2**) as illustrated in scheme A1.2. Excess bis(dimethyl( $\mu$ -dimethylsulfide))platinum(II) was decomposed by heating the solution to 60° C. Impurities were precipitated out of the resulting solution by addition of diethyl ether, and they were then removed by filtration. Removal of solvent and other volatiles under reduced pressure resulted in the isolation of **2** as a bright red solid. When dissolved in water, this complex, like **1**, forms a yellow solution.

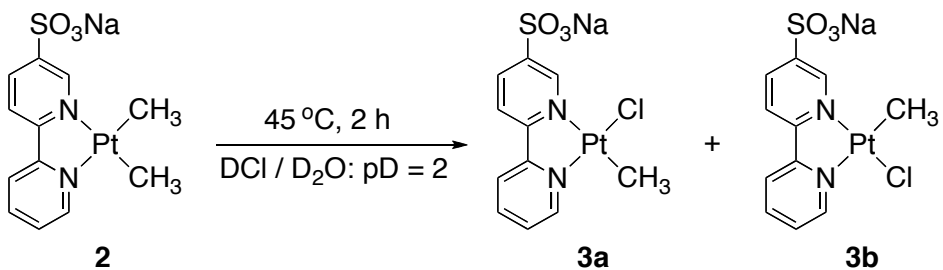


**Scheme A1.1.** The synthesis of **1**.



**Scheme A1.2.** The synthesis of **2**.

(2, 2'-bipyridine-5-sulfonate)chloromethylplatinum(II) (**3**) was generated *in situ* by heating an aqueous DCl solution of **2** with pD = 2 to 45° C for 45 minutes (scheme A1.3). Two isomers were formed as characterized by  $^1\text{H}$  NMR spectroscopy, and they showed Pt-CH<sub>3</sub> peaks at 0.87 and 0.88 ppm each with  $^{195}\text{Pt}$  satellites having a coupling constant of  $^2J_{\text{PtH}} = 75$  Hz.



**Scheme A1.3.** Protonolysis of **2** to generate isomers **3a** and **3b**.

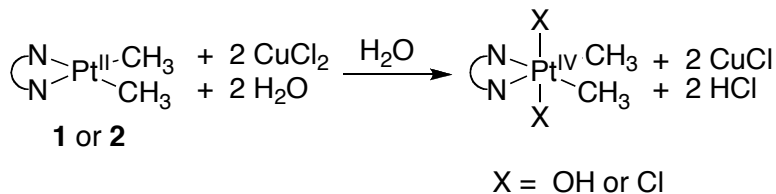
Complexes **1** and **2** seem to be oxidized by both dioxygen and hydrogen peroxide to form the respective dimethylplatinum(IV) complexes in aqueous solutions.<sup>7</sup> These complexes are a light yellow color in solution. For similar complexes, the Pt-CH<sub>3</sub> peak in the  $^1\text{H}$  NMR spectrum can often be used as a test of the platinum oxidation state; a downfield shift of this peak accompanied by decrease in  $^{195}\text{Pt}$  coupling constant from

about 80 Hz to about 70 Hz is typical for the oxidation of platinum(II) species to platinum(IV) species.<sup>8,9</sup> The Pt-CH<sub>3</sub> peak of **1** occurs at 0.63 ppm with  $^2J_{\text{PtH}}= 85$  Hz. Upon oxidation, a species was generated which was tentatively identified as platinum(IV) based on the characteristic Pt-CH<sub>3</sub> peak in the <sup>1</sup>H NMR spectrum at 1.01 ppm with a coupling constant of  $^2J_{\text{PtH}}= 69$  Hz.<sup>7,8</sup> The Pt-CH<sub>3</sub> peaks of **2** occur at 0.85 and 0.87 ppm with coupling constants of  $^2J_{\text{PtH}}= 84$  Hz, while oxidation leads to a probable platinum(IV) species in which these peaks are shifted to 1.70 and 1.72 ppm with coupling constants of  $^2J_{\text{PtH}}= \sim 70$  Hz. The products formed in the reaction of **3a** and **3b** with hydrogen peroxide in D<sub>2</sub>O containing DCl at a pH of 2 could not be identified.

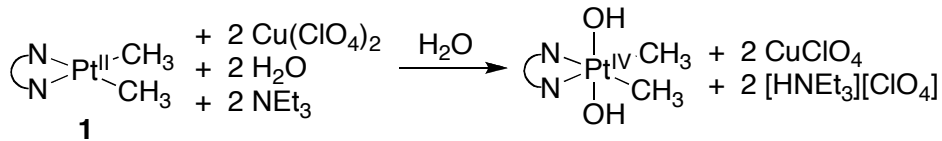
Oxidations of **1** and **2** with hydrogen peroxide occur cleanly and rapidly, and they are complete within five minutes; however, oxidations of **1** and **2** with dioxygen occur at a significantly slower rate. An approximate dioxygen oxidation rate of **1** was determined previously by UV-Vis spectroscopy; **1**, in a 0.33 mM aqueous solution, has a half-life of about 24 minutes under an atmosphere of oxygen.<sup>7</sup>

Both **1** and **2** were oxidized cleanly by excess CuCl<sub>2</sub> in aqueous solutions to species tentatively identified as platinum(IV) complexes (scheme A1.4). These reactions were complete in less than five minutes as observed by a downfield shift of the peaks in the <sup>1</sup>H NMR spectrum relative to the peaks of the initial platinum(II) complex. Following oxidation of **1**, the Pt-CH<sub>3</sub> peak in the oxidized complex was shifted downfield to 1.15 ppm with a coupling constant of  $^2J_{\text{PtH}}= 68$  Hz. The corresponding peak resulting from the oxidation of **2** was shifted downfield to 1.21 ppm with a coupling constant of  $^2J_{\text{PtH}}= 68$  Hz. Octahedral dimethylplatinum(IV) complexes containing the respective chelating ligands are likely formed in these reactions, but it is unclear what combination

of hydroxides and chlorides are in the axial positions. **1** was also oxidized by  $[\text{Cu}(\text{H}_2\text{O})_6]\text{[ClO}_4\text{]}_2$ , but the reaction was not as clean unless an excess of triethylamine was used (scheme A1.5). This could be due to the formation of acid in these reactions as depicted in schemes A1.4 and A1.5. Based on  $^1\text{H}$  NMR spectroscopy, no reaction occurred in a preliminary attempt at oxidizing the chloro(methyl)platinum(II) complex (**3**) with  $\text{CuCl}_2$  in an aqueous solution with a pH of 2.



**Scheme A1.4.** Oxidations of **1** and **2** with  $\text{CuCl}_2$ .



**Scheme A1.5.** Oxidation of **1** with  $\text{Cu}(\text{ClO}_4)_2$  in the presence of triethylamine.

### Discussion and Conclusions

While complexes **1** and **2** were oxidized slowly by dioxygen, they were both rapidly oxidized by hydrogen peroxide and  $\text{CuCl}_2$ . As  $\text{CuCl}$  can be reoxidized rapidly by dioxygen at elevated temperatures and pressures, this bodes favorably for rapid oxidation of these complexes using a catalytic amount of  $\text{CuCl}_2$  and a stoichiometric amount of

dioxygen.<sup>10,11</sup> Significant numbers of turnovers actually have been achieved in a modified Shilov system using  $\text{CuCl}_2$  to catalyze the oxidation of alkylplatinum(II) complexes with dioxygen.<sup>12</sup> Unfortunately, there are two major problems with the use of  $\text{CuCl}_2$  to catalyze these oxidations. First, the chloride ion is corrosive in aqueous solutions. Secondly, chloride is consumed in the Shilov system due to the formation of alkyl chlorides, and this could make it difficult to keep enough chloride in solution when attempting to catalyze the oxidation of alkylplatinum(II) complexes using  $\text{CuCl}_2$ .<sup>3</sup>

Due to the aforementioned problems, it could be beneficial to work with a system that does not require chloride ions in solution. The only other copper salt tested in these oxidations thus far has been  $[\text{Cu}(\text{H}_2\text{O})_6][\text{ClO}_4]_2$ . In the absence of chloride,  $[\text{Cu}(\text{H}_2\text{O})_6][\text{ClO}_4]_2$  oxidized **1** at a similar rate to  $\text{CuCl}_2$  and hydrogen peroxide; although, some side-products were formed. The reaction occurred more cleanly when there was base around, possibly due to the formation of acid (schemes A1.4 and A1.5). The oxidation of **1** with  $[\text{Cu}(\text{H}_2\text{O})_6][\text{ClO}_4]_2$  is interesting because aqueous oxidation of the monomethylplatinum(II) salts described in chapter 2 did not occur with  $[\text{Cu}(\text{H}_2\text{O})_6][\text{ClO}_4]_2$  as the oxidant. In that case, though, oxidation of the monomethylplatinum(II) species had to compete with rapid protonolysis.

Chloromethylplatinum(II) complexes with bidentate ligands have previously been shown to be more difficult to oxidize than the corresponding dimethylplatinum(II) complexes; so, it would be of interest if these complexes could be oxidized by  $\text{CuCl}_2$ , especially since the Shilov cycle requires the oxidation of alkylchloroplatinum(II) complexes.<sup>13</sup> A chloromethylplatinum(II) complex (**3**) containing the sulfonated bipyridine ligand was generated *in situ* from protonolysis of **2**. The  $\text{Pt}^{\text{II}}\text{-CH}_3$  peaks for **3a**

and **3b** in the  $^1\text{H}$  NMR spectrum were intermediate in chemical shift and  $^{195}\text{Pt}$  coupling constants between those of the dimethylplatinum(II) complexes and those of the dimethylplatinum(IV) complexes, likely indicating a complex intermediate between the two in electron density at the platinum center. This should make this complex more difficult to oxidize than the dimethylplatinum(II) complexes, as would be expected based on the oxidation potential differences determined previously for dimethyl- and chloromethyl-platinum(II) complexes.<sup>13</sup> **3** was not oxidized by  $\text{CuCl}_2$  at a pH of 2; however, it may be more easily oxidized at a higher pH.

## Experimental Section

**General considerations.** All moisture-sensitive compounds were manipulated using standard vacuum line, Schlenk or cannula techniques or in a glovebox under a dinitrogen atmosphere. Unless otherwise noted, solvents were deoxygenated and dried by thorough sparging with dinitrogen gas followed by passage through an activated alumina column.<sup>14</sup> All deuterated solvents were purchased from Cambridge Isotope Laboratories, Inc. Methanol-d<sub>4</sub> was degassed prior to use. Anhydrous methanol was purchased from Aldrich and degassed. Bis(dimethyl( $\mu$ -dimethylsulfide))platinum (II),<sup>15</sup> (1,4-bis(4-sulfonylphenyl)-2,3-dimethyl-1,4-diaza-1,3-butadiene),<sup>16</sup> and 2,2'-bipyridine-5-sulfonic acid<sup>6</sup> were prepared according to previously published procedures.

NMR spectra were acquired on a Varian Mercury 300 ( $^1\text{H}$ , 299.8 MHz;  $^{13}\text{C}$ , 75.4626 MHz) spectrometer at 23 °C.  $^1\text{H}$  NMR shifts were referenced with respect to internal solvent: 4.80 (DSS) (deuterium oxide) and 3.31 (m) (methanol-d<sub>4</sub>).

**Synthesis of (1, 4-bis(4-sulfonylphenyl)-2, 3-dimethyl-1, 4-diaza-1, 3-butadiene)dimethylplatinum(II) (1).** The sodium salt of 1,4-bis(4-sulfonate)-2,3-dimethyl-1,4-diaza-1,3-butadiene) (386 mg, 0.88 mmol) and bis(dimethyl( $\mu$ -dimethylsulfide)) (250 mg, 0.415 mmol) were dissolved in 18 mL of methanol in a Schlenk tube and sealed. While stirring, the yellow suspension was heated to 50° C, and it turned red after about 15 minutes. Heating was continued for 12 hours, and then the vessel was cooled to 23 °C. The solid was isolated by filtration and then washed with methanol. The resulting red solid, which contained some black platinum (0) from decomposition of bis(dimethyl( $\mu$ -dimethylsulfide)), was dried in under reduced pressure.  $^1\text{H}$  NMR (300 MHz,  $\text{D}_2\text{O}$ ,  $\delta$ ): 0.63 (s, 6H,  $^2J_{\text{PtH}} = 85$  Hz,  $\text{PtCH}_3$ ), 1.78 (s, 12H,  $\text{CH}_3$ ), 7.13 (d, 4H,  $^3J_{\text{HH}} = 8.3$  Hz, *o*-*H*), 7.97 (d, 4H,  $^3J_{\text{HH}} = 8.3$  Hz, *m*-*H*).

**Oxidation of 1 with copper(II) salts in  $\text{D}_2\text{O}$ .** **1** (15 mg, 0.022 mmol) and  $\text{CuCl}_2$  (9 mg, 0.07 mmol) were each dissolved in 0.02 mL of  $\text{D}_2\text{O}$ . The solution of  $\text{CuCl}_2$  was then added to the solution of **1**, and complete conversion to the oxidized product was seen immediately by  $^1\text{H}$  NMR spectroscopy.  $^1\text{H}$  NMR (300 MHz,  $\text{D}_2\text{O}$ ,  $\delta$ ): 1.16 (s, 6H,  $^2J_{\text{PtH}} = 68$  Hz,  $\text{PtCH}_3$ ), 2.45 (s, 12H,  $\text{CH}_3$ ), 7.22 (b s, 4H, *o*-*H*), 7.96 (b s, 4H, *m*-*H*). This reaction was repeated with  $\text{CuClO}_4 \cdot 6 \text{ H}_2\text{O}$  (13 mg, 0.04 mmol), **1** (11 mg, 0.02 mmol), and an excess of triethylamine to yield the same results. The reaction with  $\text{CuClO}_4 \cdot 6 \text{ H}_2\text{O}$  occurred without triethylamine, but small amounts of side-products were formed.

**Synthesis of (2,2'-bipyridine-5-sulfonate)dimethylplatinum(II) (2).** 2,2'-bipyridine-5-sulfonic acid (870 mg, 3.7 mmol) was dissolved in 50 mL  $\text{H}_2\text{O}$ . Aqueous

sodium hydroxide solution (0.024 M) was added until the solution reached a pH of 7. The solvent was then evaporated to yield a white solid (799.02 mg, 3.0945 mmol). In a Schlenk tube, this solid (238 mg, 0.414 mmol) was dissolved along with bis(dimethyl( $\mu$ -dimethylsulfide))platinum(II) (125 mg, 0.218 mmol) in 50 mL of methanol. The vessel was sealed, and the solution was stirred for about 12 hours. During that time, the solution turned from yellow to orange. The solution was then heated to 60° C for 2 hours before being cooled to room temperature. Diethyl ether was added to the solution in order to precipitate an impurity which was then removed by filtration. This was repeated, and then the solvent was removed from the filtrate under reduced pressure. The resulting solid was washed with diethyl ether, and then volatiles were removed under reduced pressure. This yielded a bright red solid (58.9%, 118 mg, 0.244 mmol).  $^1\text{H}$  NMR (300 MHz,  $\text{D}_2\text{O}$ ,  $\delta$ ): 0.85 (s, 3H,  $^2J_{\text{PtH}}=84$  Hz,  $\text{PtCH}_3$ ), 0.87 (s, 3H, 84 Hz,  $\text{CH}_3$ ), 7.62 (t, 1H,  $^3J_{\text{HH}}= 6.7$  Hz), 8.09-8.35 (m, 3H), 8.49 (dd, 1H  $^3J_{\text{HH}}= 8.7$  Hz), 8.91 (d, 1H,  $^3J_{\text{HH}}= 5.4$  Hz), 9.20 (d, 1H,  $^4J_{\text{HH}}= 2.2$  Hz,  $^3J_{\text{PtH}}= 22$  Hz, 6-H).

**Oxidations of 2 in  $\text{D}_2\text{O}$ .** **2** (5 mg, 0.01 mmol) was dissolved in 0.4 mL  $\text{D}_2\text{O}$  to form a yellow solution.  $\text{CuCl}_2$  (about 1 mg, 0.1 mmol) was then added. The solution turned a lighter yellow, and the  $^1\text{H}$  NMR spectrum revealed a mixture of an oxidized Pt(IV) species and starting material. The oxidized Pt(IV) species showed characteristic  $\text{PtCH}_3$  peaks at 1.21 ppm ( $^2J_{\text{PtH}}= 68$  Hz) and 1.22 ppm ( $^2J_{\text{PtH}}= 68$  Hz) in the  $^1\text{H}$  NMR spectrum. The oxidation of **2** was repeated with an excess of aqueous hydrogen peroxide solution (1 drop, 10 M). Bubbling occurred, and the solution turned light yellow. The  $\text{PtCH}_3$  peaks again migrated downfield, indicating formation of a

platinum(IV) complex.  $^1\text{H}$  NMR (300 MHz,  $\text{D}_2\text{O}$ ,  $\delta$ ): 1.70 ( $\text{PtCH}_3$ ), 1.72 ( $\text{PtCH}_3$ ), 7.90, 8.35, 8.65, 8.70, 9.02, 9.27.

**In situ generation of (2,2'-bipyridine-5-sulfonate)chloromethylplatinum(II) (3).** **2** (5 mg, 0.01 mmol) was dissolved in 0.4 mL of a DCl and  $\text{D}_2\text{O}$  solution ( $\text{pD}=2$ ). This solution was heated to 45 °C for 45 minutes, and it changed from yellow to orange.  $^1\text{H}$  NMR spectroscopy revealed the formation of two isomers.  $^1\text{H}$  NMR (300 MHz,  $\text{D}_2\text{O}$ ,  $\delta$ ): one isomer- 0.87 (s, 3H,  $^2\text{J}$  75 Hz,  $\text{PtCH}_3$ ), 7.42 (m, 1H, 5'- $H$ ), 8.07- 8.35 (m, 3H), 8.49 (dd, 1H,  $^3\text{J}_{\text{HH}}=8.5$  Hz,  $^4\text{J}_{\text{HH}}=1.9$  Hz, 5'- $H$ ), 8.75 (d, 1H,  $^3\text{J}_{\text{HH}}=4.9$  Hz, 6'- $H$ ), 9.05 (d, 1H,  $^4\text{J}_{\text{HH}}=1.8$  Hz, 6- $H$ ); other isomer- 0.88 (s, 3H,  $^2\text{J}_{\text{PtH}}=75$  Hz,  $\text{PtCH}_3$ ), 7.77 (m, 1H, 5'- $H$ ), 8.07-8.34 (m, 3H), 8.45 (dd, 1H,  $^3\text{J}_{\text{HH}}=8.5$  Hz,  $^4\text{J}_{\text{HH}}=2.2$  Hz, 5'- $H$ ), 8.82 (d, 1H,  $^3\text{J}_{\text{HH}}=5.6$  Hz, 6'- $H$ ), 9.12 (b s, 1H, 6- $H$ ).

**Attempted oxidation of 3.**  $\text{CuCl}_2$  (about 1 mg, 0.01 mmol) was added to the solution of **8**. No reaction was observed by  $^1\text{H}$  NMR spectroscopy.

## References and Notes

---

<sup>1</sup> Goldshlegger, N. F.; Tyabin, M. B.; Shilov, A. E.; Shteinman, A. A. *Zh. Fiz. Khim.* **1969**, *43*, 2174-2175.

<sup>2</sup> Goldshlegger, N. F.; Eskova, V. V.; Shilov, A. E.; Shteinman, A. A. *Zh. Fiz. Khim.* **1972**, *46*, 1353-1354.

<sup>3</sup> Shilov, A. E.; Shul'pin, G. B. *Activation and Catalytic Reactions of Saturated Hydrocarbons in the Presence of Metal Complexes*; Kluwer, Academic Publishers: Dordrecht, 2000; pp 259-317.

<sup>4</sup> Labinger, J. A.; Bercaw, J. E. *Nature* **2002**, *417*, 507-514.

<sup>5</sup> Lersch, M.; Tilset, M. *Chem. Rev.* **2005**, *105*, 2471-2526.

<sup>6</sup> Herrmann, W. A.; Thiel, W. R.; Kuchler, J. G. *Chem. Ber.* **1990**, *123*, 1953-1961.

<sup>7</sup> Balzarek, C.; Labinger, J. A.; Bercaw, J. E. California Institute of Technology, Pasadena, CA. Unpublished work, 2001.

<sup>8</sup> Rostovtsev, V. V.; Henling, L. M.; Labinger, J. A.; Bercaw, J. E. *Inorg. Chem.* **2002**, *41*, 3608-3619.

<sup>9</sup> In a <sup>1</sup>H NMR spectrum, a Pt<sup>IV</sup>-CH<sub>3</sub> peak would be expected to be shifted farther downfield and have a smaller coupling constant relative to the corresponding Pt<sup>II</sup>-CH<sub>3</sub> peak.

<sup>10</sup> Smidt, J.; Sedlmeier, J.; Hafner, W.; Sieber, R.; Sabel, A.; Jira, R. *Angew. Chem.* **1962**, *74*, 93-102.

<sup>11</sup> Lin, M.; Shen, C.; Garcia-Zayas, E.; Sen, A. *J. Am. Chem. Soc.* **2001**, *123*, 1000-1001.

<sup>12</sup> Lin, M.; Shen, C.; Garcia-Zayas, E. A.; Sen, A. *J. Am. Chem. Soc.* **2001**, *123*, 1000-1001.

---

<sup>13</sup> Scollard, J. D.; Day, M.; Labinger, J. A.; Bercaw, J. E. *Helv. Chim. Acta* **2001**, *84*, 3247-3268.

<sup>14</sup> Pangborn, A. B.; Giardello, M. A.; Grubbs, R. H.; Rosen, R. K.; Timmers, F. J. *Organometallics* **1996**, *15*, 1518-1520.

<sup>15</sup> Hill, G. S.; Irwin, M. J.; Levy, C. J.; Rendina, L. M.; Puddephatt, R. J. *Inorg. Synth.* **1998**, *32*, 149-153.

<sup>16</sup> Tom Dieck, H.; Svoboda, M.; Greiser, T. *Z. Naturforschung* **1981**, *36B*, 823-832.

## **Appendix 2**

### **Tables for X-ray Crystal Structures**

## Structure in Chapter 3

### Structure of 2 (CCDC 706858)

#### Special Refinement Details

Crystals were mounted on a glass fiber using Paratone oil then placed on the diffractometer under a nitrogen stream at 100K.

The diethylether sits at a center of symmetry and is therefore half occupancy. The geometry was fixed and the temperature factors were not refined.

Refinement of  $F^2$  against ALL reflections. The weighted R-factor ( $wR$ ) and goodness of fit (S) are based on  $F^2$ , conventional R-factors (R) are based on F, with F set to zero for negative  $F^2$ . The threshold expression of  $F^2 > 2\sigma(F^2)$  is used only for calculating R-factors(gt) etc. and is not relevant to the choice of reflections for refinement. R-factors based on  $F^2$  are statistically about twice as large as those based on F, and R-factors based on ALL data will be even larger.

All esds (except the esd in the dihedral angle between two l.s. planes) are estimated using the full covariance matrix. The cell esds are taken into account individually in the estimation of esds in distances, angles and torsion angles; correlations between esds in cell parameters are only used when they are defined by crystal symmetry. An approximate (isotropic) treatment of cell esds is used for estimating esds involving l.s. planes.

**Table A2.1. Atomic coordinates ( x 10<sup>4</sup>) and equivalent isotropic displacement parameters (Å<sup>2</sup> x 10<sup>3</sup>) for 2 (CCDC 706858). U(eq) is defined as the trace of the orthogonalized U<sub>ij</sub> tensor.**

	x	y	z	U <sub>eq</sub>	Occ
Pt(1)	9392(1)	9137(1)	3336(1)	17(1)	1
Na(1)	11131(1)	8176(1)	3515(1)	22(1)	1
Na(2)	7647(1)	9322(1)	3823(1)	27(1)	1
O(1)	12310(1)	7936(1)	4063(1)	24(1)	1
O(2)	12111(1)	9238(1)	3665(1)	25(1)	1
O(3)	12054(1)	8643(1)	2926(1)	25(1)	1
O(4)	11222(1)	7253(1)	2966(1)	25(1)	1
O(5)	11046(1)	6862(1)	3774(1)	25(1)	1
O(6)	6386(1)	9233(1)	3332(1)	28(1)	1
O(7)	7022(1)	10609(1)	3578(1)	38(1)	1
O(8)	8020(1)	10398(1)	4242(1)	67(1)	1
O(9)	7032(1)	9197(1)	4514(1)	55(1)	1
O(10)	6726(1)	8131(1)	3909(1)	33(1)	1
N(1)	9747(1)	9014(1)	3955(1)	19(1)	1
N(2)	10027(1)	10203(1)	3459(1)	18(1)	1
C(1)	9645(1)	8508(1)	4271(1)	19(1)	1
C(2)	9270(1)	7768(1)	4274(1)	24(1)	1
C(3)	9222(1)	7384(1)	4637(1)	27(1)	1
C(4)	9546(1)	7710(1)	4997(1)	27(1)	1
C(5)	9932(1)	8433(1)	5001(1)	24(1)	1
C(6)	9982(1)	8847(1)	4638(1)	20(1)	1
C(7)	10291(1)	9588(1)	4532(1)	20(1)	1
C(8)	10136(1)	9663(1)	4123(1)	18(1)	1
C(9)	10304(1)	10296(1)	3853(1)	18(1)	1
C(10)	10715(1)	11000(1)	3922(1)	21(1)	1
C(11)	10711(1)	11380(1)	3544(1)	20(1)	1
C(12)	11029(1)	12093(1)	3407(1)	23(1)	1
C(13)	10919(1)	12284(1)	3005(1)	26(1)	1
C(14)	10506(1)	11774(1)	2733(1)	27(1)	1
C(15)	10182(1)	11067(1)	2858(1)	24(1)	1
C(16)	10279(1)	10865(1)	3263(1)	19(1)	1
C(17)	8822(1)	8073(1)	3261(1)	25(1)	1
C(18)	9062(1)	9349(1)	2746(1)	27(1)	1
C(19)	12398(1)	8624(1)	4286(1)	29(1)	1
C(20)	12734(1)	9225(1)	3996(1)	31(1)	1
C(21)	12436(1)	9685(1)	3336(1)	31(1)	1
C(22)	11924(1)	9446(1)	2963(1)	29(1)	1

C(23)	11604(1)	8330(1)	2579(1)	28(1)	1
C(24)	11699(1)	7484(1)	2607(1)	27(1)	1
C(25)	11442(1)	6499(1)	3085(1)	28(1)	1
C(26)	10863(1)	6338(1)	3454(1)	30(1)	1
C(27)	11836(1)	6659(1)	4018(1)	30(1)	1
C(28)	12019(1)	7306(1)	4302(1)	29(1)	1
C(29)	6024(1)	9918(1)	3163(1)	37(1)	1
C(30)	6786(2)	10492(1)	3168(1)	44(1)	1
C(31)	7831(1)	11069(1)	3633(1)	69(1)	1
C(32)	7969(2)	11143(2)	4069(1)	87(1)	1
C(33)	7775(2)	10373(2)	4653(1)	99(1)	1
C(34)	7701(2)	9564(2)	4775(1)	88(1)	1
C(35)	6846(2)	8423(2)	4601(1)	72(1)	1
C(36)	6219(2)	8116(1)	4280(1)	55(1)	1
C(37)	6174(1)	7981(1)	3559(1)	38(1)	1
C(38)	5681(1)	8682(1)	3408(1)	38(1)	1
O(40)	9930(2)	5434(2)	5045(1)	50	0.50
C(41)	10364(3)	5556(3)	4663(1)	50	0.50
C(42)	9901(5)	5183(4)	4312(2)	50	0.50
C(43)	10060(3)	4680(3)	5177(2)	50	0.50
C(44)	10053(5)	4692(4)	5638(2)	50	0.50

**Table A2.2. Bond lengths [Å] and angles [°] for 2 (CCDC 706858).**

Pt(1)-C(18)	2.0469(16)	O(1)-C(19)	1.423(2)
Pt(1)-C(17)	2.0536(16)	O(1)-C(28)	1.424(2)
Pt(1)-N(2)	2.1210(12)	O(2)-C(20)	1.411(2)
Pt(1)-N(1)	2.1265(13)	O(2)-C(21)	1.422(2)
Pt(1)-Na(2)	2.9821(6)	O(3)-C(23)	1.428(2)
Pt(1)-Na(1)	3.0565(6)	O(3)-C(22)	1.429(2)
Na(1)-O(2)	2.3828(12)	O(4)-C(25)	1.4176(19)
Na(1)-O(4)	2.4419(13)	O(4)-C(24)	1.430(2)
Na(1)-O(5)	2.4672(12)	O(5)-C(26)	1.430(2)
Na(1)-O(3)	2.4943(13)	O(5)-C(27)	1.430(2)
Na(1)-O(1)	2.5103(13)	O(6)-C(38)	1.417(2)
Na(1)-N(1)	2.8602(14)	O(6)-C(29)	1.425(2)
Na(2)-O(8)	2.4073(16)	O(7)-C(30)	1.418(3)
Na(2)-O(6)	2.4305(13)	O(7)-C(31)	1.419(2)
Na(2)-O(9)	2.4619(16)	O(8)-C(33)	1.407(4)
Na(2)-O(10)	2.4869(13)	O(8)-C(32)	1.431(4)
Na(2)-O(7)	2.5630(15)	O(9)-C(35)	1.416(3)

O(9)-C(34)	1.441(3)	C(17)-Pt(1)-Na(2)	80.55(5)
O(10)-C(36)	1.428(2)	N(2)-Pt(1)-Na(2)	98.84(3)
O(10)-C(37)	1.428(2)	N(1)-Pt(1)-Na(2)	71.69(3)
N(1)-C(1)	1.3834(19)	C(18)-Pt(1)-Na(1)	118.22(5)
N(1)-C(8)	1.3849(19)	C(17)-Pt(1)-Na(1)	80.85(5)
N(2)-C(9)	1.3738(19)	N(2)-Pt(1)-Na(1)	96.01(3)
N(2)-C(16)	1.3814(19)	N(1)-Pt(1)-Na(1)	64.07(3)
C(1)-C(2)	1.407(2)	Na(2)-Pt(1)-Na(1)	129.051(19)
C(1)-C(6)	1.436(2)	O(2)-Na(1)-O(4)	130.13(5)
C(2)-C(3)	1.384(2)	O(2)-Na(1)-O(5)	133.57(5)
C(3)-C(4)	1.401(3)	O(4)-Na(1)-O(5)	68.91(4)
C(4)-C(5)	1.384(2)	O(2)-Na(1)-O(3)	66.24(4)
C(5)-C(6)	1.410(2)	O(4)-Na(1)-O(3)	66.82(4)
C(6)-C(7)	1.419(2)	O(5)-Na(1)-O(3)	127.36(4)
C(7)-C(8)	1.381(2)	O(2)-Na(1)-O(1)	65.74(4)
C(8)-C(9)	1.449(2)	O(4)-Na(1)-O(1)	113.09(4)
C(9)-C(10)	1.389(2)	O(5)-Na(1)-O(1)	67.85(4)
C(10)-C(11)	1.421(2)	O(3)-Na(1)-O(1)	105.69(4)
C(11)-C(12)	1.408(2)	O(2)-Na(1)-N(1)	83.91(4)
C(11)-C(16)	1.440(2)	O(4)-Na(1)-N(1)	139.37(4)
C(12)-C(13)	1.383(2)	O(5)-Na(1)-N(1)	105.71(4)
C(13)-C(14)	1.402(3)	O(3)-Na(1)-N(1)	126.37(4)
C(14)-C(15)	1.388(2)	O(1)-Na(1)-N(1)	100.28(4)
C(15)-C(16)	1.395(2)	O(2)-Na(1)-Pt(1)	94.76(3)
C(19)-C(20)	1.507(3)	O(4)-Na(1)-Pt(1)	105.36(3)
C(21)-C(22)	1.497(3)	O(5)-Na(1)-Pt(1)	123.03(3)
C(23)-C(24)	1.497(2)	O(3)-Na(1)-Pt(1)	95.30(3)
C(25)-C(26)	1.503(3)	O(1)-Na(1)-Pt(1)	140.92(4)
C(27)-C(28)	1.501(3)	N(1)-Na(1)-Pt(1)	41.96(3)
C(29)-C(30)	1.482(3)	O(8)-Na(2)-O(6)	126.96(5)
C(31)-C(32)	1.466(5)	O(8)-Na(2)-O(9)	67.14(7)
C(33)-C(34)	1.483(5)	O(6)-Na(2)-O(9)	110.81(5)
C(35)-C(36)	1.491(4)	O(8)-Na(2)-O(10)	135.38(7)
C(37)-C(38)	1.505(3)	O(6)-Na(2)-O(10)	68.46(4)
O(40)-C(43)	1.409(4)	O(9)-Na(2)-O(10)	68.30(6)
O(40)-C(41)	1.425(5)	O(8)-Na(2)-O(7)	64.26(6)
C(41)-C(42)	1.490(6)	O(6)-Na(2)-O(7)	65.67(4)
C(43)-C(44)	1.529(7)	O(9)-Na(2)-O(7)	104.47(5)
		O(10)-Na(2)-O(7)	126.60(4)
C(18)-Pt(1)-C(17)	87.71(7)	O(8)-Na(2)-Pt(1)	102.43(5)
C(18)-Pt(1)-N(2)	96.97(6)	O(6)-Na(2)-Pt(1)	104.18(4)
C(17)-Pt(1)-N(2)	175.22(6)	O(9)-Na(2)-Pt(1)	142.27(4)
C(18)-Pt(1)-N(1)	175.28(6)	O(10)-Na(2)-Pt(1)	114.17(4)
C(17)-Pt(1)-N(1)	96.82(6)	O(7)-Na(2)-Pt(1)	102.38(4)
N(2)-Pt(1)-N(1)	78.52(5)	C(19)-O(1)-C(28)	113.37(13)
C(18)-Pt(1)-Na(2)	107.91(5)	C(19)-O(1)-Na(1)	106.96(9)

C(28)-O(1)-Na(1)	109.85(9)	C(5)-C(6)-C(7)	134.45(15)
C(20)-O(2)-C(21)	113.66(13)	C(5)-C(6)-C(1)	119.48(14)
C(20)-O(2)-Na(1)	121.15(10)	C(7)-C(6)-C(1)	106.05(13)
C(21)-O(2)-Na(1)	117.61(10)	C(8)-C(7)-C(6)	106.22(13)
C(23)-O(3)-C(22)	113.09(13)	C(7)-C(8)-N(1)	112.45(13)
C(23)-O(3)-Na(1)	105.56(9)	C(7)-C(8)-C(9)	130.92(14)
C(22)-O(3)-Na(1)	100.92(9)	N(1)-C(8)-C(9)	116.63(13)
C(25)-O(4)-C(24)	113.05(12)	N(2)-C(9)-C(10)	112.67(13)
C(25)-O(4)-Na(1)	115.23(10)	N(2)-C(9)-C(8)	116.73(13)
C(24)-O(4)-Na(1)	117.28(9)	C(10)-C(9)-C(8)	130.60(14)
C(26)-O(5)-C(27)	113.69(12)	C(9)-C(10)-C(11)	105.72(14)
C(26)-O(5)-Na(1)	110.72(10)	C(12)-C(11)-C(10)	134.63(15)
C(27)-O(5)-Na(1)	113.08(9)	C(12)-C(11)-C(16)	119.22(14)
C(38)-O(6)-C(29)	113.03(14)	C(10)-C(11)-C(16)	106.14(13)
C(38)-O(6)-Na(2)	116.57(10)	C(13)-C(12)-C(11)	119.33(15)
C(29)-O(6)-Na(2)	118.43(10)	C(12)-C(13)-C(14)	120.92(15)
C(30)-O(7)-C(31)	113.42(19)	C(15)-C(14)-C(13)	121.30(16)
C(30)-O(7)-Na(2)	104.97(10)	C(14)-C(15)-C(16)	118.80(16)
C(31)-O(7)-Na(2)	100.39(12)	N(2)-C(16)-C(15)	129.98(14)
C(33)-O(8)-C(32)	113.9(2)	N(2)-C(16)-C(11)	109.59(13)
C(33)-O(8)-Na(2)	118.63(19)	C(15)-C(16)-C(11)	120.42(14)
C(32)-O(8)-Na(2)	118.42(16)	O(1)-C(19)-C(20)	106.95(14)
C(35)-O(9)-C(34)	115.5(2)	O(2)-C(20)-C(19)	108.02(13)
C(35)-O(9)-Na(2)	110.11(12)	O(2)-C(21)-C(22)	108.70(13)
C(34)-O(9)-Na(2)	106.57(16)	O(3)-C(22)-C(21)	106.55(14)
C(36)-O(10)-C(37)	114.84(16)	O(3)-C(23)-C(24)	107.01(13)
C(36)-O(10)-Na(2)	112.45(13)	O(4)-C(24)-C(23)	106.88(13)
C(37)-O(10)-Na(2)	110.69(10)	O(4)-C(25)-C(26)	106.35(13)
C(1)-N(1)-C(8)	105.42(12)	O(5)-C(26)-C(25)	112.51(13)
C(1)-N(1)-Pt(1)	140.57(10)	O(5)-C(27)-C(28)	107.59(13)
C(8)-N(1)-Pt(1)	113.68(9)	O(1)-C(28)-C(27)	106.75(14)
C(1)-N(1)-Na(1)	97.33(8)	O(6)-C(29)-C(30)	107.82(16)
C(8)-N(1)-Na(1)	110.76(8)	O(7)-C(30)-C(29)	106.43(15)
Pt(1)-N(1)-Na(1)	73.96(4)	O(7)-C(31)-C(32)	106.6(2)
C(9)-N(2)-C(16)	105.87(12)	O(8)-C(32)-C(31)	108.75(19)
C(9)-N(2)-Pt(1)	114.28(10)	O(8)-C(33)-C(34)	108.3(2)
C(16)-N(2)-Pt(1)	139.85(10)	O(9)-C(34)-C(33)	108.2(2)
N(1)-C(1)-C(2)	129.79(15)	O(9)-C(35)-C(36)	108.27(17)
N(1)-C(1)-C(6)	109.86(13)	O(10)-C(36)-C(35)	107.79(17)
C(2)-C(1)-C(6)	120.35(14)	O(10)-C(37)-C(38)	112.01(16)
C(3)-C(2)-C(1)	118.38(16)	O(6)-C(38)-C(37)	106.81(13)
C(2)-C(3)-C(4)	121.73(16)	C(43)-O(40)-C(41)	111.1(4)
C(5)-C(4)-C(3)	120.97(16)	O(40)-C(41)-C(42)	115.9(5)
C(4)-C(5)-C(6)	119.07(16)	O(40)-C(43)-C(44)	107.3(5)

**Table A2.3. Anisotropic displacement parameters ( $\text{\AA}^2 \times 10^4$ ) for 2 (CCDC 706858). The anisotropic displacement factor exponent takes the form:  $-2\pi^2[h^2a^*^2U11 + \dots + 2hka^*b^*U12]$ .**

	U11	U22	U33	U23	U13	U12
Pt(1)	124(1)	216(1)	159(1)	-18(1)	5(1)	4(1)
Na(1)	186(3)	197(3)	262(3)	20(3)	6(2)	4(2)
Na(2)	192(3)	340(4)	285(4)	-93(3)	40(2)	2(3)
O(1)	278(5)	217(6)	238(6)	-7(4)	35(4)	7(4)
O(2)	235(5)	217(6)	304(7)	-4(5)	23(4)	-34(4)
O(3)	265(5)	197(6)	280(6)	0(4)	27(4)	29(4)
O(4)	251(5)	223(6)	269(6)	-3(5)	-27(4)	29(4)
O(5)	218(5)	225(6)	319(7)	51(5)	0(4)	24(4)
O(6)	328(5)	219(6)	304(7)	-17(5)	-77(5)	12(4)
O(7)	268(6)	283(7)	583(10)	-139(6)	102(6)	-70(5)
O(8)	349(7)	769(12)	902(15)	-561(11)	-269(8)	230(7)
O(9)	388(7)	1028(14)	225(7)	-26(8)	-53(5)	370(8)
O(10)	210(5)	401(7)	369(8)	133(6)	73(5)	21(5)
N(1)	194(5)	195(7)	173(6)	1(5)	2(4)	-8(5)
N(2)	168(5)	207(7)	182(6)	7(5)	-8(4)	1(5)
C(1)	154(5)	209(8)	203(8)	23(6)	11(5)	12(5)
C(2)	209(7)	236(8)	272(9)	13(6)	-2(5)	-7(6)
C(3)	227(7)	235(9)	349(10)	85(7)	11(6)	-29(6)
C(4)	213(6)	321(9)	279(9)	137(7)	4(6)	20(6)
C(5)	195(6)	322(9)	209(8)	50(7)	-8(6)	31(6)
C(6)	151(5)	243(8)	197(7)	25(6)	8(5)	30(5)
C(7)	175(6)	230(8)	183(7)	-7(6)	0(5)	6(5)
C(8)	168(5)	190(7)	177(7)	-15(5)	8(5)	8(5)
C(9)	160(5)	213(8)	166(7)	-3(5)	11(5)	17(5)
C(10)	199(6)	214(8)	201(7)	-23(5)	9(5)	-4(5)
C(11)	155(6)	200(8)	232(8)	19(6)	35(5)	28(5)
C(12)	188(6)	195(8)	309(10)	8(6)	35(5)	27(5)
C(13)	194(6)	213(8)	356(10)	91(7)	61(6)	52(6)
C(14)	229(7)	322(9)	258(9)	110(7)	19(6)	57(6)
C(15)	221(7)	284(9)	231(8)	43(6)	-15(6)	25(6)
C(16)	155(5)	210(7)	197(7)	18(6)	14(4)	34(5)
C(17)	228(6)	281(9)	246(9)	-53(6)	-15(6)	-22(6)
C(18)	246(7)	353(9)	203(8)	-4(7)	-44(6)	-36(7)
C(19)	271(7)	313(9)	273(9)	-78(7)	-20(6)	43(7)
C(20)	280(7)	268(10)	382(11)	-88(7)	-18(7)	-37(7)
C(21)	297(7)	200(8)	423(11)	20(8)	107(7)	-49(6)
C(22)	295(7)	202(8)	363(10)	56(7)	116(7)	28(6)

C(23)	257(7)	340(10)	251(9)	21(7)	3(6)	29(7)
C(24)	245(7)	334(9)	242(8)	-39(7)	-11(6)	-2(7)
C(25)	284(7)	185(8)	370(10)	-49(7)	-61(7)	17(6)
C(26)	236(7)	185(9)	479(12)	26(7)	-42(7)	-37(6)
C(27)	234(7)	229(9)	425(11)	115(7)	-14(7)	9(6)
C(28)	277(7)	335(10)	267(9)	101(7)	18(6)	20(7)
C(29)	529(11)	304(10)	269(10)	-15(8)	-83(8)	137(9)
C(30)	610(13)	287(10)	423(12)	58(9)	205(10)	93(9)
C(31)	234(9)	278(12)	1570(30)	-139(14)	26(13)	-42(8)
C(32)	410(12)	498(16)	1710(40)	-593(19)	-424(17)	155(11)
C(33)	466(13)	1470(30)	1020(30)	-950(20)	-470(15)	551(17)
C(34)	473(13)	1810(30)	356(14)	-460(18)	-234(10)	659(18)
C(35)	653(14)	1230(20)	272(12)	274(13)	216(11)	648(16)
C(36)	433(11)	565(14)	644(17)	344(12)	351(11)	207(10)
C(37)	258(8)	278(10)	619(14)	42(9)	-97(8)	-67(7)
C(38)	267(8)	311(10)	567(14)	7(8)	-151(8)	-38(7)

---

## Structures in Chapter 4

### Structure of 5a (CCDC 640093)

#### Special Refinement Details

Refinement of  $F^2$  against ALL reflections. The weighted R-factor ( $wR$ ) and goodness of fit (S) are based on  $F^2$ , conventional R-factors (R) are based on F, with F set to zero for negative  $F^2$ . The threshold expression of  $F^2 > 2\sigma(F^2)$  is used only for calculating R-factors(gt) etc. and is not relevant to the choice of reflections for refinement. R-factors based on  $F^2$  are statistically about twice as large as those based on F, and R-factors based on ALL data will be even larger.

All esds (except the esd in the dihedral angle between two l.s. planes) are estimated using the full covariance matrix. The cell esds are taken into account individually in the estimation of esds in distances, angles and torsion angles; correlations between esds in cell parameters are only used when they are defined by crystal symmetry. An approximate (isotropic) treatment of cell esds is used for estimating esds involving l.s. planes.

**Table A2.4. Atomic coordinates (x 10<sup>4</sup>) and equivalent isotropic displacement parameters (Å<sup>2</sup> x 10<sup>3</sup>) for 5a (CCDC 640093). U(eq) is defined as the trace of the orthogonalized U<sup>ij</sup> tensor.**

	x	y	z	U <sub>eq</sub>
O(1A)	10111(2)	1209(1)	1178(1)	24(1)
O(2A)	8322(2)	-319(1)	1878(1)	22(1)
N(1A)	9617(2)	1334(1)	2152(1)	17(1)
C(1A)	9804(2)	2004(2)	1136(1)	18(1)
C(2A)	9736(2)	2318(2)	648(1)	19(1)
C(3A)	9437(2)	3129(2)	614(1)	19(1)
C(4A)	9204(2)	3626(2)	1035(1)	18(1)

C(5A)	9283(2)	3291(2)	1506(1)	19(1)
C(6A)	9606(2)	2486(2)	1568(1)	18(1)
C(7A)	9748(2)	2205(2)	2101(1)	17(1)
C(8A)	10047(3)	2810(2)	2516(1)	22(1)
C(9A)	10122(2)	2518(2)	3003(1)	21(1)
C(10A)	9948(2)	1632(2)	3058(1)	21(1)
C(11A)	9732(2)	1046(2)	2628(1)	17(1)
C(12A)	9589(2)	95(2)	2674(1)	18(1)
C(13A)	10164(2)	-186(2)	3108(1)	18(1)
C(14A)	10025(2)	-1051(2)	3192(1)	16(1)
C(15A)	9264(2)	-1668(2)	2834(1)	18(1)
C(16A)	8671(2)	-1450(2)	2392(1)	16(1)
C(17A)	8871(2)	-551(2)	2315(1)	16(1)
C(18A)	9969(3)	1794(2)	172(1)	23(1)
C(19A)	11280(3)	1663(2)	232(1)	33(1)
C(20A)	9848(3)	2270(2)	-314(1)	36(1)
C(21A)	9051(3)	896(2)	91(1)	30(1)
C(22A)	8895(2)	4514(2)	961(1)	18(1)
C(23A)	7865(3)	4425(2)	532(1)	32(1)
C(24A)	10047(3)	5157(2)	818(1)	31(1)
C(25A)	8502(3)	4902(2)	1444(1)	33(1)
C(26A)	10645(2)	-1362(2)	3669(1)	18(1)
C(27A)	11536(3)	-615(2)	3991(1)	29(1)
C(28A)	9651(3)	-1800(2)	4004(1)	25(1)
C(29A)	11364(2)	-2027(2)	3511(1)	22(1)
C(30A)	7849(2)	-2156(2)	2016(1)	19(1)
C(31A)	6547(2)	-2007(2)	1952(1)	26(1)
C(32A)	7723(3)	-3080(2)	2189(1)	25(1)
C(33A)	8362(3)	-2145(2)	1487(1)	26(1)
O(1B)	5055(2)	3647(1)	1899(1)	23(1)
O(2B)	8018(2)	4033(1)	2650(1)	23(1)
N(1B)	6349(2)	2571(1)	2243(1)	17(1)
C(1B)	5021(2)	3233(2)	1428(1)	19(1)
C(2B)	4482(2)	3571(2)	1006(1)	19(1)
C(3B)	4485(2)	3154(2)	530(1)	22(1)
C(4B)	4972(3)	2429(2)	445(1)	23(1)
C(5B)	5470(3)	2112(2)	871(1)	22(1)
C(6B)	5494(2)	2492(2)	1366(1)	18(1)
C(7B)	5964(2)	2069(2)	1804(1)	17(1)
C(8B)	5947(2)	1181(2)	1781(1)	20(1)
C(9B)	6336(2)	811(2)	2212(1)	21(1)
C(10B)	6726(2)	1337(2)	2657(1)	19(1)
C(11B)	6724(2)	2219(2)	2670(1)	17(1)
C(12B)	7136(2)	2813(2)	3131(1)	17(1)
C(13B)	6874(2)	2504(2)	3613(1)	20(1)
C(14B)	7288(3)	3021(2)	4059(1)	20(1)

C(15B)	8051(3)	3853(2)	4020(1)	22(1)
C(16B)	8346(2)	4204(2)	3561(1)	18(1)
C(17B)	7815(3)	3679(2)	3114(1)	19(1)
C(18B)	3923(3)	4369(2)	1077(1)	21(1)
C(19B)	2868(3)	4154(2)	1421(1)	28(1)
C(20B)	3372(3)	4606(2)	566(1)	32(1)
C(21B)	4905(3)	5178(2)	1304(1)	30(1)
C(22B)	4994(3)	1996(2)	-88(1)	30(1)
C(23B)	4373(3)	2413(2)	-506(1)	39(1)
C(24B)	4279(3)	1018(2)	-103(1)	48(1)
C(25B)	6301(3)	2048(3)	-197(1)	56(1)
C(26B)	6905(3)	2727(2)	4584(1)	26(1)
C(27B)	5979(3)	1850(2)	4538(1)	49(1)
C(28B)	8007(3)	2693(3)	4934(1)	55(1)
C(29B)	6278(3)	3400(2)	4829(1)	49(1)
C(30B)	9189(3)	5122(2)	3539(1)	20(1)
C(31B)	10245(3)	5077(2)	3212(1)	31(1)
C(32B)	9768(3)	5520(2)	4068(1)	37(1)
C(33B)	8461(3)	5742(2)	3307(1)	29(1)
O(1C)	4818(2)	362(1)	3414(1)	22(1)
O(2C)	2428(2)	1470(1)	3807(1)	23(1)
N(1C)	3340(2)	1162(1)	2913(1)	17(1)
C(1C)	4352(2)	-349(2)	3074(1)	18(1)
C(2C)	4735(2)	-1118(2)	3151(1)	16(1)
C(3C)	4202(2)	-1842(2)	2819(1)	19(1)
C(4C)	3317(2)	-1853(2)	2411(1)	18(1)
C(5C)	3016(3)	-1058(2)	2337(1)	20(1)
C(6C)	3525(2)	-299(2)	2651(1)	18(1)
C(7C)	3238(2)	544(2)	2522(1)	17(1)
C(8C)	2944(2)	719(2)	2023(1)	20(1)
C(9C)	2756(2)	1542(2)	1925(1)	22(1)
C(10C)	2879(2)	2169(2)	2326(1)	20(1)
C(11C)	3166(2)	1972(2)	2818(1)	18(1)
C(12C)	3276(2)	2607(2)	3262(1)	18(1)
C(13C)	3771(2)	3502(2)	3213(1)	21(1)
C(14C)	3803(3)	4127(2)	3606(1)	20(1)
C(15C)	3255(3)	3839(2)	4045(1)	21(1)
C(16C)	2757(2)	2969(2)	4121(1)	19(1)
C(17C)	2841(2)	2347(2)	3727(1)	19(1)
C(18C)	5680(2)	-1169(2)	3597(1)	17(1)
C(19C)	5149(3)	-1052(2)	4109(1)	29(1)
C(20C)	6041(3)	-2050(2)	3580(1)	25(1)
C(21C)	6879(2)	-454(2)	3577(1)	25(1)
C(22C)	2693(2)	-2672(2)	2065(1)	20(1)
C(23C)	1302(3)	-2884(2)	2109(1)	35(1)
C(24C)	3143(3)	-3477(2)	2208(1)	34(1)

C(25C)	2941(3)	-2501(2)	1515(1)	32(1)
C(26C)	4414(3)	5105(2)	3579(1)	24(1)
C(27C)	4996(3)	5282(2)	3074(1)	30(1)
C(28C)	3452(3)	5639(2)	3626(1)	36(1)
C(29C)	5415(3)	5395(2)	4025(1)	31(1)
C(30C)	2145(3)	2685(2)	4606(1)	21(1)
C(31C)	816(3)	2141(2)	4465(1)	30(1)
C(32C)	2067(3)	3476(2)	4956(1)	37(1)
C(33C)	2858(3)	2131(2)	4917(1)	29(1)

**Table A2.5. Bond lengths [Å] and angles [°] for 5a (CCDC 640093).**

—O(1A)-C(1A)	1.379(3)	C(22A)-C(25A)	1.521(4)
O(2A)-C(17A)	1.371(3)	C(22A)-C(23A)	1.531(4)
N(1A)-C(7A)	1.355(3)	C(22A)-C(24A)	1.532(4)
N(1A)-C(11A)	1.359(3)	C(26A)-C(27A)	1.519(4)
C(1A)-C(6A)	1.395(4)	C(26A)-C(29A)	1.527(4)
C(1A)-C(2A)	1.401(4)	C(26A)-C(28A)	1.536(4)
C(2A)-C(3A)	1.397(4)	C(30A)-C(32A)	1.520(3)
C(2A)-C(18A)	1.535(4)	C(30A)-C(31A)	1.539(4)
C(3A)-C(4A)	1.397(4)	C(30A)-C(33A)	1.548(4)
C(4A)-C(5A)	1.375(4)	O(1B)-C(1B)	1.364(3)
C(4A)-C(22A)	1.533(4)	O(2B)-C(17B)	1.382(3)
C(5A)-C(6A)	1.409(4)	N(1B)-C(7B)	1.344(3)
C(6A)-C(7A)	1.497(4)	N(1B)-C(11B)	1.359(3)
C(7A)-C(8A)	1.374(4)	C(1B)-C(6B)	1.396(4)
C(8A)-C(9A)	1.386(4)	C(1B)-C(2B)	1.410(4)
C(9A)-C(10A)	1.375(4)	C(2B)-C(3B)	1.383(4)
C(10A)-C(11A)	1.389(4)	C(2B)-C(18B)	1.539(4)
C(11A)-C(12A)	1.475(4)	C(3B)-C(4B)	1.391(4)
C(12A)-C(17A)	1.404(4)	C(4B)-C(5B)	1.382(4)
C(12A)-C(13A)	1.411(3)	C(4B)-C(22B)	1.531(4)
C(13A)-C(14A)	1.362(3)	C(5B)-C(6B)	1.399(4)
C(14A)-C(15A)	1.396(4)	C(6B)-C(7B)	1.484(4)
C(14A)-C(26A)	1.544(3)	C(7B)-C(8B)	1.387(4)
C(15A)-C(16A)	1.394(3)	C(8B)-C(9B)	1.386(4)
C(16A)-C(17A)	1.403(3)	C(9B)-C(10B)	1.376(4)
C(16A)-C(30A)	1.524(4)	C(10B)-C(11B)	1.383(4)
C(18A)-C(20A)	1.526(4)	C(11B)-C(12B)	1.465(4)
C(18A)-C(21A)	1.534(4)	C(12B)-C(17B)	1.400(4)
C(18A)-C(19A)	1.537(4)	C(12B)-C(13B)	1.407(4)

C(13B)-C(14B)	1.374(4)	C(18C)-C(21C)	1.547(4)
C(14B)-C(15B)	1.397(4)	C(22C)-C(25C)	1.520(4)
C(14B)-C(26B)	1.541(4)	C(22C)-C(24C)	1.521(4)
C(15B)-C(16B)	1.386(4)	C(22C)-C(23C)	1.540(4)
C(16B)-C(17B)	1.404(4)	C(26C)-C(28C)	1.528(4)
C(16B)-C(30B)	1.535(4)	C(26C)-C(29C)	1.533(4)
C(18B)-C(21B)	1.533(4)	C(26C)-C(27C)	1.537(4)
C(18B)-C(20B)	1.537(4)	C(30C)-C(32C)	1.531(4)
C(18B)-C(19B)	1.537(4)	C(30C)-C(33C)	1.541(4)
C(22B)-C(25B)	1.509(4)	C(30C)-C(31C)	1.546(4)
C(22B)-C(23B)	1.515(4)		
C(22B)-C(24B)	1.553(4)	C(7A)-N(1A)-C(11A)	119.3(2)
C(26B)-C(28B)	1.500(4)	O(1A)-C(1A)-C(6A)	120.6(2)
C(26B)-C(27B)	1.512(4)	O(1A)-C(1A)-C(2A)	117.7(3)
C(26B)-C(29B)	1.544(4)	C(6A)-C(1A)-C(2A)	121.6(2)
C(30B)-C(32B)	1.525(4)	C(3A)-C(2A)-C(1A)	116.8(3)
C(30B)-C(33B)	1.534(4)	C(3A)-C(2A)-C(18A)	121.5(2)
C(30B)-C(31B)	1.536(4)	C(1A)-C(2A)-C(18A)	121.7(2)
O(1C)-C(1C)	1.366(3)	C(2A)-C(3A)-C(4A)	123.7(3)
O(2C)-C(17C)	1.378(3)	C(5A)-C(4A)-C(3A)	117.4(2)
N(1C)-C(7C)	1.355(3)	C(5A)-C(4A)-C(22A)	122.6(3)
N(1C)-C(11C)	1.363(3)	C(3A)-C(4A)-C(22A)	120.0(2)
C(1C)-C(2C)	1.394(4)	C(4A)-C(5A)-C(6A)	121.8(3)
C(1C)-C(6C)	1.412(4)	C(1A)-C(6A)-C(5A)	118.7(2)
C(2C)-C(3C)	1.380(4)	C(1A)-C(6A)-C(7A)	123.5(2)
C(2C)-C(18C)	1.540(4)	C(5A)-C(6A)-C(7A)	117.8(3)
C(3C)-C(4C)	1.404(4)	N(1A)-C(7A)-C(8A)	121.6(2)
C(4C)-C(5C)	1.387(4)	N(1A)-C(7A)-C(6A)	117.1(2)
C(4C)-C(22C)	1.525(4)	C(8A)-C(7A)-C(6A)	121.3(2)
C(5C)-C(6C)	1.390(4)	C(7A)-C(8A)-C(9A)	119.2(3)
C(6C)-C(7C)	1.483(4)	C(10A)-C(9A)-C(8A)	119.2(3)
C(7C)-C(8C)	1.388(4)	C(9A)-C(10A)-C(11A)	119.8(3)
C(8C)-C(9C)	1.392(4)	N(1A)-C(11A)-C(10A)	120.6(2)
C(9C)-C(10C)	1.379(4)	N(1A)-C(11A)-C(12A)	118.3(2)
C(10C)-C(11C)	1.378(4)	C(10A)-C(11A)-C(12A)	121.0(2)
C(11C)-C(12C)	1.473(4)	C(17A)-C(12A)-C(13A)	117.9(2)
C(12C)-C(17C)	1.399(4)	C(17A)-C(12A)-C(11A)	123.2(2)
C(12C)-C(13C)	1.401(4)	C(13A)-C(12A)-C(11A)	118.9(3)
C(13C)-C(14C)	1.379(4)	C(14A)-C(13A)-C(12A)	122.4(3)
C(14C)-C(15C)	1.399(4)	C(13A)-C(14A)-C(15A)	117.5(3)
C(14C)-C(26C)	1.535(4)	C(13A)-C(14A)-C(26A)	122.6(2)
C(15C)-C(16C)	1.381(4)	C(15A)-C(14A)-C(26A)	119.9(2)
C(16C)-C(17C)	1.410(4)	C(16A)-C(15A)-C(14A)	123.9(3)
C(16C)-C(30C)	1.534(4)	C(15A)-C(16A)-C(17A)	116.3(3)
C(18C)-C(20C)	1.530(4)	C(15A)-C(16A)-C(30A)	121.3(2)
C(18C)-C(19C)	1.536(4)	C(17A)-C(16A)-C(30A)	122.3(2)

O(2A)-C(17A)-C(16A)	117.6(2)	C(10B)-C(9B)-C(8B)	118.9(3)
O(2A)-C(17A)-C(12A)	120.5(2)	C(9B)-C(10B)-C(11B)	120.0(3)
C(16A)-C(17A)-C(12A)	121.8(2)	N(1B)-C(11B)-C(10B)	120.2(3)
C(20A)-C(18A)-C(21A)	107.3(2)	N(1B)-C(11B)-C(12B)	117.2(2)
C(20A)-C(18A)-C(2A)	112.1(2)	C(10B)-C(11B)-C(12B)	122.6(2)
C(21A)-C(18A)-C(2A)	110.9(2)	C(17B)-C(12B)-C(13B)	118.2(3)
C(20A)-C(18A)-C(19A)	107.2(2)	C(17B)-C(12B)-C(11B)	122.3(2)
C(21A)-C(18A)-C(19A)	109.5(2)	C(13B)-C(12B)-C(11B)	119.5(2)
C(2A)-C(18A)-C(19A)	109.7(2)	C(14B)-C(13B)-C(12B)	121.8(3)
C(25A)-C(22A)-C(23A)	108.3(2)	C(13B)-C(14B)-C(15B)	117.4(3)
C(25A)-C(22A)-C(24A)	108.0(2)	C(13B)-C(14B)-C(26B)	122.4(2)
C(23A)-C(22A)-C(24A)	109.2(2)	C(15B)-C(14B)-C(26B)	120.1(3)
C(25A)-C(22A)-C(4A)	112.6(2)	C(16B)-C(15B)-C(14B)	124.0(3)
C(23A)-C(22A)-C(4A)	110.7(2)	C(15B)-C(16B)-C(17B)	116.4(2)
C(24A)-C(22A)-C(4A)	108.1(2)	C(15B)-C(16B)-C(30B)	122.0(2)
C(27A)-C(26A)-C(29A)	107.2(2)	C(17B)-C(16B)-C(30B)	121.6(2)
C(27A)-C(26A)-C(28A)	108.4(2)	O(2B)-C(17B)-C(12B)	120.3(2)
C(29A)-C(26A)-C(28A)	108.9(2)	O(2B)-C(17B)-C(16B)	117.9(2)
C(27A)-C(26A)-C(14A)	112.9(2)	C(12B)-C(17B)-C(16B)	121.8(2)
C(29A)-C(26A)-C(14A)	110.3(2)	C(21B)-C(18B)-C(20B)	107.5(2)
C(28A)-C(26A)-C(14A)	108.9(2)	C(21B)-C(18B)-C(19B)	110.8(2)
C(32A)-C(30A)-C(16A)	113.1(2)	C(20B)-C(18B)-C(19B)	106.5(2)
C(32A)-C(30A)-C(31A)	106.7(2)	C(21B)-C(18B)-C(2B)	110.4(2)
C(16A)-C(30A)-C(31A)	110.3(2)	C(20B)-C(18B)-C(2B)	111.6(2)
C(32A)-C(30A)-C(33A)	106.9(2)	C(19B)-C(18B)-C(2B)	109.9(2)
C(16A)-C(30A)-C(33A)	110.8(2)	C(25B)-C(22B)-C(23B)	109.2(3)
C(31A)-C(30A)-C(33A)	108.9(2)	C(25B)-C(22B)-C(4B)	109.7(3)
C(7B)-N(1B)-C(11B)	120.7(2)	C(23B)-C(22B)-C(4B)	112.7(2)
O(1B)-C(1B)-C(6B)	120.9(2)	C(25B)-C(22B)-C(24B)	109.7(3)
O(1B)-C(1B)-C(2B)	117.9(2)	C(23B)-C(22B)-C(24B)	106.9(3)
C(6B)-C(1B)-C(2B)	121.2(3)	C(4B)-C(22B)-C(24B)	108.5(3)
C(3B)-C(2B)-C(1B)	116.9(3)	C(28B)-C(26B)-C(27B)	110.5(3)
C(3B)-C(2B)-C(18B)	122.0(2)	C(28B)-C(26B)-C(14B)	110.5(3)
C(1B)-C(2B)-C(18B)	121.1(2)	C(27B)-C(26B)-C(14B)	112.0(2)
C(2B)-C(3B)-C(4B)	124.3(3)	C(28B)-C(26B)-C(29B)	108.2(3)
C(5B)-C(4B)-C(3B)	116.6(3)	C(27B)-C(26B)-C(29B)	106.5(3)
C(5B)-C(4B)-C(22B)	120.2(3)	C(14B)-C(26B)-C(29B)	109.0(2)
C(3B)-C(4B)-C(22B)	123.1(3)	C(32B)-C(30B)-C(33B)	108.3(2)
C(4B)-C(5B)-C(6B)	122.6(3)	C(32B)-C(30B)-C(16B)	111.9(2)
C(1B)-C(6B)-C(5B)	118.3(3)	C(33B)-C(30B)-C(16B)	110.1(2)
C(1B)-C(6B)-C(7B)	122.8(3)	C(32B)-C(30B)-C(31B)	106.9(2)
C(5B)-C(6B)-C(7B)	118.8(2)	C(33B)-C(30B)-C(31B)	109.0(2)
N(1B)-C(7B)-C(8B)	120.3(3)	C(16B)-C(30B)-C(31B)	110.5(2)
N(1B)-C(7B)-C(6B)	117.2(2)	C(7C)-N(1C)-C(11C)	120.1(2)
C(8B)-C(7B)-C(6B)	122.4(3)	O(1C)-C(1C)-C(2C)	118.1(2)
C(9B)-C(8B)-C(7B)	119.9(3)	O(1C)-C(1C)-C(6C)	120.9(2)

C(2C)-C(1C)-C(6C)	121.0(3)	C(15C)-C(16C)-C(30C)	122.4(3)
C(3C)-C(2C)-C(1C)	117.1(3)	C(17C)-C(16C)-C(30C)	121.4(2)
C(3C)-C(2C)-C(18C)	121.3(2)	O(2C)-C(17C)-C(12C)	120.8(3)
C(1C)-C(2C)-C(18C)	121.5(2)	O(2C)-C(17C)-C(16C)	117.7(2)
C(2C)-C(3C)-C(4C)	124.7(3)	C(12C)-C(17C)-C(16C)	121.5(2)
C(5C)-C(4C)-C(3C)	115.7(3)	C(20C)-C(18C)-C(19C)	107.8(2)
C(5C)-C(4C)-C(22C)	120.5(2)	C(20C)-C(18C)-C(2C)	112.3(2)
C(3C)-C(4C)-C(22C)	123.8(2)	C(19C)-C(18C)-C(2C)	109.9(2)
C(4C)-C(5C)-C(6C)	122.9(3)	C(20C)-C(18C)-C(21C)	106.2(2)
C(5C)-C(6C)-C(1C)	118.4(2)	C(19C)-C(18C)-C(21C)	109.7(2)
C(5C)-C(6C)-C(7C)	119.8(2)	C(2C)-C(18C)-C(21C)	110.7(2)
C(1C)-C(6C)-C(7C)	121.8(2)	C(25C)-C(22C)-C(24C)	108.6(2)
N(1C)-C(7C)-C(8C)	120.8(2)	C(25C)-C(22C)-C(4C)	109.1(2)
N(1C)-C(7C)-C(6C)	117.0(2)	C(24C)-C(22C)-C(4C)	112.6(2)
C(8C)-C(7C)-C(6C)	122.1(3)	C(25C)-C(22C)-C(23C)	109.4(2)
C(7C)-C(8C)-C(9C)	119.1(3)	C(24C)-C(22C)-C(23C)	107.5(2)
C(10C)-C(9C)-C(8C)	119.4(3)	C(4C)-C(22C)-C(23C)	109.5(2)
C(11C)-C(10C)-C(9C)	119.9(3)	C(28C)-C(26C)-C(29C)	109.2(3)
N(1C)-C(11C)-C(10C)	120.6(3)	C(28C)-C(26C)-C(14C)	109.1(2)
N(1C)-C(11C)-C(12C)	117.1(2)	C(29C)-C(26C)-C(14C)	108.9(2)
C(10C)-C(11C)-C(12C)	122.3(2)	C(28C)-C(26C)-C(27C)	109.1(2)
C(17C)-C(12C)-C(13C)	118.6(3)	C(29C)-C(26C)-C(27C)	108.8(2)
C(17C)-C(12C)-C(11C)	121.7(2)	C(14C)-C(26C)-C(27C)	111.7(2)
C(13C)-C(12C)-C(11C)	119.6(3)	C(32C)-C(30C)-C(16C)	111.8(2)
C(14C)-C(13C)-C(12C)	121.5(3)	C(32C)-C(30C)-C(33C)	107.6(2)
C(13C)-C(14C)-C(15C)	117.4(2)	C(16C)-C(30C)-C(33C)	111.3(2)
C(13C)-C(14C)-C(26C)	122.9(3)	C(32C)-C(30C)-C(31C)	106.7(2)
C(15C)-C(14C)-C(26C)	119.7(3)	C(16C)-C(30C)-C(31C)	110.3(2)
C(16C)-C(15C)-C(14C)	124.1(3)	C(33C)-C(30C)-C(31C)	109.0(2)
C(15C)-C(16C)-C(17C)	116.3(3)		

**Table A2.6. Anisotropic displacement parameters ( $\text{\AA}^2 \times 10^4$ ) for 5a (CCDC 640093). The anisotropic displacement factor exponent takes the form:  $-2\pi^2[h^2a^{*2}U^{11} + \dots + 2hka^*b^*U^{12}]$ .**

	U11	U22	U33	U23	U13	U12
O(1A)	341(13)	196(11)	215(12)	57(9)	49(11)	127(9)
O(2A)	271(12)	228(11)	171(11)	83(9)	-16(9)	74(9)
N(1A)	153(13)	184(13)	172(14)	49(11)	31(10)	37(10)
C(1A)	146(16)	174(15)	220(18)	30(13)	6(13)	38(12)
C(2A)	193(17)	200(16)	182(17)	26(13)	46(13)	36(13)
C(3A)	183(17)	220(16)	151(17)	48(13)	34(13)	35(13)
C(4A)	143(16)	225(16)	175(17)	42(13)	34(13)	70(12)
C(5A)	189(17)	224(16)	167(17)	5(13)	28(13)	86(13)
C(6A)	144(16)	214(16)	173(17)	32(13)	6(13)	50(13)
C(7A)	156(16)	202(16)	180(17)	38(13)	31(13)	62(13)
C(8A)	244(18)	219(16)	233(19)	41(14)	24(14)	100(13)
C(9A)	210(17)	263(17)	170(17)	-5(14)	-11(13)	112(13)
C(10A)	217(17)	250(17)	176(17)	50(14)	-15(13)	101(13)
C(11A)	126(16)	239(16)	162(17)	36(14)	-1(13)	68(13)
C(12A)	158(17)	221(16)	184(17)	53(13)	61(13)	78(13)
C(13A)	146(16)	238(16)	131(16)	11(13)	9(12)	19(12)
C(14A)	147(16)	169(15)	170(17)	56(13)	56(13)	42(12)
C(15A)	151(16)	190(15)	195(17)	64(13)	33(13)	39(13)
C(16A)	159(16)	200(15)	126(16)	-11(13)	34(12)	51(12)
C(17A)	126(16)	238(16)	136(16)	46(13)	15(12)	79(13)
C(18A)	282(19)	242(17)	186(18)	43(14)	61(14)	78(14)
C(19A)	400(20)	331(19)	300(20)	49(15)	164(16)	143(16)
C(20A)	580(20)	370(20)	181(19)	7(15)	103(17)	221(18)
C(21A)	350(20)	323(18)	209(18)	-53(15)	-6(15)	109(15)
C(22A)	197(17)	221(16)	149(17)	25(13)	24(13)	92(13)
C(23A)	300(20)	360(19)	320(20)	55(16)	-17(16)	149(15)
C(24A)	310(20)	264(18)	400(20)	130(16)	64(16)	111(15)
C(25A)	460(20)	294(18)	310(20)	89(15)	73(17)	228(16)
C(26A)	158(16)	204(15)	157(17)	53(13)	-17(13)	11(12)
C(27A)	320(20)	258(17)	289(19)	65(15)	-67(15)	77(15)
C(28A)	244(18)	308(18)	228(18)	61(14)	38(14)	91(14)
C(29A)	193(17)	258(17)	234(18)	83(14)	30(14)	60(13)
C(30A)	155(16)	226(16)	185(17)	17(13)	11(13)	41(13)
C(31A)	170(17)	338(18)	256(19)	-20(15)	-8(14)	23(14)
C(32A)	272(19)	207(16)	213(18)	-39(14)	-24(14)	-12(13)
C(33A)	241(18)	342(18)	211(18)	-22(14)	-9(14)	107(14)

O(1B)	278(12)	263(11)	152(12)	1(9)	1(9)	110(9)
O(2B)	267(13)	249(11)	154(11)	45(9)	12(9)	18(9)
N(1B)	135(13)	191(13)	178(14)	38(11)	33(11)	18(10)
C(1B)	171(17)	262(17)	125(17)	8(14)	-11(13)	47(13)
C(2B)	185(17)	230(16)	140(17)	35(13)	-11(13)	22(13)
C(3B)	145(17)	305(17)	216(19)	62(15)	-18(13)	74(13)
C(4B)	192(18)	358(19)	142(17)	-1(14)	-31(13)	82(14)
C(5B)	185(17)	281(17)	230(19)	23(14)	22(14)	104(13)
C(6B)	157(16)	223(16)	161(18)	9(13)	-3(13)	51(13)
C(7B)	135(16)	218(16)	150(17)	16(13)	40(13)	34(12)
C(8B)	171(17)	251(17)	202(18)	-22(14)	37(13)	80(13)
C(9B)	159(17)	217(16)	266(19)	31(14)	39(14)	72(13)
C(10B)	136(16)	246(17)	182(17)	29(14)	20(13)	27(13)
C(11B)	98(16)	244(16)	178(17)	75(14)	48(12)	49(12)
C(12B)	132(16)	214(16)	152(17)	12(13)	-17(12)	37(12)
C(13B)	193(17)	215(16)	194(18)	80(14)	13(13)	48(13)
C(14B)	235(18)	208(16)	175(18)	34(13)	-8(14)	90(13)
C(15B)	222(18)	225(16)	206(18)	-16(14)	-20(14)	68(13)
C(16B)	158(16)	194(15)	170(17)	-4(13)	-16(13)	56(12)
C(17B)	206(17)	230(16)	174(17)	74(14)	43(13)	94(13)
C(18B)	201(17)	252(17)	196(18)	33(14)	-5(13)	77(13)
C(19B)	251(19)	301(18)	310(20)	46(15)	15(15)	139(14)
C(20B)	390(20)	360(19)	290(20)	91(16)	0(16)	217(16)
C(21B)	320(20)	284(18)	300(20)	63(15)	18(15)	92(15)
C(22B)	350(20)	420(20)	184(19)	-20(15)	-10(15)	219(16)
C(23B)	440(20)	560(20)	210(20)	-31(17)	-23(16)	218(18)
C(24B)	650(30)	550(20)	280(20)	-123(18)	-34(19)	300(20)
C(25B)	410(20)	1080(30)	250(20)	-70(20)	56(18)	320(20)
C(26B)	340(20)	296(18)	140(17)	57(14)	28(14)	76(15)
C(27B)	610(30)	480(20)	350(20)	87(18)	145(19)	7(19)
C(28B)	320(20)	1130(30)	280(20)	300(20)	60(17)	290(20)
C(29B)	470(20)	640(30)	460(20)	180(20)	240(20)	240(20)
C(30B)	178(17)	187(15)	225(18)	3(13)	-7(13)	20(13)
C(31B)	196(18)	205(17)	500(20)	-13(16)	58(16)	-1(13)
C(32B)	410(20)	219(17)	390(20)	-33(16)	-60(17)	-45(15)
C(33B)	264(19)	176(16)	430(20)	54(15)	39(16)	33(14)
O(1C)	235(12)	179(11)	236(12)	14(9)	-13(9)	64(9)
O(2C)	251(12)	182(11)	246(13)	37(9)	49(10)	25(9)
N(1C)	138(13)	174(13)	201(14)	30(11)	31(11)	10(10)
C(1C)	162(17)	199(16)	156(17)	-1(13)	25(13)	21(13)
C(2C)	134(16)	179(15)	175(17)	31(13)	46(13)	28(12)
C(3C)	156(16)	184(15)	247(18)	50(14)	65(13)	69(13)
C(4C)	155(17)	229(16)	164(17)	7(13)	47(13)	47(13)
C(5C)	175(17)	262(17)	145(17)	-7(13)	-21(13)	62(13)
C(6C)	136(16)	247(16)	186(17)	28(13)	42(13)	79(13)
C(7C)	155(16)	187(15)	151(17)	-10(13)	27(13)	28(12)

C(8C)	146(17)	262(17)	206(18)	18(14)	42(13)	58(13)
C(9C)	156(17)	296(17)	221(18)	54(15)	5(13)	56(13)
C(10C)	156(17)	215(16)	241(19)	56(14)	40(13)	69(13)
C(11C)	77(15)	237(16)	230(18)	61(14)	23(13)	55(12)
C(12C)	162(16)	199(16)	196(18)	16(13)	19(13)	62(13)
C(13C)	211(17)	236(17)	187(18)	78(14)	19(13)	70(13)
C(14C)	186(17)	199(16)	226(18)	43(14)	-12(14)	70(13)
C(15C)	216(17)	204(16)	201(18)	-6(13)	-13(14)	68(13)
C(16C)	185(17)	240(17)	152(17)	19(13)	-4(13)	67(13)
C(17C)	152(16)	155(15)	259(19)	49(13)	-10(13)	23(12)
C(18C)	195(17)	167(15)	151(17)	-1(12)	9(13)	62(12)
C(19C)	291(19)	346(19)	214(19)	42(15)	-17(15)	76(15)
C(20C)	249(18)	198(16)	302(19)	46(14)	-53(15)	48(13)
C(21C)	218(18)	271(17)	263(19)	43(14)	-32(14)	84(14)
C(22C)	165(17)	222(16)	188(18)	-22(13)	-16(13)	30(13)
C(23C)	280(20)	362(19)	350(20)	-89(16)	8(16)	17(15)
C(24C)	390(20)	269(18)	340(20)	-92(15)	-40(16)	105(15)
C(25C)	380(20)	331(19)	225(19)	-20(15)	-9(15)	53(16)
C(26C)	203(18)	178(16)	311(19)	17(14)	-5(14)	20(13)
C(27C)	294(19)	247(17)	360(20)	64(15)	7(16)	34(14)
C(28C)	205(19)	235(17)	630(20)	49(17)	43(17)	35(14)
C(29C)	260(19)	246(17)	390(20)	5(15)	-20(16)	-1(14)
C(30C)	227(18)	258(17)	132(17)	7(13)	44(13)	51(13)
C(31C)	263(19)	470(20)	178(18)	59(15)	66(14)	112(16)
C(32C)	450(20)	410(20)	220(20)	-6(16)	78(16)	70(17)
C(33C)	259(19)	420(20)	236(19)	106(15)	60(15)	107(15)

---

## Structure of 6 (CCDC 635046)

### Special Refinement Details

Refinement of  $F^2$  against ALL reflections. The weighted R-factor ( $wR$ ) and goodness of fit (S) are based on  $F^2$ , conventional R-factors (R) are based on F, with F set to zero for negative  $F^2$ . The threshold expression of  $F^2 > 2\sigma(F^2)$  is used only for calculating R-factors(gt) etc. and is not relevant to the choice of reflections for refinement. R-factors based on  $F^2$  are statistically about twice as large as those based on F, and R-factors based on ALL data will be even larger.

All esds (except the esd in the dihedral angle between two l.s. planes) are estimated using the full covariance matrix. The cell esds are taken into account individually in the estimation of esds in distances, angles and torsion angles; correlations between esds in cell parameters are only used when they are defined by crystal symmetry. An approximate (isotropic) treatment of cell esds is used for estimating esds involving l.s. planes.

**Table A2.7. Atomic coordinates ( $\times 10^4$ ) and equivalent isotropic displacement parameters ( $\text{\AA}^2 \times 10^3$ ) for 6 (CCDC 635046).  $U_{\text{eq}}$  is defined as the trace of the orthogonalized  $U_{ij}$  tensor.**

	x	y	z	$U_{\text{eq}}$
Ir	10238(1)	6292(1)	7803(1)	14(1)
O(1)	11904(2)	5620(2)	7349(2)	17(1)
O(2)	7190(2)	5461(2)	7430(2)	22(1)
N(1)	10945(2)	4254(2)	7144(2)	16(1)
N(2)	9387(2)	5324(2)	6751(2)	17(1)
C(1)	12410(2)	4560(2)	7446(2)	14(1)
C(2)	13466(2)	4089(2)	7608(2)	16(1)
C(3)	14061(2)	2994(3)	7712(3)	18(1)
C(4)	13628(2)	2286(2)	7660(2)	16(1)
C(5)	12575(2)	2744(3)	7498(2)	16(1)
C(6)	11967(2)	3860(2)	7379(2)	14(1)

C(7)	10647(2)	3559(3)	6814(3)	21(1)
C(8)	9593(3)	4319(3)	6491(3)	26(1)
C(9)	8541(2)	6286(2)	6417(2)	16(1)
C(10)	7439(2)	6287(3)	6805(3)	17(1)
C(11)	6653(2)	7290(3)	6446(3)	21(1)
C(12)	6939(2)	8176(3)	5768(3)	21(1)
C(13)	8029(2)	8147(3)	5384(3)	17(1)
C(14)	8815(2)	7167(2)	5728(2)	16(1)
C(15)	10155(2)	5259(2)	7152(2)	14(1)
C(16)	14304(3)	1078(3)	7737(3)	21(1)
C(17)	15273(3)	951(3)	6767(3)	34(1)
C(18)	14762(3)	596(3)	8695(3)	31(1)
C(19)	13646(3)	434(3)	7782(3)	30(1)
C(20)	8379(2)	9109(3)	4658(3)	19(1)
C(21)	9174(3)	8813(3)	3642(3)	28(1)
C(22)	7413(3)	10111(3)	4373(3)	30(1)
C(23)	8945(3)	9416(3)	5188(3)	29(1)
C(24)	8718(2)	6402(3)	8868(3)	19(1)
C(25)	8567(2)	7365(3)	8074(3)	18(1)
C(26)	8405(2)	8448(3)	8238(3)	21(1)
C(27)	9495(2)	8647(3)	7901(3)	20(1)
C(28)	10455(2)	7605(2)	8054(3)	17(1)
C(29)	10480(2)	6783(3)	8958(3)	18(1)
C(30)	9540(3)	6823(3)	9929(3)	21(1)
C(31)	8740(3)	6333(3)	9938(3)	21(1)
K	5960(1)	4381(1)	7765(1)	17(1)
O(41)	4900(2)	3516(2)	9880(2)	21(1)
O(42)	3751(2)	5546(2)	8813(2)	23(1)
O(43)	4646(2)	6297(2)	6753(2)	22(1)
O(44)	6288(2)	4757(2)	5629(2)	25(1)
O(45)	7650(2)	2784(2)	6665(2)	27(1)
O(46)	6582(2)	2063(2)	8697(2)	25(1)
C(41)	3752(3)	4059(3)	10253(3)	23(1)
C(42)	3511(3)	5249(3)	9912(3)	25(1)
C(43)	3533(3)	6669(3)	8381(3)	26(1)
C(44)	3571(3)	6881(3)	7263(3)	26(1)
C(45)	4739(3)	6385(3)	5700(3)	28(1)
C(46)	5926(3)	5891(3)	5185(3)	31(1)
C(47)	7435(3)	4259(4)	5202(3)	36(1)
C(48)	7731(3)	3059(4)	5594(3)	36(1)
C(49)	7800(3)	1668(3)	7115(3)	31(1)
C(50)	7678(3)	1459(3)	8245(3)	31(1)
C(51)	6362(3)	1834(3)	9795(3)	30(1)
C(52)	5163(3)	2375(3)	10223(3)	27(1)
C(61)	937(3)	9684(3)	9222(3)	31(1)
C(62)	440(3)	8938(3)	9899(3)	33(1)

C(63)	-495(3)	9265(3)	10668(3)	34(1)
-------	---------	---------	----------	-------

**Table A2.8. Bond lengths [Å] and angles [°] for 6 (CCDC 635046).**

Ir-C(15)	2.041(3)	C(26)-C(27)	1.539(4)
Ir-O(1)	2.0423(19)	C(27)-C(28)	1.513(4)
Ir-C(24)	2.093(3)	C(28)-C(29)	1.397(5)
Ir-C(25)	2.145(3)	C(29)-C(30)	1.522(4)
Ir-C(28)	2.159(3)	C(30)-C(31)	1.540(5)
Ir-C(29)	2.174(3)	K-O(43)	2.766(2)
O(1)-C(1)	1.326(4)	K-O(44)	2.803(3)
O(2)-C(10)	1.287(4)	K-O(45)	2.883(3)
O(2)-K	2.576(2)	K-O(42)	2.909(2)
N(1)-C(15)	1.369(4)	K-O(46)	2.915(3)
N(1)-C(6)	1.412(3)	K-O(41)	2.916(2)
N(1)-C(7)	1.474(4)	K-C(47)	3.510(4)
N(2)-C(15)	1.348(4)	O(41)-C(52)	1.422(4)
N(2)-C(9)	1.427(4)	O(41)-C(41)	1.431(4)
N(2)-C(8)	1.471(4)	O(42)-C(43)	1.415(4)
C(1)-C(2)	1.403(4)	O(42)-C(42)	1.424(4)
C(1)-C(6)	1.414(4)	O(43)-C(44)	1.422(4)
C(2)-C(3)	1.383(4)	O(43)-C(45)	1.428(4)
C(3)-C(4)	1.403(4)	O(44)-C(46)	1.425(5)
C(4)-C(5)	1.401(4)	O(44)-C(47)	1.433(4)
C(4)-C(16)	1.534(4)	O(45)-C(48)	1.413(5)
C(5)-C(6)	1.408(4)	O(45)-C(49)	1.422(5)
C(7)-C(8)	1.522(4)	O(46)-C(50)	1.425(4)
C(9)-C(14)	1.387(4)	O(46)-C(51)	1.427(4)
C(9)-C(10)	1.435(4)	C(41)-C(42)	1.488(5)
C(10)-C(11)	1.424(4)	C(43)-C(44)	1.504(5)
C(11)-C(12)	1.394(5)	C(45)-C(46)	1.501(5)
C(12)-C(13)	1.407(4)	C(47)-C(48)	1.494(6)
C(13)-C(14)	1.400(4)	C(49)-C(50)	1.494(6)
C(13)-C(20)	1.534(4)	C(51)-C(52)	1.498(5)
C(16)-C(19)	1.517(5)	C(61)-C(63)#1	1.377(6)
C(16)-C(18)	1.534(5)	C(61)-C(62)	1.394(6)
C(16)-C(17)	1.544(5)	C(62)-C(63)	1.385(6)
C(20)-C(22)	1.527(4)	C(63)-C(61)#1	1.377(6)
C(20)-C(23)	1.532(5)		
C(20)-C(21)	1.538(5)	C(15)-Ir-O(1)	87.56(10)
C(24)-C(25)	1.417(5)	C(15)-Ir-C(24)	93.31(12)
C(24)-C(31)	1.509(5)	O(1)-Ir-C(24)	153.01(11)
C(25)-C(26)	1.531(5)	C(15)-Ir-C(25)	100.71(12)

O(1)-Ir-C(25)	165.77(10)	N(2)-C(15)-Ir	132.1(2)
C(24)-Ir-C(25)	39.06(12)	N(1)-C(15)-Ir	120.4(2)
C(15)-Ir-C(28)	164.27(12)	C(19)-C(16)-C(18)	109.2(3)
O(1)-Ir-C(28)	88.10(10)	C(19)-C(16)-C(4)	112.5(3)
C(24)-Ir-C(28)	97.40(12)	C(18)-C(16)-C(4)	110.2(3)
C(25)-Ir-C(28)	80.84(11)	C(19)-C(16)-C(17)	107.3(3)
C(15)-Ir-C(29)	156.85(12)	C(18)-C(16)-C(17)	108.6(3)
O(1)-Ir-C(29)	86.99(10)	C(4)-C(16)-C(17)	108.9(3)
C(24)-Ir-C(29)	81.68(12)	C(22)-C(20)-C(23)	107.7(3)
C(25)-Ir-C(29)	89.62(12)	C(22)-C(20)-C(13)	112.8(3)
C(28)-Ir-C(29)	37.61(12)	C(23)-C(20)-C(13)	109.3(3)
C(1)-O(1)-Ir	121.82(18)	C(22)-C(20)-C(21)	107.1(3)
C(10)-O(2)-K	141.1(2)	C(23)-C(20)-C(21)	109.4(3)
C(15)-N(1)-C(6)	127.9(3)	C(13)-C(20)-C(21)	110.5(3)
C(15)-N(1)-C(7)	112.4(2)	C(25)-C(24)-C(31)	124.3(3)
C(6)-N(1)-C(7)	119.7(2)	C(25)-C(24)-Ir	72.47(17)
C(15)-N(2)-C(9)	126.3(3)	C(31)-C(24)-Ir	112.3(2)
C(15)-N(2)-C(8)	113.8(2)	C(24)-C(25)-C(26)	122.1(3)
C(9)-N(2)-C(8)	119.0(2)	C(24)-C(25)-Ir	68.48(16)
O(1)-C(1)-C(2)	118.7(3)	C(26)-C(25)-Ir	114.08(19)
O(1)-C(1)-C(6)	124.5(2)	C(25)-C(26)-C(27)	111.8(2)
C(2)-C(1)-C(6)	116.8(3)	C(28)-C(27)-C(26)	112.3(3)
C(3)-C(2)-C(1)	122.9(3)	C(29)-C(28)-C(27)	124.9(3)
C(2)-C(3)-C(4)	121.0(3)	C(29)-C(28)-Ir	71.78(19)
C(5)-C(4)-C(3)	116.7(3)	C(27)-C(28)-Ir	111.3(2)
C(5)-C(4)-C(16)	122.3(3)	C(28)-C(29)-C(30)	124.2(3)
C(3)-C(4)-C(16)	120.9(3)	C(28)-C(29)-Ir	70.61(19)
C(4)-C(5)-C(6)	122.8(3)	C(30)-C(29)-Ir	112.2(2)
C(5)-C(6)-N(1)	118.4(3)	C(29)-C(30)-C(31)	112.6(3)
C(5)-C(6)-C(1)	119.7(2)	C(24)-C(31)-C(30)	113.0(3)
N(1)-C(6)-C(1)	121.8(3)	O(2)-K-O(43)	85.10(7)
N(1)-C(7)-C(8)	103.4(2)	O(2)-K-O(44)	89.83(8)
N(2)-C(8)-C(7)	102.7(3)	O(43)-K-O(44)	61.15(7)
C(14)-C(9)-N(2)	119.2(3)	O(2)-K-O(45)	94.48(8)
C(14)-C(9)-C(10)	123.0(3)	O(43)-K-O(45)	121.30(8)
N(2)-C(9)-C(10)	117.8(3)	O(44)-K-O(45)	60.15(7)
O(2)-C(10)-C(11)	123.7(3)	O(2)-K-O(42)	108.16(8)
O(2)-C(10)-C(9)	122.8(3)	O(43)-K-O(42)	58.08(7)
C(11)-C(10)-C(9)	113.5(3)	O(44)-K-O(42)	113.86(7)
C(12)-C(11)-C(10)	122.8(3)	O(45)-K-O(42)	156.87(8)
C(11)-C(12)-C(13)	122.6(3)	O(2)-K-O(46)	122.13(7)
C(14)-C(13)-C(12)	115.5(3)	O(43)-K-O(46)	152.37(7)
C(14)-C(13)-C(20)	120.1(3)	O(44)-K-O(46)	110.21(8)
C(12)-C(13)-C(20)	124.4(3)	O(45)-K-O(46)	57.41(7)
C(9)-C(14)-C(13)	122.6(3)	O(42)-K-O(46)	111.18(7)
N(2)-C(15)-N(1)	107.4(3)	O(2)-K-O(41)	119.80(8)

O(43)-K-O(41)	115.20(7)	C(48)-O(45)-C(49)	112.4(3)
O(44)-K-O(41)	150.26(7)	C(48)-O(45)-K	114.7(2)
O(45)-K-O(41)	115.29(7)	C(49)-O(45)-K	119.2(2)
O(42)-K-O(41)	57.39(7)	C(50)-O(46)-C(51)	111.9(3)
O(46)-K-O(41)	57.88(7)	C(50)-O(46)-K	113.5(2)
O(2)-K-C(47)	79.38(10)	C(51)-O(46)-K	112.2(2)
O(43)-K-C(47)	80.83(9)	O(41)-C(41)-C(42)	109.1(3)
O(44)-K-C(47)	22.92(8)	O(42)-C(42)-C(41)	108.3(3)
O(45)-K-C(47)	42.14(9)	O(42)-C(43)-C(44)	107.7(3)
O(42)-K-C(47)	136.49(8)	O(43)-C(44)-C(43)	108.3(3)
O(46)-K-C(47)	98.51(9)	O(43)-C(45)-C(46)	108.4(3)
O(41)-K-C(47)	154.59(10)	O(44)-C(46)-C(45)	109.0(3)
C(52)-O(41)-C(41)	110.4(3)	O(44)-C(47)-C(48)	108.3(3)
C(52)-O(41)-K	117.9(2)	O(44)-C(47)-K	49.60(16)
C(41)-O(41)-K	117.71(19)	C(48)-C(47)-K	85.4(2)
C(43)-O(42)-C(42)	114.4(3)	O(45)-C(48)-C(47)	109.3(3)
C(43)-O(42)-K	108.39(19)	O(45)-C(49)-C(50)	108.6(3)
C(42)-O(42)-K	115.13(18)	O(46)-C(50)-C(49)	108.0(3)
C(44)-O(43)-C(45)	112.3(3)	O(46)-C(51)-C(52)	108.7(3)
C(44)-O(43)-K	122.3(2)	O(41)-C(52)-C(51)	108.9(3)
C(45)-O(43)-K	116.6(2)	C(63)#1-C(61)-C(62)	119.5(4)
C(46)-O(44)-C(47)	111.0(3)	C(63)-C(62)-C(61)	119.6(4)
C(46)-O(44)-K	110.0(2)	C(61)#1-C(63)-C(62)	120.9(4)
C(47)-O(44)-K	107.5(2)		

Symmetry transformations used to generate equivalent atoms: #1 -x,-y+2,-z+2

**Table A2.9. Anisotropic displacement parameters ( $\text{\AA}^2 \times 10^4$ ) for 6 (CCDC 635046). The anisotropic displacement factor exponent takes the form:  $-2\pi^2[h^2a^*{}^2U^{11} + \dots + 2hka^*b^*U^{12}]$ .**

	U <sup>11</sup>	U <sup>22</sup>	U <sup>33</sup>	U <sup>23</sup>	U <sup>13</sup>	U <sup>12</sup>
Ir	114(1)	150(1)	180(1)	-45(1)	-41(1)	-50(1)
O(1)	113(8)	141(10)	264(13)	-68(9)	-23(8)	-48(7)
O(2)	205(10)	210(12)	281(14)	-39(10)	-66(10)	-117(9)
N(1)	146(9)	137(11)	231(15)	-50(10)	-83(10)	-34(8)
N(2)	174(10)	130(11)	253(15)	-36(10)	-109(10)	-51(8)
C(1)	128(10)	149(13)	145(15)	-27(10)	-35(11)	-57(9)

C(2)	136(10)	170(14)	189(16)	-49(11)	-49(11)	-51(9)
C(3)	160(11)	190(14)	206(17)	-39(11)	-78(12)	-61(10)
C(4)	179(11)	162(14)	145(16)	-25(11)	-58(11)	-54(10)
C(5)	162(11)	175(14)	185(16)	-34(11)	-66(11)	-69(10)
C(6)	135(10)	161(13)	134(15)	-33(10)	-41(11)	-45(9)
C(7)	191(12)	165(14)	320(20)	-84(13)	-120(13)	-47(10)
C(8)	243(14)	163(15)	450(20)	-113(14)	-200(15)	-18(11)
C(9)	157(11)	157(13)	193(16)	-49(11)	-85(11)	-48(9)
C(10)	165(11)	171(14)	214(17)	-55(11)	-68(12)	-63(10)
C(11)	147(11)	205(15)	300(20)	-91(13)	-52(13)	-65(10)
C(12)	171(12)	191(15)	276(19)	-58(13)	-83(13)	-43(11)
C(13)	170(11)	166(14)	202(17)	-28(11)	-87(12)	-64(10)
C(14)	148(10)	173(14)	189(17)	-51(11)	-64(11)	-54(10)
C(15)	136(10)	149(13)	136(15)	-16(10)	-45(11)	-60(9)
C(16)	214(13)	148(14)	264(19)	-35(12)	-112(13)	-38(11)
C(17)	284(16)	236(19)	400(20)	-96(16)	-39(17)	-36(14)
C(18)	372(18)	182(17)	410(20)	4(15)	-256(18)	-54(14)
C(19)	332(17)	168(16)	470(20)	-26(15)	-238(17)	-70(13)
C(20)	215(12)	161(14)	226(18)	-22(12)	-94(13)	-70(11)
C(21)	357(18)	218(17)	280(20)	-41(14)	-53(16)	-141(14)
C(22)	306(16)	191(17)	380(20)	12(15)	-152(17)	-63(13)
C(23)	407(19)	252(18)	330(20)	3(15)	-179(17)	-195(15)
C(24)	138(11)	207(15)	238(18)	-90(12)	-11(12)	-79(10)
C(25)	107(10)	197(15)	226(18)	-94(12)	-25(11)	-25(10)
C(26)	167(11)	178(15)	267(19)	-89(12)	-79(13)	-8(10)
C(27)	190(12)	168(14)	248(18)	-52(12)	-75(13)	-50(10)
C(28)	138(10)	150(14)	237(18)	-55(11)	-44(12)	-53(9)
C(29)	137(10)	205(15)	241(18)	-80(12)	-62(12)	-58(10)
C(30)	222(13)	233(16)	172(17)	-48(12)	-57(13)	-83(12)
C(31)	206(13)	224(16)	196(18)	-56(12)	-10(13)	-96(12)
K	157(2)	179(3)	188(4)	-27(2)	-50(2)	-73(2)
O(41)	200(9)	212(12)	245(13)	-34(9)	-44(9)	-114(9)
O(42)	244(10)	210(12)	249(14)	-83(10)	-56(10)	-72(9)
O(43)	200(9)	250(12)	227(13)	-14(9)	-88(9)	-88(9)
O(44)	233(10)	295(14)	217(13)	-18(10)	-73(10)	-100(10)
O(45)	246(11)	295(14)	278(15)	-98(11)	-99(11)	-54(10)
O(46)	219(10)	224(12)	270(14)	-40(10)	-90(10)	-40(9)
C(41)	190(13)	350(20)	195(18)	-90(14)	9(13)	-153(13)
C(42)	197(13)	340(20)	250(20)	-150(15)	-21(13)	-96(13)
C(43)	219(13)	216(17)	380(20)	-131(15)	-55(15)	-66(12)
C(44)	206(13)	183(16)	390(20)	-51(14)	-119(15)	-47(11)
C(45)	350(17)	260(18)	260(20)	16(14)	-177(16)	-99(14)
C(46)	410(20)	350(20)	200(20)	11(15)	-99(17)	-193(17)
C(47)	239(15)	580(30)	170(20)	-18(17)	-32(15)	-142(17)
C(48)	213(15)	560(30)	260(20)	-200(19)	-53(15)	-10(16)
C(49)	184(13)	300(20)	410(20)	-164(17)	-46(15)	-11(13)

C(50)	232(14)	203(17)	410(20)	-56(15)	-94(16)	-4(12)
C(51)	364(18)	226(18)	280(20)	12(14)	-156(17)	-86(14)
C(52)	348(17)	253(18)	240(20)	-5(14)	-72(15)	-172(14)
C(61)	313(17)	370(20)	290(20)	-98(16)	-61(16)	-156(16)
C(62)	340(18)	263(19)	470(30)	-119(17)	-138(18)	-123(15)
C(63)	367(19)	360(20)	340(20)	-15(17)	-62(18)	-235(17)

---

## Structure of 7 (CCDC 704157)

### Special Refinement Details

Crystals were mounted on a glass fiber using Paratone oil then placed on the diffractometer under a nitrogen stream at 100K.

Refinement of  $F^2$  against ALL reflections. The weighted R-factor ( $wR$ ) and goodness of fit (S) are based on  $F^2$ , conventional R-factors (R) are based on F, with F set to zero for negative  $F^2$ . The threshold expression of  $F^2 > 2\sigma(F^2)$  is used only for calculating R-factors(gt) etc. and is not relevant to the choice of reflections for refinement. R-factors based on  $F^2$  are statistically about twice as large as those based on F, and R-factors based on ALL data will be even larger.

All esds (except the esd in the dihedral angle between two l.s. planes) are estimated using the full covariance matrix. The cell esds are taken into account individually in the estimation of esds in distances, angles and torsion angles; correlations between esds in cell parameters are only used when they are defined by crystal symmetry. An approximate (isotropic) treatment of cell esds is used for estimating esds involving l.s. planes.

**Table A2.10. Atomic coordinates ( $\times 10^4$ ) and equivalent isotropic displacement parameters ( $\text{\AA}^2 \times 10^3$ ) for 7 (CCDC 704157).  $U_{\text{eq}}$  is defined as the trace of the orthogonalized  $U_{ij}$  tensor.**

	x	y	z	$U_{\text{eq}}$
Ir(1)	7820(1)	4989(1)	909(1)	17(1)
Ir(2)	9029(1)	6015(1)	-85(1)	16(1)
P(1)	9425(3)	7025(3)	1455(2)	15(1)
O(1)	7246(9)	5849(8)	92(5)	48(3)
N(1)	8837(9)	6319(8)	929(5)	20(3)

C(1)	9008(10)	4958(11)	-853(5)	21(3)
C(2)	8991(12)	5973(12)	-1121(5)	22(3)
C(3)	10072(12)	6485(12)	-1460(6)	25(4)
C(4)	10794(12)	7119(11)	-954(6)	28(3)
C(5)	10668(10)	6693(10)	-242(6)	11(3)
C(6)	10818(10)	5657(9)	-106(6)	14(3)
C(7)	11165(11)	4834(12)	-573(6)	28(4)
C(8)	10039(12)	4273(12)	-863(7)	33(4)
C(9)	7234(13)	3566(11)	568(7)	30(4)
C(10)	6350(10)	4032(11)	988(6)	19(3)
C(11)	6146(13)	3657(11)	1689(6)	28(4)
C(12)	7277(14)	3560(12)	2084(7)	32(4)
C(13)	8208(11)	4295(10)	1838(6)	18(3)
C(14)	9081(11)	4029(11)	1368(5)	17(3)
C(15)	9139(12)	2998(10)	1033(6)	24(3)
C(16)	7943(12)	2660(10)	761(6)	23(3)
C(17)	10840(13)	6588(10)	1793(6)	19(3)
C(18)	11862(12)	6760(12)	1455(7)	24(4)
C(19)	12910(12)	6295(10)	1665(6)	24(3)
C(20)	12909(13)	5720(11)	2235(7)	31(4)
C(21)	11890(12)	5575(11)	2592(7)	26(4)
C(22)	10854(11)	5990(11)	2383(6)	20(3)
C(23)	9721(11)	8315(11)	1148(6)	19(3)
C(24)	9060(12)	8713(10)	603(6)	21(3)
C(25)	9202(11)	9702(10)	404(6)	21(3)
C(26)	9992(12)	10377(11)	714(6)	21(4)
C(27)	10635(10)	10007(14)	1251(6)	21(3)
C(28)	10509(11)	8998(12)	1454(6)	20(3)
C(29)	8489(11)	7205(10)	2177(6)	13(3)
C(30)	7394(11)	6752(11)	2211(6)	19(3)
C(31)	6671(12)	6913(12)	2756(7)	27(4)
C(32)	7017(12)	7533(10)	3259(6)	21(3)
C(33)	8074(12)	8043(12)	3229(6)	27(4)
C(34)	8810(11)	7878(11)	2684(6)	20(3)

**Table A2.11. Bond lengths [Å] and angles [°] for 7 (CCDC 704157).**

Ir(1)-N(1)	2.069(10)	Ir(1)-C(14)	2.112(12)
Ir(1)-C(9)	2.071(14)	Ir(1)-C(13)	2.127(12)
Ir(1)-C(10)	2.088(12)	Ir(1)-Ir(2)	2.7709(9)
Ir(1)-O(1)	2.093(9)	Ir(2)-C(1)	2.067(13)

Ir(2)-O(1)	2.076(11)	C(9)-Ir(1)-C(10)	40.8(5)
Ir(2)-C(5)	2.089(11)	N(1)-Ir(1)-O(1)	75.7(4)
Ir(2)-C(6)	2.093(11)	C(9)-Ir(1)-O(1)	96.1(5)
Ir(2)-C(2)	2.096(11)	C(10)-Ir(1)-O(1)	97.0(4)
Ir(2)-N(1)	2.098(10)	N(1)-Ir(1)-C(14)	95.4(5)
P(1)-N(1)	1.551(11)	C(9)-Ir(1)-C(14)	81.2(6)
P(1)-C(23)	1.807(15)	C(10)-Ir(1)-C(14)	99.6(5)
P(1)-C(29)	1.823(12)	O(1)-Ir(1)-C(14)	150.4(4)
P(1)-C(17)	1.842(14)	N(1)-Ir(1)-C(13)	102.4(4)
C(1)-C(2)	1.416(19)	C(9)-Ir(1)-C(13)	89.3(5)
C(1)-C(8)	1.471(17)	C(10)-Ir(1)-C(13)	81.4(5)
C(2)-C(3)	1.557(18)	O(1)-Ir(1)-C(13)	169.8(4)
C(3)-C(4)	1.547(18)	C(14)-Ir(1)-C(13)	39.1(4)
C(4)-C(5)	1.547(16)	N(1)-Ir(1)-Ir(2)	48.8(3)
C(5)-C(6)	1.374(16)	C(9)-Ir(1)-Ir(2)	110.0(4)
C(6)-C(7)	1.474(17)	C(10)-Ir(1)-Ir(2)	137.5(3)
C(7)-C(8)	1.586(18)	O(1)-Ir(1)-Ir(2)	48.1(3)
C(9)-C(10)	1.449(18)	C(14)-Ir(1)-Ir(2)	105.0(3)
C(9)-C(16)	1.473(18)	C(13)-Ir(1)-Ir(2)	137.5(3)
C(10)-C(11)	1.513(17)	C(1)-Ir(2)-O(1)	92.9(4)
C(11)-C(12)	1.523(19)	C(1)-Ir(2)-C(5)	99.9(5)
C(12)-C(13)	1.507(18)	O(1)-Ir(2)-C(5)	161.2(4)
C(13)-C(14)	1.419(16)	C(1)-Ir(2)-C(6)	81.4(5)
C(14)-C(15)	1.494(18)	O(1)-Ir(2)-C(6)	159.4(4)
C(15)-C(16)	1.534(18)	C(5)-Ir(2)-C(6)	38.4(4)
C(17)-C(18)	1.370(18)	C(1)-Ir(2)-C(2)	39.8(5)
C(17)-C(22)	1.419(17)	O(1)-Ir(2)-C(2)	98.6(5)
C(18)-C(19)	1.403(18)	C(5)-Ir(2)-C(2)	82.9(5)
C(19)-C(20)	1.369(17)	C(6)-Ir(2)-C(2)	89.6(5)
C(20)-C(21)	1.381(19)	C(1)-Ir(2)-N(1)	148.9(5)
C(21)-C(22)	1.364(17)	O(1)-Ir(2)-N(1)	75.5(4)
C(23)-C(28)	1.402(18)	C(5)-Ir(2)-N(1)	99.4(4)
C(23)-C(24)	1.430(17)	C(6)-Ir(2)-N(1)	99.4(4)
C(24)-C(25)	1.347(17)	C(2)-Ir(2)-N(1)	168.3(5)
C(25)-C(26)	1.400(17)	C(1)-Ir(2)-Ir(1)	103.0(4)
C(26)-C(27)	1.395(17)	O(1)-Ir(2)-Ir(1)	48.6(3)
C(27)-C(28)	1.37(2)	C(5)-Ir(2)-Ir(1)	139.1(3)
C(29)-C(30)	1.381(17)	C(6)-Ir(2)-Ir(1)	113.3(3)
C(29)-C(34)	1.391(17)	C(2)-Ir(2)-Ir(1)	134.5(4)
C(30)-C(31)	1.391(17)	N(1)-Ir(2)-Ir(1)	47.9(3)
C(31)-C(32)	1.352(19)	N(1)-P(1)-C(23)	112.7(6)
C(32)-C(33)	1.374(18)	N(1)-P(1)-C(29)	111.7(6)
C(33)-C(34)	1.402(17)	C(23)-P(1)-C(29)	105.5(6)
		N(1)-P(1)-C(17)	117.0(6)
N(1)-Ir(1)-C(9)	157.1(5)	C(23)-P(1)-C(17)	104.2(6)
N(1)-Ir(1)-C(10)	159.7(5)	C(29)-P(1)-C(17)	104.8(6)

Ir(2)-O(1)-Ir(1)	83.3(4)	C(12)-C(13)-Ir(1)	114.2(9)
P(1)-N(1)-Ir(1)	137.9(6)	C(13)-C(14)-C(15)	123.4(13)
P(1)-N(1)-Ir(2)	137.1(6)	C(13)-C(14)-Ir(1)	71.0(7)
Ir(1)-N(1)-Ir(2)	83.4(4)	C(15)-C(14)-Ir(1)	110.6(8)
C(2)-C(1)-C(8)	124.1(12)	C(14)-C(15)-C(16)	112.1(11)
C(2)-C(1)-Ir(2)	71.2(7)	C(9)-C(16)-C(15)	111.0(11)
C(8)-C(1)-Ir(2)	113.3(9)	C(18)-C(17)-C(22)	119.8(13)
C(1)-C(2)-C(3)	123.3(12)	C(18)-C(17)-P(1)	120.7(10)
C(1)-C(2)-Ir(2)	69.0(7)	C(22)-C(17)-P(1)	119.2(10)
C(3)-C(2)-Ir(2)	114.4(8)	C(17)-C(18)-C(19)	120.3(13)
C(4)-C(3)-C(2)	110.7(10)	C(20)-C(19)-C(18)	119.0(14)
C(5)-C(4)-C(3)	112.2(11)	C(19)-C(20)-C(21)	120.9(14)
C(6)-C(5)-C(4)	121.3(11)	C(22)-C(21)-C(20)	120.9(13)
C(6)-C(5)-Ir(2)	71.0(7)	C(21)-C(22)-C(17)	118.9(12)
C(4)-C(5)-Ir(2)	111.9(8)	C(28)-C(23)-C(24)	117.0(13)
C(5)-C(6)-C(7)	127.2(12)	C(28)-C(23)-P(1)	123.1(10)
C(5)-C(6)-Ir(2)	70.7(7)	C(24)-C(23)-P(1)	119.7(10)
C(7)-C(6)-Ir(2)	115.7(9)	C(25)-C(24)-C(23)	120.4(13)
C(6)-C(7)-C(8)	110.3(11)	C(24)-C(25)-C(26)	122.2(13)
C(1)-C(8)-C(7)	111.6(12)	C(27)-C(26)-C(25)	118.3(13)
C(10)-C(9)-C(16)	123.7(12)	C(28)-C(27)-C(26)	120.1(14)
C(10)-C(9)-Ir(1)	70.2(8)	C(27)-C(28)-C(23)	122.0(13)
C(16)-C(9)-Ir(1)	115.9(10)	C(30)-C(29)-C(34)	117.7(12)
C(9)-C(10)-C(11)	121.5(12)	C(30)-C(29)-P(1)	121.1(10)
C(9)-C(10)-Ir(1)	69.0(7)	C(34)-C(29)-P(1)	121.0(10)
C(11)-C(10)-Ir(1)	112.6(9)	C(29)-C(30)-C(31)	120.9(13)
C(10)-C(11)-C(12)	112.7(11)	C(32)-C(31)-C(30)	120.6(13)
C(13)-C(12)-C(11)	111.8(11)	C(31)-C(32)-C(33)	120.4(13)
C(14)-C(13)-C(12)	124.3(13)	C(32)-C(33)-C(34)	119.2(13)
C(14)-C(13)-Ir(1)	69.9(7)	C(29)-C(34)-C(33)	121.0(12)

**Table A2.12. Anisotropic displacement parameters ( $\text{\AA}^2 \times 10^4$ ) for 7 (CCDC 704157). The anisotropic displacement factor exponent takes the form:**  
 **$-2\pi^2[h^2a^*2U11 + \dots + 2hka^*b^*U12]$ .**

	U11	U22	U33	U23	U13	U12
Ir(1)	149(2)	233(3)	114(2)	6(3)	-19(2)	-13(3)
Ir(2)	137(2)	266(3)	90(2)	-14(2)	-7(2)	-13(3)
P(1)	145(19)	230(20)	92(16)	-16(15)	-6(13)	-8(17)
O(1)	610(60)	540(60)	300(50)	70(50)	-160(50)	140(60)
N(1)	170(50)	320(60)	100(40)	60(50)	-10(40)	-40(50)
C(1)	210(50)	210(60)	210(50)	30(60)	40(50)	20(70)
C(2)	120(50)	310(70)	230(50)	-120(60)	-10(50)	40(60)
C(3)	230(70)	330(80)	190(60)	10(60)	10(50)	0(60)
C(4)	300(70)	400(70)	150(60)	110(60)	130(60)	-10(60)
C(5)	120(60)	100(60)	110(50)	-60(50)	-20(40)	-40(50)
C(6)	40(50)	270(60)	110(50)	0(50)	20(50)	10(50)
C(7)	310(70)	270(70)	250(60)	-20(60)	-20(50)	80(60)
C(8)	330(70)	410(80)	260(60)	-90(60)	-40(60)	-20(60)
C(9)	350(70)	340(70)	220(60)	60(60)	160(60)	20(60)
C(10)	200(60)	220(60)	170(50)	110(60)	-40(50)	-20(60)
C(11)	270(70)	300(80)	280(60)	30(60)	100(60)	10(60)
C(12)	350(70)	310(80)	300(70)	0(60)	70(60)	-160(60)
C(13)	150(60)	190(70)	200(60)	60(50)	-110(50)	20(50)
C(14)	40(50)	280(70)	180(50)	100(60)	-20(50)	0(60)
C(15)	300(70)	200(70)	210(60)	-40(50)	-40(60)	30(60)
C(16)	200(60)	270(70)	220(60)	10(50)	70(50)	20(60)
C(17)	240(60)	240(70)	100(50)	-80(50)	10(50)	20(60)
C(18)	200(70)	320(70)	210(60)	60(60)	-80(50)	40(60)
C(19)	150(60)	320(70)	270(60)	-30(60)	-20(50)	-60(60)
C(20)	260(70)	290(70)	370(70)	-10(60)	-100(60)	100(60)
C(21)	290(70)	250(70)	230(60)	100(60)	-20(50)	10(60)
C(22)	150(60)	240(70)	210(50)	20(60)	0(50)	10(60)
C(23)	190(60)	240(70)	130(60)	-40(50)	60(50)	-10(60)
C(24)	210(60)	230(70)	190(50)	-50(50)	60(50)	0(60)
C(25)	220(60)	260(80)	140(50)	50(50)	170(50)	70(60)
C(26)	250(70)	180(70)	210(60)	-10(50)	160(50)	90(50)
C(27)	180(60)	260(70)	170(50)	-70(60)	50(40)	-10(60)
C(28)	270(60)	210(70)	130(50)	-40(60)	90(50)	50(60)
C(29)	160(60)	130(70)	90(50)	-20(50)	50(50)	20(50)
C(30)	130(60)	280(70)	160(60)	-10(60)	10(50)	0(60)
C(31)	170(60)	380(80)	250(60)	90(60)	50(50)	20(60)
C(32)	240(70)	220(70)	170(60)	-70(50)	110(50)	-50(60)

---

C(33)	330(70)	350(70)	140(60)	-80(60)	30(50)	-50(60)
C(34)	190(60)	310(70)	100(50)	-10(50)	10(50)	-130(60)

---

## Structure of 12/15 (CCDC 700172)

### Special Refinement Details

Crystals were mounted on a glass fiber using Paratone oil then placed on the diffractometer under a nitrogen stream at 100K.

The axial ligand on Ir is disordered between acetonitrile (78%) and carbonyl (22%). Disorder is also observed in the counterion.

Refinement of  $F^2$  against ALL reflections. The weighted R-factor ( $wR$ ) and goodness of fit (S) are based on  $F^2$ , conventional R-factors (R) are based on F, with F set to zero for negative  $F^2$ . The threshold expression of  $F^2 > 2\sigma(F^2)$  is used only for calculating R-factors(gt) etc. and is not relevant to the choice of reflections for refinement. R-factors based on  $F^2$  are statistically about twice as large as those based on F, and R-factors based on ALL data will be even larger.

All esds (except the esd in the dihedral angle between two l.s. planes) are estimated using the full covariance matrix. The cell esds are taken into account individually in the estimation of esds in distances, angles and torsion angles; correlations between esds in cell parameters are only used when they are defined by crystal symmetry. An approximate (isotropic) treatment of cell esds is used for estimating esds involving l.s. planes.

**Table A2.13. Atomic coordinates (x 10<sup>4</sup>) and equivalent isotropic displacement**

**parameters (Å<sup>2</sup> x 10<sup>3</sup>) for 12/15 (CCDC 700172). U(eq) is defined as the trace of the orthogonalized  $U^{ij}$  tensor.**

	x	y	z	U <sub>eq</sub>	Occ
Ir(1)	8077(1)	4908(1)	5396(1)	15(1)	1
P(1)	7564(1)	3624(1)	5357(1)	15(1)	1
P(2)	8389(1)	6236(1)	5417(1)	20(1)	1

O(1)	8124(1)	4924(1)	4432(1)	18(1)	1
O(2)	7943(1)	4891(1)	6353(1)	20(1)	1
N(1)	9796(1)	4539(1)	4972(1)	16(1)	1
N(2)	9700(1)	4509(1)	6006(1)	16(1)	1
N(3A)	6833(5)	5215(4)	5340(4)	16(1)	0.777(5)
C(3B)	6790(30)	5200(20)	5221(17)	24(7)	0.223(5)
C(1)	9274(1)	4631(1)	5462(1)	15(1)	1
C(2)	8810(1)	4796(1)	4087(1)	16(1)	1
C(3)	8724(1)	4838(1)	3430(1)	22(1)	1
C(4)	9387(1)	4728(1)	3016(1)	23(1)	1
C(5)	10198(1)	4585(1)	3239(1)	18(1)	1
C(6)	10289(1)	4536(1)	3894(1)	20(1)	1
C(7)	9619(1)	4624(1)	4319(1)	15(1)	1
C(8)	10652(1)	4334(1)	5174(1)	22(1)	1
C(9)	10583(1)	4302(1)	5891(1)	23(1)	1
C(10)	9385(1)	4541(1)	6632(1)	18(1)	1
C(11)	9950(2)	4407(1)	7127(1)	23(1)	1
C(12)	9725(2)	4431(1)	7754(1)	28(1)	1
C(13)	8879(2)	4595(1)	7886(1)	31(1)	1
C(14)	8314(2)	4728(1)	7402(1)	28(1)	1
C(15)	8540(1)	4723(1)	6770(1)	20(1)	1
C(16)	10956(1)	4519(1)	2795(1)	21(1)	1
C(17)	10692(2)	4210(2)	2149(1)	37(1)	1
C(18)	11626(2)	3997(2)	3061(1)	43(1)	1
C(19)	11339(2)	5291(1)	2705(1)	36(1)	1
C(20)	10385(2)	4358(2)	8281(1)	38(1)	1
C(21)	10019(2)	3929(2)	8845(2)	78(1)	1
C(22)	10594(3)	5145(2)	8499(2)	138(2)	1
C(23)	11150(2)	3945(2)	8071(2)	65(1)	1
C(24)	7517(1)	3322(1)	4508(1)	17(1)	1
C(25)	6795(1)	3704(1)	4151(1)	21(1)	1
C(26)	6853(2)	3548(1)	3436(1)	26(1)	1
C(27)	6884(2)	2716(1)	3299(1)	28(1)	1
C(28)	7597(2)	2345(1)	3663(1)	28(1)	1
C(29)	7519(2)	2480(1)	4370(1)	24(1)	1
C(30)	8160(2)	2861(1)	5739(1)	23(1)	1
C(31)	9064(1)	2830(1)	5484(1)	23(1)	1
C(32)	9533(2)	2152(2)	5736(1)	37(1)	1
C(33)	9530(2)	2145(2)	6443(1)	36(1)	1
C(34)	8636(1)	2147(1)	6695(1)	30(1)	1
C(35)	8148(2)	2829(1)	6455(1)	28(1)	1
C(36)	6478(1)	3546(1)	5685(1)	18(1)	1
C(37)	6129(1)	2742(1)	5696(1)	22(1)	1
C(38)	5226(1)	2716(1)	5948(1)	25(1)	1
C(39)	5160(2)	3058(1)	6605(1)	31(1)	1
C(40)	5463(2)	3860(1)	6579(1)	32(1)	1

C(41)	6370(1)	3910(1)	6346(1)	24(1)	1
C(42)	8472(1)	6589(1)	4591(1)	23(1)	1
C(43)	7610(1)	6616(1)	4253(1)	26(1)	1
C(44)	7712(2)	6774(2)	3559(1)	37(1)	1
C(45)	8222(2)	7470(2)	3426(2)	43(1)	1
C(46)	9074(2)	7431(2)	3767(1)	39(1)	1
C(47)	8954(2)	7320(1)	4476(1)	34(1)	1
C(48)	9358(1)	6588(1)	5803(1)	25(1)	1
C(49)	10169(1)	6301(1)	5495(1)	28(1)	1
C(50)	10935(2)	6695(2)	5779(1)	38(1)	1
C(51)	10981(2)	6548(2)	6484(1)	47(1)	1
C(52)	10186(2)	6799(2)	6817(1)	42(1)	1
C(53)	9390(1)	6478(1)	6514(1)	27(1)	1
C(54)	7503(1)	6763(1)	5781(1)	23(1)	1
C(55)	7186(1)	6478(1)	6426(1)	29(1)	1
C(56)	6392(2)	6886(1)	6634(1)	32(1)	1
C(57)	6523(2)	7726(1)	6657(1)	35(1)	1
C(58)	6841(2)	8010(1)	6029(1)	34(1)	1
C(59)	7640(2)	7612(1)	5819(1)	32(1)	1
C(60A)	6135(2)	5383(2)	5355(2)	18(1)	0.777(5)
O(3B)	6231(8)	5350(7)	5138(5)	29(3)	0.223(5)
C(61A)	5237(2)	5590(2)	5408(2)	32(1)	0.777(5)
P(3)	2978(1)	4962(1)	5335(1)	46(1)	1
F(1A)	2505(6)	4215(4)	5350(6)	91(4)	0.526(8)
F(2A)	3547(4)	4619(3)	5933(3)	72(2)	0.526(8)
F(3A)	3630(6)	4678(6)	4893(4)	80(3)	0.526(8)
F(4A)	3470(3)	5738(2)	5478(4)	64(2)	0.526(8)
F(5A)	2339(4)	5230(4)	5903(4)	93(2)	0.526(8)
F(6A)	2408(5)	5296(4)	4863(4)	103(3)	0.526(8)
F(1B)	2538(3)	4727(7)	4609(3)	118(4)	0.474(8)
F(5B)	3422(3)	5608(4)	4904(5)	92(3)	0.474(8)
F(4B)	2198(3)	5476(3)	5416(8)	117(5)	0.474(8)
F(3B)	3391(4)	5182(9)	5889(4)	157(6)	0.474(8)
F(2B)	3763(6)	4453(6)	5154(5)	76(3)	0.474(8)
F(6B)	2444(7)	4324(6)	5556(6)	93(4)	0.474(8)

**Table A2.14. Bond lengths [Å] and angles [°] for 12/15 (CCDC 700172).**

Ir(1)-C(1)	1.9694(19)	C(20)-C(21)	1.534(4)
Ir(1)-O(2)	2.0331(14)	C(24)-C(25)	1.534(3)
Ir(1)-O(1)	2.0390(13)	C(24)-C(29)	1.539(3)
Ir(1)-N(3A)	2.055(8)	C(25)-C(26)	1.539(3)
Ir(1)-C(3B)	2.14(4)	C(26)-C(27)	1.523(3)
Ir(1)-P(2)	2.4348(5)	C(27)-C(28)	1.521(3)
Ir(1)-P(1)	2.4437(5)	C(28)-C(29)	1.517(3)
P(1)-C(30)	1.850(2)	C(30)-C(35)	1.515(3)
P(1)-C(36)	1.865(2)	C(30)-C(31)	1.535(3)
P(1)-C(24)	1.876(2)	C(31)-C(32)	1.522(3)
P(2)-C(48)	1.854(2)	C(32)-C(33)	1.493(4)
P(2)-C(42)	1.861(3)	C(33)-C(34)	1.516(3)
P(2)-C(54)	1.862(2)	C(34)-C(35)	1.534(3)
O(1)-C(2)	1.332(2)	C(36)-C(37)	1.545(3)
O(2)-C(15)	1.329(3)	C(36)-C(41)	1.550(3)
N(1)-C(1)	1.337(3)	C(37)-C(38)	1.531(3)
N(1)-C(7)	1.417(3)	C(38)-C(39)	1.522(3)
N(1)-C(8)	1.472(3)	C(39)-C(40)	1.518(3)
N(2)-C(1)	1.352(3)	C(40)-C(41)	1.526(3)
N(2)-C(10)	1.417(3)	C(42)-C(47)	1.537(3)
N(2)-C(9)	1.471(3)	C(42)-C(43)	1.545(3)
N(3A)-C(60A)	1.150(8)	C(43)-C(44)	1.503(4)
C(3B)-O(3B)	0.95(4)	C(44)-C(45)	1.514(4)
C(2)-C(3)	1.398(3)	C(45)-C(46)	1.535(4)
C(2)-C(7)	1.409(3)	C(46)-C(47)	1.525(4)
C(3)-C(4)	1.382(3)	C(48)-C(53)	1.517(3)
C(4)-C(5)	1.395(3)	C(48)-C(49)	1.532(3)
C(5)-C(6)	1.396(3)	C(49)-C(50)	1.529(3)
C(5)-C(16)	1.531(3)	C(50)-C(51)	1.515(4)
C(6)-C(7)	1.401(3)	C(51)-C(52)	1.514(4)
C(8)-C(9)	1.521(3)	C(52)-C(53)	1.528(3)
C(10)-C(11)	1.398(3)	C(54)-C(55)	1.539(4)
C(10)-C(15)	1.411(3)	C(54)-C(59)	1.541(3)
C(11)-C(12)	1.374(3)	C(55)-C(56)	1.522(3)
C(12)-C(13)	1.403(4)	C(56)-C(57)	1.523(3)
C(12)-C(20)	1.535(4)	C(57)-C(58)	1.510(4)
C(13)-C(14)	1.380(3)	C(58)-C(59)	1.522(3)
C(14)-C(15)	1.384(3)	C(60A)-C(61A)	1.478(4)
C(16)-C(19)	1.524(3)	P(3)-F(3B)	1.399(6)
C(16)-C(18)	1.525(3)	P(3)-F(6A)	1.475(5)
C(16)-C(17)	1.532(3)	P(3)-F(3A)	1.485(9)
C(20)-C(23)	1.490(4)	P(3)-F(6B)	1.498(8)
C(20)-C(22)	1.524(4)	P(3)-F(1A)	1.536(6)

P(3)-F(4B)	1.555(5)	C(1)-N(2)-C(10)	127.69(18)
P(3)-F(2B)	1.592(9)	C(1)-N(2)-C(9)	112.27(18)
P(3)-F(4A)	1.626(4)	C(10)-N(2)-C(9)	120.02(18)
P(3)-F(5B)	1.635(6)	C(60A)-N(3A)-Ir(1)	175.1(7)
P(3)-F(5A)	1.643(6)	O(3B)-C(3B)-Ir(1)	178(4)
P(3)-F(2A)	1.671(6)	N(1)-C(1)-N(2)	109.07(17)
P(3)-F(1B)	1.738(6)	N(1)-C(1)-Ir(1)	125.19(16)
		N(2)-C(1)-Ir(1)	125.73(16)
C(1)-Ir(1)-O(2)	91.57(8)	O(1)-C(2)-C(3)	117.04(17)
C(1)-Ir(1)-O(1)	92.21(7)	O(1)-C(2)-C(7)	126.46(19)
O(2)-Ir(1)-O(1)	176.10(5)	C(3)-C(2)-C(7)	116.50(19)
C(1)-Ir(1)-N(3A)	178.8(2)	C(4)-C(3)-C(2)	123.1(2)
O(2)-Ir(1)-N(3A)	87.8(2)	C(3)-C(4)-C(5)	121.1(2)
O(1)-Ir(1)-N(3A)	88.5(2)	C(4)-C(5)-C(6)	116.2(2)
C(1)-Ir(1)-C(3B)	174.1(10)	C(4)-C(5)-C(16)	122.4(2)
O(2)-Ir(1)-C(3B)	94.4(10)	C(6)-C(5)-C(16)	121.4(2)
O(1)-Ir(1)-C(3B)	81.9(10)	C(5)-C(6)-C(7)	123.4(2)
N(3A)-Ir(1)-C(3B)	6.7(12)	C(6)-C(7)-C(2)	119.7(2)
C(1)-Ir(1)-P(2)	92.79(6)	C(6)-C(7)-N(1)	117.43(19)
O(2)-Ir(1)-P(2)	91.00(5)	C(2)-C(7)-N(1)	122.91(19)
O(1)-Ir(1)-P(2)	89.77(4)	N(1)-C(8)-C(9)	103.38(18)
N(3A)-Ir(1)-P(2)	86.2(2)	N(2)-C(9)-C(8)	102.89(18)
C(3B)-Ir(1)-P(2)	87.5(11)	C(11)-C(10)-C(15)	119.8(2)
C(1)-Ir(1)-P(1)	94.97(6)	C(11)-C(10)-N(2)	117.74(19)
O(2)-Ir(1)-P(1)	89.17(5)	C(15)-C(10)-N(2)	122.5(2)
O(1)-Ir(1)-P(1)	89.56(4)	C(12)-C(11)-C(10)	123.3(2)
N(3A)-Ir(1)-P(1)	86.0(2)	C(11)-C(12)-C(13)	116.5(2)
C(3B)-Ir(1)-P(1)	84.8(11)	C(11)-C(12)-C(20)	121.3(2)
P(2)-Ir(1)-P(1)	172.229(16)	C(13)-C(12)-C(20)	121.9(2)
C(30)-P(1)-C(36)	104.75(10)	C(14)-C(13)-C(12)	120.8(2)
C(30)-P(1)-C(24)	102.90(10)	C(13)-C(14)-C(15)	123.1(2)
C(36)-P(1)-C(24)	107.25(10)	O(2)-C(15)-C(14)	117.0(2)
C(30)-P(1)-Ir(1)	120.86(8)	O(2)-C(15)-C(10)	126.5(2)
C(36)-P(1)-Ir(1)	111.52(7)	C(14)-C(15)-C(10)	116.5(2)
C(24)-P(1)-Ir(1)	108.58(7)	C(19)-C(16)-C(18)	109.1(2)
C(48)-P(2)-C(42)	103.75(10)	C(19)-C(16)-C(5)	108.71(18)
C(48)-P(2)-C(54)	105.82(11)	C(18)-C(16)-C(5)	111.8(2)
C(42)-P(2)-C(54)	105.51(10)	C(19)-C(16)-C(17)	109.1(2)
C(48)-P(2)-Ir(1)	120.72(8)	C(18)-C(16)-C(17)	107.2(2)
C(42)-P(2)-Ir(1)	109.34(7)	C(5)-C(16)-C(17)	110.9(2)
C(54)-P(2)-Ir(1)	110.55(7)	C(23)-C(20)-C(22)	112.0(3)
C(2)-O(1)-Ir(1)	125.06(12)	C(23)-C(20)-C(21)	106.9(3)
C(15)-O(2)-Ir(1)	125.98(12)	C(22)-C(20)-C(21)	108.2(3)
C(1)-N(1)-C(7)	128.09(18)	C(23)-C(20)-C(12)	112.6(2)
C(1)-N(1)-C(8)	112.37(18)	C(22)-C(20)-C(12)	106.8(2)
C(7)-N(1)-C(8)	119.53(18)	C(21)-C(20)-C(12)	110.3(3)

C(25)-C(24)-C(29)	110.26(18)	C(57)-C(58)-C(59)	112.2(2)
C(25)-C(24)-P(1)	111.79(14)	C(58)-C(59)-C(54)	111.16(19)
C(29)-C(24)-P(1)	117.80(16)	N(3A)-C(60A)-C(61A)	177.1(7)
C(24)-C(25)-C(26)	110.93(19)	F(3B)-P(3)-F(6A)	137.6(6)
C(27)-C(26)-C(25)	111.52(19)	F(3B)-P(3)-F(3A)	107.3(4)
C(28)-C(27)-C(26)	110.9(2)	F(6A)-P(3)-F(3A)	98.1(5)
C(29)-C(28)-C(27)	111.6(2)	F(3B)-P(3)-F(6B)	102.7(7)
C(28)-C(29)-C(24)	110.1(2)	F(6A)-P(3)-F(6B)	100.0(5)
C(35)-C(30)-C(31)	111.2(2)	F(3A)-P(3)-F(6B)	109.2(6)
C(35)-C(30)-P(1)	117.23(16)	F(3B)-P(3)-F(1A)	117.3(7)
C(31)-C(30)-P(1)	110.60(15)	F(6A)-P(3)-F(1A)	93.9(5)
C(32)-C(31)-C(30)	111.28(19)	F(3A)-P(3)-F(1A)	93.1(6)
C(33)-C(32)-C(31)	110.9(2)	F(6B)-P(3)-F(1A)	18.4(9)
C(32)-C(33)-C(34)	110.7(2)	F(3B)-P(3)-F(4B)	96.5(6)
C(33)-C(34)-C(35)	111.1(2)	F(6A)-P(3)-F(4B)	49.0(4)
C(30)-C(35)-C(34)	110.7(2)	F(3A)-P(3)-F(4B)	145.9(6)
C(37)-C(36)-C(41)	109.90(18)	F(6B)-P(3)-F(4B)	88.2(5)
C(37)-C(36)-P(1)	114.09(15)	F(1A)-P(3)-F(4B)	97.2(4)
C(41)-C(36)-P(1)	113.91(14)	F(3B)-P(3)-F(2B)	89.8(5)
C(38)-C(37)-C(36)	111.72(19)	F(6A)-P(3)-F(2B)	123.5(5)
C(39)-C(38)-C(37)	111.66(19)	F(3A)-P(3)-F(2B)	26.6(4)
C(40)-C(39)-C(38)	109.1(2)	F(6B)-P(3)-F(2B)	94.6(6)
C(39)-C(40)-C(41)	111.4(2)	F(1A)-P(3)-F(2B)	83.6(6)
C(40)-C(41)-C(36)	111.78(19)	F(4B)-P(3)-F(2B)	172.4(6)
C(47)-C(42)-C(43)	109.99(19)	F(3B)-P(3)-F(4A)	51.5(5)
C(47)-C(42)-P(2)	118.30(19)	F(6A)-P(3)-F(4A)	94.1(3)
C(43)-C(42)-P(2)	112.45(15)	F(3A)-P(3)-F(4A)	94.3(4)
C(44)-C(43)-C(42)	111.2(2)	F(6B)-P(3)-F(4A)	150.3(6)
C(43)-C(44)-C(45)	113.2(2)	F(1A)-P(3)-F(4A)	168.1(6)
C(44)-C(45)-C(46)	110.3(2)	F(4B)-P(3)-F(4A)	81.6(3)
C(47)-C(46)-C(45)	110.9(2)	F(2B)-P(3)-F(4A)	99.2(5)
C(46)-C(47)-C(42)	109.2(2)	F(3B)-P(3)-F(5B)	93.7(5)
C(53)-C(48)-C(49)	110.4(2)	F(6A)-P(3)-F(5B)	66.4(4)
C(53)-C(48)-P(2)	114.82(16)	F(3A)-P(3)-F(5B)	65.9(4)
C(49)-C(48)-P(2)	113.37(17)	F(6B)-P(3)-F(5B)	163.6(6)
C(50)-C(49)-C(48)	110.3(2)	F(1A)-P(3)-F(5B)	147.2(6)
C(51)-C(50)-C(49)	110.1(2)	F(4B)-P(3)-F(5B)	89.1(4)
C(52)-C(51)-C(50)	111.4(2)	F(2B)-P(3)-F(5B)	86.3(4)
C(51)-C(52)-C(53)	112.5(2)	F(4A)-P(3)-F(5B)	44.6(3)
C(48)-C(53)-C(52)	113.1(2)	F(3B)-P(3)-F(5A)	66.2(4)
C(55)-C(54)-C(59)	109.2(2)	F(6A)-P(3)-F(5A)	89.7(4)
C(55)-C(54)-P(2)	116.36(16)	F(3A)-P(3)-F(5A)	172.1(4)
C(59)-C(54)-P(2)	114.64(16)	F(6B)-P(3)-F(5A)	69.3(6)
C(56)-C(55)-C(54)	111.6(2)	F(1A)-P(3)-F(5A)	86.4(5)
C(55)-C(56)-C(57)	111.8(2)	F(4B)-P(3)-F(5A)	41.7(4)
C(58)-C(57)-C(56)	110.5(2)	F(2B)-P(3)-F(5A)	145.8(4)

F(4A)-P(3)-F(5A)	84.9(3)	F(3B)-P(3)-F(1B)	174.8(4)
F(5B)-P(3)-F(5A)	117.8(4)	F(6A)-P(3)-F(1B)	41.8(3)
F(3B)-P(3)-F(2A)	38.5(6)	F(3A)-P(3)-F(1B)	69.0(4)
F(6A)-P(3)-F(2A)	173.4(5)	F(6B)-P(3)-F(1B)	82.1(6)
F(3A)-P(3)-F(2A)	88.5(3)	F(1A)-P(3)-F(1B)	67.1(5)
F(6B)-P(3)-F(2A)	77.9(5)	F(4B)-P(3)-F(1B)	85.4(5)
F(1A)-P(3)-F(2A)	85.9(5)	F(2B)-P(3)-F(1B)	87.9(4)
F(4B)-P(3)-F(2A)	124.5(6)	F(4A)-P(3)-F(1B)	124.4(4)
F(2B)-P(3)-F(2A)	63.1(4)	F(5B)-P(3)-F(1B)	81.5(4)
F(4A)-P(3)-F(2A)	85.1(3)	F(5A)-P(3)-F(1B)	117.8(3)
F(5B)-P(3)-F(2A)	116.7(4)	F(2A)-P(3)-F(1B)	142.8(4)
F(5A)-P(3)-F(2A)	83.7(3)		

**Table A2.15. Anisotropic displacement parameters ( $\text{\AA}^2 \times 10^4$ ) for 12/15**

(CCDC 700172). The anisotropic displacement factor exponent takes the

form:  $-2\pi^2 [ h^2 a^* \mathbf{U}^{11} + \dots + 2 h k a^* b^* \mathbf{U}^{12} ]$ 

	U <sup>11</sup>	U <sup>22</sup>	U <sup>33</sup>	U <sup>23</sup>	U <sup>13</sup>	U <sup>12</sup>
Ir(1)	96(1)	134(1)	211(1)	-6(1)	24(1)	-5(1)
P(1)	132(2)	138(2)	176(3)	-2(3)	22(3)	9(2)
P(2)	115(2)	149(2)	335(4)	-7(3)	31(3)	-19(2)
O(1)	117(5)	211(7)	221(8)	48(6)	-15(5)	-7(8)
O(2)	160(7)	255(8)	194(8)	-59(7)	51(6)	-5(7)
N(1)	93(8)	252(10)	131(10)	-22(8)	-19(7)	18(7)
N(2)	123(8)	267(10)	103(10)	-17(8)	2(7)	11(7)
N(3A)	180(17)	101(16)	210(30)	0(20)	-50(20)	-42(9)
C(1)	153(9)	166(9)	130(11)	-5(9)	7(9)	-23(7)
C(2)	142(9)	179(11)	172(11)	55(9)	-22(8)	-22(8)
C(3)	182(9)	275(12)	209(12)	63(11)	-41(9)	-12(9)
C(4)	283(12)	298(13)	112(12)	56(10)	-34(9)	-51(9)
C(5)	228(11)	160(11)	167(13)	6(9)	25(10)	-21(8)
C(6)	161(10)	190(11)	248(14)	-15(10)	1(10)	29(8)
C(7)	159(10)	158(10)	134(12)	4(9)	-9(9)	-8(8)
C(8)	111(10)	371(14)	193(13)	-38(10)	-45(9)	69(9)
C(9)	132(10)	314(13)	235(14)	-39(11)	-6(9)	37(9)
C(10)	242(11)	180(11)	119(12)	-20(9)	18(9)	-29(8)

C(11)	255(12)	203(11)	221(14)	-20(10)	3(10)	-3(9)
C(12)	433(15)	200(12)	217(14)	-6(11)	-22(12)	-62(11)
C(13)	475(16)	280(13)	181(14)	-28(11)	98(12)	-72(11)
C(14)	316(13)	274(13)	238(14)	-77(10)	94(11)	-67(9)
C(15)	211(10)	150(11)	228(13)	-33(9)	45(10)	-45(8)
C(16)	261(12)	217(12)	153(13)	4(10)	34(10)	8(9)
C(17)	395(15)	452(17)	256(16)	-110(13)	50(13)	-7(12)
C(18)	410(16)	614(19)	258(16)	105(14)	128(13)	265(14)
C(19)	324(14)	337(15)	410(17)	-36(12)	116(13)	-86(11)
C(20)	680(20)	271(14)	176(15)	20(11)	-126(14)	-5(13)
C(21)	1000(30)	1080(30)	246(19)	260(20)	80(20)	460(30)
C(22)	2260(60)	350(20)	1530(40)	-10(30)	-1620(40)	-130(30)
C(23)	425(19)	1250(30)	265(18)	150(20)	-135(15)	60(20)
C(24)	176(10)	167(10)	179(14)	-10(9)	20(9)	-2(7)
C(25)	172(11)	198(11)	250(13)	-2(9)	-3(9)	-18(8)
C(26)	228(11)	297(12)	239(13)	18(10)	-6(11)	-33(11)
C(27)	273(12)	334(12)	243(14)	-68(10)	22(12)	-26(12)
C(28)	291(13)	276(13)	264(15)	-80(11)	27(11)	13(10)
C(29)	317(13)	167(11)	247(14)	-32(10)	16(10)	5(9)
C(30)	212(11)	216(11)	268(14)	31(9)	24(11)	68(10)
C(31)	205(10)	248(11)	232(14)	19(11)	59(10)	69(8)
C(32)	277(13)	392(16)	444(18)	45(13)	72(13)	146(11)
C(33)	218(12)	404(16)	443(19)	141(13)	-35(12)	48(11)
C(34)	230(12)	343(14)	316(16)	130(12)	-26(11)	12(10)
C(35)	226(12)	291(12)	328(15)	26(10)	-1(12)	-9(11)
C(36)	152(10)	163(10)	209(12)	-1(9)	17(9)	-9(8)
C(37)	204(11)	188(11)	255(14)	-21(10)	16(10)	-58(8)
C(38)	217(11)	310(13)	233(14)	-43(11)	40(10)	-97(10)
C(39)	226(12)	406(15)	293(15)	-72(12)	97(11)	-118(11)
C(40)	247(12)	364(15)	365(17)	-147(12)	116(12)	-73(11)
C(41)	210(11)	243(12)	278(15)	-72(10)	73(10)	-68(9)
C(42)	168(9)	197(10)	332(14)	10(12)	33(12)	-31(7)
C(43)	182(11)	207(12)	402(18)	82(11)	-6(11)	-14(9)
C(44)	329(14)	367(16)	402(19)	88(13)	-102(13)	-66(12)
C(45)	368(17)	418(16)	510(20)	249(14)	-110(14)	-58(13)
C(46)	248(13)	389(15)	550(20)	218(14)	14(13)	-59(11)
C(47)	230(11)	245(12)	530(20)	112(13)	-20(12)	-41(9)
C(48)	152(10)	186(11)	419(17)	-14(11)	11(10)	-47(8)
C(49)	168(10)	269(12)	396(17)	5(12)	34(11)	-40(8)
C(50)	202(12)	450(17)	500(20)	-71(14)	27(12)	-110(11)
C(51)	238(14)	680(20)	480(20)	-136(17)	-48(13)	-99(13)
C(52)	275(14)	518(18)	480(20)	-117(15)	-18(14)	-123(13)
C(53)	188(11)	280(13)	345(16)	-53(11)	-1(11)	-43(9)
C(54)	153(10)	191(11)	334(16)	-28(10)	14(10)	-10(8)
C(55)	219(11)	223(12)	424(17)	-69(12)	72(11)	0(9)
C(56)	238(12)	310(14)	426(18)	-90(12)	85(12)	12(10)

C(57)	262(13)	297(14)	491(19)	-151(13)	8(13)	65(10)
C(58)	329(14)	211(11)	488(18)	-79(11)	6(14)	66(11)
C(59)	244(12)	190(12)	528(19)	-46(12)	75(12)	-9(9)
C(60A)	105(13)	150(14)	290(20)	12(18)	37(18)	-24(9)
C(61A)	124(13)	415(18)	410(20)	30(20)	25(16)	57(11)
P(3)	244(3)	404(4)	745(5)	20(5)	61(4)	-56(3)
F(1A)	350(40)	190(20)	2190(120)	20(40)	-410(50)	-84(18)
F(2A)	620(30)	790(40)	760(50)	80(30)	-350(30)	70(30)
F(3A)	520(40)	1330(100)	550(40)	-450(50)	130(30)	-220(50)
F(4A)	500(20)	450(20)	980(60)	20(30)	150(30)	-189(16)
F(5A)	440(30)	960(50)	1400(60)	-130(40)	360(30)	130(30)
F(6A)	1250(60)	620(40)	1210(70)	590(40)	-810(50)	-310(40)
F(1B)	560(30)	2550(110)	420(30)	-260(50)	110(30)	-570(40)
F(5B)	560(30)	830(40)	1360(80)	520(40)	150(40)	30(30)
F(4B)	280(20)	520(40)	2720(140)	-450(70)	160(60)	-20(20)
F(3B)	610(50)	3300(170)	800(60)	-1240(90)	150(40)	-800(70)
F(2B)	380(30)	700(40)	1200(110)	-210(50)	40(50)	140(20)
F(6B)	260(30)	1160(90)	1360(80)	1000(70)	160(40)	20(40)

---

**Structure of 16 (CCDC 676694)****Special Refinement Details**

Crystals were mounted on a glass fiber using Paratone oil then placed on the diffractometer under a nitrogen stream at 100K.

There are two molecules in the asymmetric unit, each of which is disordered, differently. Molecule A (figure 4.10a) is disordered in the tertiary butyl group composed of carbons 21-23. Molecule B (figure 4.10b) is disordered in two of the cyclohexyl groups composed of carbon atoms 24-35.

Refinement of  $F^2$  against ALL reflections. The weighted R-factor ( $wR$ ) and goodness of fit (S) are based on  $F^2$ , conventional R-factors (R) are based on F, with F set to zero for negative  $F^2$ . The threshold expression of  $F^2 > 2\sigma(F^2)$  is used only for calculating R-factors(gt) etc. and is not relevant to the choice of reflections for refinement. R-factors based on  $F^2$  are statistically about twice as large as those based on F, and R-factors based on ALL data will be even larger. All esds (except the esd in the dihedral angle between two l.s. planes) are estimated using the full covariance matrix. The cell esds are taken into account individually in the estimation of esds in distances, angles and torsion angles; correlations between esds in cell parameters are only used when they are defined by crystal symmetry. An approximate (isotropic) treatment of cell esds is used for estimating esds involving l.s. planes.

**Table A2.16. Atomic coordinates (x 10<sup>4</sup>) and equivalent isotropic displacement parameters (Å<sup>2</sup> x 10<sup>3</sup>) for 16 (CCDC 676694). U(eq) is defined as the trace of the orthogonalized U<sup>ij</sup> tensor.**

	x	y	z	U <sub>eq</sub>	Occ
Ir(1)	3561(1)	1999(1)	2207(1)	10(1)	1
Cl(1)	4027(1)	1386(1)	2083(1)	14(1)	1
P(1A)	2390(1)	1925(1)	1319(1)	13(1)	1
P(2A)	4702(1)	1978(1)	3107(1)	13(1)	1
O(1A)	2474(1)	1822(1)	2675(1)	13(1)	1
O(2A)	4686(1)	2134(1)	1739(1)	17(1)	1
N(1A)	2496(2)	2600(1)	2624(1)	13(1)	1
N(2A)	3645(2)	2763(1)	2071(1)	13(1)	1
C(1A)	1884(2)	2028(1)	2951(1)	11(1)	1
C(2A)	1209(2)	1862(1)	3280(1)	14(1)	1
C(3A)	571(2)	2042(1)	3600(1)	20(1)	1
C(4A)	568(2)	2405(1)	3614(1)	20(1)	1
C(5A)	1222(2)	2571(1)	3280(1)	18(1)	1
C(6A)	1870(2)	2398(1)	2951(1)	14(1)	1
C(7A)	2413(2)	2982(1)	2621(1)	17(1)	1
C(8A)	3188(2)	3094(1)	2227(1)	16(1)	1
C(9A)	4375(2)	2760(1)	1675(1)	13(1)	1
C(10A)	4625(2)	3075(1)	1414(1)	17(1)	1
C(11A)	5305(2)	3098(1)	1010(1)	19(1)	1
C(12A)	5771(2)	2790(1)	875(1)	22(1)	1
C(13A)	5546(2)	2478(1)	1132(1)	19(1)	1
C(14A)	4859(2)	2448(1)	1530(1)	14(1)	1
C(15A)	3206(2)	2484(1)	2308(1)	12(1)	1
C(16A)	-97(2)	2616(1)	3980(1)	30(1)	1
C(17A)	-808(4)	2838(1)	3579(2)	108(2)	1
C(18A)	551(3)	2842(1)	4409(2)	91(2)	1
C(19A)	-719(3)	2392(1)	4324(2)	79(2)	1
C(20A)	5523(2)	3444(1)	714(2)	31(1)	1
C(21A)	4517(5)	3518(2)	261(4)	66(3)	0.555(6)
C(22A)	6322(5)	3416(2)	292(3)	38(2)	0.555(6)
C(23A)	5694(9)	3725(2)	1107(4)	79(4)	0.555(6)
C(21C)	5472(9)	3420(2)	99(3)	56(4)	0.445(6)
C(22C)	6655(5)	3537(2)	964(4)	41(3)	0.445(6)
C(23C)	4916(6)	3753(2)	926(4)	33(2)	0.445(6)
C(24A)	1226(2)	1729(1)	1540(1)	14(1)	1
C(25A)	233(2)	1785(1)	1147(1)	17(1)	1
C(26A)	-629(2)	1653(1)	1469(1)	22(1)	1

C(27A)	-512(2)	1267(1)	1627(1)	22(1)	1
C(28A)	479(2)	1202(1)	1994(1)	20(1)	1
C(29A)	1356(2)	1338(1)	1692(1)	17(1)	1
C(30A)	1904(2)	2304(1)	864(1)	14(1)	1
C(31A)	1410(2)	2578(1)	1231(1)	17(1)	1
C(32A)	920(2)	2867(1)	839(1)	22(1)	1
C(33A)	1679(2)	3041(1)	495(1)	23(1)	1
C(34A)	2163(2)	2776(1)	123(1)	19(1)	1
C(35A)	2649(2)	2477(1)	502(1)	19(1)	1
C(36A)	2845(2)	1613(1)	787(1)	15(1)	1
C(37A)	2144(2)	1561(1)	209(1)	20(1)	1
C(38A)	2513(2)	1263(1)	-158(1)	28(1)	1
C(39A)	3578(2)	1319(1)	-285(1)	29(1)	1
C(40A)	4261(2)	1373(1)	290(1)	24(1)	1
C(41A)	3912(2)	1676(1)	650(1)	18(1)	1
C(42A)	4080(2)	1764(1)	3702(1)	15(1)	1
C(43A)	3820(2)	1377(1)	3580(1)	21(1)	1
C(44A)	3136(2)	1241(1)	4013(1)	22(1)	1
C(45A)	3579(2)	1286(1)	4650(1)	24(1)	1
C(46A)	3872(2)	1665(1)	4774(1)	27(1)	1
C(47A)	4563(2)	1796(1)	4341(1)	23(1)	1
C(48A)	5875(2)	1728(1)	3057(1)	14(1)	1
C(49A)	6319(2)	1774(1)	2473(1)	18(1)	1
C(50A)	7238(2)	1542(1)	2452(1)	22(1)	1
C(51A)	8026(2)	1608(1)	2968(1)	24(1)	1
C(52A)	7583(2)	1551(1)	3547(1)	24(1)	1
C(53A)	6686(2)	1785(1)	3583(1)	19(1)	1
C(54A)	5147(2)	2391(1)	3474(1)	16(1)	1
C(55A)	4332(2)	2609(1)	3715(1)	22(1)	1
C(56A)	4795(2)	2908(1)	4095(1)	26(1)	1
C(57A)	5416(2)	3140(1)	3740(1)	30(1)	1
C(58A)	6215(2)	2931(1)	3477(1)	28(1)	1
C(59A)	5768(2)	2622(1)	3106(1)	20(1)	1
Ir(2)	2114(1)	4465(1)	2621(1)	15(1)	1
Cl(2)	2327(1)	3830(1)	2633(1)	22(1)	1
P(1B)	3494(1)	4459(1)	3392(1)	18(1)	1
P(2B)	726(1)	4379(1)	1860(1)	19(1)	1
O(1B)	3031(1)	4462(1)	1977(1)	19(1)	1
O(2B)	1215(1)	4443(1)	3277(1)	20(1)	1
N(1B)	2568(2)	5188(1)	2314(1)	16(1)	1
N(2B)	1389(2)	5166(1)	2897(1)	17(1)	1
C(1B)	3504(2)	4743(1)	1804(1)	17(1)	1
C(2B)	4244(2)	4693(1)	1437(1)	27(1)	1
C(3B)	4837(2)	4958(1)	1263(1)	29(1)	1
C(4B)	4680(2)	5302(1)	1434(1)	23(1)	1
C(5B)	3925(2)	5357(1)	1781(1)	19(1)	1

C(6B)	3327(2)	5093(1)	1971(1)	16(1)	1
C(7B)	2343(2)	5556(1)	2411(1)	19(1)	1
C(8B)	1521(2)	5542(1)	2804(1)	19(1)	1
C(9B)	658(2)	5047(1)	3245(1)	15(1)	1
C(10B)	-24(2)	5288(1)	3428(1)	19(1)	1
C(11B)	-755(2)	5199(1)	3774(1)	21(1)	1
C(12B)	-797(2)	4849(1)	3949(1)	25(1)	1
C(13B)	-136(2)	4607(1)	3770(1)	22(1)	1
C(14B)	603(2)	4691(1)	3414(1)	18(1)	1
C(15B)	2013(2)	4971(1)	2612(1)	15(1)	1
C(16B)	5376(2)	5605(1)	1308(1)	25(1)	1
C(17B)	4770(2)	5941(1)	1163(1)	30(1)	1
C(18B)	6089(2)	5662(1)	1869(1)	31(1)	1
C(19B)	5941(2)	5524(1)	778(1)	33(1)	1
C(20B)	-1454(2)	5471(1)	3994(1)	29(1)	1
C(21B)	-1434(3)	5815(1)	3662(2)	43(1)	1
C(22B)	-1080(3)	5547(1)	4653(1)	46(1)	1
C(23B)	-2507(2)	5343(1)	3958(2)	53(1)	1
C(24B)	4697(6)	4400(2)	3087(3)	22(2)	0.731(5)
C(25B)	5681(3)	4475(1)	3539(2)	38(1)	0.731(5)
C(26B)	6591(4)	4469(2)	3218(3)	50(2)	0.731(5)
C(27B)	6700(4)	4123(1)	2914(3)	47(2)	0.731(5)
C(28B)	5758(5)	4031(2)	2508(3)	33(2)	0.731(5)
C(29B)	4835(14)	4049(4)	2783(8)	29(3)	0.731(5)
C(24C)	4797(16)	4408(5)	3200(9)	2(3)	0.269(5)
C(25C)	5226(8)	4704(2)	2825(5)	22(3)	0.269(5)
C(26C)	6334(9)	4629(3)	2837(7)	34(3)	0.269(5)
C(27C)	6508(8)	4291(3)	2501(6)	24(3)	0.269(5)
C(28C)	6017(13)	3991(5)	2797(9)	38(5)	0.269(5)
C(29C)	4840(30)	4071(11)	2840(20)	20(7)	0.269(5)
C(30B)	3722(6)	4849(2)	3842(3)	22(2)	0.754(5)
C(31B)	4094(3)	5163(1)	3589(2)	24(1)	0.754(5)
C(32B)	4453(4)	5436(1)	4064(2)	23(1)	0.754(5)
C(33B)	3630(4)	5533(1)	4422(2)	25(1)	0.754(5)
C(34B)	3191(4)	5214(1)	4700(2)	26(1)	0.754(5)
C(35B)	2834(11)	4934(3)	4233(7)	20(2)	0.754(5)
C(30C)	3611(18)	4854(6)	3965(10)	17(5)	0.246(5)
C(31C)	4645(9)	4972(2)	4139(5)	21(3)	0.246(5)
C(32C)	4636(12)	5359(3)	4323(7)	25(4)	0.246(5)
C(33C)	3772(12)	5425(4)	4690(7)	28(4)	0.246(5)
C(34C)	2793(11)	5328(3)	4385(7)	35(4)	0.246(5)
C(35C)	2900(40)	4966(10)	4190(20)	31(11)	0.246(5)
C(36B)	3445(2)	4092(1)	3929(1)	22(1)	1
C(37B)	4144(2)	4133(1)	4504(1)	28(1)	1
C(38B)	4240(2)	3795(1)	4854(1)	31(1)	1
C(39B)	3230(3)	3663(1)	4988(1)	36(1)	1

C(40B)	2494(2)	3641(1)	4434(1)	33(1)	1
C(41B)	2423(2)	3984(1)	4083(1)	27(1)	1
C(42B)	1148(2)	4350(1)	1120(1)	21(1)	1
C(43B)	1773(2)	4017(1)	1053(1)	23(1)	1
C(44B)	2236(2)	4024(1)	476(1)	29(1)	1
C(45B)	1476(2)	4067(1)	-58(1)	26(1)	1
C(46B)	842(2)	4392(1)	8(1)	27(1)	1
C(47B)	366(2)	4392(1)	580(1)	27(1)	1
C(48B)	73(2)	3967(1)	1985(1)	23(1)	1
C(49B)	-384(2)	3980(1)	2573(1)	28(1)	1
C(50B)	-774(3)	3625(1)	2737(2)	42(1)	1
C(51B)	-1490(3)	3473(1)	2247(2)	46(1)	1
C(52B)	-1009(3)	3451(1)	1683(2)	50(1)	1
C(53B)	-646(2)	3807(1)	1491(1)	34(1)	1
C(54B)	-198(2)	4736(1)	1839(1)	21(1)	1
C(55B)	172(2)	5075(1)	1562(1)	21(1)	1
C(56B)	-499(2)	5382(1)	1676(1)	30(1)	1
C(57B)	-1558(2)	5312(1)	1447(2)	35(1)	1
C(58B)	-1930(2)	4979(1)	1717(1)	31(1)	1
C(59B)	-1267(2)	4667(1)	1593(1)	31(1)	1
C(61)	8052(3)	2497(1)	1599(2)	45(1)	1
Cl(3)	8328(1)	2508(1)	869(1)	54(1)	1
Cl(4)	9122(1)	2512(1)	2116(1)	53(1)	1
C(62)	2133(2)	190(1)	4796(2)	41(1)	1
Cl(5)	3284(1)	307(1)	4585(1)	43(1)	1
Cl(6)	1713(1)	490(1)	5294(1)	50(1)	1

---

**Table A2.17. Bond lengths [ $\text{\AA}$ ] and angles [ $^\circ$ ] for 16 (CCDC 676694).**

Ir(1)-C(15A)	1.944(2)	C(24A)-C(25A)	1.540(3)
Ir(1)-O(2A)	2.0257(17)	C(24A)-C(29A)	1.545(3)
Ir(1)-O(1A)	2.0343(16)	C(25A)-C(26A)	1.536(3)
Ir(1)-P(2A)	2.4194(7)	C(26A)-C(27A)	1.527(3)
Ir(1)-P(1A)	2.4365(7)	C(27A)-C(28A)	1.516(4)
Ir(1)-Cl(1)	2.4584(5)	C(28A)-C(29A)	1.530(3)
P(1A)-C(36A)	1.859(2)	C(30A)-C(35A)	1.528(3)
P(1A)-C(30A)	1.860(2)	C(30A)-C(31A)	1.546(3)
P(1A)-C(24A)	1.867(2)	C(31A)-C(32A)	1.525(3)
P(2A)-C(54A)	1.858(2)	C(32A)-C(33A)	1.517(4)
P(2A)-C(42A)	1.868(3)	C(33A)-C(34A)	1.520(3)
P(2A)-C(48A)	1.871(2)	C(34A)-C(35A)	1.537(3)
O(1A)-C(1A)	1.332(3)	C(36A)-C(41A)	1.531(3)
O(2A)-C(14A)	1.328(2)	C(36A)-C(37A)	1.544(4)
N(1A)-C(15A)	1.342(3)	C(37A)-C(38A)	1.533(3)
N(1A)-C(6A)	1.422(3)	C(38A)-C(39A)	1.519(4)
N(1A)-C(7A)	1.468(3)	C(39A)-C(40A)	1.526(4)
N(2A)-C(15A)	1.366(3)	C(40A)-C(41A)	1.529(3)
N(2A)-C(9A)	1.415(3)	C(42A)-C(47A)	1.532(4)
N(2A)-C(8A)	1.475(3)	C(42A)-C(43A)	1.544(3)
C(1A)-C(2A)	1.403(3)	C(43A)-C(44A)	1.523(3)
C(1A)-C(6A)	1.420(3)	C(44A)-C(45A)	1.513(4)
C(2A)-C(3A)	1.378(3)	C(45A)-C(46A)	1.524(3)
C(3A)-C(4A)	1.392(3)	C(46A)-C(47A)	1.522(4)
C(4A)-C(5A)	1.389(3)	C(48A)-C(49A)	1.534(4)
C(4A)-C(16A)	1.529(4)	C(48A)-C(53A)	1.542(4)
C(5A)-C(6A)	1.389(3)	C(49A)-C(50A)	1.535(3)
C(7A)-C(8A)	1.520(3)	C(50A)-C(51A)	1.513(4)
C(9A)-C(10A)	1.406(3)	C(51A)-C(52A)	1.527(4)
C(9A)-C(14A)	1.420(3)	C(52A)-C(53A)	1.522(3)
C(10A)-C(11A)	1.380(3)	C(54A)-C(55A)	1.536(3)
C(11A)-C(12A)	1.392(3)	C(54A)-C(59A)	1.538(3)
C(11A)-C(20A)	1.534(3)	C(55A)-C(56A)	1.527(3)
C(12A)-C(13A)	1.382(3)	C(56A)-C(57A)	1.520(4)
C(13A)-C(14A)	1.380(3)	C(57A)-C(58A)	1.525(4)
C(16A)-C(19A)	1.489(4)	C(58A)-C(59A)	1.539(3)
C(16A)-C(18A)	1.508(5)	Ir(2)-C(15B)	1.944(2)
C(16A)-C(17A)	1.508(5)	Ir(2)-O(1B)	2.0307(17)
C(20A)-C(21C)	1.399(8)	Ir(2)-O(2B)	2.0380(18)
C(20A)-C(23A)	1.402(7)	Ir(2)-P(1B)	2.4102(8)
C(20A)-C(22A)	1.534(7)	Ir(2)-P(2B)	2.4260(8)
C(20A)-C(23C)	1.550(8)	Ir(2)-Cl(2)	2.4529(5)
C(20A)-C(22C)	1.610(8)	P(1B)-C(30B)	1.822(7)
C(20A)-C(21A)	1.635(8)	P(1B)-C(24C)	1.88(2)

P(1B)-C(36B)	1.870(3)	C(28C)-C(29C)	1.63(5)
P(1B)-C(24B)	1.857(9)	C(30B)-C(31B)	1.450(7)
P(1B)-C(30C)	1.99(2)	C(30B)-C(35B)	1.612(15)
P(2B)-C(42B)	1.846(3)	C(31B)-C(32B)	1.542(6)
P(2B)-C(54B)	1.850(3)	C(32B)-C(33B)	1.503(7)
P(2B)-C(48B)	1.852(2)	C(33B)-C(34B)	1.528(6)
O(1B)-C(1B)	1.337(3)	C(34B)-C(35B)	1.549(13)
O(2B)-C(14B)	1.324(3)	C(30C)-C(35C)	1.22(5)
N(1B)-C(15B)	1.354(3)	C(30C)-C(31C)	1.48(3)
N(1B)-C(6B)	1.411(3)	C(31C)-C(32C)	1.543(17)
N(1B)-C(7B)	1.468(3)	C(32C)-C(33C)	1.54(2)
N(2B)-C(15B)	1.352(3)	C(33C)-C(34C)	1.47(2)
N(2B)-C(9B)	1.415(3)	C(34C)-C(35C)	1.47(4)
N(2B)-C(8B)	1.470(3)	C(36B)-C(41B)	1.523(4)
C(1B)-C(2B)	1.390(4)	C(36B)-C(37B)	1.531(4)
C(1B)-C(6B)	1.425(3)	C(37B)-C(38B)	1.518(3)
C(2B)-C(3B)	1.380(3)	C(38B)-C(39B)	1.523(4)
C(3B)-C(4B)	1.400(3)	C(39B)-C(40B)	1.517(4)
C(4B)-C(5B)	1.381(4)	C(40B)-C(41B)	1.538(3)
C(4B)-C(16B)	1.545(3)	C(42B)-C(47B)	1.535(4)
C(5B)-C(6B)	1.395(3)	C(42B)-C(43B)	1.551(3)
C(7B)-C(8B)	1.509(3)	C(43B)-C(44B)	1.522(4)
C(9B)-C(10B)	1.406(3)	C(44B)-C(45B)	1.507(4)
C(9B)-C(14B)	1.420(3)	C(45B)-C(46B)	1.530(3)
C(10B)-C(11B)	1.380(4)	C(46B)-C(47B)	1.519(4)
C(11B)-C(12B)	1.401(3)	C(48B)-C(53B)	1.528(4)
C(11B)-C(20B)	1.534(4)	C(48B)-C(49B)	1.541(4)
C(12B)-C(13B)	1.385(3)	C(49B)-C(50B)	1.522(3)
C(13B)-C(14B)	1.399(4)	C(50B)-C(51B)	1.510(5)
C(16B)-C(18B)	1.524(4)	C(51B)-C(52B)	1.510(4)
C(16B)-C(19B)	1.537(4)	C(52B)-C(53B)	1.535(4)
C(16B)-C(17B)	1.542(3)	C(54B)-C(59B)	1.514(4)
C(20B)-C(23B)	1.502(4)	C(54B)-C(55B)	1.554(3)
C(20B)-C(21B)	1.523(4)	C(55B)-C(56B)	1.527(3)
C(20B)-C(22B)	1.555(4)	C(56B)-C(57B)	1.490(4)
C(24B)-C(25B)	1.609(9)	C(57B)-C(58B)	1.531(4)
C(24B)-C(29B)	1.539(18)	C(58B)-C(59B)	1.541(4)
C(25B)-C(26B)	1.503(6)	C(61)-Cl(3)	1.748(4)
C(26B)-C(27B)	1.515(6)	C(61)-Cl(4)	1.759(4)
C(27B)-C(28B)	1.524(8)	C(62)-Cl(5)	1.743(3)
C(28B)-C(29B)	1.464(18)	C(62)-Cl(6)	1.758(3)
C(24C)-C(29C)	1.53(5)		
C(24C)-C(25C)	1.57(2)	C(15A)-Ir(1)-O(2A)	91.66(8)
C(25C)-C(26C)	1.525(15)	C(15A)-Ir(1)-O(1A)	93.06(8)
C(26C)-C(27C)	1.538(14)	O(2A)-Ir(1)-O(1A)	175.24(6)
C(27C)-C(28C)	1.52(2)	C(15A)-Ir(1)-P(2A)	94.16(7)

O(2A)-Ir(1)-P(2A)	90.58(5)	C(10A)-C(9A)-C(14A)	119.0(2)
O(1A)-Ir(1)-P(2A)	88.45(5)	N(2A)-C(9A)-C(14A)	122.1(2)
C(15A)-Ir(1)-P(1A)	93.67(7)	C(11A)-C(10A)-C(9A)	123.4(2)
O(2A)-Ir(1)-P(1A)	92.81(5)	C(10A)-C(11A)-C(12A)	116.6(2)
O(1A)-Ir(1)-P(1A)	87.51(5)	C(10A)-C(11A)-C(20A)	121.8(2)
P(2A)-Ir(1)-P(1A)	171.367(19)	C(12A)-C(11A)-C(20A)	121.5(2)
C(15A)-Ir(1)-Cl(1)	179.44(8)	C(13A)-C(12A)-C(11A)	120.9(3)
O(2A)-Ir(1)-Cl(1)	87.99(4)	C(14A)-C(13A)-C(12A)	123.3(2)
O(1A)-Ir(1)-Cl(1)	87.29(4)	O(2A)-C(14A)-C(13A)	118.2(2)
P(2A)-Ir(1)-Cl(1)	85.40(2)	O(2A)-C(14A)-C(9A)	125.2(2)
P(1A)-Ir(1)-Cl(1)	86.79(2)	C(13A)-C(14A)-C(9A)	116.7(2)
C(36A)-P(1A)-C(30A)	105.13(11)	N(1A)-C(15A)-N(2A)	108.96(18)
C(36A)-P(1A)-C(24A)	105.83(11)	N(1A)-C(15A)-Ir(1)	125.68(16)
C(30A)-P(1A)-C(24A)	102.17(11)	N(2A)-C(15A)-Ir(1)	125.36(18)
C(36A)-P(1A)-Ir(1)	112.52(9)	C(19A)-C(16A)-C(18A)	108.2(3)
C(30A)-P(1A)-Ir(1)	121.69(8)	C(19A)-C(16A)-C(17A)	106.5(3)
C(24A)-P(1A)-Ir(1)	108.05(8)	C(18A)-C(16A)-C(17A)	110.5(3)
C(54A)-P(2A)-C(42A)	101.42(11)	C(19A)-C(16A)-C(4A)	112.7(2)
C(54A)-P(2A)-C(48A)	103.39(11)	C(18A)-C(16A)-C(4A)	108.8(3)
C(42A)-P(2A)-C(48A)	106.00(11)	C(17A)-C(16A)-C(4A)	110.1(3)
C(54A)-P(2A)-Ir(1)	119.69(8)	C(21C)-C(20A)-C(11A)	113.1(3)
C(42A)-P(2A)-Ir(1)	109.43(9)	C(23A)-C(20A)-C(11A)	114.2(4)
C(48A)-P(2A)-Ir(1)	115.31(9)	C(23A)-C(20A)-C(22A)	112.3(5)
C(1A)-O(1A)-Ir(1)	123.99(13)	C(11A)-C(20A)-C(22A)	113.6(3)
C(14A)-O(2A)-Ir(1)	126.57(15)	C(21C)-C(20A)-C(23C)	113.5(6)
C(15A)-N(1A)-C(6A)	127.51(18)	C(11A)-C(20A)-C(23C)	112.9(3)
C(15A)-N(1A)-C(7A)	112.72(19)	C(21C)-C(20A)-C(22C)	107.6(6)
C(6A)-N(1A)-C(7A)	119.76(19)	C(23C)-C(20A)-C(22C)	103.8(5)
C(15A)-N(2A)-C(9A)	127.87(18)	C(23A)-C(20A)-C(21A)	109.5(6)
C(15A)-N(2A)-C(8A)	111.4(2)	C(11A)-C(20A)-C(21A)	103.7(3)
C(9A)-N(2A)-C(8A)	120.42(18)	C(22A)-C(20A)-C(21A)	102.3(4)
O(1A)-C(1A)-C(2A)	116.5(2)	C(25A)-C(24A)-C(29A)	109.57(19)
O(1A)-C(1A)-C(6A)	127.1(2)	C(25A)-C(24A)-P(1A)	119.50(17)
C(2A)-C(1A)-C(6A)	116.4(2)	C(29A)-C(24A)-P(1A)	111.92(17)
C(3A)-C(2A)-C(1A)	122.9(2)	C(26A)-C(25A)-C(24A)	109.6(2)
C(2A)-C(3A)-C(4A)	121.2(2)	C(27A)-C(26A)-C(25A)	111.7(2)
C(5A)-C(4A)-C(3A)	116.2(2)	C(28A)-C(27A)-C(26A)	110.5(2)
C(5A)-C(4A)-C(16A)	120.6(2)	C(27A)-C(28A)-C(29A)	112.3(2)
C(3A)-C(4A)-C(16A)	123.2(2)	C(28A)-C(29A)-C(24A)	110.9(2)
C(6A)-C(5A)-C(4A)	124.2(2)	C(35A)-C(30A)-C(31A)	110.47(19)
C(5A)-C(6A)-C(1A)	119.1(2)	C(35A)-C(30A)-P(1A)	115.41(17)
C(5A)-C(6A)-N(1A)	118.5(2)	C(31A)-C(30A)-P(1A)	112.20(17)
C(1A)-C(6A)-N(1A)	122.4(2)	C(32A)-C(31A)-C(30A)	111.3(2)
N(1A)-C(7A)-C(8A)	103.27(18)	C(33A)-C(32A)-C(31A)	110.3(2)
N(2A)-C(8A)-C(7A)	103.58(17)	C(32A)-C(33A)-C(34A)	111.0(2)
C(10A)-C(9A)-N(2A)	118.8(2)	C(33A)-C(34A)-C(35A)	111.6(2)

C(30A)-C(35A)-C(34A)	111.3(2)	P(1B)-Ir(2)-Cl(2)	84.32(2)
C(41A)-C(36A)-C(37A)	110.3(2)	P(2B)-Ir(2)-Cl(2)	87.30(2)
C(41A)-C(36A)-P(1A)	115.14(16)	C(30B)-P(1B)-C(24C)	96.6(6)
C(37A)-C(36A)-P(1A)	114.96(17)	C(30B)-P(1B)-C(36B)	105.5(2)
C(38A)-C(37A)-C(36A)	110.7(2)	C(24C)-P(1B)-C(36B)	100.4(6)
C(39A)-C(38A)-C(37A)	112.0(2)	C(30B)-P(1B)-C(24B)	102.2(3)
C(38A)-C(39A)-C(40A)	110.4(2)	C(24C)-P(1B)-C(24B)	8.5(8)
C(39A)-C(40A)-C(41A)	111.7(2)	C(36B)-P(1B)-C(24B)	104.7(3)
C(40A)-C(41A)-C(36A)	110.4(2)	C(30B)-P(1B)-C(30C)	8.6(8)
C(47A)-C(42A)-C(43A)	108.20(19)	C(24C)-P(1B)-C(30C)	103.1(9)
C(47A)-C(42A)-P(2A)	118.48(18)	C(36B)-P(1B)-C(30C)	98.6(7)
C(43A)-C(42A)-P(2A)	113.92(17)	C(24B)-P(1B)-C(30C)	109.3(7)
C(44A)-C(43A)-C(42A)	110.8(2)	C(30B)-P(1B)-Ir(2)	117.9(3)
C(45A)-C(44A)-C(43A)	112.4(2)	C(24C)-P(1B)-Ir(2)	120.0(6)
C(44A)-C(45A)-C(46A)	110.7(2)	C(36B)-P(1B)-Ir(2)	113.67(9)
C(47A)-C(46A)-C(45A)	111.2(2)	C(24B)-P(1B)-Ir(2)	111.5(2)
C(46A)-C(47A)-C(42A)	111.3(2)	C(30C)-P(1B)-Ir(2)	117.7(7)
C(49A)-C(48A)-C(53A)	110.0(2)	C(42B)-P(2B)-C(54B)	107.61(12)
C(49A)-C(48A)-P(2A)	114.49(17)	C(42B)-P(2B)-C(48B)	107.10(12)
C(53A)-C(48A)-P(2A)	114.29(17)	C(54B)-P(2B)-C(48B)	107.63(12)
C(48A)-C(49A)-C(50A)	111.2(2)	C(42B)-P(2B)-Ir(2)	111.36(9)
C(51A)-C(50A)-C(49A)	112.3(2)	C(54B)-P(2B)-Ir(2)	112.45(9)
C(50A)-C(51A)-C(52A)	109.6(2)	C(48B)-P(2B)-Ir(2)	110.46(10)
C(53A)-C(52A)-C(51A)	111.1(2)	C(1B)-O(1B)-Ir(2)	124.17(15)
C(52A)-C(53A)-C(48A)	111.9(2)	C(14B)-O(2B)-Ir(2)	125.93(15)
C(55A)-C(54A)-C(59A)	110.01(19)	C(15B)-N(1B)-C(6B)	127.01(19)
C(55A)-C(54A)-P(2A)	114.61(18)	C(15B)-N(1B)-C(7B)	112.3(2)
C(59A)-C(54A)-P(2A)	114.50(17)	C(6B)-N(1B)-C(7B)	120.63(19)
C(56A)-C(55A)-C(54A)	110.3(2)	C(15B)-N(2B)-C(9B)	127.39(19)
C(57A)-C(56A)-C(55A)	110.7(2)	C(15B)-N(2B)-C(8B)	112.4(2)
C(56A)-C(57A)-C(58A)	111.3(2)	C(9B)-N(2B)-C(8B)	120.22(19)
C(57A)-C(58A)-C(59A)	111.7(2)	O(1B)-C(1B)-C(2B)	118.1(2)
C(54A)-C(59A)-C(58A)	110.4(2)	O(1B)-C(1B)-C(6B)	125.4(2)
C(15B)-Ir(2)-O(1B)	92.75(9)	C(2B)-C(1B)-C(6B)	116.5(2)
C(15B)-Ir(2)-O(2B)	90.14(9)	C(3B)-C(2B)-C(1B)	123.8(2)
O(1B)-Ir(2)-O(2B)	177.00(6)	C(2B)-C(3B)-C(4B)	120.1(3)
C(15B)-Ir(2)-P(1B)	93.81(8)	C(5B)-C(4B)-C(3B)	116.7(2)
O(1B)-Ir(2)-P(1B)	92.32(5)	C(5B)-C(4B)-C(16B)	120.0(2)
O(2B)-Ir(2)-P(1B)	86.70(5)	C(3B)-C(4B)-C(16B)	122.9(2)
C(15B)-Ir(2)-P(2B)	94.60(8)	C(4B)-C(5B)-C(6B)	124.2(2)
O(1B)-Ir(2)-P(2B)	88.27(5)	C(5B)-C(6B)-N(1B)	118.1(2)
O(2B)-Ir(2)-P(2B)	92.29(6)	C(5B)-C(6B)-C(1B)	118.6(2)
P(1B)-Ir(2)-P(2B)	171.53(2)	N(1B)-C(6B)-C(1B)	123.3(2)
C(15B)-Ir(2)-Cl(2)	177.33(8)	N(1B)-C(7B)-C(8B)	103.60(18)
O(1B)-Ir(2)-Cl(2)	85.42(4)	N(2B)-C(8B)-C(7B)	103.36(18)
O(2B)-Ir(2)-Cl(2)	91.66(4)	C(10B)-C(9B)-N(2B)	118.6(2)

C(10B)-C(9B)-C(14B)	119.7(2)	C(33B)-C(32B)-C(31B)	110.9(4)
N(2B)-C(9B)-C(14B)	121.7(2)	C(32B)-C(33B)-C(34B)	112.1(3)
C(11B)-C(10B)-C(9B)	123.1(2)	C(33B)-C(34B)-C(35B)	112.0(7)
C(10B)-C(11B)-C(12B)	117.1(2)	C(34B)-C(35B)-C(30B)	109.1(9)
C(10B)-C(11B)-C(20B)	121.9(2)	C(35C)-C(30C)-C(31C)	123(3)
C(12B)-C(11B)-C(20B)	120.9(2)	C(35C)-C(30C)-P(1B)	122(3)
C(13B)-C(12B)-C(11B)	120.7(3)	C(31C)-C(30C)-P(1B)	114.1(12)
C(12B)-C(13B)-C(14B)	123.0(2)	C(30C)-C(31C)-C(32C)	109.2(12)
O(2B)-C(14B)-C(13B)	118.6(2)	C(33C)-C(32C)-C(31C)	109.7(11)
O(2B)-C(14B)-C(9B)	124.9(2)	C(34C)-C(33C)-C(32C)	113.7(13)
C(13B)-C(14B)-C(9B)	116.4(2)	C(35C)-C(34C)-C(33C)	106(2)
N(2B)-C(15B)-N(1B)	108.36(19)	C(30C)-C(35C)-C(34C)	125(4)
N(2B)-C(15B)-Ir(2)	126.51(18)	C(41B)-C(36B)-C(37B)	108.5(2)
N(1B)-C(15B)-Ir(2)	125.13(18)	C(41B)-C(36B)-P(1B)	117.18(19)
C(18B)-C(16B)-C(19B)	111.3(3)	C(37B)-C(36B)-P(1B)	114.67(18)
C(18B)-C(16B)-C(17B)	109.1(2)	C(38B)-C(37B)-C(36B)	111.7(2)
C(19B)-C(16B)-C(17B)	107.7(2)	C(37B)-C(38B)-C(39B)	111.5(2)
C(18B)-C(16B)-C(4B)	107.0(2)	C(40B)-C(39B)-C(38B)	111.5(2)
C(19B)-C(16B)-C(4B)	111.3(2)	C(39B)-C(40B)-C(41B)	112.5(2)
C(17B)-C(16B)-C(4B)	110.4(2)	C(36B)-C(41B)-C(40B)	110.4(2)
C(23B)-C(20B)-C(21B)	109.2(3)	C(47B)-C(42B)-C(43B)	109.8(2)
C(23B)-C(20B)-C(11B)	112.1(2)	C(47B)-C(42B)-P(2B)	117.9(2)
C(21B)-C(20B)-C(11B)	112.3(2)	C(43B)-C(42B)-P(2B)	111.72(18)
C(23B)-C(20B)-C(22B)	108.3(3)	C(44B)-C(43B)-C(42B)	110.7(2)
C(21B)-C(20B)-C(22B)	107.3(2)	C(45B)-C(44B)-C(43B)	112.8(2)
C(11B)-C(20B)-C(22B)	107.4(2)	C(44B)-C(45B)-C(46B)	110.3(2)
C(25B)-C(24B)-C(29B)	107.9(9)	C(47B)-C(46B)-C(45B)	112.5(2)
C(25B)-C(24B)-P(1B)	115.9(4)	C(46B)-C(47B)-C(42B)	111.5(2)
C(29B)-C(24B)-P(1B)	115.6(8)	C(53B)-C(48B)-C(49B)	111.7(2)
C(26B)-C(25B)-C(24B)	110.5(4)	C(53B)-C(48B)-P(2B)	120.1(2)
C(25B)-C(26B)-C(27B)	111.4(4)	C(49B)-C(48B)-P(2B)	110.69(17)
C(26B)-C(27B)-C(28B)	111.1(4)	C(50B)-C(49B)-C(48B)	111.7(2)
C(29B)-C(28B)-C(27B)	115.1(9)	C(51B)-C(50B)-C(49B)	112.0(3)
C(28B)-C(29B)-C(24B)	112.8(12)	C(50B)-C(51B)-C(52B)	110.4(3)
C(29C)-C(24C)-C(25C)	106(2)	C(51B)-C(52B)-C(53B)	112.1(2)
C(29C)-C(24C)-P(1B)	108(2)	C(48B)-C(53B)-C(52B)	110.1(3)
C(25C)-C(24C)-P(1B)	117.9(12)	C(59B)-C(54B)-C(55B)	109.6(2)
C(26C)-C(25C)-C(24C)	106.1(11)	C(59B)-C(54B)-P(2B)	119.57(17)
C(25C)-C(26C)-C(27C)	111.0(9)	C(55B)-C(54B)-P(2B)	112.36(18)
C(28C)-C(27C)-C(26C)	108.4(11)	C(56B)-C(55B)-C(54B)	110.5(2)
C(27C)-C(28C)-C(29C)	111(2)	C(57B)-C(56B)-C(55B)	111.7(2)
C(24C)-C(29C)-C(28C)	107(3)	C(56B)-C(57B)-C(58B)	111.0(2)
C(31B)-C(30B)-C(35B)	111.6(6)	C(57B)-C(58B)-C(59B)	110.4(2)
C(31B)-C(30B)-P(1B)	120.2(4)	C(54B)-C(59B)-C(58B)	110.4(2)
C(35B)-C(30B)-P(1B)	112.9(6)	Cl(3)-C(61)-Cl(4)	112.71(19)
C(30B)-C(31B)-C(32B)	112.3(4)	Cl(5)-C(62)-Cl(6)	112.10(17)

**Table A2.18. Anisotropic displacement parameters ( $\text{\AA}^2 \times 10^4$ ) for 16 (CCDC 676694).**

The anisotropic displacement factor exponent takes the form:  $-2\pi^2 [ h^2 a^*{}^2 U_{11} + \dots + 2 h k a^* b^* U_{12} ]$

	U <sub>11</sub>	U <sub>22</sub>	U <sub>33</sub>	U <sub>23</sub>	U <sub>13</sub>	U <sub>12</sub>
Ir(1)	116(1)	77(1)	115(1)	6(1)	7(1)	6(1)
Cl(1)	171(3)	93(2)	162(4)	-3(2)	0(3)	13(2)
P(1A)	145(4)	117(3)	119(4)	13(2)	9(3)	1(2)
P(2A)	144(4)	87(3)	144(4)	-8(3)	-8(3)	6(3)
O(1A)	138(10)	85(7)	162(10)	30(7)	13(8)	-5(6)
O(2A)	190(11)	115(7)	191(11)	41(7)	29(9)	-2(7)
N(1A)	155(12)	69(8)	155(13)	12(8)	36(10)	29(8)
N(2A)	173(13)	55(8)	171(13)	-2(8)	45(10)	23(8)
C(1A)	77(12)	175(11)	90(14)	-11(10)	3(10)	-13(10)
C(2A)	164(15)	131(11)	133(15)	28(10)	4(12)	1(10)
C(3A)	163(15)	286(14)	164(16)	13(11)	19(12)	-27(11)
C(4A)	198(16)	237(13)	172(17)	11(11)	51(13)	52(11)
C(5A)	210(16)	158(12)	189(17)	-8(11)	53(13)	36(11)
C(6A)	129(14)	149(11)	145(15)	-2(10)	14(12)	5(10)
C(7A)	248(16)	101(10)	159(15)	0(10)	39(12)	47(10)
C(8A)	217(15)	86(10)	177(16)	-11(10)	25(12)	40(10)
C(9A)	121(14)	133(11)	117(15)	20(10)	-17(11)	-6(10)
C(10A)	172(15)	126(11)	217(17)	10(10)	-4(13)	1(10)
C(11A)	172(15)	168(12)	220(17)	69(11)	5(13)	-16(10)
C(12A)	205(16)	242(13)	245(18)	63(12)	110(14)	-1(11)
C(13A)	189(16)	150(11)	228(17)	29(11)	57(13)	32(10)
C(14A)	154(14)	131(11)	123(15)	17(10)	-11(12)	-14(10)
C(15A)	113(13)	123(10)	108(15)	6(9)	-23(11)	14(9)
C(16A)	350(20)	246(14)	340(20)	-11(13)	224(16)	45(13)
C(17A)1190(50)	1320(40)	810(40)	240(30)	470(30)	1080(40)	
C(18A)	680(30)	1100(30)	1050(40)	-820(30)	550(30)	-310(30)
C(19A)	860(40)	540(20)	1120(40)	-280(20)	780(30)	-70(20)
C(20A)	360(20)	210(14)	390(20)	134(13)	182(17)	7(13)
C(21A)	390(50)	670(50)	970(70)	700(50)	270(40)	190(30)
C(22A)	280(40)	390(30)	470(50)	240(30)	90(40)	-50(30)
C(23A)1490(110)	240(30)	790(70)	-50(40)	740(80)	-320(50)	
C(21C)1230(120)	260(40)	200(50)	60(30)	90(60)	-170(50)	
C(22C)	250(40)	240(30)	770(70)	100(40)	180(40)	-90(30)
C(23C)	260(40)	140(30)	610(60)	180(30)	130(50)	20(30)
C(24A)	127(14)	165(11)	119(15)	8(10)	16(11)	-18(10)
C(25A)	150(15)	202(12)	150(16)	29(10)	5(12)	-27(10)
C(26A)	152(16)	273(14)	228(18)	28(12)	-32(13)	-20(11)

C(27A)	164(16)	292(14)	194(17)	32(12)	27(13)	-46(11)
C(28A)	167(15)	221(12)	198(17)	23(11)	12(13)	-37(11)
C(29A)	154(15)	160(11)	180(16)	28(10)	-1(12)	-4(10)
C(30A)	152(15)	141(11)	133(15)	34(10)	-10(12)	24(10)
C(31A)	185(15)	177(12)	146(16)	2(10)	10(12)	29(11)
C(32A)	223(17)	228(13)	208(17)	19(11)	-19(13)	93(11)
C(33A)	291(17)	153(12)	221(17)	48(11)	-61(14)	43(11)
C(34A)	241(17)	179(12)	160(16)	52(11)	9(13)	6(11)
C(35A)	179(15)	182(12)	188(17)	30(11)	-5(13)	22(11)
C(36A)	180(15)	131(11)	134(15)	2(10)	42(12)	-2(10)
C(37A)	232(17)	228(13)	148(16)	-37(11)	18(13)	-13(11)
C(38A)	380(20)	270(14)	193(18)	-94(12)	58(15)	-27(13)
C(39A)	380(20)	262(14)	242(19)	-93(12)	119(16)	-11(13)
C(40A)	261(17)	208(13)	266(18)	-14(12)	108(14)	30(11)
C(41A)	202(16)	171(12)	163(16)	14(10)	51(13)	12(10)
C(42A)	159(15)	137(11)	140(16)	7(10)	-4(12)	18(10)
C(43A)	303(18)	132(11)	176(17)	10(10)	12(14)	29(11)
C(44A)	290(18)	177(12)	183(17)	30(11)	6(14)	-35(11)
C(45A)	288(18)	291(14)	140(17)	73(12)	30(14)	-36(12)
C(46A)	340(19)	341(15)	136(17)	-18(12)	16(14)	-139(13)
C(47A)	237(17)	280(14)	167(17)	23(12)	-42(14)	-83(12)
C(48A)	139(14)	104(10)	181(16)	15(10)	13(12)	20(9)
C(49A)	161(15)	172(12)	199(17)	-2(11)	-4(13)	28(10)
C(50A)	200(16)	237(13)	227(18)	-18(11)	53(13)	42(12)
C(51A)	151(16)	246(13)	320(20)	0(12)	5(14)	48(11)
C(52A)	182(16)	247(13)	274(19)	-4(12)	-53(14)	56(12)
C(53A)	140(15)	235(13)	192(17)	-17(11)	-29(13)	35(11)
C(54A)	163(15)	121(11)	183(16)	-27(10)	-43(12)	3(10)
C(55A)	212(16)	177(12)	262(18)	-81(11)	-26(13)	26(11)
C(56A)	283(18)	168(12)	303(19)	-125(11)	-33(15)	43(11)
C(57A)	410(20)	144(12)	330(20)	-70(12)	-79(16)	-26(12)
C(58A)	340(19)	163(13)	330(20)	7(12)	15(15)	-73(12)
C(59A)	275(17)	133(11)	183(17)	4(10)	-8(13)	-29(11)
Ir(2)	185(1)	86(1)	192(1)	9(1)	43(1)	10(1)
Cl(2)	287(4)	91(2)	282(4)	0(3)	58(3)	15(2)
P(1B)	218(4)	123(3)	203(4)	-2(3)	29(3)	24(3)
P(2B)	191(4)	142(3)	231(5)	-8(3)	32(3)	-6(3)
O(1B)	217(11)	107(8)	248(12)	-9(7)	64(9)	-10(7)
O(2B)	223(11)	147(8)	247(12)	38(8)	65(9)	45(7)
N(1B)	195(13)	80(9)	198(13)	-8(8)	51(11)	0(8)
N(2B)	202(13)	83(9)	223(14)	7(8)	40(11)	6(9)
C(1B)	182(15)	135(11)	205(17)	9(10)	45(13)	-9(10)
C(2B)	346(19)	110(11)	390(20)	14(12)	201(16)	47(11)
C(3B)	289(18)	213(13)	410(20)	9(13)	230(16)	39(12)
C(4B)	260(17)	151(12)	282(18)	36(11)	70(14)	-11(11)
C(5B)	239(17)	116(11)	229(17)	22(10)	63(13)	-3(10)

C(6B)	152(15)	144(11)	184(16)	5(10)	28(12)	8(10)
C(7B)	217(16)	90(11)	269(17)	-19(11)	42(13)	26(10)
C(8B)	217(16)	84(10)	274(17)	6(11)	53(13)	-11(11)
C(9B)	157(15)	164(11)	135(16)	2(10)	23(12)	-3(10)
C(10B)	205(16)	144(11)	214(17)	10(11)	15(13)	23(11)
C(11B)	215(16)	200(13)	232(18)	-9(11)	45(14)	41(11)
C(12B)	234(17)	263(14)	267(19)	17(12)	85(14)	-6(12)
C(13B)	250(17)	143(12)	268(18)	34(11)	99(14)	34(11)
C(14B)	202(16)	156(12)	179(16)	12(10)	29(13)	19(11)
C(15B)	143(14)	117(10)	183(16)	-1(10)	6(12)	8(10)
C(16B)	236(17)	156(12)	370(20)	44(12)	130(15)	1(11)
C(17B)	325(19)	133(12)	470(20)	111(12)	160(16)	-6(12)
C(18B)	301(19)	218(13)	440(20)	-26(13)	110(17)	-46(12)
C(19B)	350(20)	228(13)	430(20)	51(14)	151(17)	-59(13)
C(20B)	299(19)	223(14)	390(20)	21(13)	178(16)	77(12)
C(21B)	430(20)	280(16)	610(30)	82(15)	210(20)	186(14)
C(22B)	630(30)	377(17)	410(20)	-45(16)	210(20)	130(17)
C(23B)	290(20)	365(17)	970(30)	-85(19)	200(20)	58(15)
C(24B)	270(40)	300(30)	50(40)	-30(20)	-90(30)	80(20)
C(25B)	330(30)	540(30)	270(30)	-130(20)	10(20)	90(20)
C(26B)	190(30)	710(40)	590(40)	-320(30)	0(30)	80(30)
C(27B)	260(30)	690(40)	450(40)	-180(30)	30(30)	140(30)
C(28B)	280(40)	330(30)	380(50)	-130(30)	40(30)	100(20)
C(29B)	390(50)	180(30)	330(60)	-60(30)	130(30)	120(20)
C(24C)	30(30)	20(30)	20(30)	-1(10)	4(11)	1(10)
C(25C)	230(70)	130(40)	310(70)	-10(40)	10(50)	0(40)
C(26C)	90(60)	290(60)	650(110)	-170(60)	130(70)	-30(50)
C(27C)	120(60)	330(60)	290(80)	-20(50)	110(50)	50(50)
C(28C)	160(100)	370(80)	620(150)	-300(100)	100(90)	40(70)
C(29C)	200(70)	200(70)	200(70)	1(10)	22(13)	-1(10)
C(30B)	250(30)	210(20)	230(40)	-120(20)	190(30)	-26(17)
C(31B)	310(20)	166(17)	230(20)	50(15)	27(19)	-11(15)
C(32B)	330(30)	150(20)	200(30)	7(18)	-10(20)	-70(19)
C(33B)	310(30)	108(19)	330(30)	-16(18)	-20(20)	7(18)
C(34B)	330(30)	194(19)	260(30)	-14(17)	70(20)	47(19)
C(35B)	260(40)	110(20)	240(40)	-40(30)	110(30)	-10(20)
C(30C)	170(50)	160(50)	170(50)	1(10)	20(11)	-3(10)
C(31C)	280(70)	180(50)	160(70)	-20(40)	-20(50)	70(50)
C(32C)	300(90)	90(60)	340(110)	80(60)	-70(80)	-130(50)
C(33C)	370(90)	170(70)	340(110)	-20(60)	170(80)	90(60)
C(34C)	360(90)	260(70)	460(110)	-130(60)	90(80)	150(60)
C(35C)	310(110)	310(110)	310(110)	3(10)	36(16)	-2(10)
C(36B)	327(18)	132(11)	199(17)	14(11)	59(14)	46(11)
C(37B)	420(20)	188(13)	214(18)	16(11)	19(15)	73(12)
C(38B)	480(20)	201(13)	218(19)	3(12)	-28(16)	76(13)
C(39B)	580(30)	262(15)	260(20)	106(13)	73(18)	115(15)

C(40B)	370(20)	269(15)	360(20)	122(13)	79(17)	36(13)
C(41B)	350(20)	196(13)	277(19)	100(12)	76(15)	55(12)
C(42B)	207(16)	183(12)	241(18)	-28(11)	9(13)	-14(11)
C(43B)	228(17)	180(12)	263(18)	-53(11)	13(14)	-6(11)
C(44B)	244(18)	263(14)	360(20)	-56(13)	86(16)	-9(12)
C(45B)	268(18)	272(14)	235(18)	-35(12)	50(14)	-35(12)
C(46B)	318(19)	270(14)	238(19)	-20(12)	50(15)	-7(12)
C(47B)	300(18)	238(14)	252(19)	-51(12)	12(15)	16(12)
C(48B)	230(17)	139(12)	332(19)	-12(11)	90(14)	-28(11)
C(49B)	308(19)	206(13)	350(20)	-9(12)	111(16)	-55(12)
C(50B)	420(20)	276(15)	610(30)	46(16)	250(20)	-66(14)
C(51B)	470(20)	287(15)	670(30)	-123(17)	300(20)	-194(15)
C(52B)	580(30)	327(17)	640(30)	-235(17)	330(20)	-260(16)
C(53B)	294(19)	320(15)	420(20)	-129(14)	98(17)	-136(13)
C(54B)	204(16)	165(12)	264(18)	-18(11)	37(14)	5(11)
C(55B)	189(16)	222(13)	206(17)	13(11)	-7(13)	-10(11)
C(56B)	302(19)	209(13)	390(20)	61(13)	43(16)	9(12)
C(57B)	310(20)	312(15)	420(20)	71(14)	32(17)	69(14)
C(58B)	179(17)	343(16)	410(20)	45(14)	17(15)	47(13)
C(59B)	276(19)	259(14)	390(20)	13(13)	45(16)	14(13)
C(61)	330(20)	472(19)	570(30)	-47(17)	76(19)	22(16)
Cl(3)	395(6)	614(5)	636(7)	156(5)	122(5)	169(4)
Cl(4)	457(6)	398(4)	701(7)	-93(4)	-8(5)	20(4)
C(62)	340(20)	334(16)	550(30)	-17(16)	89(19)	5(14)
Cl(5)	467(6)	287(4)	581(6)	55(4)	197(5)	-13(4)
Cl(6)	577(6)	453(5)	488(6)	40(4)	198(5)	137(4)

---